RESIDUAL STRESS EFFECTS IN FATIGUE

ASTM STP 776

RESIDUAL STRESS EFFECTS IN FATIGUE

A symposium
sponsored by ASTM
Committee E-9 on Fatigue
Phoenix, Ariz., 11 May 1981

ASTM SPECIAL TECHNICAL PUBLICATION 776
J. F. Throop and H. S. Reemsnyder,
symposium chairmen

ASTM Publication Code Number (PCN)
04-776000-30

1916 Race Street, Philadelphia, Pa. 19103

Library of Congress Catalog Card Number: 81-71054

NOTE

The Society is not responsible, as a body, for the statements and opinions advanced in this publication.

Printed in Baltimore, Md.
July 1982

Foreword

The Symposium on Residual Stress Effects in Fatigue was held in Phoenix, Arizona, on 11 May 1981. ASTM Committee E-9 on Fatigue was sponsor. J. F. Throop and H. S. Reemsnyder served as symposium chairmen.

Related ASTM Publications

Low-Cycle Fatigue and Life Prediction, STP 770 (1982), 04-770000-30

Design of Fatigue and Fracture Resistant Structures, STP 761 (1982), 04-761000-30

Methods and Models for Predicting Fatigue Crack Growth under Random Loading, STP 748 (1981), 04-748000-30

Statistical Analysis of Fatigue Data, STP 744 (1981), 04-744000-30

Fatigue Crack Growth Measurement and Data Analysis, STP 738 (1981), 04-738000-30

Tables for Estimating Median Fatigue Limits, STP 731 (1981), 04-731000-30

Fatigue of Fibrous Composite Materials, STP 723 (1981), 04-723000-33

Effect of Load Variables on Fatigue Crack Initiation and Propagation, STP 714 (1980), 04-714000-30

Part-Through Crack Fatigue Life Prediction, STP 687 (1979), 04-687000-30

A Note of Appreciation to Reviewers

This publication is made possible by the authors and, also, the unheralded efforts of the reviewers. This body of technical experts whose dedication, sacrifice of time and effort, and collective wisdom in reviewing the papers must be acknowledged. The quality level of ASTM publications is a direct function of their respected opinions. On behalf of ASTM we acknowledge with appreciation their contribution.

ASTM Committee on Publications

Editorial Staff

Contents

Introduction

The Symposium on Residual Stress Effects in Fatigue was organized to bring together new observations and analyses developed mainly from the application of fracture mechanics and local strain concepts to the estimation of fatigue life when residual stresses are present in a component. The use of superposition of stress intensity factor relationships, including expressions that consider residual stresses, has become widely accepted in recent years. Such superposition allows the analytical estimation of fatigue life rate to include residual stress effects on fatigue crack propagation.

Investigators active in the field of fatigue of materials are well aware, however, that if reliable fatigue life estimates are to be made, it is necessary to characterize the residual stress fields in test specimens and engineering components. Such characterization must include both analytical and experimental determinations of the residual stress distributions and their possible changes during the life of the component. Indeed, ASTM Subcommittee E09.02 on Residual Stress Effects in Fatigue and this symposium are the outgrowth of a 1976 task group study on organizing an activity for investigating the effects of residual stress in fatigue crack initiation, growth, performance, and life; seeking ways to measure those effects; and studying means of alleviating the adverse effects and exploiting the beneficial effects on fatigue behavior.

New techniques for analytical solutions of residual stresses, employing analogous thermal stress distributions, are becoming available. Also, experimental methods and instruments for residual stress measurement by X-ray diffraction, hole-drilling, and other techniques are being improved and becoming more widely available. Moreover, in the years since 1976 a rapid increase in awareness of the importance of residual stresses in material behavior has developed worldwide.

Because of these developments, May 1981 seemed a propitious time for ASTM Committee E-9 on Fatigue to sponsor a symposium exploring the present state of the art on residual stress effects on the fatigue behavior of materials. Many of the papers indicate that the newest developments of knowledge in the field are strongly influenced by the concepts of local strain analysis and linear elastic fracture mechanics. Some of the papers also treat recently developed techniques for observing the effects of residual stresses experimentally, such as ultrasonic methods, fretting fatigue experiments, and *in situ* observations of surface microcrack opening displacements in a scanning electron microscope. Along with a summary of methods for residual stress measurement and a presentation of standards for residual stress measurement, a variety of subjects was covered, including stress intensity factors, notches, weld fatigue, crack propagation in welds, welded joints, welded attachments, railroad rails, case-hardened steels, and aircraft landing-gear maintenance. These contributions show how the presence of residual stresses, either intentionally or unintentionally introduced, may affect the fatigue behavior of various specimens and structural components. They also indicate how one may take these effects into account quantitatively by measurement or analysis.

It is well known that large changes in fatigue life may result from varying the residual stress magnitude or distribution, especially if it is a compressive residual stress as in a shot-peened surface. It follows logically that considerable scatter in fatigue life at a given load level will result if the residual stress state in the component is not controlled within close limits. It has only recently been recognized that even in laboratory testing of specimens the fatigue performance may be incorrectly evaluated if the residual stress state of the specimens is not considered. Furthermore, while it has long been recognized that residual stresses may change during continuous load cycling (sometimes called "fading") it is only recently that analytical approaches—for example, local strain—have been developed for evaluating their changing magnitude during cycling. These aspects of fatigue behavior are discussed in several of the symposium papers.

This volume, then, should help the student, researcher, and engineer to become aware of the possible magnitude, nature, and consequences of residual stress effects in fatigue of materials. It also offers examples of analysis, instrumentation, and procedures currently used in evaluating these effects. We hope that future research and developments in the field will bring about improvements in, and new and better methods of, inspection, analysis, and measurement of the residual stress effects throughout the useful life of a component or structure.

We express our thanks and appreciation to the authors for their symposium presentations and papers. Special thanks are also due Darrell F. Socie and the members of the Joint ASTM E-9/E-24 Task Group on Fatigue of Short Cracks for their part in the consideration of that aspect of the subject. In addition, we thank the many reviewers for their time, effort, and helpful criticisms of the manuscripts.

J. F. Throop
Benét Weapons Laboratory,
Large Caliber Weapons Systems
Laboratory, U. S. Army Research
and Development Command,
Watervliet, New York;
symposium chairman

H. S. Reemsnyder
Homer Research Laboratory,
Bethlehem Steel Corporation,
Bethlehem, Pennsylvania;
symposium chairman

C. O. Ruud[1]

Nondestructive and Semidestructive Methods for Residual Stress Measurement

REFERENCE: Ruud, C. O., "**Nondestructive and Semidestructive Methods for Residual Stress Measurement,**" *Residual Stress Effects in Fatigue, ASTM STP 776,* American Society for Testing and Materials, 1982, pp. 3-5.

ABSTRACT: The effect of residual stresses on the fatigue life in metallic components has long been recognized. However, the most commonly employed methods for its measurement are destructive or at least partially so. This has led to an active interest in nondestructive methods for residual stress measurement. A review and evaluation has recently been published that describes the essence of the principles of nearly all the applied and proposed methods for nondestructive and semidestructive residual stress measurement. This review is summarized herein.

KEY WORDS: residual stresses, stress measurement, nondestructive stress measurement, semidestructive stress measurement, hole drilling stress measurement, X-ray diffraction stress measurement, ultrasonic stress measurement, Barkhausen noise analysis

Residual stresses have been given many labels, including *internal, bulk, self, welding, forming, fabrication*, and *in situ stresses*. However, these other names are not as specific or else they are less comprehensive than the preferred term, *residual stresses*. Residual stresses are produced in metals by most processes used to form and fabricate them into engineering components. This includes welding, forging, heat treating, rolling, grinding, machining, etc. These processes cause residual stresses by inducing plastic deformation of the metal through severe temperature gradients or mechanical forces. A less common source of residual stress which is not the direct result of plastic deformation is localized permanent elastic expansion or contraction of the metallic lattice in processes such as nitriding, carburizing, or heat treatment which induces phase transformation.

Background

For many reasons, residual stresses are receiving increased attention by the engineering community. These reasons are primarily concerned with pressures to reduce the cost of materials used in structures, extending the useful lifetime of

[1] NDT&E Program Director, The Pennsylvania State University, University Park, Pa. 16802.

existing structures, and the demand for greater reliability of structural components. This has led to much activity in the study of residual stress measurement methodologies, especially those which may be applied to nondestructive inspection. Unfortunately, those methods of residual stress measurement with which the engineering community is most familiar are completely destructive. This has precipitated greater activity in the research and development of nondestructive, or at least semidestructive, methods of residual stress measurement.

An in-depth review and evaluation has recently been completed on nondestructive methods of residual stress measurement.[2] This EPRI Report is summarized herein. It focuses upon nine generic types of stress measurement-related phenomena:

1. Ultrasonic (Acoustics)
2. Electromagnetic (including Barkhausen)
3. Neutron Diffraction
4. X-Ray Diffraction
5. Positron Annihilation
6. Nuclear Hyperfine (including Mossbauer)
7. Chemical Etchant
8. Indentation
9. Hole Drilling

A condensation of this full report was recently published,[3] which focused upon the four most useful and/or most studied nondestructive and semidestructive methods. These were ultrasonic, Barkhausen, X-ray diffraction (XRD), and hole drilling.

Conclusions

The EPRI Report concluded that the most reliable methods, besides the completely destructive mechanical methods, for the measurement of residual stresses are hole drilling and X-ray diffraction. The semidestructive method of hole drilling is capable of measuring stresses to a depth of a few millimetres into the specimen, and the instrumentation is portable and inexpensive. However, the application of this method could well weaken the component to the extent that it would no longer be functional. Furthermore, there are many other limitations of the hole-drilling techniques; these are described in the EPRI Report.

The X-ray diffraction method is recognized as the only truly nondestructive residual stress measurement technique that is reliable. Its most severe limitations are that it can be applied nondestructively only on the surface, instrumentation is expensive, and procedures for the newly available portable instrumentation are not yet ready for general application. Other less serious limitations are detailed in the EPRI Report.

[2] Ruud, C. O., "A Review and Evaluation of Nondestructive Methods For Residual Stress Measurement," EPRI Report NP-1971, Project 1395-5, Electric Power Research Institute, Palo Alto, Calif., Sept. 1981.

[3] Ruud, C. O., *Journal of Metals*, Vol. 33, No. 7, July 1981, pp. 35-40.

The ultrasound methods hold the greatest promise for wide practical application, especially for three-dimensional stress fields; however, their general implementation is by no means likely to evolve in the near future. Most of the other methods that have been proposed, including Barkhausen Noise Analysis, are either of such limited use or in such an elementary state of development that their practical implementation is likely to be further away than that of ultrasound.

The prognosis offered is that the semidestructive method of hole drilling will continue to find limited application, especially where its use can be tolerated and where investment in XRD instrumentation is fiscally prohibitive. However, the technology for portable XRD equipment capable of rapid, accurate residual stress measurement is advancing, and more versatile devices will become available over the next few years. This will set the stage for much more widespread field and shop use of XRD, even for dynamic and high-temperature applications. The ultrasonic techniques will enjoy the most intense research investment and will continue to offer the promise of three-dimensional nondestructive residual stress measurement; however, general practical implementation is years away, even though instrumentation for ultrasound is by nature easier to make portable than the XRD counterpart. The major impediments to ultrasound residual stress technology will remain the need for better understanding of the effect of microstructural characteristics of metals on the ultrasonic wave, development of vectorial algorithms for acoustic propagation and velociometric effects, higher-quality more-versatile transducers, and better transducer/metal coupling technology. The Barkhausen technique of residual stress measurement suffers from as many inherent unknowns and limitations as does ultrasound without offering as much promise for general practical applicability. Any advancements in the magnetic or other methods are likely to come by chance from research applied to basic knowledge or goals other than NDE for residual stress measurement.

Leonard Mordfin [1]

Standards for Residual Stress Measurement

REFERENCE: Mordfin, Leonard, "**Standards for Residual Stress Measurement,**" *Residual Stress Effects in Fatigue, ASTM STP 776*, American Society for Testing and Materials, 1982, pp. 6-12.

ABSTRACT: It has been long appreciated that residual stresses can exert significant influences on fatigue and fracture behavior, but only recently have analytical models been developed which enable the influences to be quantified. These new capabilities have fostered increased demands for residual stress measurements and these, in turn, have revealed that the reliability and the reproducibility of such measurements are often less than adequate. The need for standards for residual stress measurements is now recognized as being urgent. Few standards presently exist, and they do not provide the required levels of measurement reproducibility.

Several organizations are attempting to respond to this critical need. This paper is a status report on the growing national effort to develop voluntary consensus standards to enhance the reproducibility of residual stress measurements. This effort has achieved noteworthy progress in only a few years, but it has also become evident that further progress will be increasingly more difficult because our understanding of some residual stress phenomena is limited. There is need for a national *research* effort to parallel and to support the standardization effort.

KEY WORDS: fatigue, hole drilling, nondestructive evaluation, photoelasticity, research needs, residual stress, standards, stress measurement, terminology, ultrasonics, X-ray diffraction

The phenomenon of residual stresses has been recognized for a long time and some methods for measuring residual stresses have been known for almost as long. Until recently, however, there were virtually no standards for residual stress measurement, because there was no general requirement to measure residual stresses accurately. Simply knowing whether the stresses in a certain region of a given part were tensile or compressive, or high or low, was usually sufficient to make a qualitative determination of whether the fabrication process for the part was acceptable or whether it had to be modified. In other words, there was no particular benefit to be derived from knowing whether the residual stress level was, say, 60 percent or 75 percent of the material yield strength.

This relatively comfortable situation (ignorance is bliss?) no longer prevails in many engineering applications. The development of analytical fracture mechanics and methods for predicting fatigue crack growth rates has made it possible to make quantitative estimates of the performance and durability of load-bearing

[1] Acting Chief, Office of Nondestructive Evaluation, National Bureau of Standards, Washington, D.C. 20234.

elements. With these new capabilities, critical parts can be designed and fabricated with greater reliability than ever before, provided that the stresses acting on the parts are well characterized. A design engineer can often estimate applied stresses rather accurately if he knows the service loads and the conditions under which a part is expected to operate. However, the residual stresses, which can be just as detrimental as applied stresses, can only be characterized on the basis of measurements. The reliable measurement of residual stress has therefore become an elusive goal in many organizations that are concerned with the fatigue and fracture of critical parts.

There are numerous situations in which the design engineer would like to be able to specify maximum and minimum residual stress levels. One can also visualize inspection procedures that will monitor the residual stress distributions of critical parts in service in order to assure safety and durability. In scenarios such as these, which are not at all unrealistic for the latter part of this decade, it is imperative that residual stress measuring techniques be quantitative and reproducible; this requires measurement standards. The realization of this need prompted the creation of several groups, over the past few years, which are vigorously pursuing the development of standards for residual stress measurement.

Some Recent History

In 1976 ASTM Committee E-9 on Fatigue established the Task Group on Residual Stress Effects in Fatigue under the chairmanship of Joseph Throop of Watervliet Arsenal. Throop appreciated the importance of the measurement problem and formed a section, within the task group, to concern itself with the measurement and characterization of residual stress fields; this despite the fact that the topic was not in the mainstream of the task group's interest. In 1980 the task group became Subcommittee E9.02 on Residual Stress Effects in Fatigue.

The Society for Experimental Stress Analysis (SESA), under the instigation of Paul Prevey of Lambda Research, created the Technical Committee on Residual Stress Measurement in 1978. The principal functions of the committee are to promote research and to disseminate information on residual stress measurement. With Prevey as chairman, however, the committee also pursued round-robin testing programs aimed at providing some of the data needed to establish meaningful standards for residual stress measurements. Michael Flaman of Ontario Hydro is the present chairman of the committee, with Richard Chrenko of General Electric serving as chairman of the committee's executive board.

Also in 1978, Alfred Fox of Bell Laboratories, then chairman of ASTM Committee E-28 on Mechanical Testing, recognized the need for residual stress measurement standards and asked the author to organize the Task Group on Measurement Methods for Residual Stress. A year later the task group became Subcommittee E28.13 on Residual Stress Measurement, its principal mission being the development of consensus standards for residual stress measurement. The subcommittee is presently comprised of five sections: 01 on Nomenclature, 02 on Hole-Drilling Methods, 03 on X-Ray Diffraction Methods, 04 on Dissection and Layer-Removal Methods, and 05 on Ultrasonic Methods. With the establishment of E28.13, Throop was able to de-emphasize E9.02's direct concern with measurement methods.

In 1980 ASTM Committee D-20 on Plastics initiated Section D20.10.23 on Residual Strain Measurement, with Alex Redner of Vishay Intertechnology as its chairman. The chief interest of the section is the measurement of strains in plastics by photoelastic techniques.

It is a source of great satisfaction that the cooperation between all these groups has been excellent, since this is unquestionably enhancing the standards-development process.

Present Activities

There are, today, no national standards in the United States that address generic methods for measuring residual stresses. There are some company standards and some product standards, but the engineer or the technician who needs a standardized methodology or a traceable calibration procedure to guide him and to help him to make reliable and reproducible measurements of residual stress is generally at a loss in this respect. Fortunately, however, rapid progress is being made on this front, and it is reasonable to expect that consensus standards will begin to become available later in 1981.

X-Ray Diffraction

The well-known manual on "Residual Stress Measurement by X-Ray Diffraction" was published by the Society of Automotive Engineers (SAE) in 1960; an updated edition was issued in 1971 [*1*].[2] This is unquestionably one of the finest technical documents assembled by a committee and, until recently, it represented the single most complete and reliable American document on the subject. Few practitioners of the art can be found who are not intimately familiar with its hundred-plus pages. Recently, however, some detailed review articles have appeared (for example, Ref *2*) which provide more up-to-date treatments of certain aspects of the subject than are available in the ten-year-old manual.

SAE J784a, as the manual is commonly known, has frequently been cited as a standard, but it is not nor was it intended as such. Although it describes various testing techniques clearly and thoroughly, it prescribes none. Two laboratories could well conduct residual stress measurements "in accordance with SAE J784a" and yet do virtually nothing in common. The three-point parabola procedure for determining peak diffraction angles, for example, has occasionally been termed "the SAE method" but, in fact, SAE J784a describes other procedures as well.

The committee that prepared the manual has undergone several changes over the past few years under SAE reorganizations and is presently known as the X-Ray Task Group of the Materials Properties and Processing Effects Division, an arm of the SAE Fatigue Design and Evaluation Committee. John Larson of

[2] The italic numbers in brackets refer to the list of references appended to this paper.

Ingersoll-Rand, an associate editor of SAE J784a, is the chairman of the group. In recent years the group directed its principal attention to the measurement of retained austenite by X-ray methods and has, apparently, ceased to address the residual stress problem. This is unfortunate, because the group has the competence to successfully formulate some of the needed test method standards for residual stress measurements. That such standards are feasible has already been demonstrated abroad.[3]

ASTM Subcommittee E28.13 has elected to pursue a different, although equally important, standards aspect of the X-ray diffraction method, namely the alignment and the calibration of the diffraction apparatus. Section 03 of the subcommittee, under Prevey's leadership, has prepared a "Standard Method for Verifying the Alignment of Instrumentation for Residual Stress Measurement by X-Ray Diffraction," which is expected to be balloted at the subcommittee level late in 1981. The method relies on the use of a stress-free metal powder as a reference specimen. The data that verify the stress-free nature were obtained in an SESA round-robin testing program initiated by Prevey, assisted by John Cammett of Metcut Research, for the SESA committee.

A second project in Section 03 of Subcommittee E28.13 is concerned with the calibration of the diffraction instrument. Based on earlier work by Prevey [*3*], a standard procedure will be formulated for evaluating the effective elastic constants which are needed to convert lattice strain measurements to stress values.

Hole Drilling

The most rapid progress in Subcommittee E28.13, thus far, has been achieved by Section 02 under Redner's direction. With considerable assistance from M. R. Baren of the Budd Company, Redner prepared a "Standard Method for Determining Residual Stresses by the Hole-Drilling Strain-Gage Method". The method has been approved by the Society and will be published in the *1982 ASTM Book of Standards*. The section is now making plans for a round-robin testing program, perhaps in collaboration with the SESA committee, to support the development of a more quantitative estimate of the precision of the method.

Photoelasticity

The photoelastic approach to evaluating the residual stresses in optically birefringent materials is also benefiting from Redner's leadership. Although some standards for this method have been available for some time,[4] they do not provide the quantitative precision needed for fracture mechanics analyses and, furthermore, they are applicable only to glass. In response to these limitations, ASTM Section D20.10.23 has developed a "Standard Method for Photoelastic Mea-

[3] "Standard Method for X-Ray Stress Measurement," Committee on Mechanical Behaviour of Materials, The Society of Materials Science, Japan, 20 April 1973.

[4] ASTM Tests for Polariscopic Examination of Glass Containers (C 148) and ASTM Test for Analyzing Stress in Glass (F 218).

surements of Strains in Transparent or Translucent Plastic Materials," which is expected to be approved by the Society in 1982.

Terminology

The difficulties in achieving consensus definitions of terms related to residual stress can only be appreciated by those who have tried it. There are very good reasons why standard definitions do not already exist for such "obvious" terms as *residual stress* and *residual strain*. After several years of persistent effort Section 01 of Subcommittee E28.13 has finally come up with definitions for these and other terms and a subcommittee letter ballot is expected late in 1981. The eventual intent—at this stage, at least—is to incorporate these definitions into ASTM Definitions of Terms Relating to Methods of Mechanical Testing (E 6).

Future Directions

The consensus standards for residual stress measurement that are now under development are based upon reasonably well-established practices. Well-established practices are not always available, however, to support every standard that merits development. In some cases there is inadequate understanding of *all* the physical phenomena involved and even some uncertainty regarding the most promising standardization approaches which should be pursued. This is a problem that has existed, for example, in connection with ultrasonic and magnetic methods for measuring residual stress.

Thomas Proctor of NBS, chairman of Section 05 in Subcommittee E28.13, addressed this problem by organizing the ASTM Symposium on Ultrasonic Measurements of Stress in collaboration with Joseph Heyman of NASA/Langley. The symposium, which was held in April 1981, brought together a number of experts on the subject and did, indeed, provide some of the guidance and direction that were sought. It became clear, as paper after paper was presented, that the principal barrier inhibiting further development and widespread application of ultrasonic techniques for residual stress measurement is inadequate understanding of the effects of microstructural features on ultrasonic wave propagation. That points up a need for an intensive research effort which an ASTM committee can certainly encourage but cannot hope to conduct. In fact, the effects of microstructure on ultrasonic wave propagation represents only one of several unsolved problems relating to residual stress measurement. NBS, through its Office of Nondestructive Evaluation, has proposed a framework for a comprehensive research program on this subject that is responsive to national priorities for enhanced productivity and product quality [*4*].

A panel discussion in the Symposium on Ultrasonic Measurements of Stress revealed that, in spite of the gaps in our understanding, there are at least three standardization activities, pertaining to the ultrasonic measurement of residual stress, which Subcommittee E28.13 can and should pursue: (*1*) the formulation of standard definitions of relevant terms, particularly those related to the acoustoelastic constants; (*2*) the development of a standard method for making ultrasonic velocity measurements (perhaps in collaboration with Committee E-7 on Nondestructive Testing) that is more directly applicable to residual stress determinations than existing documents;[5] and (*3*) the development and evaluation of concepts for reference artifacts, containing well-characterized residual stress distributions, which can be used for the calibration and verification of ultrasonic stress-measuring systems. A promising concept of this kind was proposed in the symposium,[6] and preliminary plans for a round-robin evaluation by Section E28.13.05 were initiated.

Is it meaningful or worthwhile to pursue the standardization of methods or techniques that are not already well established? It is disturbing to hear this question posed time and again when the ASTM experience shows, beyond doubt, that the answer is an overwhelming *yes*. There are few activities that stimulate research on test methods and measurement techniques more than the healthy pursuit of consensus standards. The records of ASTM Committees D-30 on Composite Materials and E-24 on Fracture, to name only two, bear this out. In fact, NBS recognition of this fertile relationship between standards development and research [*5*] is the basis for the Bureau's support of, and the author's participation in, Subcommittee E28.13 on Residual Stress Measurement.

Concluding Remarks

Since the inception of Subcommittee E28.13 on Residual Stress Measurement and the task group which preceded it, well over one hundred written requests have been received from individuals expressing interest in the subcommittee's progress. Yet the subcommittee's membership roster stands at only 27 and, as is evident from this paper, most of the subcommittee's progress has resulted from the dedicated efforts of a handful of highly competent and very busy people. The officers of Committee E-28 are grateful to them, as is everyone who has a need for more reliable and more reproducible measurements of residual stress. This is an excellent opportunity to invite other interested persons to join the subcommittee and to participate in its important work.

In addition to this need for volunteers to help in the development of standards, the residual stress measurement problem requires the involvement of organizations. Mention has been made of the comprehensive research program on residual stress measurement problems that must be addressed. The timely execution of such a program will require substantial resources; more, in fact, than any single organization may be willing to commit in the face of today's budgetary constraints.

[5] ASTM Practice for Measuring Ultrasonic Velocity in Materials (E 494) and ASTM Test for Pulse Velocity Through Concrete (C 597).

[6] Hsu, N., Proctor, T., and Blessing, G., "An Analytical Approach to Reference Samples for Ultrasonic Residual Stress Measurement."

References

[1] Hilley, M. E., Ed., "Residual Stress Measurement by X-Ray Diffraction," SAE J784a, 2nd ed., Society of Automotive Engineers, Warrendale, Pa., 1971.
[2] James, M. R. and Cohen, J. B., "The Measurement of Residual Stresses by X-Ray Diffraction Techniques," in *Treatise on Materials Science and Technology*, Vol. 19A, H. Herman, Ed., Academic Press, New York, 1980, pp. 1-62.
[3] Prevey, P. S., "A Method of Determining the Elastic Properties of Alloys in Selected Crystallographic Directions for X-Ray Diffraction Residual Stress Measurement," in *Advances in X-Ray Analysis*, Vol. 20, Plenum Press, New York, 1977, pp. 345-354.
[4] Mordfin, L., "Measurement of Residual Stresses: Problems and Opportunities," in *Residual Stress for Designers and Metallurgists*, L. J. Vande Walle, Ed., American Society for Metals, 1981, pp. 189-210.
[5] Mordfin, L. and Berger, H., "NDE Standards for Nuclear Power Systems: An NBS Perspective," in *Nondestructive Evaluation in the Nuclear Industry-1980*, American Society for Metals, 1981, pp. 303-318.

A. P. Parker[1]

Stress Intensity Factors, Crack Profiles, and Fatigue Crack Growth Rates in Residual Stress Fields

REFERENCE: Parker, A. P., "**Stress Intensity Factors, Crack Profiles, and Fatigue Crack Growth Rates in Residual Stress Fields,**" *Residual Stress Effects in Fatigue, ASTM STP 776,* American Society for Testing and Materials, 1982, pp. 13-31.

ABSTRACT: A linear elastic fracture mechanics approach to crack growth rate prediction implies the need to calculate accurate, effective stress intensity (K) factors, and hence effective R-values, (K_{min}/K_{max}), for components containing residual stress. To this end the weight function and associated superposition techniques are described, with emphasis on stress intensity and crack shape prediction for residual stress problems. Stress intensity factors are presented for various geometries with residual stress fields. The nonlinear, crack surface 'overlapping' effect is noted, and the case of cracks emanating from notches in residual stress fields is shown to be an associated problem.

The application of such results in crack growth rate prediction is addressed. The characteristic crack growth rate features of several different loading systems are predicted, and shown to agree with available experimental data. Finally, the qualitative changes in the form of standard *S-N* curves for welded details are predicted, and shown to conform with limited available *S-N* curve experimental data.

KEY WORDS: crack growth, crack propagation, cylinders, fracture (materials), residual stress, retardation, stress intensity factor, weldments

Nomenclature

- a Crack length (edge crack)
  Semicrack length (internal crack)
- b Crack spacing
- C Coefficient in Paris's crack growth law
- E Modulus of elasticity
- H Material property, $H = E$ (plane stress),
  $H = E/(1 - \nu^2)$ (plane strain)
- K Stress intensity factor
- K_I Opening mode stress intensity factor
- K_0 Nondimensionalizing stress intensity factor
- ΔK Stress intensity factor range
- m Weight function with stress boundary conditions

[1]Principal Lecturer, Materials Branch, Royal Military College of Science, Shrivenham, Swindon, Wiltshire, England.

m^*	Weight function with displacement boundary conditions
M	Exponent in Paris's crack growth law
max	Maximum value
min	Minimum value
N	Number of loading cycles
p	Crack face pressure loading which produces same K as crack-line stress system in the unflawed configuration
R	Ratio of K_{min}/K_{max}
R_1	Inner tube radius
R_2	Outer tube radius
th	Threshold
Y	Material yield stress
v	Crack opening
ν	Poisson's ratio
σ	Direct stress
τ	Shear stress

The Weight Function

In a particular crack geometry subjected to loading system 'A' (Fig. 1) the opening mode stress intensity factor is K_I^A, the associated crack length is a, and the vertical displacement of the crack surface is v. We may define a weight function $m(x, a)$ as

$$m(x,a) = \frac{H}{2K_I^A} \cdot \frac{\partial v(x,a)}{\partial a} \tag{1}$$

where

$$H = \begin{cases} E \text{ (plane stress)} \\ \dfrac{E}{1-\nu^2} \text{ (plane strain)} \end{cases}$$

where E is the modulus of elasticity and ν is Poisson's ratio.

It may be demonstrated [*1, 2*] that this weight function is unique to the given geometry, and is independent of the loading from which it was derived.[2] The stress intensity factor K_I^B for the same geometry subjected to a crack-line loading system 'B' may be obtained from

$$K_I^B = \int_a p(x)m(x,a)\,dx \tag{2}$$

where $p(x)$ is the crack-line pressure loading for system 'B'.

Some remarks are in order:

1. The weight function is more general than is indicated by Eqs 1 and 2. Firstly, the weight function is applicable to boundaries other than the crack line,

[2] The italic numbers in brackets refer to the list of references appended to this paper.

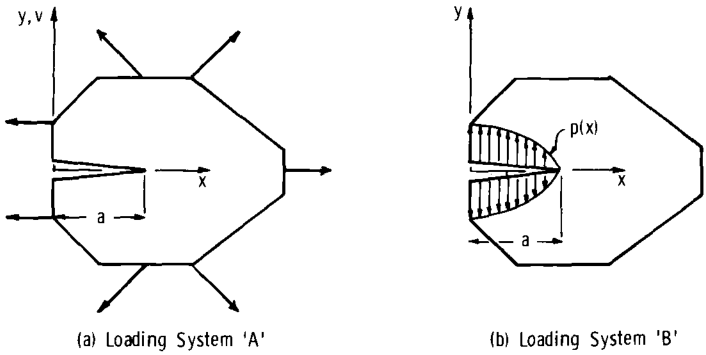

FIG. 1—*Loading system used in weight function description.*

and hence may be used to calculate K_I as a result of loading on other boundaries. Secondly, an additional term may be included in Eq 2 to include the effects of body force loading. Thirdly, there is an associated weight function, $m^*(x, a)$, which may be employed in the derivation of new K-solutions resulting from displacement boundary conditions [3].

2. Loading system 'A' must not possess more symmetries than loading system 'B'. Thus, if the weight function is derived from a loading system having biaxial symmetry, it may only be used to obtain stress intensity factors for biaxially symmetric systems.

3. It is particularly important to ensure that the correct stress and/or displacement boundary conditions are imposed on all boundaries, and that systems 'A' and 'B' are compatible in the respect [4, 5].

4. A little used property, noted by Rice [2], is that once Eq 2 is solved to obtain K_I^B it is then possible to reconstruct the displacement field by substitution into Eq 1 and subsequent integration to obtain

$$\mathrm{v}(x, a) = \frac{2}{H} \int K_I^B(a) \cdot m(x, a)\, da \tag{3}$$

where the constant of integration is obtained from the condition $\mathrm{v} = 0$ at $x = a$.

5. Although little used to date, the weight function approach appears equally applicable to Mode II stress intensity calculations.

6. Weight functions are applicable to three-dimensional configurations [2] and have been derived for three-dimensional axisymmetric configurations [6].

7. Weight functions may be derived from experimental data [7] and from stress intensity variation alone [8].

Superposition

Given that the stress intensity factors are derived from a linear elastic analysis, the superposition principle will apply. This states that the stress system due to two or more loads acting together is equal to the sum of the stresses due to each load acting separately. The superposition applied to an uncracked body is illustrated in Fig. 2. The residual stress field is simply added to that due to the boundary loading in order to determine the total field; provided that the body behaves in a linearly elastic fashion during the addition of boundary tractions to the residual stress field the superposition is valid. This is the technique employed in the prediction of stress fields in overstrained, thick cylinders [*9*].

If a crack is now introduced into the body (Fig. 3), there will be a general redistribution of stress, and the stress intensity factor may be calculated using the superposition illustrated in Fig. 3. Note that redistribution arising from the presence of the crack does *not* imply that the superposition principle is invalidated, as has been either explicitly or implicitly assumed by some workers [*10,11*]. It is not necessary to employ special methods to determine K in cracked bodies containing residual stresses.

Stress Intensity Factors for Cracks in Residual Stress Fields

There is a limited number of stress intensity factor solutions for cracks in residual stress fields. The important feature to note with respect to bodies contain-

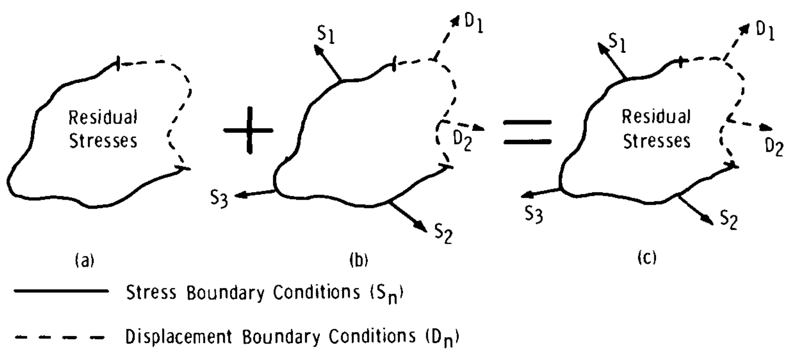

FIG. 2—*Superposition of stress fields in uncracked body.*

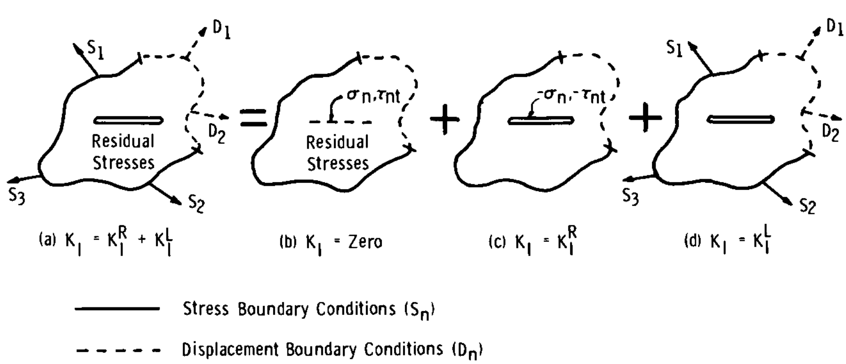

FIG. 3—*Superposition of stress fields to obtain stress intensity factor solutions.*

ing residual stress fields is that the residual stresses at any complete section produce self-equilibrating forces and moments. The cracked, autofrettaged cylinder of Fig. 4 has the residual stress field illustrated. When it is cracked into two or more pieces, as illustrated in Fig. 4*b*, there is no tendency of the separate segments to spring apart or to approach one another; hence the stress intensity tends to zero at long crack lengths. This effect is demonstrated clearly in the results shown in Fig. 4*c*, which indicate the variation of stress intensity with crack length in such a cylinder for a variety of wall thicknesses. (These results were obtained using the Modified Mapping Collocation Technique described in Refs *12* and *13*).

A residual stress field more typical of a welded component is shown in Fig. 5. This field varies parabolically across the width of the specimen. In the event that

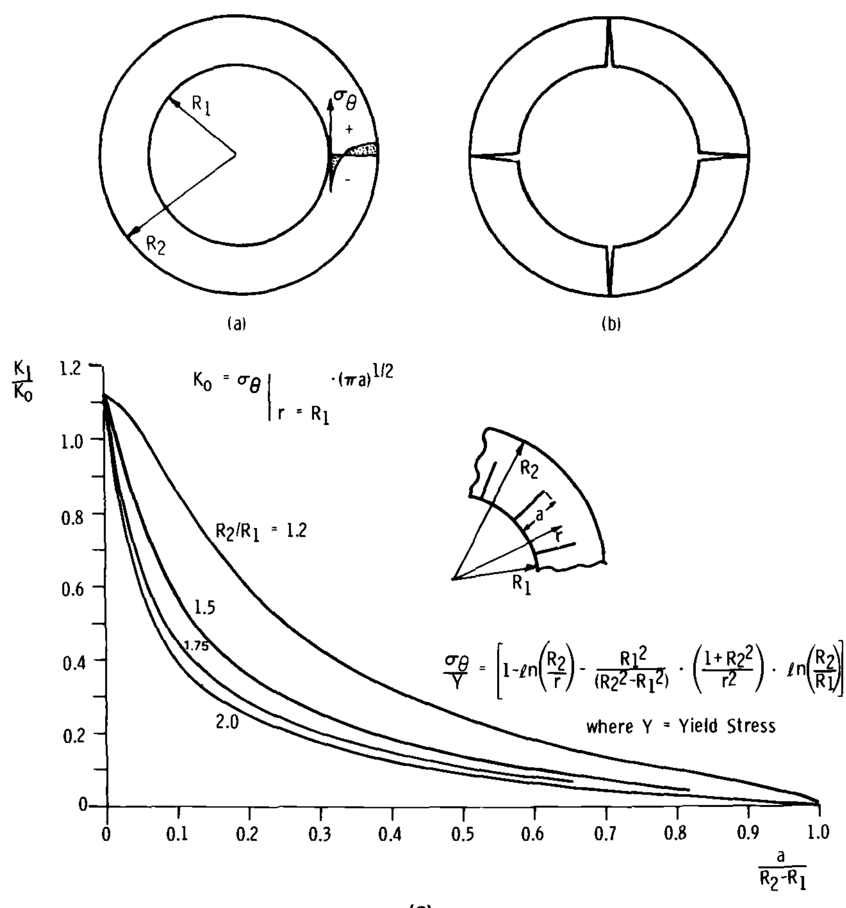

FIG. 4—(a) *Variation of hoop* σ_θ *residual stress in fully autofrettaged thick cylinder, after Ref.* 9. (b) *Autofrettaged tube cracked into separate segments.* (c) *Stress intensity factors for fully autofrettaged tube with 50 equal length radial cracks emanating from the bore.*

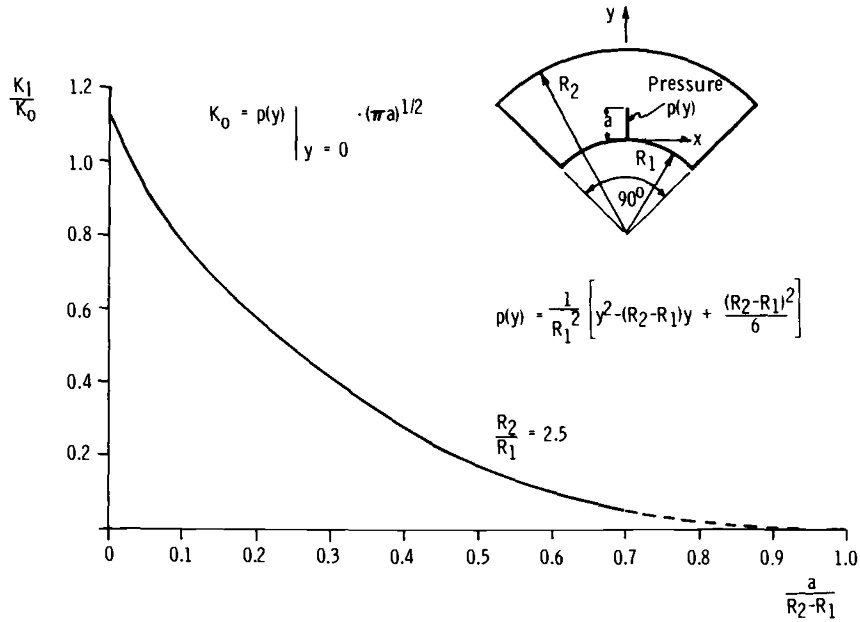

FIG. 5—*Residual stress intensity factors—edge cracked ring segment (determined by use of weight function, see Ref 12).*

the stresses are tensile at the edges, the stress intensity factors for an edge crack are positive and remain positive at all crack lengths, tending to zero as the crack length approaches the specimen width. (These results were obtained from the numerically determined weight function detailed in Ref *12*).

Consider the case of an internal crack introduced into a residual tensile field. Figure 6 illustrates the case of an array of such cracks of length $2a$, with spacing between centers of $2b$. The residual stress is equivalent to pressure $p(x)$. (Solving this problem by utilizing weight function methods is presented in the Appendix.) In the case $p(x) = \mathrm{p}\cos 2(\pi x/2b)$ the stress intensity is always positive; in the case $p(x) = \mathrm{p}\cos 4(\pi x/2b)$ the stress intensity changes sign as the crack extends. In all cases, the variation in stress intensity is smooth and tends to zero at long crack lengths. This effect appears to be characteristic of bodies with residual stress fields, provided the propagation of the crack through the specimen produces separate pieces. However, if this condition is not satisfied, K may not tend smoothly to zero as the crack extends. This includes the case of fixed displacement boundary conditions, which is equivalent to a connectivity with infinite elastic modulus. Consider, for example, a double box section containing residual stresses caused by welding together edges *AB* and *CD* in Fig. 7*a* to create the configuration shown in Fig. 7b. At failure the surfaces spring apart, implying high positive K_I^R values at very long crack lengths.

It appears to be incorrect to infer some sudden change in stress intensity and hence crack behavior as the crack propagates through the point at which the

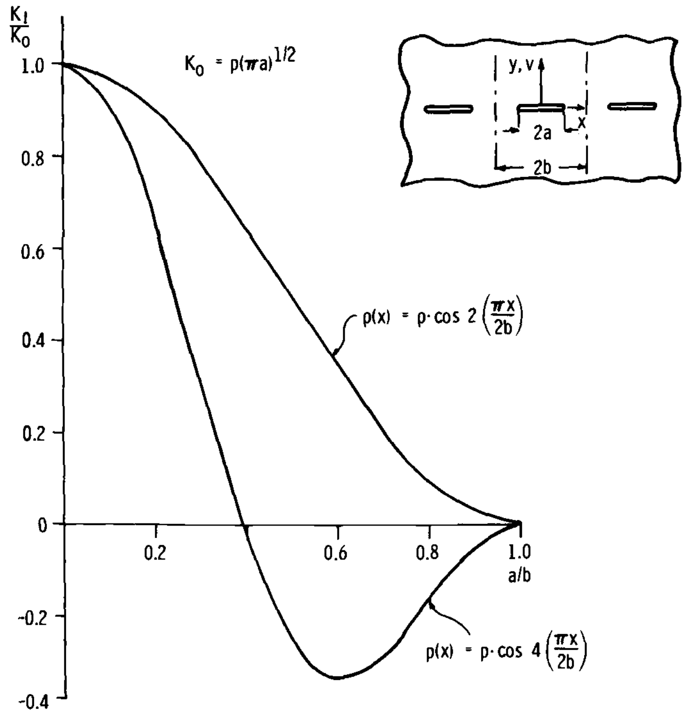

FIG. 6—*Stress intensity factors for an array of cracks in a periodic residual stress field.*

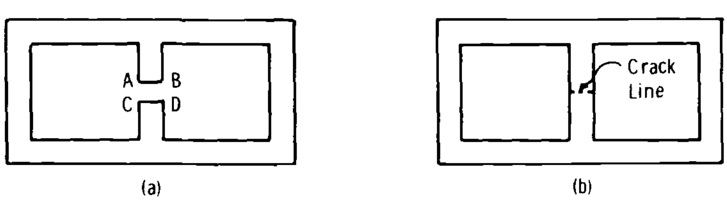

FIG. 7—*Example of residual stresses in double box section.* (a) *Before welding.* (b) *After welding.*

unflawed crack line loading changes sign. Nevertheless, this effect is inferred by several workers [*10*,*11*,*14*]. Furthermore, since stress distribution within a body is continuous, and the stress intensity is the result of integrating these stress fields along a particular path, this type of nonsmooth modeling of stress fields in order to determine K may produce physically unacceptable results and sudden changes in crack growth rate predictions, as in Ref *14*.

Overlapping Effects

One situation in which a slavish superposition of stress intensity contributions from residual and boundary loading may produce a physically unacceptable answer is that in which the problem includes a nonlinear contact condition. Bowie and Freese [15] have observed that it is possible to predict positive values of stress intensity, despite the fact that the crack surfaces are mathematically 'overlapped' at some distance from the crack tip (Fig. 8). An iterative technique is then required to correct for this effect and to prevent overlapping. The necessary crack-line loading required to eliminate the overlapping will be a varying pressure applied to the faces, which will tend to increase the stress intensity.

Whilst the overlapping effect in Ref 15 was produced by means of a combination of tension and bending, it is clear that this could be induced by a residual stress field, with or without other loading. For instance, in the example of the array of cracks, it is possible to reconstruct the crack shape by employing the appropriate weight function and stress intensity in Eq 3. With the loading $p(x) = -p \cos 4(\pi x/2b)$ the variation of K is equal and opposite to Fig. 6. The crack shape in this case is calculated in the Appendix, and is illustrated in Fig. 9 for crack lengths in the range of $0.3 \leq a/b \leq 1.0$. Note that for a large proportion of their length, the crack surfaces are mathematically 'overlapped' and the stress intensity solution would not be valid for this case.

At this point we observe that the introduction of a notch which permits 'overlapping' to occur will make the solution valid once again, provided the geometrical effects of the notch on K are minimal.

Fatigue Crack Growth in Residual Stress Fields

The prediction of life using Linear Elastic Fracture Mechanics and a crack growth law is well known [16]. It consists of defining the stress intensity range ΔK as

$$\Delta K = K_{max} - K_{min} \qquad K_{min} > 0 \tag{4}$$

$$\Delta K = K_{max} \qquad K_{min} \leq 0 \tag{5}$$

where K_{max} and K_{min} are the effective maximum and minimum stress intensity values respectively during a given loading cycle. Equation 5 implies that the part of the fatigue cycle during which the crack is closed at its tip (that is, $K \leq 0$) makes no contribution to crack growth. We shall assume that the above relationships are valid whenever material behavior is linearly elastic, even though contact conditions may be nonlinear. Whilst it is not considered further in this

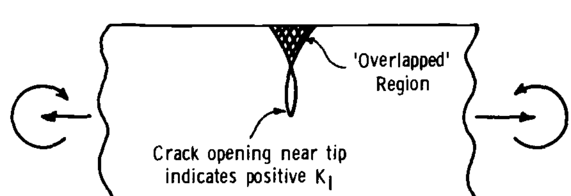

FIG. 8—*Physically unacceptable overlapping of crack surfaces due to combination of tension and bending.*

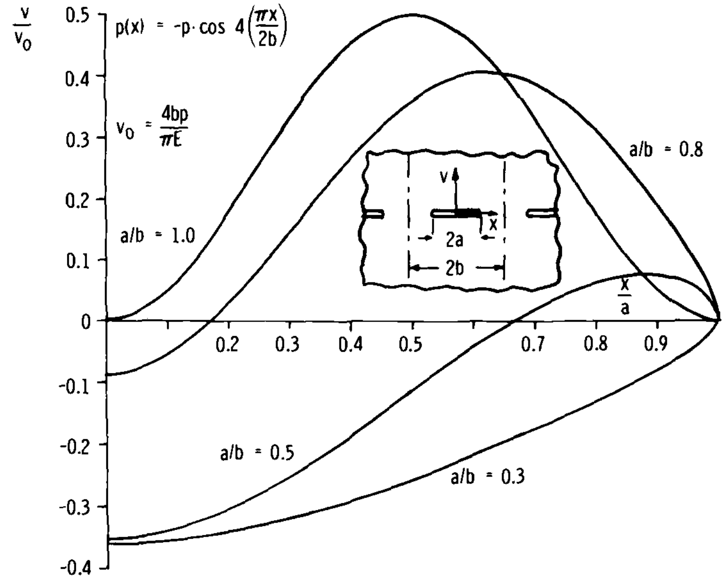

FIG. 9—*Crack profiles for an array of cracks in a residual stress field (plane stress).*

paper, the correction for nonlinear contact is straightforward, using an iterative weight function based scheme to achieve the required displacements.

For much of a component's lifetime, the fatigue crack growth rate is related to the stress intensity factor range by [*16*]

$$\frac{da}{dN} = C(\Delta K)^M \tag{6}$$

where N represents the number of cycles, and C and M are experimentally determined constants. In this paper, we deliberately avoid any modification to Eq 6 to account for the effect of R-ratio, where

$$R = K_{min}/K_{max} \qquad K_{min} > 0 \tag{7}$$

$$R = 0 \qquad K_{min} \leq 0 \tag{8}$$

Thus we anticipate a family of curves relating stress intensity range to crack growth rate (Fig. 10).

There does not appear to be any reason to assume that the superposition principle is violated by 'stress fading' during fatigue crack growth in residual stress fields at stress levels which only produce localized (crack tip) yielding. The original paper by Morrow [*17*] in which the "stress fading" concept is expounded contains details of experimental work on uncracked specimens without residual stresses, loaded cyclically to stress levels near to the yield stress of the material. The work was subsequently referenced by Forsyth [*18*] in a section entitled "Residual Stress and Cyclic Stress Fading", and finally became interpreted [*11*]

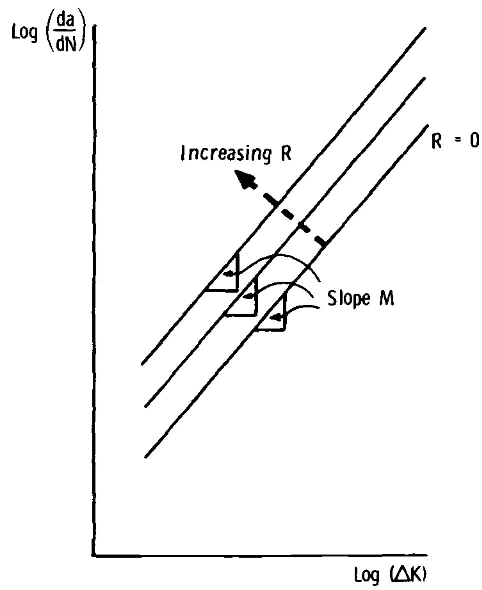

FIG. 10—*Portion of lifetime represented by Paris's law.*

as a validation of the fading of residual stress fields under cyclic loading. The latter interpretation does not appear to be justified by Morrow's original work.

Consider a plate containing a residual stress field. When a crack is introduced, it has a residual stress intensity K_I^R. The sheet is then subjected to a cyclic loading. The stress intensity contributions produced by this loading are $K_{I_{max}}^L$ and $K_{I_{min}}^L$, the maximum and minimum values of stress intensity produced by the remote loading.

In general we note that Eqs 4 and 5 give

$$\left.\begin{aligned} \Delta K &= K_{I_{max}}^L - K_{I_{min}}^L \\ R &= \frac{K_{I_{min}}^L + K_I^R}{K_{I_{max}}^L + K_I^R} \end{aligned}\right\} K_{I_{min}}^L + K_I^R > 0 \tag{9}$$

$$\left.\begin{aligned} \Delta K &= K_{I_{max}}^L + K_I^R \\ R &= 0 \end{aligned}\right\} K_{I_{min}}^L + K_I^R \leq 0 \tag{10}$$

We now consider the effects on crack growth rate of three types of loading on the basis of Eqs 9 and 10.

Configuration 1

Configuration 1 is an edge-cracked plate with a residual field producing compressive crack-line stresses at the edge. In this case K_I^R will be negative. If the component is subjected to cyclic tensile loading, the latter contribution to K_I will be positive. A composite schematic diagram (Fig. 11) illustrates the changes in

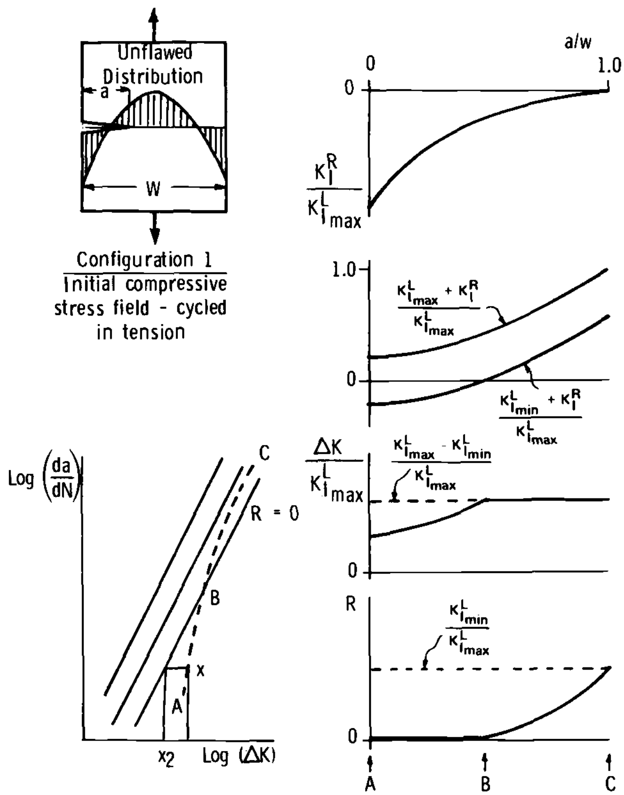

FIG. 11—*Schematic of Configuration 1 (compressive stress field, cycled in tension), stress intensity, stress intensity range,* R*-value, and crack growth rate.*

stress intensity, stress intensity range, and R-value at various crack lengths. At short crack lengths K_I^R has a large effect, reducing K_I below the value it would have in the absence of such residual stresses, and maintaining R at zero. As the effect of K_I^R diminishes at longer crack lengths, ΔK gradually increases until it reaches a fixed value $K_{I_{max}}^L - K_{I_{min}}^L$, at which point R increases above zero, reaching a maximum value of $K_{I_{min}}^L/K_{I_{max}}^L$.

In order to consider the influence of these effects on crack growth rate, we have reproduced the characteristic log (da/dN) versus log (ΔK) curves in Fig. 11. If the crack growth data obtained from the component with residual stresses are plotted by ignoring the contribution of K_I^R it will produce curves of the type shown as dotted lines in Fig. 11. Such results are reported for the case $K_{I_{min}}^L = 0$ in Ref *10*. Results of this form contain a great deal of information. Firstly, at any point X between A and B it is known that $R = 0$, and we may read off at X_2 the correct value of ΔK, and hence solve for K_I^R from Eq 10; namely

$$K_I^R = \Delta K - K_{I_{max}}^L \tag{11}$$

At any point between B and C the correct value of ΔK is being used, and we may interpolate to obtain an R-value. It is then possible to solve for K_I^R from Eq 9.

$$K_I^R = \frac{R K_{I_{max}}^L - K_{I_{min}}^L}{(1 - R)} \tag{12}$$

Thus we may define a complete curve of K_I^R versus (a/W). This information in turn is sufficient to reconstruct the residual stress field along the crack line *before* the appearance of the crack, either by an analytical technique similar to that proposed in Ref *19* or an iterative weight function based scheme.

As a special case of this configuration, we note that the introduction of a notch into the residual stress field may permit movement of the crack surfaces at minimum load (Fig. 12). Such an effect has been noted by several workers [*20,22*]. The significance of this crack deformation is that it indicates a *positive* stress intensity. Thus it is possible for a compressive residual stress field to produce a positive stress intensity when the crack surfaces touch one another at some point, whilst it will still produce a negative contribution when the crack surfaces are completely open. This will tend to reduce ΔK even further when a notch is present and hence reduce the crack growth rate. Such an effect on crack growth rate in notched specimens containing residual stresses is noted by Underwood et al [*10*].

The arguments put forward for this configuration apply equally to the case of an internal crack in a compressive residual stress field.

Configuration 2

Configuration 2 is a centrally located crack in a component having tensile stresses along the crack line at the center of the crack, and cycled in compression. Similar arguments to those enunciated for Configuration 1 apply in this case, but the effects are significantly different. Figure 13 illustrates the changes in stress intensity, stress intensity range, and R-value at various crack lengths for this configuration. At short crack lengths, the effect of K_I^R is to ensure that the crack experiences a stress intensity range given by $|K_{I_{max}}^L - K_{I_{min}}^L|$, and a nonzero R-value. At a given crack length $K_{I_{min}}^L + K_I^R$ reduces to zero, R becomes zero, and ΔK reduces as the crack propagates further until $K_{I_{max}}^L + K_I^R$ becomes zero, and arrest is certain at an easily determined crack length.

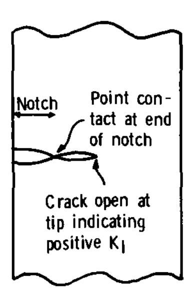

FIG. 12—*Possible effect of notch in residual compressive stress field.*

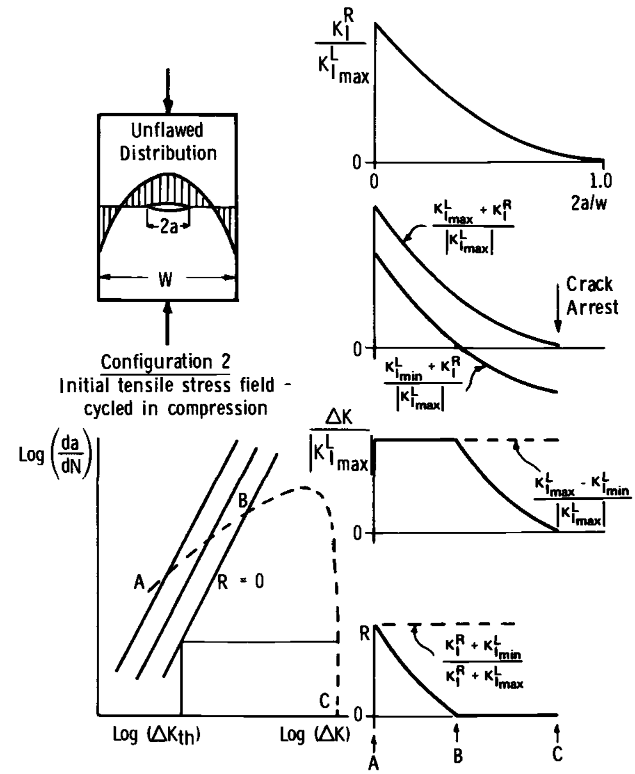

FIG. 13—*Schematic of Configuration 2 (tensile stress field, cycled in compression), stress intensity, stress intensity range,* R-*value, and crack growth rate.*

The expected plot of log (da/dN) versus log (ΔK) is illustrated in Fig. 13. The chronological order of events is ABC. The crack may actually be expected to arrest just prior to point C when ΔK falls to some threshold value ΔK_{th} [*23*] associated with $R = 0$. Following the same argument as that for Configuration 1, we may determine K_I^R in this case from

$$K_I^R = \frac{RK_{I_{max}}^L - K_{I_{min}}^L}{(1 - R)} \quad \text{between } A \text{ and } B \tag{13}$$

$$K_I^R = \Delta K - K_{I_{max}}^L \quad \text{between } B \text{ and } C \tag{14}$$

The type of behavior proposed in Fig. 13 has been observed in work performed at the Welding Institute [*24*] and in fatigue crack growth experiments in rings containing residual stress fields [*25*], although in the latter case the change in the 'active' K_I^L is a major contribution to the crack retardation.

Configuration 3

Configuration 3 is identical to Configuration 2, but cycled in tension. Applying similar arguments to those presented for the previous two configurations we

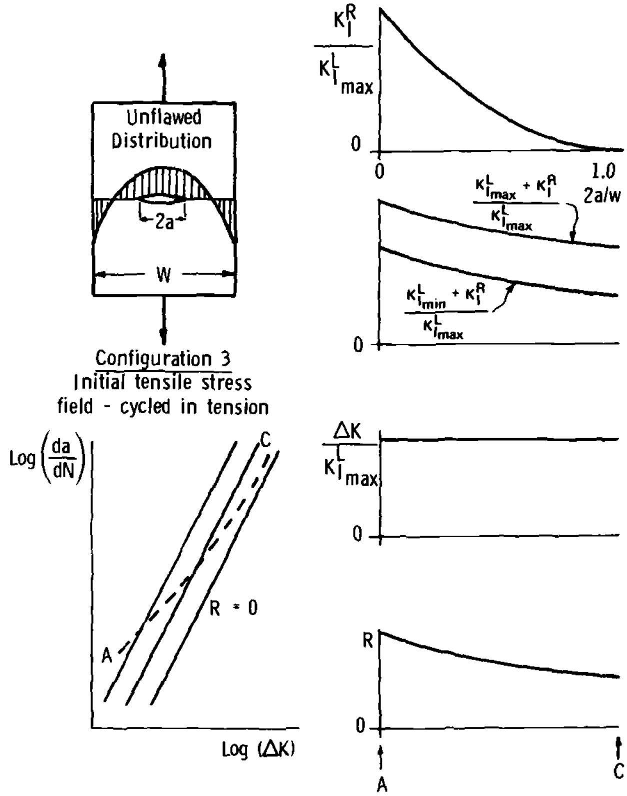

FIG. 14—*Schematic of Configuration 3 (tensile stress field, cycled in tension), stress intensity, stress intensity range,* R*-value, and crack growth rate.*

obtain the predictions illustrated schematically in Fig. 14. This figure shows the variation in stress intensity, stress intensity range, and R-value for various crack lengths. The associated prediction for log (da/dN) versus log (ΔK) is also shown.

Implications for S-N Curves for Welded Components

In this section we deduce qualitatively the effects on the form of the standard S-N curve of the presence of residual stress fields in welds. (S is the range of remotely applied stress, and N is the number of cycles to failure.)

Maddox [26] has demonstrated that in the case of a welded component (that is, a structure with pre-existing crack-like defects) without residual stresses, in which a large proportion of lifetime is expended in the straight-line portion of the log (da/dN) versus log (ΔK) curve, the slope of the S-N curve is the negative reciprocal of the crack growth curve (that is, the initial slope of the S-N curve is $-(1/M)$, where M is the exponent in Eq. 6 (see Fig. 15a). A variation in R-value thus has the predominant effect of altering the intercept but not the slope of the initial portion of the S-N curve.

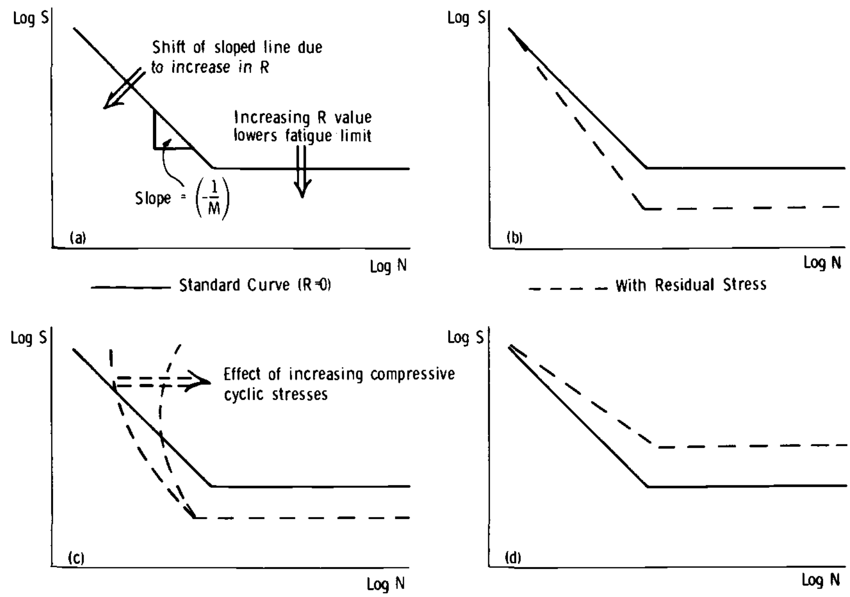

FIG. 15 — S-N *curves (schematic).* (a) *General form and effect of changing* R. (b) *Tensile residual stresses with remote tensile loading.* (c) *Tensile residual stresses with remote compressive loading.* (d) *Compressive residual stresses with remote tensile loading.*

Pook [*23*] has shown that the threshold value of the stress intensity range, ΔK_{th}, is reduced as a result of increasing R-ratio. The equivalent effect on the S-N curve is a reduction in the fatigue limit, below which load cycles have no effect on component lifetime.

Assuming that the critical defects in welds will normally be in regions of positive K_I^R, consider the two cases of defects in residual tensile fields, namely Configurations 2 and 3. The variation of R for the case of tensile loading (that is, positive K_I^L) is shown in Fig. 14. The effect is generally to reduce the apparent slope of the crack growth curve and hence to increase the slope of the S-N curve. At high applied stress levels the values of the observed and expected slopes will tend asymptotically towards one another on the crack growth plot, from which we infer that the equivalent S-N curves will also approach asymptotically at high S-values. The predicted effect is shown in the S-N plot in Fig. 15*b*. Furthermore, since the R-value is effectively higher than expected, the fatigue limit will be reduced in line with Pook's observations [*23*]. Results closely resembling this proposed behavior have been reported for fatigue tests on longitudinal non-load-carrying fillets subjected to tensile loading (see Fig. 4 of Ref *24* and Fig. 2 of Ref *27*).

In the case of compressive loading, we refer to Fig. 13. Between A and B the R-value is higher than predicted, and the slope of the growth curve is less steep, producing a steeper slope in the equivalent S-N diagram. In this case, however, a loading in the region B-C will produce crack closure during part of the load application, effectively reducing ΔK and S and producing a significant nonlinearity in the S-N curve (Fig. 15*c*). Once again, at low stress levels R is higher than anticipated, and the fatigue limit is therefore lowered. Results presented in Fig. 5 of Ref *24* for fatigue tests on transverse non-load-carrying fillets tested under predominantly compressive loading show them to exhibit a similar behavior to that proposed in Fig. 15*c*. Furthermore, in the event that higher compressive cyclic stresses are applied during the fatigue loading, a large proportion of component lifetime may be in the near horizontal region of the da/dN curve. This in turn will produce a vertical line on the S-N plot, or even one which leans to the right in an unexpected fashion. Such behavior is reported in Ref *28*, page 243. Whilst crack arrest is likely at high compressive stress levels in our idealized, single crack model, the effects of multiple, interacting cracks may produce complete failure.

It is, of course, possible to produce compressive residual stresses in a previously identified critical region of a weld. For tensile cyclic loading applied to a compressive residual stress field we refer to Fig. 10. The apparent curve is effectively steeper than anticipated; thus the equivalent S-N curve slope will be shallower, the R-value is also lower, and the fatigue limit will be raised (see Fig. 15*d*). Notice also that at high cyclic stress levels the S-N curves approach asymptotically. Results of this form are reported in Ref *29*, wherein the compressive stresses were induced either by spot-heating or localized compressive treatment.

Discussion and Conclusions

The weight function is a flexible tool for the rapid, accurate determination of crack-tip stress intensity factors and associated crack profiles in the presence of residual stress fields. Use of the weight function permits the prediction of crack surface 'overlapping' effects which will give rise to nonlinear contact conditions. Although not addressed in this paper, the weight function may also be used in an iterative process to correct for 'overlapping' effects.

The information required to determine numerical weight function data is the stress intensity factor and the associated variation in crack shape with incremental crack extension. The additional computing effort involved in deriving the weight function once a stress intensity has been obtained is minimal when contrasted with the flexibility of the weight function, particularly for problems involving cracks in residual stress fields. Weight functions should always be obtained during a numerical stress intensity solution, and there may be advantages to a standardized 'packaging' of such weight function data for subsequent use by designers. A cubic spline fit, for use with a standard spline program package, would appear to be an obvious choice for fitting such data.

The redistribution of stress arising from the presence of a crack does not imply that the superposition principle is violated, provided that the overall behavior is effectively linearly elastic. For a variety of different geometrical and loading situations the variation of stress intensity with crack length is smooth, and there is no sudden change in stress intensity when the crack tip reaches the point at which the unflawed crack-line loading changes sign. Notches may alter or eliminate the nonlinearity of a system in which crack surfaces would otherwise 'overlap'.

The characteristic crack growth rate features of several loading systems appear to agree with available experimental data, provided the R-values are corrected for residual stress effects. In similar vein the qualitative changes in the form of standard S-N curves for welded details as predicted using a fracture mechanics approach conform with available S-N curve experimental data.

It appears to be possible to infer S-N behavior in the presence of residual stress fields from a proper fracture mechanics and crack growth rate analysis. However, it would not generally be possible to predict the effects of a change in the residual stress field from S-N data alone or the effects of altering the R-value. Since no additional information is available from S-N curves, and a large predictive capability is lost, it appears reasonable to ask whether the S-N presentation has any significant contribution to make in the life prediction of welded components with residual stresses.

Acknowledgments

This work was performed during the author's attachment to the U. S. Army Materials and Mechanics Research Center, Watertown, Massachusetts, under the aegis of the Tri-Partite Technical Cooperation Program. The author wishes to thank Mr. O. L. Bowie of AMMRC for several useful discussions during the course of the work.

APPENDIX

Stress Intensity and Crack Profiles for an Array of Cracks

The weight function $m(x, a)$ for a crack of length a in an array of colinear, equal length cracks with distance between crack centers of b is given in Ref *30* as

$$m(x,a) = \left(2b \tan \frac{\pi a}{2b}\right)^{1/2} \frac{1}{2b} \left[\frac{\cos \dfrac{\pi x}{2b}}{\left(\sin^2 \dfrac{\pi a}{2b} - \sin^2 \dfrac{\pi x}{2b}\right)^{1/2}} \right] \tag{15}$$

where x is the distance from the crack center (Fig. 6).

Any stress intensity factor $K_{\mathrm{I}}^{\mathrm{B}}$ for an appropriate loading system B may be obtained from Eq 1; that is,

$$K_{\mathrm{I}}^{\mathrm{B}} = \int_{-a}^{a} p(x) m(x,a)\, dx \tag{16}$$

where $p(x)$ is the crack-line pressure loading which is equal and opposite to the crack-line loading in the unflawed structure subjected to residual stresses and/or remote loading. Consider first the pressure distribution

$$p(x) = p \cos 2\left(\frac{\pi x}{2b}\right) \tag{17}$$

Substituting into Eq 16 from Eqs 15 and 17 we obtain

$$K_{\mathrm{I}}^{\mathrm{B}} = p\left(2b \tan \frac{\pi a}{2b}\right)^{1/2} \cos^2\left(\frac{\pi a}{2b}\right) \tag{18}$$

which is illustrated graphically in Fig. 6.

Now consider the case

$$p(x) = p \cos 4\left(\frac{\pi x}{2b}\right) \tag{19}$$

Substituting into Eq 16 from Eqs 15 and 19 we obtain

$$K_{\mathrm{I}}^{\mathrm{B}} = p\left(2b \tan \frac{\pi a}{2b}\right)^{1/2} \left[3 \cos^4 \frac{\pi a}{2b} - 2 \cos^2 \frac{\pi a}{2b}\right] \tag{20}$$

which is also shown in Fig. 6.

To obtain the crack shape we employ Eq 3; that is,

$$\mathrm{v}(x, a) = \frac{2}{H} \int K_{\mathrm{I}}^{\mathrm{B}}(a) m(x, a)\, da \tag{21}$$

where the constant of integration is obtained from the condition $\mathrm{v} = 0$ at $x = a$.

For the case $p(x) = p \cos 2(\pi x/2b)$, we substitute from Eqs 15 and 18 into Eq 21 to obtain

$$\mathrm{v} = \frac{4bp}{\pi H} \cos\left(\frac{\pi x}{2b}\right)\left[\sin^2\left(\frac{\pi a}{2b}\right) - \sin^2\left(\frac{\pi x}{2b}\right)\right]^{1/2} \tag{22}$$

whilst for $p(x) = p \cos 4(\pi x/2b)$ we substitute from Eqs 15 and 20 into Eq 21 to obtain

$$\mathrm{v} = \frac{4bp}{\pi H} \cos\left(\frac{\pi x}{2b}\right) \sin\left(\frac{\pi x}{2b}\right)\left[z - 3 \sin^2\left(\frac{\pi x}{2b}\right)\frac{z^3}{3} + z\right] \tag{23}$$

where

$$z = \left[\left(\frac{\sin\left(\frac{\pi a}{2b}\right)}{\cos\left(\frac{\pi x}{2b}\right)}\right)^2 - 1\right]^{1/2} \tag{24}$$

Crack profiles based on Eq 23 and 24 are presented in Fig. 9 for the case of plane stress, $H = E$.

References

[1] Bueckner, H. F., *Zeitschrift für Angewandte Mathematik und Mechanik*, Vol. 50, 1970, pp. 529-546.

[2] Rice, J. R., *International Journal of Solids and Structures*, Vol. 8, 1972, pp. 751-758.

[3] Parker, A. P. and Bowie, O. L., "The Weight Function for Various Boundary Condition Problems," 27th Conference of Army Mathematicians, West Point, N. Y., 1981.

[4] Cartwright, D. J., "Stress Intensity Factor Determination," in *Developments in Fracture Mechanics*, G. G. Chell, Ed., Applied Science Publishers Ltd., London, 1980.

[5] Chell, G. G. and Ewing D. J. F., *International Journal of Fracture*, Vol. 13, No. 4, 1977, pp. 467-479.

[6] Labbens, R., Heliot, J., and Pellissier-Tanon, A. in *Cracks and Fracture, ASTM STP 601*, American Society for Testing and Materials, 1976, pp. 341-364.

[7] Bar-Tikva, D., "An Experimental Method for Stress Intensity Factor Calibration," Technical Report AFWAL-TR-80-4001, Air Force Wright Aeronautical Laboratories, Wright-Patterson AFB, Ohio, 1980.

[8] Petroski, H. J. and Achenbach, J. D., *Engineering Fracture Mechanics*, Vol. 10, 1978, pp. 320-336.

[9] Hill, R., *The Mathematical Theory of Plasticity*, Clarendon Press, Oxford, 1950.

[10] Underwood, J. H., Pook, L. P., and Sharples, J. K. in *Flaw Growth and Fracture, ASTM STP 631*, American Society for Testing and Materials, 1977, pp. 402-415.

[11] Kapadia, B. M. in *Fatigue Testing of Weldments, ASTM STP 648*, American Society for Testing and Materials, 1978, pp. 244-260.

[12] Parker, A. P. and Andrasic, C. P., "Weight Functions for Cracked, Curved Beams," in *Numerical Methods in Fracture Mechanic*, Proceedings of 2nd International Conference, Swansea, 1980, pp. 67-82.

[13] Parker, A. P. and Andrasic, C. P., "Stress Intensity Prediction for a Multiply-Cracked, Pressurized Gun Tube with Residual and Thermal Stresses," in *AMMRC MS 80-5*, Army Materials and Mechanics Research Center, Watertown, Mass., 1980, pp. 35-39.

[14] Glinka, G. in *Fracture Mechanics, ASTM STP 677*, American Society for Testing and Materials, 1979, pp. 198-214.

[15] Bowie, O. L. and Freese, C. E., *Engineering Fracture Mechanics*, Vol. 8, 1976, pp. 373-379.

[16] Paris, P. C. and Erdogan, F., *Journal of Basic Engineering, Transactions of ASME*, Vol. 85, 1963, pp. 528-534.

[17] Morrow, J. and Sinclair, G. M. in *Basic Mechanisms of Fatigue, ASTM STP 237*, American Society for Testing and Materials, 1958, pp. 83-109.

[18] Forsyth, P. J. E., *The Physical Basis of Metal Fatigue*, Elsevier, New York, 1969, p. 175.

[19] Vaidyanathan, S. and Finnie, I., *Journal of Basic Engineering, Transactions of ASME*, Vol. 93, 1971, pp. 242-246.

[20] Pitoniak, F. J., Grandt, A. F., Montulli, L. T., and Packman, P. F., *Engineering Fracture Mechanics*, Vol. 6, 1974, pp. 663-670.

[21] Ladelski, A., "A Study of Residual Stress Induced by Different Fatigue Crack Histories," M. Sc. thesis, Mechanical Engineering Department, Technion, Israel, 1975.

[22] Tirosh, J. and Ladelski, A., *Engineering Fracture Mechanics*, Vol. 13, 1980, pp. 453-461.

[23] Pook, L. P., "Fatigue Crack Growth Data for Various Materials Deduced from the Fatigue Lives of Precracked Plates," NEL Report 484, National Engineering Laboratory, East Kilbride, Scotland, 1971.

[24] Gurney, T. R., "Some Recent Work Relating to the Influence of Residual Stresses on Fatigue Strength," in *Proceedings*, International Conference on Residual Stress in Welded Construction and Their Effects, Vol. 1, The Welding Institute, Abington Hall, Cambridge, England, 1977, pp. 151-163.

[25] Kapp, J. A. and Eisenstadt, R. in *Fracture Mechanics, ASTM STP 677*, American Society for Testing and Materials, 1979, pp. 746-756.

[26] Maddox, S. J., "Fracture Mechanics Applied to Fatigue in Welded Structures," in *Welding Institute Conference on Fatigue of Welded Structures*, Brighton, England, 1970, pp. 73-96.

[27] Trufyakov, V. I., *British Welding Journal*, Vol. 5, 1958, pp. 491-498.

[28] Gurney, T. R., *Fatigue of Welded Structures*, 2nd ed., Cambridge University Press, 1979.

[29] Gurney, T. R., *British Welding Journal*, Vol. 7, 1960, pp. 415-431.

[30] Parker, A. P. and Mason, J. C., "Stress Intensity Factors for an Infinite Array of Colinear Cracks Subjected to Varying Pressure," in *Proceedings of the Institution of Civil Engineers*, Part 2, Vol. 71, 1981, pp. 543-549.

H. S. Reemsnyder[1]

Evaluating the Effect of Residual Stresses on Notched Fatigue Resistance

REFERENCE: Reemsnyder, H. S., **"Evaluating the Effect of Residual Stresses on Notched Fatigue Resistance,"** *Residual Stress Effects in Fatigue, ASTM STP 776,* American Society for Testing and Materials, 1982, p. 32.

ABSTRACT: Many current fatigue design criteria for structural details present allowable stress ranges for specified design lives but neglect mean and residual stresses. The paper reviews published test results and shows that residual stresses and concomitant mean stresses can have a significant influence on fatigue resistance in certain cases. The beneficial effects of compressive residual stresses due to shot-peening are well-known. For example, shot-peening of non-load-carrying fillet-welded carbon steel and butt-welded constructional alloy steel has increased the fatigue strengths at two million cycles by 20 to 40 percent. Also, the fatigue resistance of weldments can be influenced significantly by the presence of residual stresses, provided the stress ratio is equal to or less than zero and the lives are greater than one million cycles. The fatigue strength of transverse butt welds with reinforcement intact at two million cycles has been increased by 12 percent and 24 to 33 percent for stress ratios of, respectively, 0 and −1 through thermal stress relief. Such improvement has also been shown for longitudinal non-load-carrying fillet welds (for example, attachments, gussets, etc.) where the increases in fatigue strength at two million cycles due to thermal stress relief for stress ratios of 0, −1, and −4 were, respectively, 15, 57, and 168 percent.

The paper presents an extension of the local-strain fatigue life initiation model to accommodate residual and mean stresses. The model is based upon the stress-strain function of Smith, Watson, and Topper and includes iterative solutions for K_σ and $2N_f$. Changes in residual stresses due to cyclic loading and fatigue lives of notches at nonzero mean stresses are predicted and compared with experimental results. Also, further extensions of the model to accommodate plane strain — that is, thickness effects — and surface roughness are discussed.

KEY WORDS: fatigue tests, fatigue of metals, residual stress, stress concentrations, crack initiation, weldments, stress relief, shot peening, local strain

This paper has been previously published in *Materials, Experimentation, and Design in Fatigue — Proceedings of Fatigue '81*, Westbury Press, Guildford, England, 1981, pp. 273-295; distributed in the United States by Ann Arbor Science Publishers, Woburn, Massachusetts.

[1]Principal Scientist, Product Research, Research Department, Bethlehem Steel Corporation, Bethlehem, Pa. 18016.

F. V. Lawrence, Jr.,[1] *J. D. Burk,*[2] *and J-Y Yung*[3]

Influence of Residual Stress on the Predicted Fatigue Life of Weldments

REFERENCE: Lawrence, F. V., Jr., Burk, J. D., and Yung, J-Y, **"Influence of Residual Stress on the Predicted Fatigue Life of Weldments,"** *Residual Stress Effects in Fatigue, ASTM STP 776,* American Society for Testing and Materials, 1982, pp. 33-43.

ABSTRACT: A model was developed that predicts the influence of residual stress and stress ratio on the total fatigue life of a weld. The total fatigue life of a weld was considered to be composed of both crack initiation and crack propagation. Weld toe residual stresses were considered to influence the crack initiation life but not the crack propagation life.

The crack initiation life was estimated using cumulative damage concepts. Actual weld material properties (weld metal and heat-affected zone) were considered in the initiation life estimation. Neuber's rule was used to determine the local cyclic stress-strain behavior at the weld toe, and the fatigue notch factor was evaluated by using Peterson's equation. Residual stresses were introduced into the analysis as a simulated pre-stressing of the weld. Cyclic relaxation of the mean stress established during the set-up cycle was modeled by a power function and allowed relaxation to be considered in the life estimates.

Fatigue tests of steel weldments and aluminum butt welds having tensile and compressive residual stresses were conducted to verify the analytically predicted total fatigue life predictions. Agreement between analytical predictions and experimental results was quite good.

KEY WORDS: fatigue, fatigue life prediction, welds, fatigue of welds, residual stress

Predicting the Fatigue Resistance of Welds

In order to provide a means of interrelating the parameters which influence the fatigue life of welds, and to permit the accurate prediction of weldment fatigue resistance, an analytical model for estimating the total fatigue life of welds has been developed [*1*].[4] This model assumes that the total fatigue life of a weldment (N_T) is composed of a fatigue crack initiation period (N_I) and a fatigue crack propagation period (N_P); that is,

$$N_T = N_I + N_P \tag{1}$$

The initiation portion of life (N_I) is estimated using strain-control fatigue data and is considered to consist of the number of cycles for the initiation of a fatigue crack(s) and its (their) early growth and coalescence into a dominant fatigue crack

[1] Professor of Civil Engineering and Metallurgy, University of Illinois at Urbana-Champaign.

[2] Research Engineer, Shell Development Company, Houston, Tex.

[3] Research Assistant, Department of Metallurgy and Mining Engineering, University of Illinois at Urbana-Champaign.

[4] The italic numbers in brackets refer to the list of references appended to this paper.

which obeys the Paris power law. Using this definition, N_I constitutes a large fraction of the total fatigue life, particularly at lives greater than 10^6 cycles. The fatigue crack propagation portion of life (N_P) is estimated using (long-crack) fatigue crack propagation data assuming the "appropriate" value of the initiated crack length (a_I).

This model is quite general and can be applied to sound welds or to welds containing internal defects [2]. Naturally, in the case of welds containing crack-life defects, N_I may be very short; however, for rounded internal defects such as slag or porosity, N_I may be appreciable, and neglecting it may be excessively conservative. In some applications, lack of knowledge of the defect population of a welded structure may force one to assume the existence of an active fatigue crack immediately after fabrication and, thus, the total absence of any life devoted to fatigue crack initiation. Conversely, for welds such as production welds in machine elements, it is unlikely that serious weld defects are always present; thus a major fraction of their fatigue life may be devoted to fatigue crack initiation. It is for this latter case, particularly, that the model has been developed.

In its present state of development, the model is useful for predicting the fatigue resistance of weldments under constant-amplitude loadings and, as will be discussed here, provides a systematic means for estimating the effect of variables such as residual stress on weldment fatigue life.

Predicting the Fatigue Crack Initiation Life

For initiation lives of 10^5 or greater, cyclic hardening and softening effects can usually be ignored, and generally elastic conditions may be assumed. For such cases, N_I can be estimated using the Basqin relationship

$$\sigma_a = (\sigma_f' - \sigma_o)\,[2N_I]^b \tag{2}$$

where

σ_a = stress amplitude,
σ_f' = fatigue strength coefficient,
σ_o = mean stress,
$2N_I$ = reversals to fatigue crack initiation, and
b = fatigue strength exponent (approximately -0.1 for mild steel).

The notch-root stress amplitude, the stress at the critical region in the weld (weld toe or internal defect), can be taken as $(\Delta S/2)\,K_f$ so that Eq 2 becomes

$$\frac{\Delta S}{2} K_f = (\sigma_f' - \sigma_o)\,[2N_I]^b \tag{3}$$

where

ΔS = remote stress, and
K_f = fatigue notch factor.

A difficulty in proceeding with the life estimation calculation suggested by Eq 3 is determining the appropriate value of K_f for the weld toe or for the weld defect. This difficulty arises from the fact that the notch-root radius of a discontinuity such as the weld toe is unknown and is variable. Microscopic examination of weld toes reveals that practically any value of radius can be observed; thus notches such as weld toes must be considered to have all possible values of notch-root radius. This difficulty has lead to the idea of a maximum value of K_f for a given weld shape K_{fmax} [1].

Predicting the Total Fatigue Life (N_T)

The total fatigue life (N_T) is considered to be the sum of the crack initiation life (N_I) and the fatigue crack propagation life (N_P) (Eq 1). When initiation occurs at a defect such as a pore, slag pocket, or deep notch, the size of the initiated crack length (a_I) may be taken as the dimension of the defect. Thus the fatigue crack propagation life (N_P) may be calculated directly by taking the defect size as a_I, and may be added to the estimate of N_I using Eq 3 (naturally, in the case of serious defects, N_I may be rather short) to obtain N_T. The proper value of a_I is unclear for weld discontinuities such as weld toes, which are serious defects but not deep notches. It has been past practice in these cases to assume arbitrarily that a_I was 0.254 mm (0.01-in.), regardless of the stress level or the material [1]. Recent work by Chen and Lawrence [3] has provided an alternative strategy for the definition of a_I. For fatigue failure to occur, an a_I just greater than the length of a nonpropagating crack (a_{th}) must be provided by the process of fatigue crack initiation. Thus, at long lives, a_I is assumed to be a little larger than a_{th}.

Predicting the Influence of Weld Residual Stresses on N_I

If the mean stress relaxes during cycling, the current value of mean stress (σ_o) may be estimated by [4]

$$\sigma_o/\sigma_{os} = (2N_I - 1)^k \tag{4}$$

where

σ_o = current value of mean stress (notch root),
σ_{os} = initial value of mean stress (notch root),
$2N_I$ = elapsed reversals, and
k = relaxation exponent (a function of strain amplitude; see Fig. 1.)

Assuming that the notch root strains are essentially elastic ($2N_I > 2N_{tr}$), the damage per cycle is

$$(1/2N_I) = [(\sigma_f'/\sigma_a)(1 - \sigma_o/\sigma_f')]^{1/b} \tag{5}$$

Using the Palmgren-Miner rule of cumulative damage and Eqs 4 and 5, the fatigue crack initiation life under conditions of relaxing mean stress can be calculated by integrating Eq 6 (below) and solving for the upper limit of integration using approximate methods [5].

$$\int_1^{2N_I} [(\sigma_f'/\sigma_a)(1 - \sigma_{os}(2N_I)^k/\sigma_f')]^{1/b}\, d(2N_I) = 1 \tag{6}$$

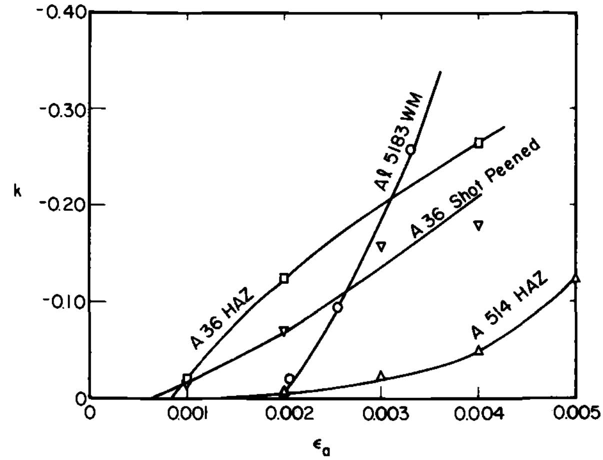

FIG. 1—*Relaxation exponent* (k) *as a function of the strain amplitude for A36 HAZ, A514 HAZ, and 5083-0 weld materials.*

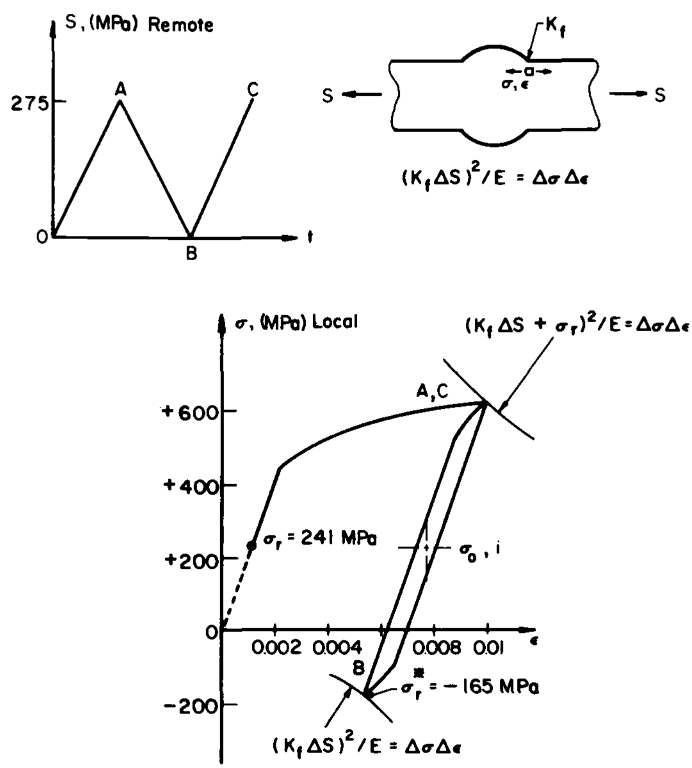

FIG. 2—*Simulated local stress-strain response at the weld toe for a butt weldment with weld-toe residual stresses* (σ_r). *A36-HAZ material;* σ_r = *241 MPa (35 ksi). The initial residual stress of 241 MPa (35 ksi) becomes −165 MPa (−24 ksi) after two reversals (one cycle, OAB).*

Equation 6 affords a means of predicting the potential effects of weld toe residual stresses (σ_r) on the fatigue crack initiation life N_I. It is assumed that σ_r approaches the yield point of the base metal (S_y) in the small volume at the weld toe in which initiation takes place (Fig. 2). This residual stress and any remotely imposed mean stress may relax with cycling (Eq 4) (Fig. 5). The notch root residual stresses have been ignored in the calculation of N_P, but the remote mean stress effects are considered to persist and to influence the propagation portion of life through the reported variation of crack opening factor as a function of stress ratio (R) [*6*].

The residual stress (σ_r) is assumed to be either $+S_y$, 0, or $-S_y$. These three cases bound most possibilities. The worst case, $\sigma_r = S_y$, is often approached in practice. The intermediate case, $\sigma_r = 0$, could result from stress relief. The most favorable case, $\sigma_r = -S_y$, could be realized through some mechanical pretreatment such as shot-peening or over-stressing.

As shown in Fig. 3, the initial value of notch root mean stress (σ_{os}) resulting from the residual stress (σ_r) may vary greatly depending upon the material. For many aluminums, the heat-affected zone (HAZ) at the weld toe is in the annealed state; consequently, the notch-root plasticity in the first cycle results in $\sigma_{os} = 0$. Other materials, such as high-strength steels, exhibit very little notch-root plasticity; consequently, σ_{os} may be larger than σ_r. The results obtained using the model agree with the experimentally observed behavior [*5*]. Figure 4 shows the qualitative behavior of N_I predictions based on Eq 6.

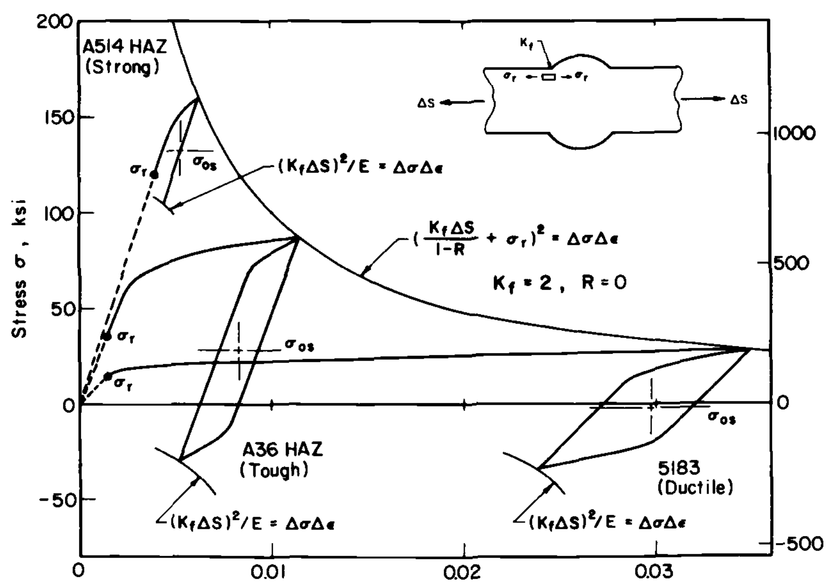

FIG. 3—*The initial value of mean stress* (σ_{os}) *resulting from three different extremes of material behavior. Results shown are for a single arbitrary value of* $\Delta\sigma\ \Delta\varepsilon$.

The predictions for the high-strength, quenched-and-tempered steels (Fig. 5) indicate that such materials can sustain high residual stresses which do not relax. The total fatigue life of such materials is strongly influenced by both residual stress (σ_r) and stress ratio (R). Stress relief of mechanically induced compressive residuals should be highly effective.

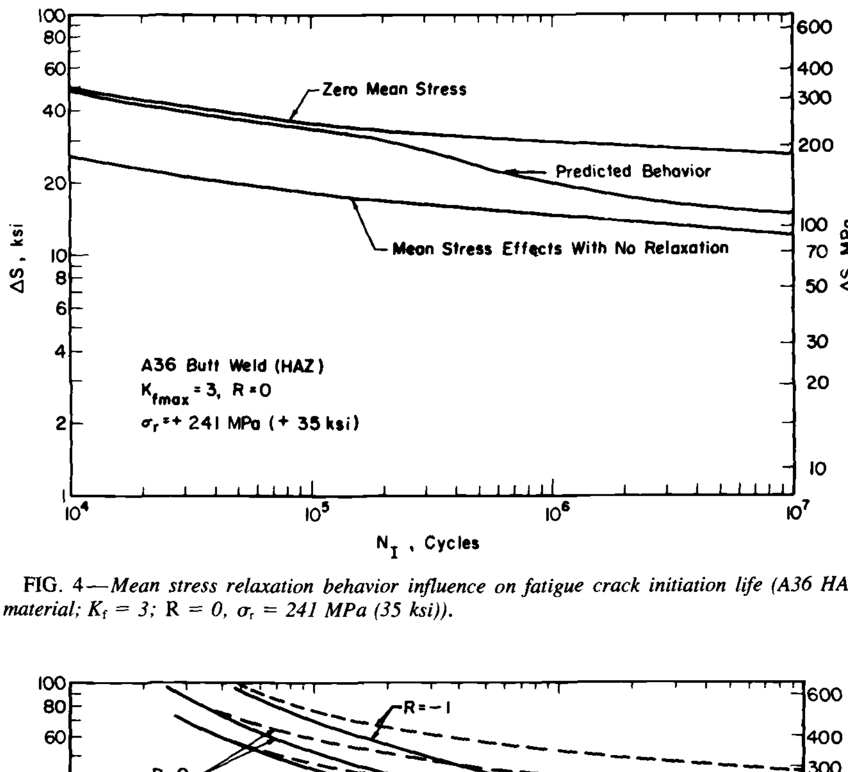

FIG. 4—*Mean stress relaxation behavior influence on fatigue crack initiation life (A36 HAZ material; K_f = 3;* R *= 0, σ_r = 241 MPa (35 ksi)).*

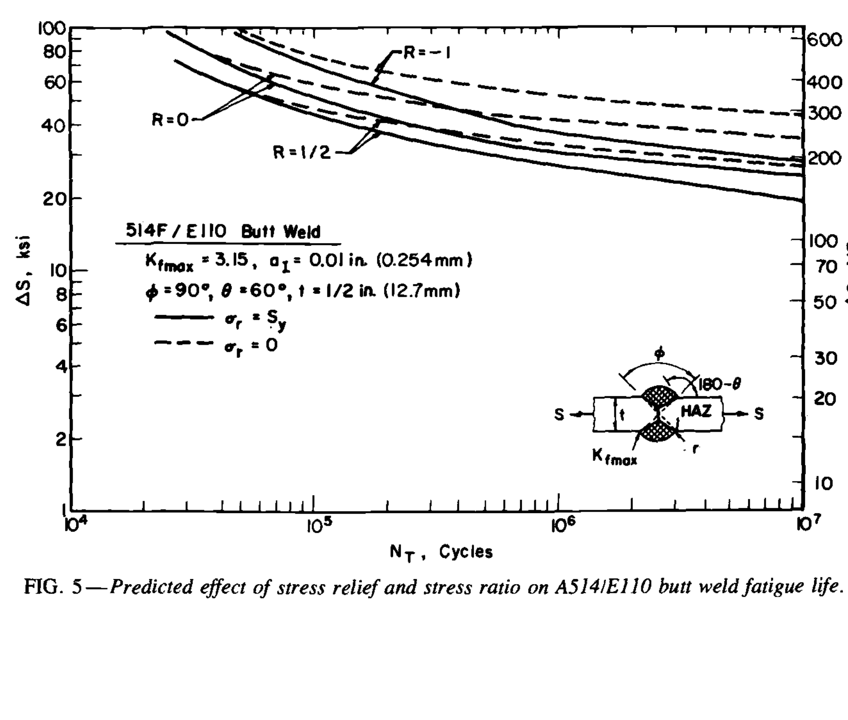

FIG. 5—*Predicted effect of stress relief and stress ratio on A514/E110 butt weld fatigue life.*

An intermediate case is mild steel (Fig. 6). Mild steels can have appreciable residual stresses; however, since the transition fatigue life (N_{tr}) is often very long ($\approx$500 000 cycles), there is a large amount of plasticity at the notch root even at long lives (10^6 cycles). This notch-root plasticity tends to rapidly relax the notch-root residual and mean stresses, with the result that N_I is little affected for lives less than 10^6 cycles. The observed dependence of N_P on stress ratio does, however, result in a predicted variation of total fatigue life with stress ratio R.

Because of the high notch root plasticity during the first few cycles before the material cyclically hardens, the predictions for the aluminum weld considered here (5083/5183) exhibit little dependence upon either residual stress or stress ratio, even though the relaxation of the stabilized mean stress (σ_{os}) is very slow (Fig. 7).

Comparisons of these predictions with experimental data are given in Figs. 8 to 10. Generally, the mean stress relaxation exponent (k) in Eq 4 decreases with the transition fatigue life (N_{tr}). Other things being equal, materials should be influenced by σ_r and R. (The aluminum considered is an exception to this rule for the reasons discussed.)

Influence of Ultimate Strength on N_I

Using the observed variation in steel fatigue properties (σ_f' and b) and tensile strength (S_u), Eq 3 can be rewritten [7] as

$$S_a = \frac{S_u + 345 - \sigma_r}{1 + 0.0015\alpha S_u t^{1/2}}[2N_I]^{-1/6 \log 2 (1 + 345/S_u)} \text{ (SI units)} \quad (7)$$

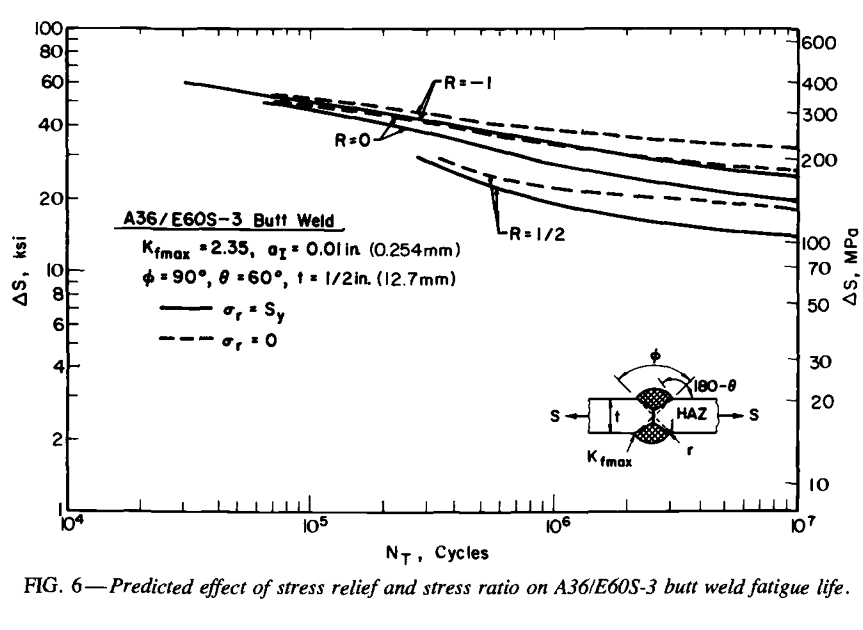

FIG. 6—*Predicted effect of stress relief and stress ratio on A36/E60S-3 butt weld fatigue life.*

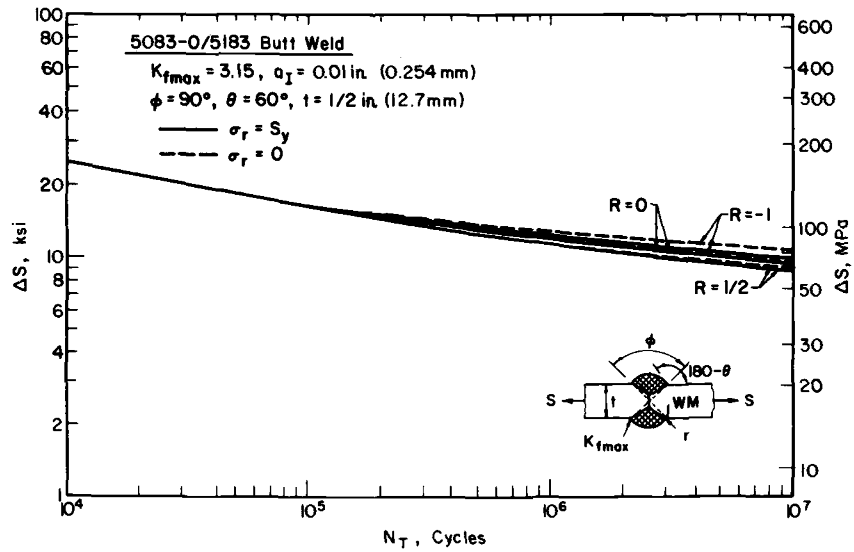

FIG. 7—*Predicted effect of stress relief and stress ratio on 5083-0/5183 butt weld fatigue life.*

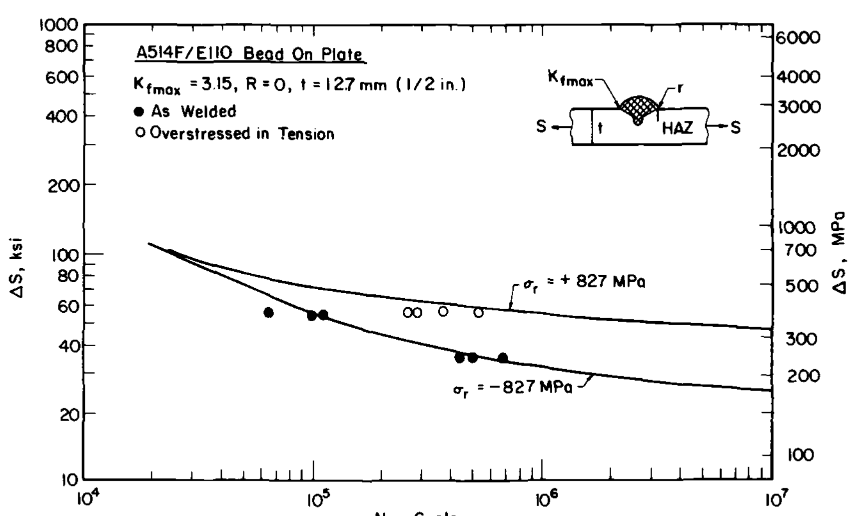

FIG. 8—*Total fatigue life predictions and experimental results (solid and open symbols) for A514F/E110 weldments with tensile and compressive residual stresses, respectively.*

where

S_a = fatigue limit at $2N_1$ ($R = -1$), and
σ_r = residual stress at weld toe.

The fatigue limit of steel weldments predicted by Eq 7 is a function of S_u and is plotted in Fig. 11 for three assumptions of weld toe residual stress (σ_r). For the assumption of no residual stress, it can be seen that the fatigue resistance of a steel

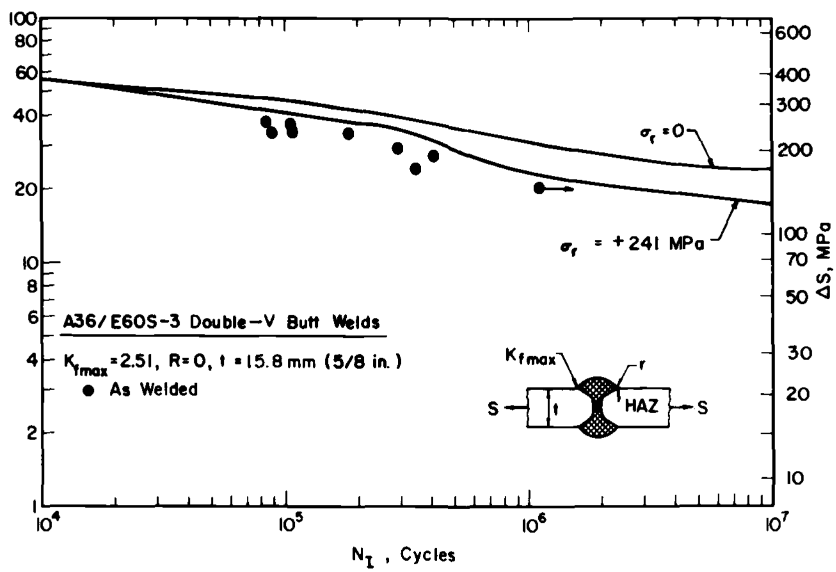

FIG. 9—*Fatigue crack initiation life predictions and experimental results (solid symbols) for 15.8-mm (5/8-in.) A36/E60S-3 butt welds.*

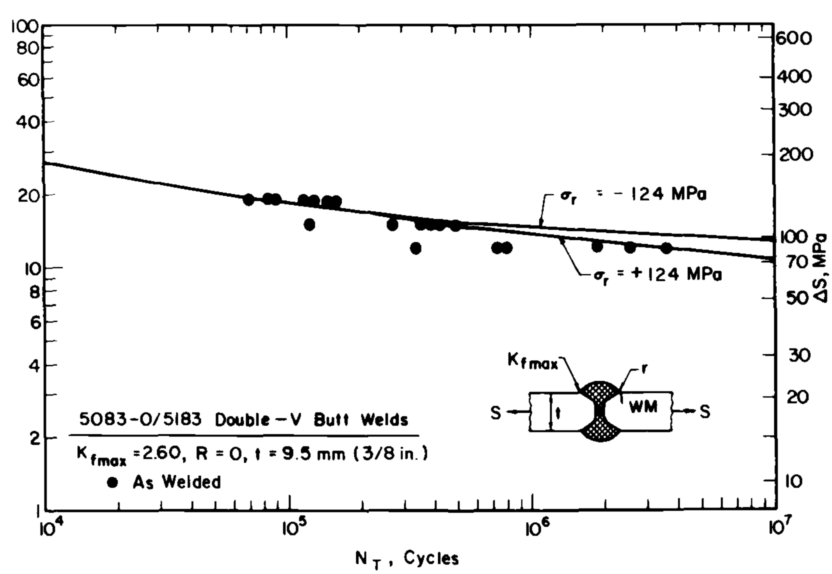

FIG. 10—*Total fatigue life predictions and experimental results (solid symbols) for 5083-0/5183 9.5-mm (3/8-in.) butt welds.*

weldment continues to increase with increasing S_u even though the increase in σ_f' due to the increase in S_u is partially offset by a larger K_{fmax}. Under the assumption of positive residual stresses equal to the base metal yield strength ($\sigma_r = +S_y$), the fatigue limit is no longer a strong function of S_u but increases only slightly and

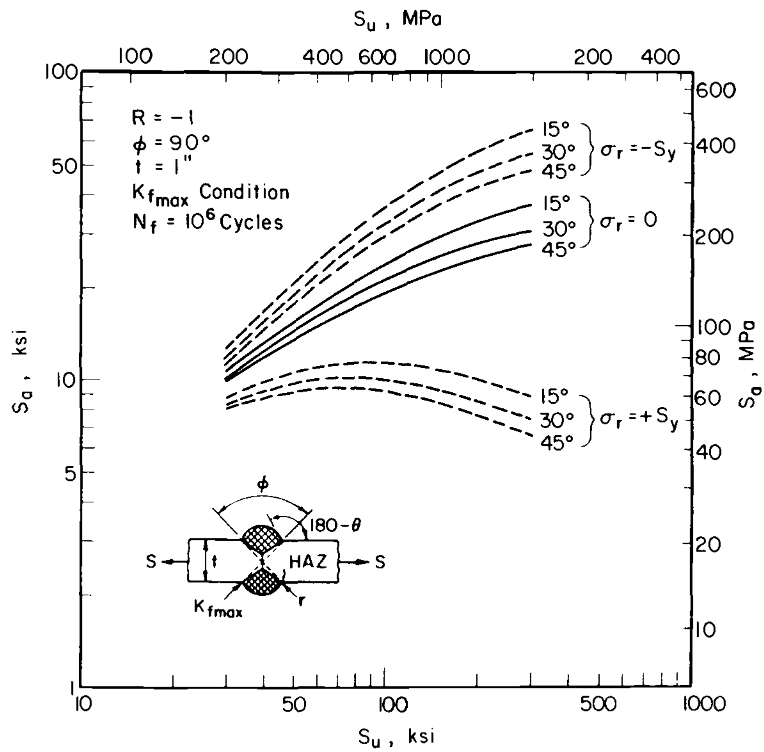

FIG. 11 —*Predicted influence of ultimate strength (S_u) on the fatigue strength (S_a) of a steel butt weldment at 10^6 cycles. The effect of weld shape (θ) and weld toe residual stresses (σ_r) are considered for assumed K_{fmax} conditions.*

then decreases with increases in S_u above 550 MPa (80 ksi). Thus, increasing the strength (S_u) of weldments (particularly in the as-welded condition) may actually decrease their fatigue limit due to the combined effects of increasing K_{fmax} and σ_r. The full potential of higher strength steels may be realized if the welds are stress relieved; that is, if the residual stresses (σ_r) are reduced from $+S_y$ to 0. Furthermore, the higher strength steels should show the greatest benefit from overstressing or inducing compressive residual stresses ($\sigma_r = -S_y$) at the weld toe.

Acknowledgments

This study was principally supported by the University of Illinois Fracture Control Program, which is funded by a consortium of Midwest industries. The authors wish to thank Professor JoDean Morrow of the Department of Theoretical and Applied Mechanics for his advice and help.

References

[1] Lawrence, F. V., Jr., Mattos, R. J., Higashida, Y., and Burk, J. D. in *Fatigue Testing of Weldments, ASTM STP 648,* D. W. Hoeppner, Ed., American Society for Testing and Materials, 1978, pp. 134-158.
[2] Tobe, Y. and Lawrence, F. V., Jr., *Welding Journal,* Vol. 56, No. 9, 1977, pp. 259s-266s.
[3] Chen, W. C. and Lawrence, F. V., Jr., *Fracture Control Program Report No. 32,* University of Illinois, Urbana-Champaign, 1979.
[4] Jhansale, H. R. and Topper, T. H. in *Cyclic Stress-Strain Behavior—Analysis, Experimentation, and Failure Prediction, ASTM STP 519,* American Society for Testing and Materials, 1973, pp. 246-270.
[5] Burk, J. D. and Lawrence, F. V., Jr., *Fracture Control Program Report No. 29,* University of Illinois, Urbana-Champaign, 1978.
[6] Elber, W. in *Damage Tolerance in Aircraft Structures, ASTM STP 486,* American Society for Testing and Materials, 1971, pp. 230-242.
[7] Lawrence, F. V., Jr., Ho, N. J., and Mazumdar, P. K., *Predicting the Fatigue Resistance of Welds, Fracture Control Program Report No. 36,* University of Illinois, Urbana-Champaign, 1980.

G. E. Nordmark,[1] *L. N. Mueller,*[1] *and R. A. Kelsey*[1]

Effect of Residual Stresses on Fatigue Crack Growth Rates in Weldments of Aluminum Alloy 5456 Plate

REFERENCE: Nordmark, G. E., Mueller, L. N., and Kelsey, R. A., "**Effect of Residual Stresses on Fatigue Crack Growth Rates in Weldments of Aluminum Alloy 5456 Plate,**" *Residual Stress Effects in Fatigue, ASTM STP 776,* American Society for Testing and Materials, 1982, pp. 44-62.

ABSTRACT: Rates of fatigue crack propagation were determined for CT specimens taken from the weld metal, heat-affected zone, and base metal of an Alcoa 649A Process 5556 butt weld in a 51-mm (2-in.)-thick 5456-H117 plate. Crack-opening displacement measurements were taken during the fatigue crack propagation tests so that the effects of crack-opening loads and residual stresses could be determined. The use of the concept of Elber's effective stress intensity range, based on the measurements of crack-opening loads, indicates that the crack propagation rates are equivalent in the weld metal, heat-affected zone, and base metal. Furthermore, the effect of stress ratio also can be correlated using the effective stress intensity range concept.

KEY WORDS: aluminum alloy, fatigue crack growth rates, residual stresses, effective stress intensity factors

Fatigue failures in welded aluminum structures generally initiate at points of stress concentration produced by weld discontinuities or the geometry of the weld crown. Because crack propagation may occur in the weld metal, heat-affected zone (HAZ), and base metal, it is necessary to determine fatigue crack growth rates (FCGR) for all three zones. Previous investigators of fatigue crack growth in thick aluminum weldments [*1,2*] reported that the FCGR for 5183 weld metal was slower than that in 5083-0 parent material at low stress intensities.[2] However, recent work [*3,4*] has indicated that these measured rates of propagation were probably affected by residual stresses in the specimens. The effect of residual stress in aluminum weldments is particularly evident in tests of full thickness specimens from thick welds where the propagation in the interior lags greatly behind the propagation at the surface [*3,5*] because of compressive residual stresses in the interior. That residual stresses may greatly affect crack propagation in smaller, partial thickness specimens has also been reported [*4*]. The purpose

[1]Senior Engineers and Section Head, respectively, Alcoa Technical Center, Alcoa Center, Pa. 15069.

[2]The italic numbers in brackets refer to the list of references appended to this paper.

of this investigation is to study the effect of residual stress on the FCGR behavior of high deposition rate (HDR) butt welds in tnick 5456-H117 plate.

Material and Welding Procedure

The material used in this investigation is aluminum alloy 5456-H117 51-mm (2-in.) plate welded with 5556 electrode. Alloy 5456 is a weldable, strain-hardened alloy with magnesium as its major alloying element. Nominal chemical composition and typical tensile properties are listed in Tables 1 and 2, respectively. Because the heat of the welding partially anneals the material in the vicinity of the weld, the tensile properties for the annealed temper, 5456-0, also are listed. HDR welding was done automatically in the flat position using the procedures listed in Table 3.

Residual Stress Distribution

Residual stresses are produced in welded structures by thermal expansion, plastic deformation, and shrinkage during cooling. The amount of constraint determines the level of the residual stress and, when sufficient, these stresses can approach the tensile yield strength of the material. Figure 1 shows schematically the residual stress distribution in a multipass butt welded plate. For a given plate thickness, the magnitude of the transverse stresses varies inversely with the size of the weld passes; however, longitudinal stresses increase somewhat with the size of the passes [7]. In a previous investigation [3], the transverse residual stresses for the HDR welded 5456 plate used in this study were measured at the

TABLE 1—*Nominal chemical composition, percent of alloying elements* [6].

	Mn	Mg	Cr	Ti
5456	0.8	5.1	0.12	...
5556	0.8	5.1	0.12	0.12

TABLE 2—*Typical tensile properties* [6].

	Tensile Strength, MPa (ksi)	Yield Strength, MPa (ksi)	Elongation % in 51 mm (2 in.)
5456-H116, 5456-H117	352 (51)	255 (37)	16
5456-0	310 (45)	159 (23)	24

TABLE 3—*Welding procedures for 51-mm (2-in.) plate, Alcoa 649A Process welds.*[a]

	Electrode					
Plate Alloy	Alloy	Diameter, mm (in.)	No. of Passes	Current, A	Voltage, V	Travel Speed, mm/s (in./min)
5456-H117	5556	3.2 (0.125)	4	570	35	4.2 (10)

[a]60-deg double V with a 6.4-mm (0.25-in.) radius and a 19-mm (0.75-in.) land. 118 L/min (250 ft^3/h) shielding gas of an argon-helium mixture.

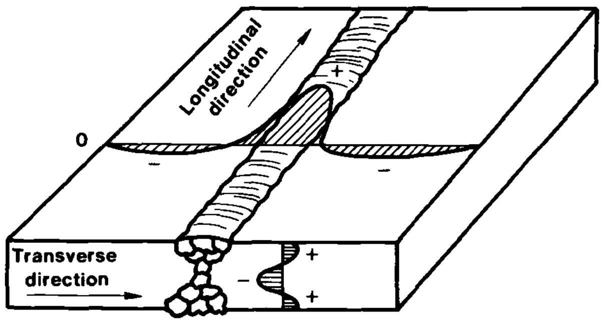

FIG. 1—*Residual stress distributions in a conventional welded plate (indicated directions are with respect to the weld).*

edge of the weld by a strain gage sectioning technique; they were determined to be only 5.5 MPa (0.8 ksi) compression–essentially zero. However, for a comparable conventional weld made in 12 passes, the residual transverse stresses were 92 MPa (13 ksi).

FCGR Specimens

Compact-type (CT) specimens (Fig. 2) were used to measure fatigue crack growth rates in this investigation. Figures 3*a* and 3*b* show specimen locations in the HDR welded 5456-H117 plate. Specimens were taken from the base metal, HAZ, and weld metal, and were oriented so that crack propagation was in the direction of the weld.

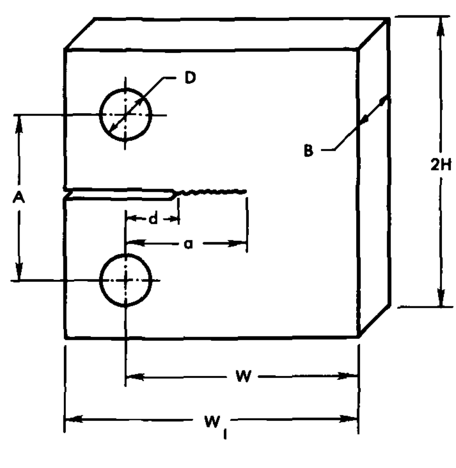

	B	2H	W	A	D	d	W_I	H/W
mm	6.35	76.2	63.5	34.9	9.58	15.9	79.4	0.6
in.	0.25	3.00	2.500	1.375	0.377	0.625	3.125	0.6

FIG. 2—*Dimensions for compact fatigue crack propagation specimen.*

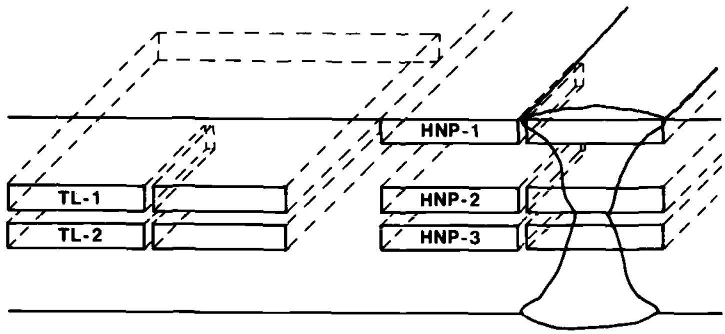

FIG. 3a—*TL and HNP specimen locations; Alcoa 649A butt weld in 51-mm (2-in.) 5456-H117 plate.*

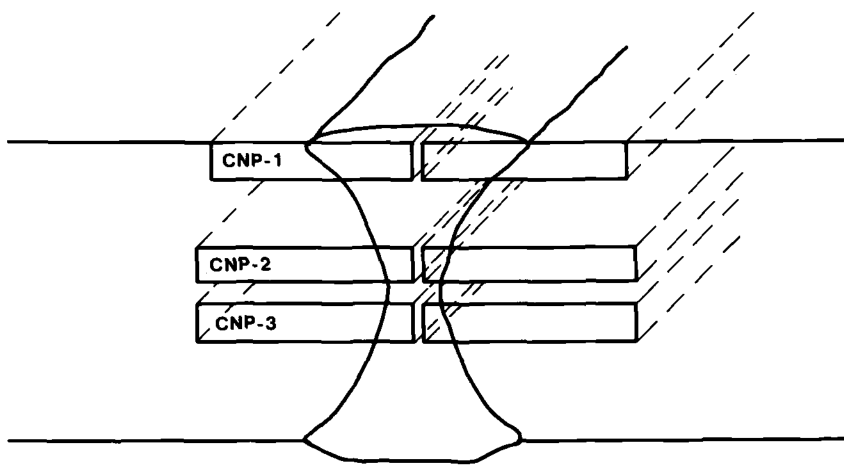

FIG. 3b—*CNP specimen locations; Alcoa 649A butt weld in 51-mm (2-in.) 5456-H117 plate.*

As shown in Fig. 4, longitudinal residual stresses can close the crack tip by producing a moment around it. In fact, Ref *4* reported that longitudinal residual stresses had more effect on closure than transverse residual stresses for specimens from a die forging. A technique described in Ref *4* was used to qualitatively check the level of residual stresses present in the specimens. Mechanical displacement measurements were taken over a 51-mm (2-in.) gage length on the front edge of the CT specimens. These were used to determine the movement produced by machining the crack starter notch. Closures of 0.0051 mm (0.0002 in.) or less were measured for the TL and the CNP specimens (Figs. 3*a* and 3*b*). However, for HNP specimens, whose test sections were located in the HAZ, the closures were 0.023 to 0.051 mm (0.0009 to 0.0020 in.) with the specimens from midthickness having the largest closures. The larger closures indicate higher levels of residual stresses; therefore higher loads would be required to open the cracks.

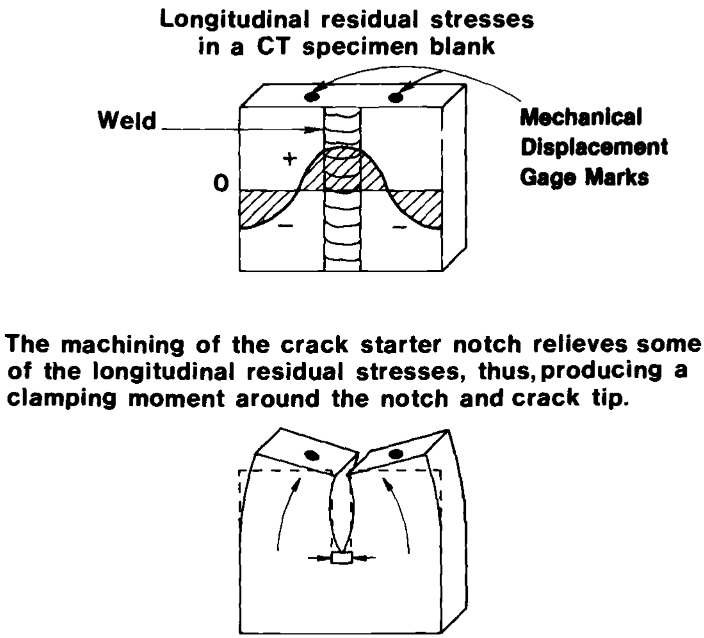

FIG. 4—*Crack closure produced in a CT specimen by longitudinal residual welding stresses.*

FCGR Test Procedures

Fatigue crack growth data were obtained at stress ratios of 0 and $\frac{1}{3}$ in moist air (relative humidity greater than 90 percent).[3] Crack length measurements were determined visually at 0.5-mm (0.02-in.) increments using grids on the specimen surfaces. The tests were conducted using a closed-loop servohydraulic machine at a frequency of 20 Hz in accordance with ASTM Tentative Test Method for Constant-Load-Amplitude Fatigue Crack Growth Rates Above 10^{-8} m/Cycle (E 647). The crack growth rates were determined by the secant method, and stress intensity factors were calculated by using Srawley's equation as outlined in this method. A compliance gage was mounted on the front edge of the specimen and plots of applied load, P_{APPL}, versus crack-opening displacement, COD, were made periodically during the test to determine the crack-opening load, P_{op}.

Definition of P_{op}

The concept of an effective stress intensity range, ΔK_{EFF}, described by Elber [*8*], assumes that crack propagation only occurs when the crack tip is completely open (that is, when $P_{APPL} > P_{op}$). Residual stresses, as well as fretting/corrosion debris or crack tip plasticity, can clamp the crack tip closed or wedge it open. In either case the P versus COD plot will have a dual slope as shown in Fig. 5 for

[3]Stress ratio (R) = minimum stress/maximum stress.

Specimen HNP2. The initial slope is attributed to the load needed to overcome the internal force system; the upper slope is that associated with opening of the crack tip. No universally accepted definition of P_{op} exists; thus different positions on the curve might be selected as representing P_{op}. The points of tangency to either the upper or lower straight line portions or the intersection of the extrapolated straight lines of the loading or unloading curves are possible definitions. Elber defined P_{op} as the lowest point on the loading curve which is tangent to a line having the slope of the prior unloading curve measured at maximum load. This slope defines the elastic stiffness of the fully opened crack. Bucci [*4*] recently used the intersection method as being the most convenient, and it is probably the most reliable for visual determination. For direct measurement, Vasquez et al [*9*] used the upper tangency point on the unloading curve. For the test data described herein, there would be little difference between opening loads determined by the Elber and Vasquez definitions. Figure 6 shows a comparison of three definitions of P_{op} plotted against crack length for Specimen HNP2. In the succeeding data and discussion, P_{op} is based on the upper tangency definition; however, a comparison of results obtained with the upper tangency and intersection definitions is included in the Discussion.

Figure 7 shows the upper tangency P_{op} versus crack length for the specimens tested at $R = 0$. Notice that P_{op} decreases with increasing crack length, which indicates relief of residual stresses.

Analysis of FCGR Data

A four-parameter Weibull function was statistically fitted to the FCGR data for each specimen on the basis of both ΔK_{APPL} and ΔK_{EFF}. This sigmoidal type function is defined as

$$\frac{da}{dN} = e + (v - e)\left[-\ell n\left(1 - \frac{\Delta K}{Kb}\right)\right]^{1/k} \tag{1}$$

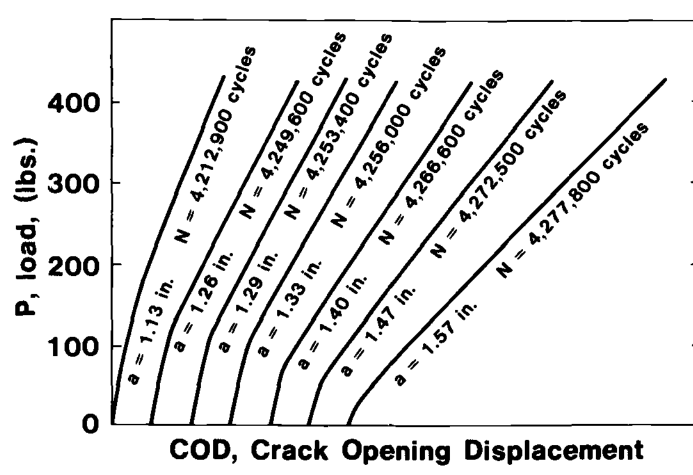

FIG. 5—*Load versus COD traces for Specimen HNP2 (1 in. = 25.4 mm; 1 lbf = 4.4 N).*

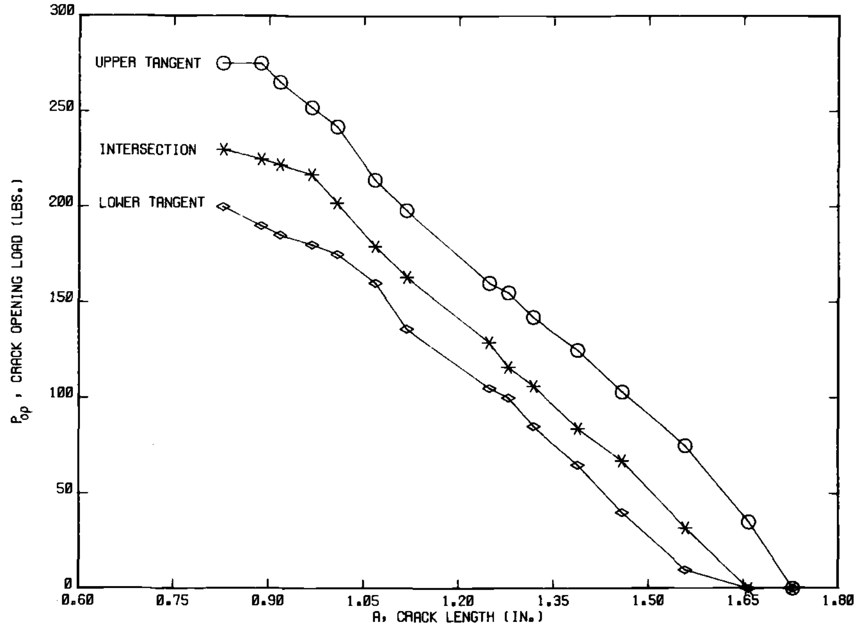

FIG. 6—*Comparison of three methods for defining* P_{op} *for Specimen HNP2 (1 in. = 25.4 mm; 1 lbf = 4.4 N).*

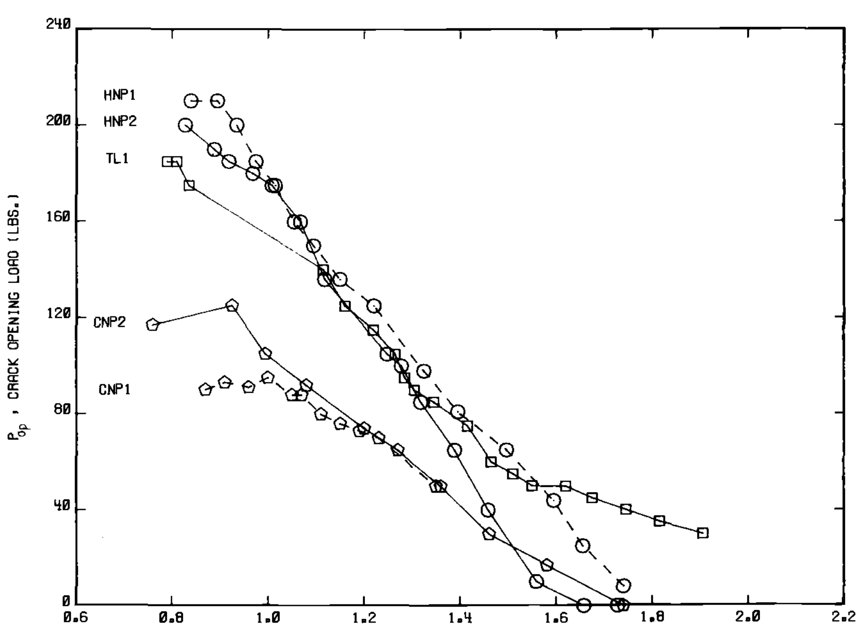

FIG. 7—*Crack-opening load versus crack length for specimens tested at* R = 0 *(1 in. = 25.4 mm; 1 lbf = 4.4 N).*

where e = threshold parameter, and has the dimensions of da/dN,
v = characteristic value parameter, and has the dimensions of da/dN,
k = shape parameter, and is a dimensionless exponent, and
Kb = instability asymptote parameter, and has the dimensions of ΔK.

This function was fitted to each data set by optimizing the parameters with a unique nonlinear regression analysis technique described in Ref *10*. Briefly, this technique minimizes the sum of the squared normalized perpendicular residuals between a data set and the Weibull function. All four parameters can be optimized to a data set, or one parameter can be held constant while the other three are optimized. The parameter Kb is an upper asymptote of the function and represents a toughness characteristic of the material. For tests conducted at $R = 0$, Kb was held constant at 121 Mpa$\sqrt{\text{m}}$ (110 ksi$\sqrt{\text{in.}}$). For the test conducted at $R = 1/3$, Kb was reduced by $(1 - R)$ and rounded off to 77 Mpa$\sqrt{\text{m}}$ (70 ksi $\sqrt{\text{in.}}$). This toughness value was estimated from published work at Alcoa on welded 5456-H117.

Figures 8 to 15 show the FCGR plots and their mean curve fits for the weld, HAZ, and base metal for both ΔK_{APPL} and ΔK_{EFF}. Table 4 lists the fitted parameters for each data set. It also lists an error statistic, MSSQ, the mean sum of the squared normalized perpendicular residuals, which can be used for relative comparisons. When fits for each data set were made by optimizing all four parameters

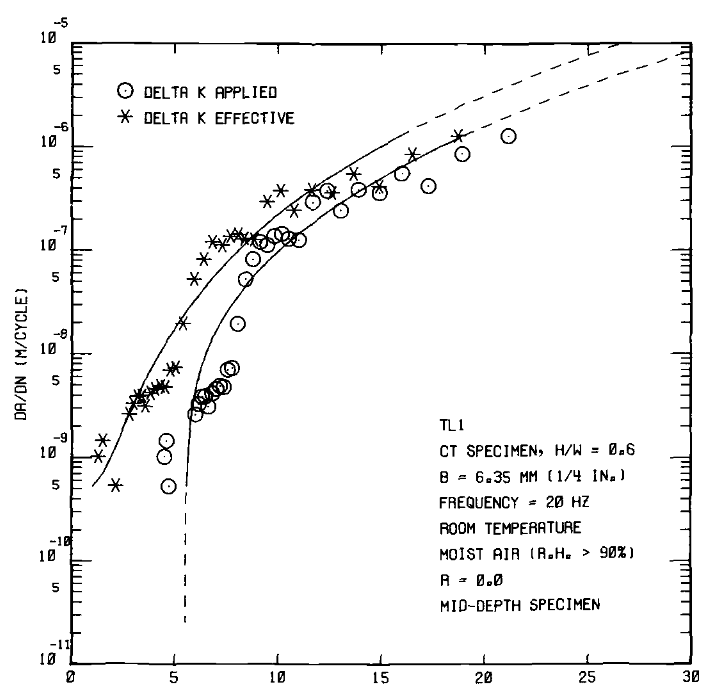

FIG. 8—*FCGR response and fitted Weibull curves for Specimen TL1, base metal, 5456-H117, 51-mm (2-in.) plate, 32 points.*

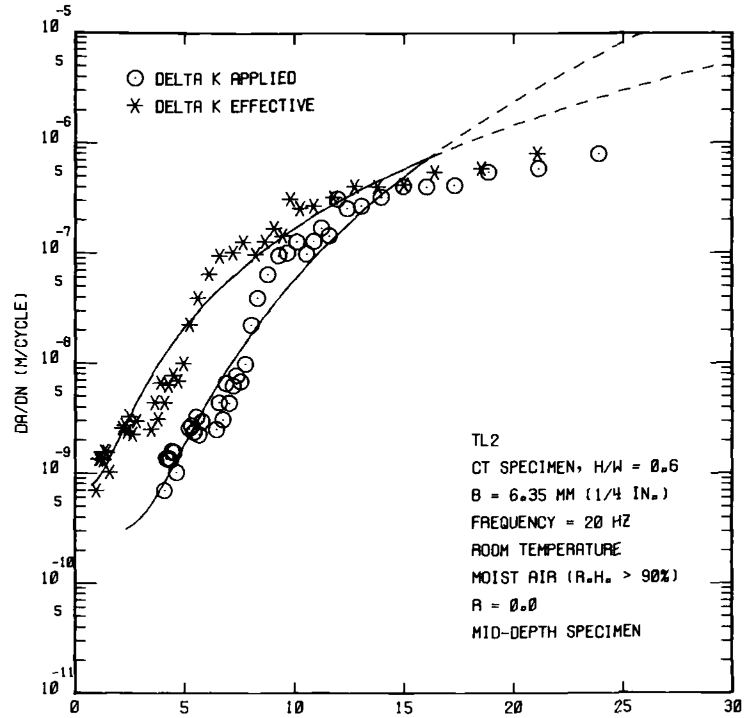

FIG. 9—*FCGR response and fitted Weibull curves for Specimen TL2, base metal, 5456-H117, 51-mm (2-in.) plate, 42 points.*

of the model, instead of holding *Kb* constant, the MSSQ statistic never changed by more than 4 percent.

Load versus COD traces were not made for Specimen TL2, so ΔK_{EFF} was calculated using the P_{op} measurements from Specimen TL1. Since the ΔK_{EFF} data sets for the TL specimens were not independent of each other they were not joined together as were the data sets for the CNP and HNP specimens.

Modeling FCGR data allows its use during design. The effect of "what if" questions relative to the life of a structure can be quickly ascertained by using a table of FCGR model parameters and a life prediction program. The Weibull model and the fitting procedure have produced good life predictions in ASTM E24.04.04 FCGR Description Round-Robin [*10*], where 80 to 90 percent of the life predictions made with the Weibull model fell within 20 percent of the actual lives.

Discussion

ΔK_{APPL} versus ΔK_{EFF}

The FCGR of Specimens CNP2, HNP2, and TL1, taken from the midplane, are shown in Fig. 16 plotted on the basis of ΔK_{APPL}. From this plot it appears that the rates of fatigue crack propagation in the HAZ are slower than those in the base metal which are in turn, slower than those in the weld metal. Previous work

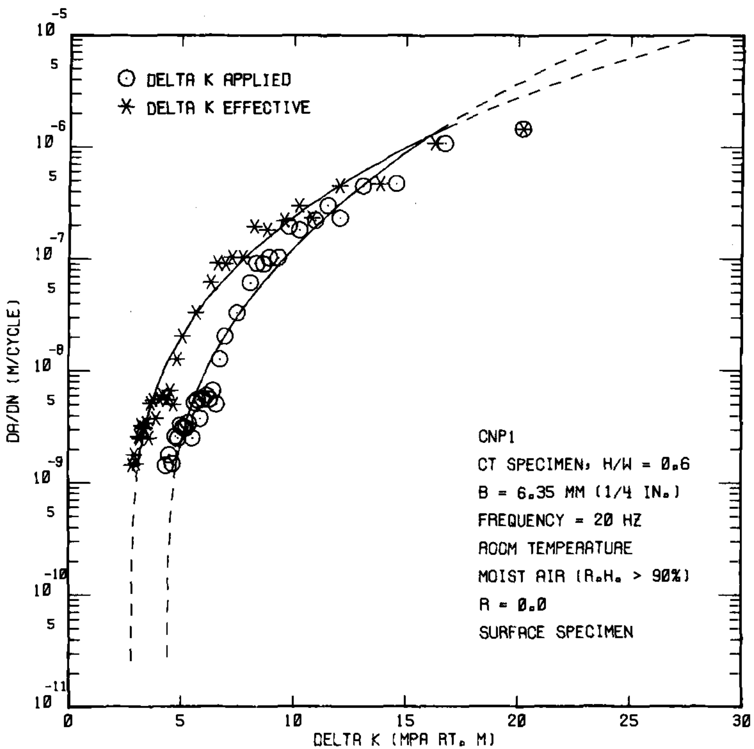

FIG. 10—*FCGR response and fitted Weibull curves for Specimen CNP1, 5556 weld metal in 5456-H117, 51-mm (2-in.) plate, 35 points.*

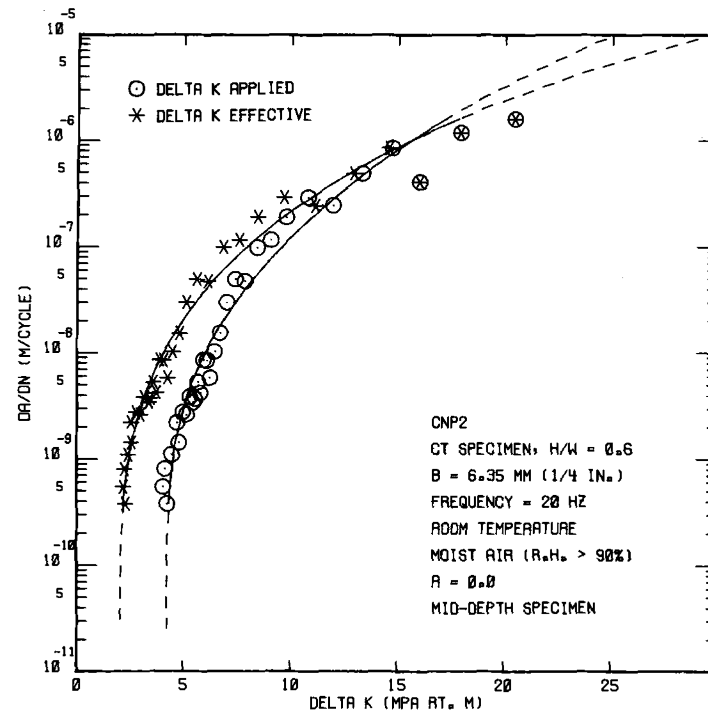

FIG. 11—*FCGR response and fitted Weibull curves for Specimen CNP2, 5556 weld metal in 5456-H117, 51-mm (2-in.) plate, 31 points.*

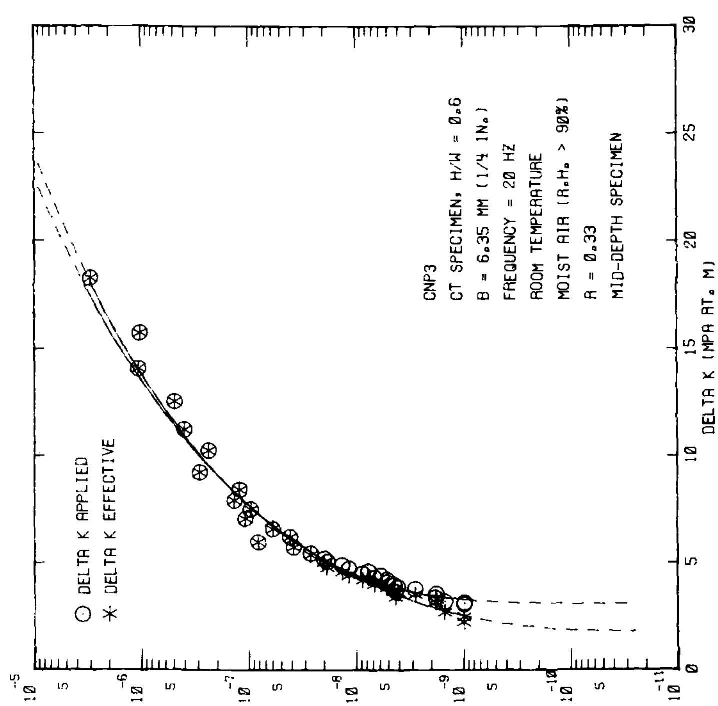

FIG. 12—*FCGR response and fitted Weibull curves for Specimen CNP3, 5556 weld metal in 5456-H117, 51-mm (2-in.) plate, 35 points.*

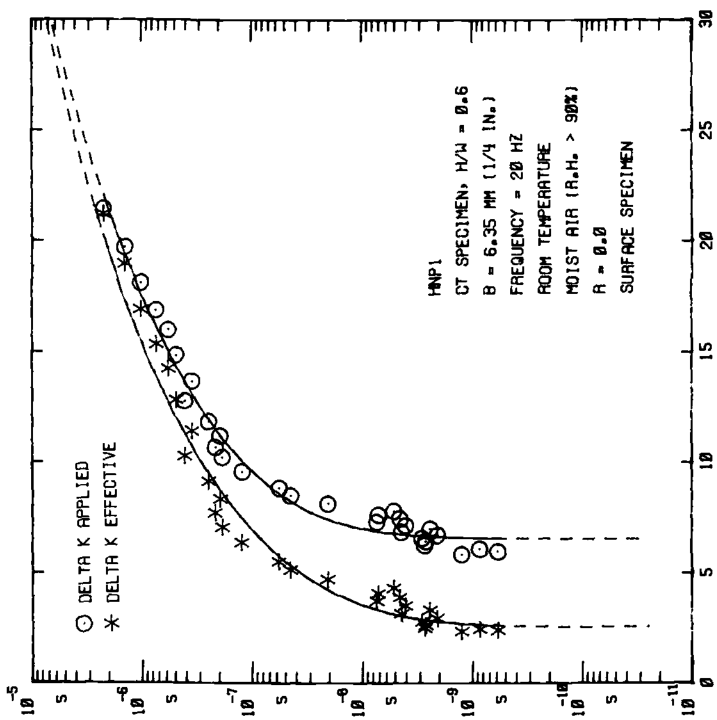

FIG. 13—*FCGR response and fitted Weibull curves for Specimen HNP1, heat-affected zone, 5456-H117, 51-mm (2-in.) plate, 30 points.*

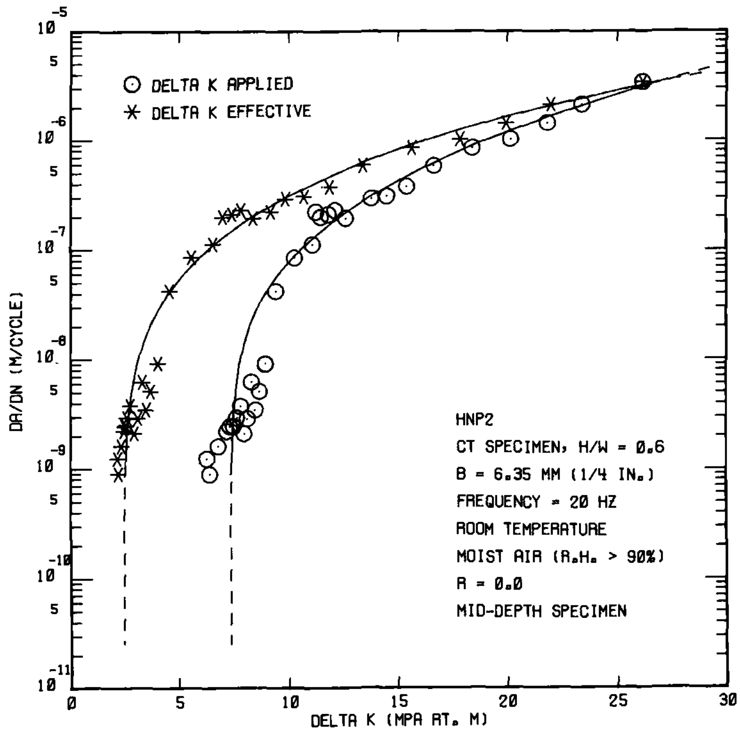

FIG. 14—*FCGR response and fitted Weibull curves for Specimen HNP2, heat-affected zone, 5456-H117, 51-mm (2-in.) plate, 31 points.*

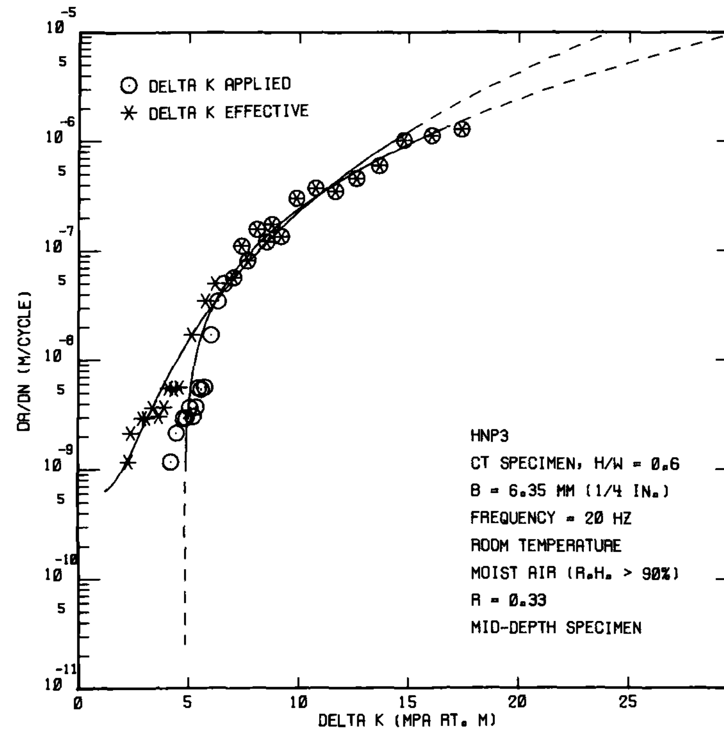

FIG. 15—*FCGR response and fitted Weibull curves for Specimen HNP3, heat-affected zone, 5456-H117, 51-mm (2-in.) plate, 28 points.*

TABLE 4—*Fitted Weibull FCGR parameters for each data set.*[a]

Specimen	ΔK Type	R[b]	Number of Points	e, μin./cycle	v, μin./cycle	K	Kb, ksi$\sqrt{\text{in.}}$	MSSQ[c]
CNP1	applied	0	35	−0.1055	3.615E5	0.2188	110	0.0060
	effective			−0.1257	3.104E4	0.3024	110	0.0074
CNP2	applied	0	31	−0.0988	2.420E5	0.2266	110	0.0064
	effective			−0.0448	2.364E4	0.3090	110	0.0086
CNP3	applied	⅓	35	−0.1358	1.324E4	0.2782	70	0.0038
	effective			−0.0118	2.043E6	0.2626	70	0.0051
Joined CNP	effective		101	−0.0223	7.360E4	0.2742	110	0.0084
HNP1	applied	0	30	−1.6290	1.305E4	0.3212	110	0.0041
	effective			−0.2649	8.420E3	0.3718	110	0.0144
HNP2	applied	0	31	−1.8217	9.597E3	0.3232	110	0.0054
	effective			−0.5552	2.762E3	0.4559	110	0.0117
HNP3	applied	⅓	28	−1.2392	2.912E3	0.3515	70	0.0041
	effective			−0.0224	1.591E4	0.2629	70	0.0074
Joined HNP	effective		89	−0.1260	1.474E4	0.3386	110	0.0167
TL1	applied	0	32	−0.4660	3.124E4	0.2755	110	0.0152
	effective			0.0189	5.676E4	0.2790	110	0.0307
TL2	applied	0	42	0.0110	5.103E5	0.1985	110	0.0135
	effective			0.0274	8.481E3	0.3413	110	0.0314

[a] 1 μin./cycle = 2.54E-5 mm/cycle; 1 ksi$\sqrt{\text{in.}}$ = 1.1 MPa$\sqrt{\text{m}}$.
[b] R = stress ratio = minimum stress/maximum stress.
[c] MSSQ = mean sum of squared normalized perpendicular residuals.

[1,2] seemingly contradicts this ranking by concluding that the FCGR in welds are slower than those in the base metal, but those rankings were for full thickness specimens from conventionally welded plates with high transverse residual stresses. The HDR welds for this work have negligible transverse residual stresses. Nonetheless, the longitudinal residual stresses affected both sets of results, and when these data are plotted on the basis of ΔK_{EFF} in Fig. 17 the rates of crack propagation appear to be equivalent. Except for the effect of residual stresses on P_{op}, the rate of fatigue crack growth is similar in base metal, weld metal, and HAZ. However, the residual stresses present in a weldment may significantly affect FCGR in different zones of a structure.

ΔK_{EFF} *Calculations*

The effect that the upper tangency and intersection methods for defining crack-opening load have on calculating ΔK_{EFF} is shown in Fig. 18 for Specimen HNP2. Predictably, ΔK_{EFF} calculated by the upper tangency method is slightly smaller than ΔK_{EFF} calculated by the intersection method.

Figure 19 shows the upper tangency ΔK_{EFF} FCGR plot for all the CNP specimens. Figure 20 presents the comparable plot generated by the intersection method. Figures 21 and 22 show the same two respective plots for the HNP specimens. For the CNP specimens, the upper tangent definition gives a tighter fit than the intersection definition. This is confirmed by the fact that the MSSQ statistic of the fitted curves is smaller for the upper tangent definition (0.0084 versus 0.0111). The calculated fit of the curves for the HNP data is not as good for either definition, but the intersection definition has the advantage with respect to the MSSQ statistic. However, the upper tangent definition does give a tighter fit at high and low stress intensities.

R-Ratio Effect

Figure 23 shows the R-ratio effect for the FCGR response of the CNP specimens plotted on the basis ΔK_{APPL}. When plotted using ΔK_{EFF}, however, as in Fig. 19, the data for the two stress ratios appear equivalent. Figures 24 and 21 show comparable plots for the specimens from the heat-affected zone and, except for the middle stress intensities, the use of ΔK_{EFF} also brings these data into good agreement. Schijve [11] also reported that ΔK_{EFF} was a good basis for correlating FCGR data for Alclad 2024-T3 sheet tested at several positive stress ratios.

Conclusions

1. The fatigue crack propagation properties of CT specimens taken from an Alcoa 649A Process (high deposition rate) welded 5456-H117 51-mm (2-in.) plate ranked on the basis of ΔK_{APPL} from slowest to fastest were: the heat-affected zone, the base metal, and the 5556 weld metal. However, when the data are plotted on the basis of ΔK_{EFF}, as determined from the crack-opening load, the crack propagation rates are equivalent. Therefore the different fatigue crack propagation rates measured for the three materials are the result of differences in residual stresses.

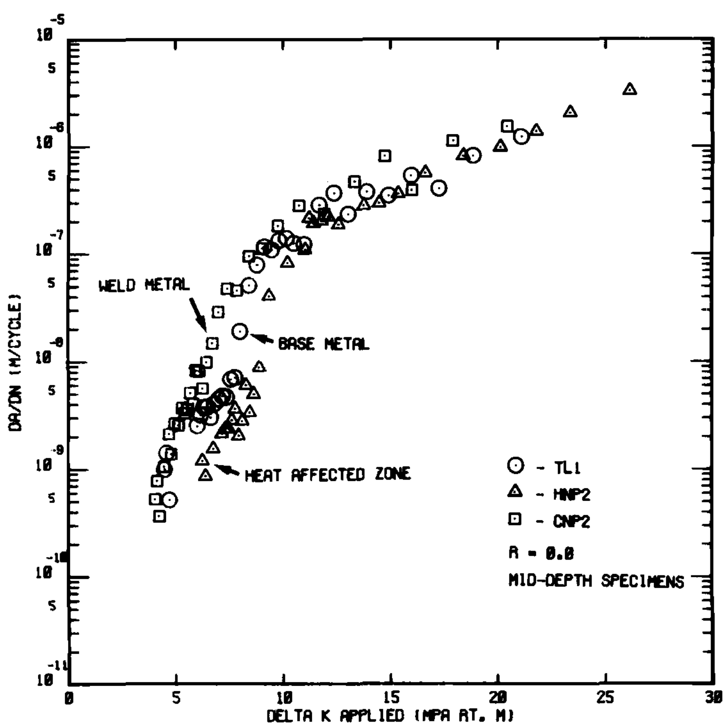

FIG. 16—*FCGR response of specimens taken from the midplane of the 5456-H117 plate plotted on the basis of applied* ΔK.

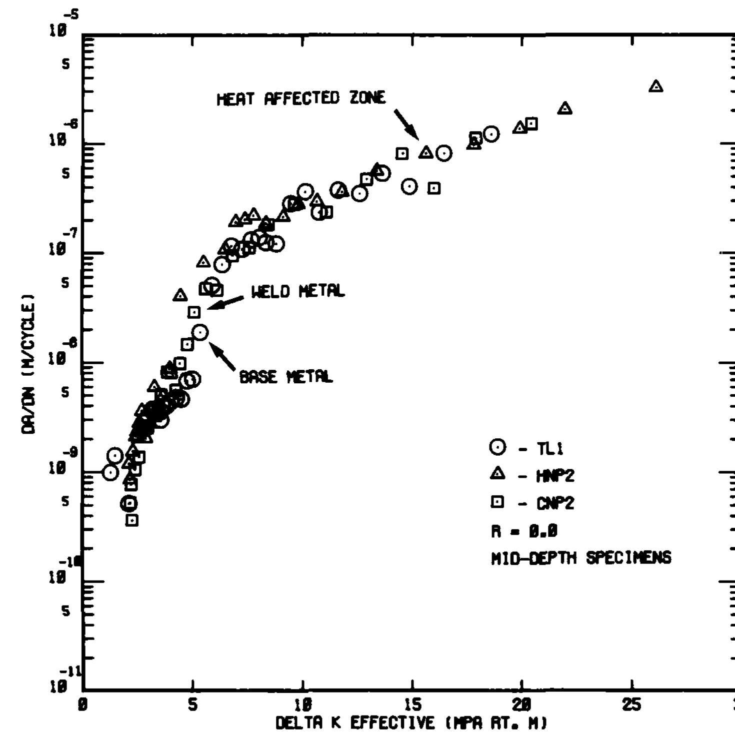

FIG. 17—*FCGR response of specimens taken from the midplane of the 5456-H117 plate plotted on the basis of effective* ΔK.

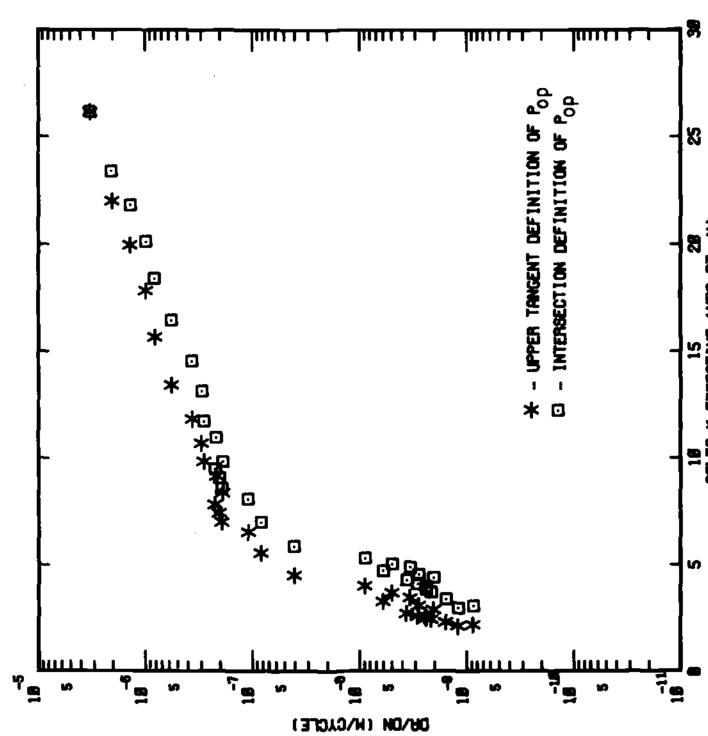

FIG. 18—*Comparison of two methods of defining effective ΔK for Specimen HNP2.*

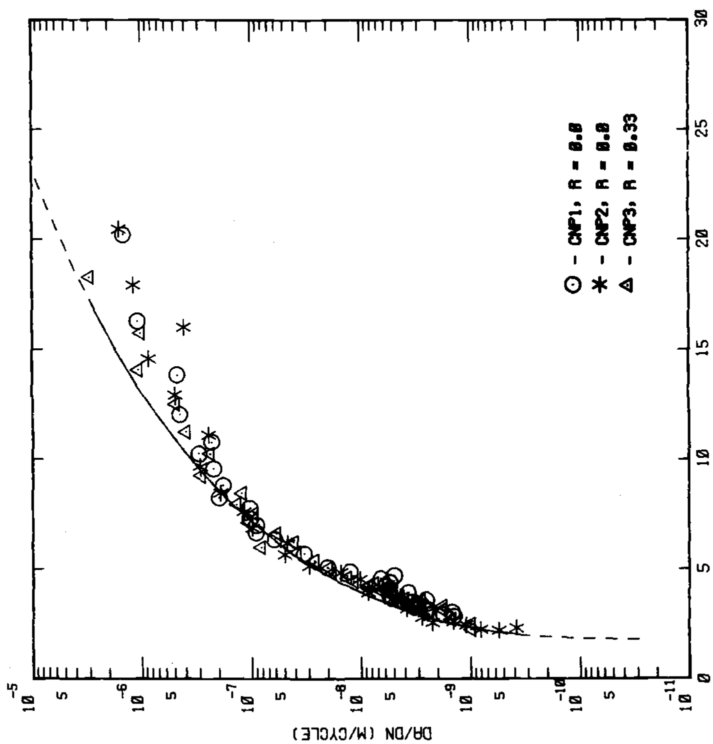

FIG. 19—*FCGR response and fitted Weibull curve of the combined CNP specimens plotted on the basis of ΔK_{EFF}, 101 points.*

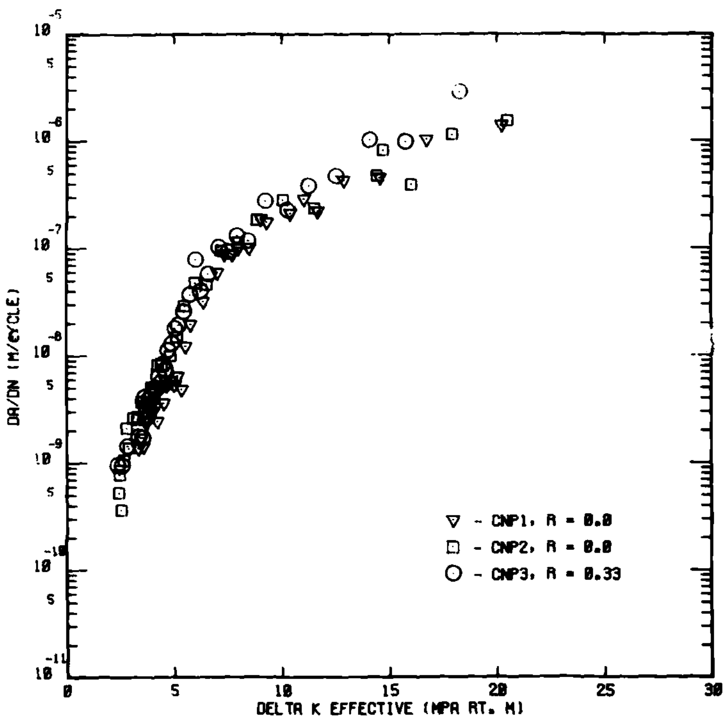

FIG. 20—*FCGR response of the combined CNP specimens plotted against* ΔK_{EFF} *calculated with* P_{op} *defined by the intersection method.*

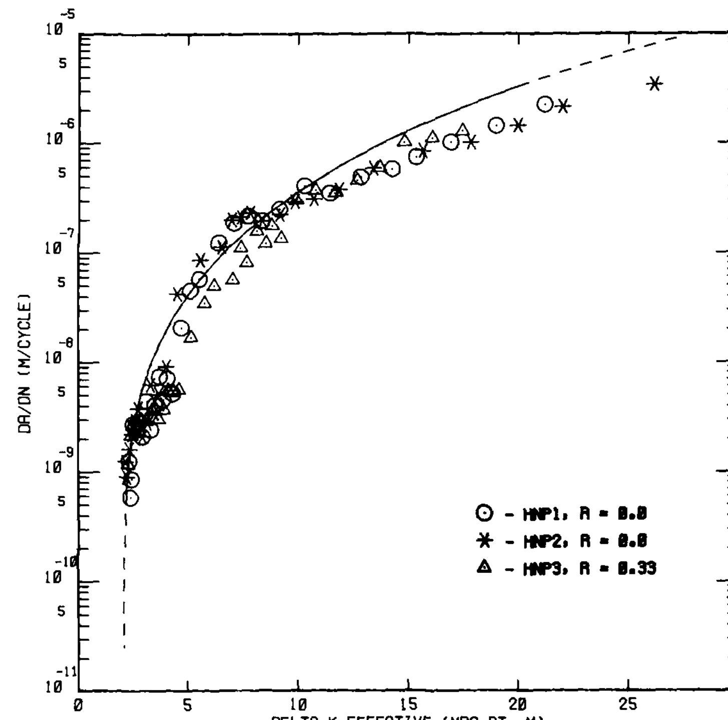

FIG. 21—*FCGR response and fitted Weibull curve of the combined HNP specimens plotted on the basis of* ΔK_{EFF}, *89 points.*

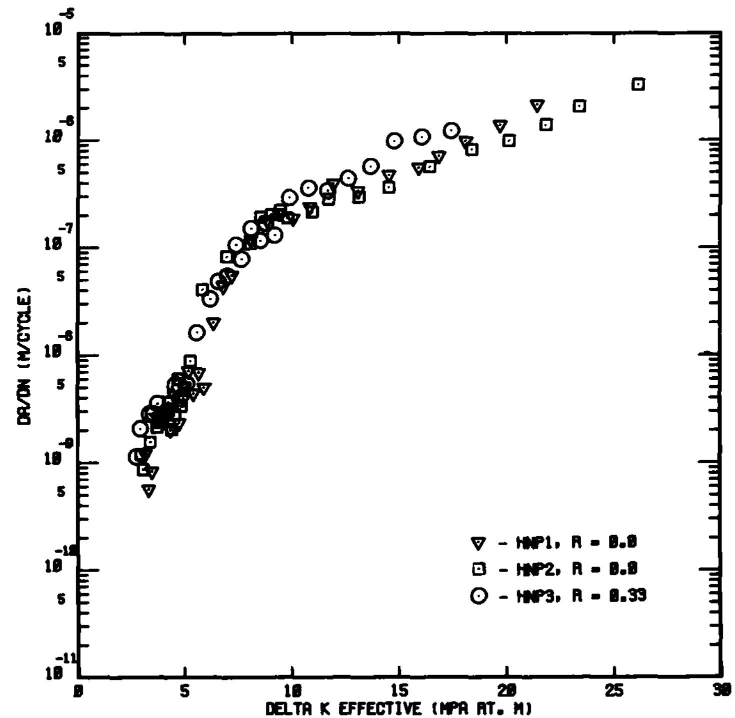

FIG. 22—*FCGR response of the combined HNP specimens plotted against* ΔK_{EFF} *calculated with* P_{op} *defined by the intersection method.*

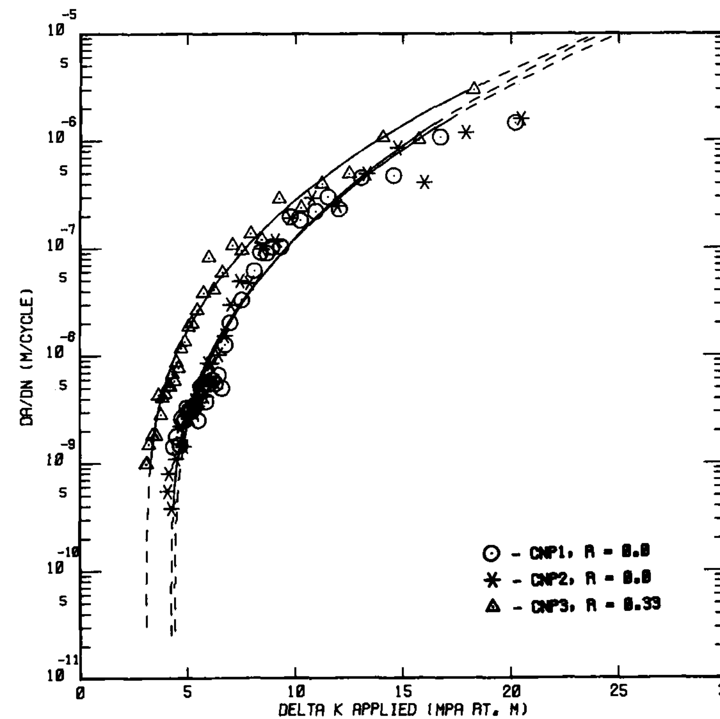

FIG. 23—*FCGR response and fitted Weibull curves of the CNP specimens.*

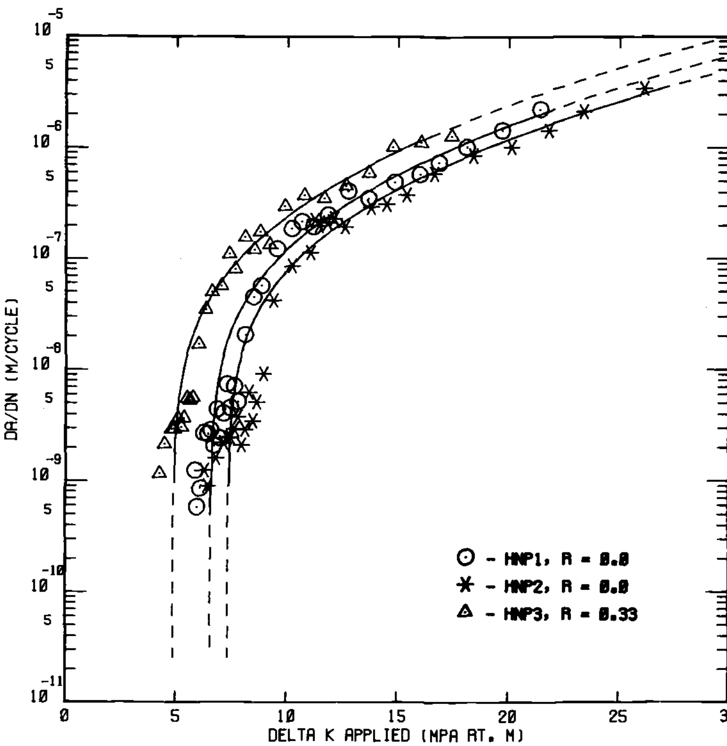

FIG. 24—*FCGR response and fitted Weibull curves of the HNP specimens.*

2. The concept of ΔK_{EFF} also correlates the FCGR data obtained at stress ratios of 0 and ⅓.

References

[*1*] Kelsey, R. A., Nordmark, G. E., and Clark, J. W. in *Fatigue and Fracture Toughness—Cryogenic Behavior, ASTM STP 556,* American Society for Testing and Materials, pp. 159-185.

[*2*] Kaufman, J. G. and Kelsey, R. A. in *Properties of Materials for Liquified Natural Gas Tankage, ASTM STP 579,* American Society for Testing and Materials, 1975, pp. 138-158.

[*3*] Kelsey, R. A. and Nordmark, G. E., *Aluminium,* June 1979, pp. 391-394.

[*4*] Bucci, R. J., "Effect of Residual Stress on Fatigue Crack Growth Rate Measurement," 13th National Symposium on Fracture Mechanics, Philadelphia, 16 June 1980.

[*5*] Nelson, F. G. and Kaufman, J. G. in *Progress in Flaw Growth and Fracture Toughness Testing, ASTM STP 536,* American Society for Testing and Materials, pp. 350-376.

[*6*] *Aluminum Standards and Data,* Aluminum Association, 1976.

[*7*] Kelsey, R. A., *Welding Journal,* Welding Research Supplement, Vol. 50, 1971, pp. 507-514.

[*8*] Elber, W. in *Damage Tolerance in Aircraft Structures, ASTM STP 486,* American Society for Testing and Materials, 1971, pp. 230-242.

[*9*] Vasquez, J. A., Morrone, A., and Ernst, H., *Engineering Fracture Mechanics,* Vol. 12, pp. 231-240.

[*10*] Miller, M. S. and Gallagher, J. P. in *Fatigue Crack Growth Measurement and Data Analysis, ASTM STP 738,* S. J. Hudak, Jr., and R. J. Bucci, Eds., American Society for Testing and Materials, 1981, pp. 205-251.

[*11*] Schijve, J., "The Stress Ratio Effect on Fatigue Crack Growth in 2024-T3 Alclad and the Relationship to Crack Closure," Technische Hogeschool, Delft Memorandum M-336, Delft, Aug. 1979.

S. J. Maddox[1]

Influence of Tensile Residual Stresses on the Fatigue Behavior of Welded Joints in Steel

REFERENCE: Maddox, S. J., **"Influence of Tensile Residual Stresses on the Fatigue Behavior of Welded Joints in Steel,"** *Residual Stress Effects in Fatigue, ASTM STP 776,* American Society for Testing and Materials, 1982, pp. 63-96.

ABSTRACT: Fatigue tests were carried out on fillet welded joints in four steels, with yield strengths ranging from 332 to 727 N/mm^2, under various applied load ratios. Some specimens were stress-relieved but most were spot-heated to ensure that high tensile residual stresses, as would be present in as-welded joints in real structures, were present in the specimens. The aim was to investigate the effect of tensile residual stresses on the fatigue behavior of fillet welded joints under different load ratios and the relevance of the tensile strength of the steel, particularly in relation to the magnitude of residual stresses developed.

In the present specimens, the residual stresses were no higher in the high-strength steels than the mild steels, with the result that the tensile strength of the steel had no effect on the fatigue strength of the joints in both the as-welded and the stress-relieved conditions. Furthermore, it was found that for the range of R-values used ($R = -\infty$ (zero compression to $R = 0.67$) applied load ratio had little effect on the fatigue strength of the as-welded joints provided that "failure" under compressive loading was taken to be a crack length less than or equal to that at which the rate of crack growth began to decrease. Stress relief was only partially effective, with the result that applied compressive stresses were still damaging. Thus under partly compressive loading the fatigue strength of the joint increased but not greatly. However, stress relief had no effect on the fatigue strength of the joint when it was subjected to tension loading.

KEY WORDS: fatigue tests, weldments, fillet welds, structural steels, low alloy steels, residual stresses, stress relieving, ultimate tensile strength, crack propagation, design

Nomenclature

a	Half-crack length (measured on plate surface)
K_t	Elastic stress concentration factor
S	Applied stress range[2]
σ_R	Residual stress
σ_L	Residual stress acting along specimen
σ_{max}	Maximum principal residual stress
R	Stress ratio, $\dfrac{\text{algebraic minimum applied stress}}{\text{algebraic maximum applied stress}}$

[1]Head of Fatigue Laboratory, The Welding Institute, Cambridge, England.
[2]Stresses are given in N/mm^2 (1 N/mm^2 = 1 MPa = 0.1450 ksi).

Most recent fatigue design rules for steel welded structures [*1-5*] are based on stress range regardless of applied mean stress in order to take account of the presence of high tensile residual stresses which arise as a result of welding [*6*].[3] In some cases—for example, the U. S. rules [*1*]—purely compressive applied cyclic stresses can be ignored, but in others [*2-4*] even they are treated as if they were tensile. The actual effect of tensile residual stresses will depend on their magnitude; in this context it may be noted that most laboratory test specimens used to generate the data upon which fatigue design *S-N* curves are based were too small to contain very high residual stresses [*7,8*]. However, for design purposes the conservative assumption must be made that in real structures tensile residual stresses will be at their highest, that is, of yield stress magnitude. For such conditions, it can be shown [*6*] that even applied stresses which cycle from zero to compression are effectively as damaging as applied tensile stresses when they are superimposed onto the residual stress.

Although the stress range approach to design has a sound theoretical basis, relatively few test data have been obtained to justify it for all conditions [*7*] and further work is needed to explore circumstances under which the approach may be over-conservative or even unsafe. This need is heightened by the fact that few laboratory test specimens will have contained residual stresses whose magnitudes were representative of those which could arise in real structures, so that conclusions based on such tests may be misleading when applied to welded joints containing high tensile residual stresses. In this paper, some aspects of the influence of tensile residual stresses are considered on the basis of fatigue tests carried out on fillet welded joints in steel.

Firstly, the consequences of fatigue damage occurring under purely compressive applied stresses need clarifying. There is no doubt that fatigue cracks will initiate under compressive stresses in fields of residual tensile stress [*7*], but it can be argued that they will eventually propagate outside the zone of influence of the original residual stress and stop propagating before they reach a critical size. The progress of fatigue cracks under compressive applied stresses was investigated in the present work.

The fact that fatigue cracking can occur under applied compressive stresses is probably the most striking effect of tensile residual stresses, and investigations have tended to concentrate on demonstrating the equivalence of applied part or fully compressive stress ranges and the stress range for zero-tension loading [*7*]. However, it is possible that the combination of high tensile residual stresses and a high tensile applied mean stress will lead to further reduction in fatigue strength, which would make the current design rules unconservative. Theoretically, the equivalence should hold for high tensile mean stresses [*6*], but the theoretical analysis assumes elastic conditions and the validity of this assumption would decrease with increased tensile applied stress. To investigate this possibility, fatigue tests were carried out under high positive stress ratios.

[3]The italic numbers in brackets refer to the list of references appended to this paper.

Another factor which might make the current design rules unconservative is the effect of the tensile strength of the steel. Work so far has concentrated on medium strength steels, but if it is found that the magnitude of residual stresses increases with increased material yield strength, the higher residual stresses produced in welded high-strength steels could lead to a reduction in their fatigue strengths as compared with those for lower strength steels. Residual stress measurements in butt welds in high-strength steels reported by Satoh [*9*] show that residual stresses can be higher in high-strength steels than in mild steels, but not in proportion to their yield strengths. For example, whereas yield strength residual stresses were found in a mild steel, those in HY80 high-strength low-alloy steel (yield strength 550 N/mm^2) were only 70 percent of yield and those in a higher strength alloy steel with a yield strength of 900 N/mm^2 were only 60 percent of yield. Satoh [*9*] discusses the level of residual stress which can arise during welding in terms of the transformation temperature, the amount of expansion which accompanies transformation from austenite, and the variation of material yield strength with temperature. He shows that in alloy steels, chiefly because of the lower transformation temperature range, and therefore higher strength at transformation, and greater amount of expansion during transformation, yield stress residual stresses will not arise, whereas in mild steel they could.

The magnitude of residual stress is likely to be most significant in joints loaded in compression. As discussed by Gurney [*6*], there is a limiting applied compressive stress S, which, when superimposed onto the tensile residual stress, produces an effective stress of zero. Thus, above S the effective stress is compressive, and therefore not damaging, and there will be no further reduction in fatigue life. This stress depends on the stress concentration due to the weld detail (K_t) and the magnitude of the tensile residual stress (σ_R), so that

$$K_t S = \sigma_R \tag{1}$$

or

$$S = \frac{\sigma_R}{K_t} \tag{2}$$

Clearly, for a given weld detail, S increases with σ_R so that the limiting stress S will be higher in a high-strength steel than in mild steel.

In order to investigate the effect of material strength on residual stress developed and fatigue strength, comparative tests were performed on four steels (two structural and two high strength).

Current fatigue design rules do not distinguish between as-welded and stress-relieved welded joints, it being assumed that stress-relieved joints will be treated in the same way as as-welded joints and designed on the basis of applied stress range regardless of stress ratio. This should prove reasonable for joints loaded in tension, since then the behavior of as-welded and stress-relieved joints is similar [*6*], apart from a possible increase in the fatigue limit due to stress-relief [*7*] accompanied by a slight rotation of the S-N curve [*8*]. However, the stress range approach will be overconservative for stress-relieved joints subjected to compressive stresses since, in the absence of tensile residual stresses, such stresses should be largely nondamaging. An extensive program of work involving tests on many types of joints is needed before the design rules can be modified to take account of stress relief. However, the opportunity was taken in the present investigation to test some specimens in the stress-relieved condition in order to provide an initial indication of the benefits of stress relief.

Experimental Details

Materials

The test specimens were fabricated from four different steels: a mild steel, a carbon-manganese structural steel (to British Standard Specification BS 4360 Grade 50B), and two higher strength low-alloy quenched and tempered steels (Superelso S70, made in France by Creusot-Loire, and QT445A, which is made by the British Steel Corporation). The chemical analyses and tensile properties of the steels are given in Table 1. As will be seen, the steels covered a range of yield strengths from 332 to 727 N/mm^2. The specimens were fabricated so that the direction of stressing would be parallel to the rolling direction of the plate.

Specimen Design

Welded joints can fail by fatigue in a number of ways, depending on the weld detail and orientation with respect to the loading, but by far the most common way is by fatigue crack propagation from the weld toe under stresses acting essentially transverse to the weld. Therefore a weld detail which would fail in this way was chosen for the present investigation.

The test specimen used consisted of a 12.5-mm-thick plate with a longitudinal attachment fillet welded to one surface (Fig. 1). The fillet weld was carried on around the ends of the attachment, thus providing two regions where the weld toe lay transverse to the direction of loading and therefore two sites for fatigue cracking. This design was chosen because, from experience, the fatigue results obtained from such joints tend to exhibit little scatter. In addition, by limiting the sites for fatigue cracking to two small areas of weld, the detection and monitoring of fatigue cracking was made easier.

The welds were made in the flat position using the conditions given in Table 2. In every case the weld was continuous around the ends of the attachment, the stop–start positions being in the middle of the attachments.

Residual Stresses

To ensure that the required high tensile residual stresses were present in the regions where fatigue cracking would take place, some test specimens were spot-heated [*6*]. Two high-output oxy-propane heating torches were used to heat the specimens (Fig. 2*a*) for sufficient time to leave a 50-mm-diameter spot after heating. The conditions corresponded to the attainment of a heat spot which was

TABLE 1—*Material properties.*

Steel	Chemical Composition, Element Weight, %														
	C	S	P	Si	Mn	Ni	Cr	Mo	V	Cu	Cb	Ti	Al	Sn	Co
Mild steel	0.34	0.014	0.017	0.31	0.84	0.01	0.01	<0.01	<0.01	0.02	<0.005	<0.01	0.049	<0.01	<0.01
BS 4360 Grade 50B	0.16	0.012	0.011	0.41	1.37	0.02	0.01	<0.01	<0.01	0.02	0.031	<0.01	0.035	<0.01	<0.01
Superelso S70	0.17	0.013	0.011	0.35	1.43	0.81	0.79	0.22	0.01	0.33	<0.005	<0.01	0.042	0.02	0.02
QT445A	0.18	0.017	0.023	0.46	1.00	0.03	0.82	0.30	0.01	0.05	<0.005	<0.01	0.072	<0.01	<0.01

Tensile Properties

Steel	Yield Strength, N/mm^2	Ultimate Tensile Strength, N/mm^2	Elongation, %	Reduction in Area, %
Mild steel	332	600	33	52
BS 4360 Grade 50B	364	540	39	72
Superelso S70	672	800	25	55
QT445A	727[a]	834	23	65

[a] 0.2 percent proof stress.

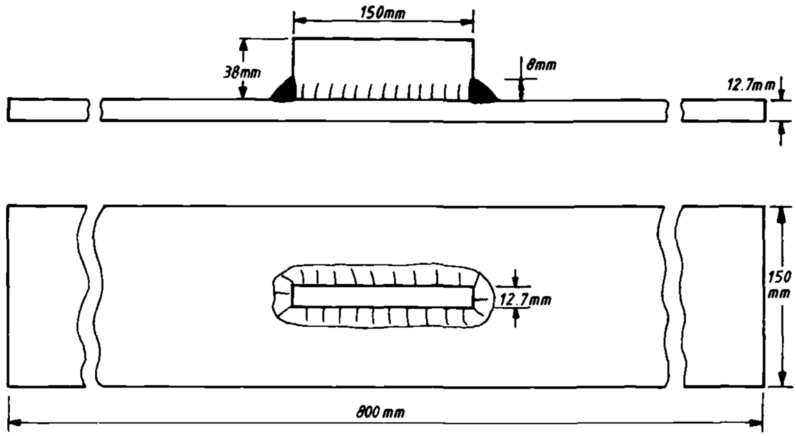

FIG. 1—*Test specimen.*

TABLE 2—*Welding conditions.*

Steel	Number of Weld Passes	Weld Leg Length, mm	Electrode Diameters, mm 1	2	3	Electrode Type	Additional Comments
Mild steel	2	8	3.25	4.0	···	BS 639, E 4333R (AWS E6013)	···
BS 4360 Grade 50B	2	8	3.25	5.0	···	BS 639, E 4333R (AWS E6013)	···
Superelso S70	3	8	4.0	4.0	4.0	BS 639, E 5133B (AWS E7016)	preheat to 100 °C; electrodes dried at 450 °C for 1 h
QT445A	2	8	3.25	4.0	···	BS 639, E 5133B (AWS E7016)	preheat to 100 °C; electrodes dried at 450 °C for 1 h

cherry red in color. The specimens were left to cool in still air. Spot-heating produces radial tensile residual stresses within the spot, balanced by compressive residual stresses acting tangentially outside the spot [*6*] (Fig. 2*b*). Thus the whole of the weld toe at the ends of the attachments should have been left in a field of tensile residual stress. These specimens are referred to as "as-welded".

To ensure that high tensile residual stresses were produced, they were measured using the center-hole drilling technique [*10*], usually in two specimens of each steel. Strains were converted to stresses assuming elastic behavior.

Some specimens were thermally stress-relieved by heating them for 1 h in the range of 580 to 620°C in the case of the carbon steels and at 600°C in the case

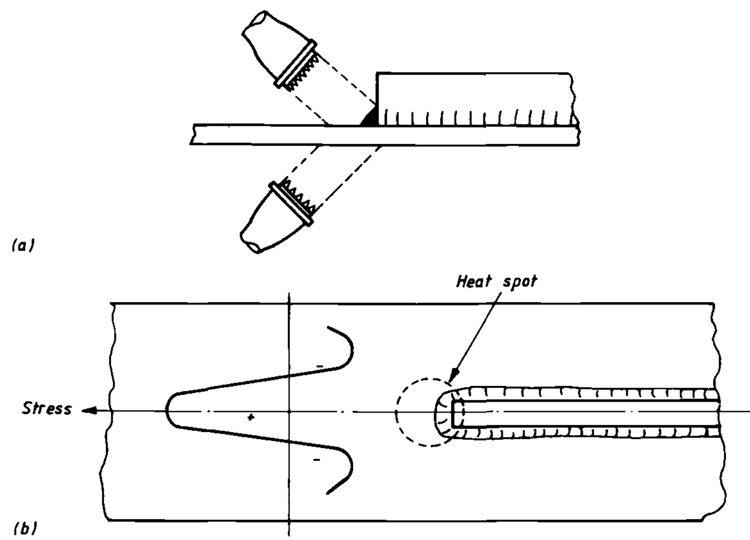

FIG. 2—(a) *Positions of heating torches during spot-heating.* (b) *Form of residual stress distribution produced.*

of the two low-alloy quenched and tempered steels. Again, residual stress levels were checked.

Fatigue Testing

The specimens were tested axially under a number of stress ratios R. Five stress ratios were used in the tests of the "as-welded" specimens, namely zero-compression ($R = -\infty$), alternating loading ($R = -1$), zero-tension loading ($R = 0$), and tension-tension loading with $R = 0.5$ and 0.67, although due to a shortage of material the high-strength steel specimens were not tested with $R = 0$. The stress-relieved specimens were tested only with $R = -1$, 0.5, and 0.67. It has already been shown that fatigue failure is unlikely to occur under zero-compression loading in such specimens [7]. The tests were carried out in hydraulic and servo-hydraulic testing machines at frequencies between 5 and 17 Hz. Care was taken to ensure that a tensile load was not applied to the specimens which were to be tested in compression when they were being set up for test, since this could influence the fatigue behavior of the joint.

Fine wires connected to the testing machine cut-out circuit were glued to the plain surfaces of the specimens opposite the weld in order to interrupt the test when a through-thickness crack was present. The test was then continued and the progress of cracking observed. In the case of specimens tested under zero-compression loading, as anticipated, it was found that the rate of crack growth decreased as a crack propagated from the weld and the associated tensile residual stress field, and in those cases the tests were terminated before failure. For all other stress ratios, fatigue cracks continued to propagate and the specimens were tested to complete failure.

Test Results

The residual stresses acting in the longitudinal direction (σ_L)—that is, in the direction of loading in the fatigue tests—are given in Table 3. Normally, they were close to the maximum principal stress (σ_{max}), which is also given.

The fatigue test results are given in Tables 4 to 7. Two values of the fatigue endurance are given. The first of these, if detected, was the number of cycles needed to produce a through-thickness crack, while the second was "failure". For specimens tested in compression, this was defined as the endurance at which the rate of crack growth started to decrease, as discussed later. The surface crack length at that time is included in the Tables. The results are also plotted on *S-N* diagrams in terms of the number of cycles to "failure", the as-welded in Fig. 3 to 6*a* and the stress-relieved in Figs. 7 to 10.

Discussion

Residual Stresses

Referring to the results for the "as-welded" specimens in Table 3, it will be seen that, as anticipated, high tensile residual stresses were present. However, their magnitudes did not increase with material tensile strength. In fact, the highest measured were those in the lowest strength steel and then they exceeded yield, whereas in the high-strength steels the level of residual stress was less than half yield. This was surprising in view of the results reported by Satoh [9], from which residual stresses of 400 to 500 N/mm^2, 60 to 70 percent of yield, would be expected. However, using the hole-drilling technique, residual stresses 10 mm from the weld toe were measured and it is possible that they may not have been as high as those at the toe. Another possible explanation for the low residual stresses in the high-strength steels is that the test specimens were too narrow to accommodate the high levels expected. Insufficient material was available to explore this using the present steels, but residual stress measurements made on a larger specimen, 300 mm wide, in a steel similar to QT445A confirmed that higher residual stresses could occur. In that case, the yield strength of the steel was 824 N/mm^2 and residual stresses of 400 to 500 N/mm^2 were introduced by spot heating.

The results in Table 3 for stress-relieved joints show that stress relief may not have been as effective as might have been expected. Although the residual

TABLE 3—*Residual stress measurements.*

Steel	Yield Strength, N/mm^2	Residual Stress, N/mm^2			
		Spot-Heated		Stress-Relieved	
		σ_{max}	σ_L	σ_{max}	σ_L
Mild steel	332	370 to 448	260 to 448	19 to 41	19 to 41
BS 4360 Grade 50B	364	263 to 395	207 to 260	7 to 61	0 to 60
Superelso S70	672	256	226	61	60
QT445A	727	325 to 346	325 to 343	84 to 124	83 to 124

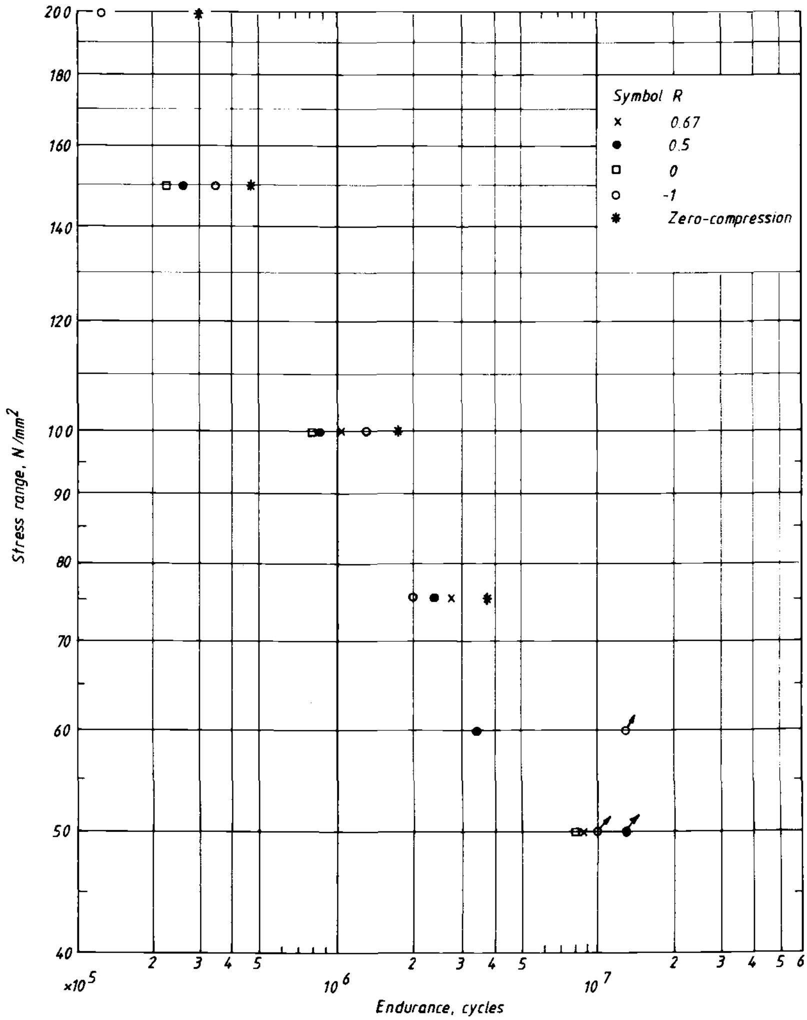

FIG. 3—*Fatigue test results for as-welded mild steel specimens.*

stresses were virtually eliminated in some specimens, comparatively high stresses in relation to typical fatigue design stresses were left in most of them.

Fatigue Crack Propagation

In the present specimens, fatigue cracks propagated from the weld toe through the plate thickness and then across the plate width as a through-thickness crack (Fig. 11). The specimen shown in Fig. 11 was tested in tension and eventually failed when the ligament fractured. The same occurred in specimens tested with $R = -1$. However, as anticipated, specimens loaded purely in compression did not fracture. Some typical results illustrating how cracking developed are shown

TABLE 4—*Fatigue test results obtained from mild steel specimens.*

Condition	Specimen Number	Stress Ratio (R)	Stress Range, N/mm^2	Cycles to Through-Thickness Cracking	Surface Crack Length, mm	Cycles to Failure	Criterion of Failure
As-welded	544	0.67	100	956 600	...	1 004 000	rupture
	548	0.67	75	2 466 500	45	2 746 100	rupture
	541	0.67	50	7 549 600	44	8 343 000	rupture
	547	0.5	150	252 800	45	266 900	rupture
	545	0.5	100	754 600	44	844 000	rupture
	536	0.5	75	2 023 000	43	2 293 300	rupture
	549	0.5	60	...	...	3 294 500	rupture
	535	0.5	50	...	...	12 223 000	unbroken
	753	0	150	199 700	46	226 350	rupture
	754	0	100	705 800	53	787 880	rupture
	755	0	50	7 101 000	45	8 014 700	rupture
	546	−1	200	106 900	50	124 000	rupture
	537	−1	150	293 000	43	342 700	rupture
	539	−1	100	...	—	1 245 800	rupture
	538	−1	75	1 660 800	48	1 966 000	rupture
	581	−1	60	...	—	12 605 000	unbroken
	584	−1	50	...	—	10 000 000	unbroken
	550	zero-compression	200	188 000	46	300 000	80 mm crack
	542	zero-compression	150	419 600	48	475 000	75 mm crack

	543	zero-compression	100	1 649 000	47	1 750 000	72 mm crack
	540	zero-compression	75	3 267 800	39	3 736 500	86 mm crack
Stress-relieved	552	0.67	100	830 000	40	896 400	rupture
	553	0.67	75	2 321 500	46	2 602 700	rupture
	585	0.67	60	...	...	10 000 000	unbroken
	556	0.67	50	...	...	10 004 000	unbroken
	551	0.5	150	254 100	53	259 900	rupture
	557	0.5	100	860 000	46	940 600	rupture
	555	0.5	75	1 799 100	48	1 976 500	rupture
	752	0	150	206 800	39	243 100	rupture
	750	0	100	933 000	47	1 036 900	rupture
	589	0	75	...	...	11 423 000	unbroken
	587	0	60	...	...	10 000 000	unbroken
	751	0	50	...	...	12 260 000	unbroken
	558	−1	200	173 000	46	221 600	rupture
	554	−1	150	1 272 900	...	1 508 800	rupture
	749	−1	150	672 300	45	797 000	rupture
	559	−1	100	1 042 000	44	1 327 400	rupture
	588	−1	100	...	...	16 648 000	unbroken
	748	−1	75	...	...	18 328 000	unbroken

TABLE 5—*Fatigue test results obtained from BS 4360 Grade 50B specimens.*

Condition	Specimen Number	Stress Ratio (R)	Stress Range, N/mm^2	Cycles to Through-Thickness Cracking	Surface Crack Length, mm	Cycles to Failure	Criterion of Failure
As-welded	466	0.67	100	960 400	...	1 012 200	rupture
	473	0.67	75	3 028 700	42	3 414 300	rupture
	460	0.67	50	6 501 100	46	7 106 000	rupture
	471	0.5	150	252 300	48	270 700	rupture
	470	0.5	100	809 700	46	893 900	rupture
	461	0.5	75	1 769 500	43	2 138 200	rupture
	462	0.5	50	6 703 200	43	7 762 600	rupture
	766	0	150	186 300	47	217 960	rupture
	764	0	100	670 200	47	766 990	rupture
	765	0	50	512 143	43	6 065 600	rupture
	472	−1	200	115 240	53	136 470	rupture
	469	−1	150	180 100	47	236 800	rupture
	468	−1	100	693 400	46	873 800	rupture
	464	−1	75	1 352 000	50	1 716 600	rupture
	593	−1	50	...	...	21 800 000	unbroken
	474	zero-compression	200	548 500	43	650 000	65 mm crack
	763	zero-compression	200	223 000	45	325 000	75 mm crack
	463	zero-compression	150	223 500	48	300 000	80 mm crack

	467	zero-compression	100	1 010 400	50	1 093 600	75 mm crack
	465	zero-compression	75	1 568 800	50	1 796 000	94 mm crack
	594	zero-compression	60	...	...	11 300 000	unbroken
	592	zero-compression	50	...	...	10 000 000	unbroken
Stress-relieved	478	0.67	100	882 900	39	973 100	rupture
	475	0.67	75	2 539 800	47	2 858 400	rupture
	484	0.67	50	6 834 000	42	7 619 800	rupture
	483	0.5	150	215 700	47	235 400	rupture
	481	0.5	100	811 270	47	911 000	rupture
	479	0.5	75	1 794 800	44	2 044 000	rupture
	476	0.5	50	...	...	13 425 300	unbroken
	759	0	150	255 200	37	309 400	rupture
	758	0	100	1 500 000	41	1 664 500	rupture
	599	0	75	...	...	7 400 000	unbroken
	597	0	60	...	...	12 254 000	unbroken
	760	0	50	...	...	19 092 000	unbroken
	762	−1	200	405,300	50	461 100	rupture
	477	−1	150	1 751 530	46	1 953 900	rupture
	596	−1	110	...	...	2 438 000	rupture
	598	−1	110	...	...	2 323 000	rupture
	482	−1	100	...	...	12 127 500	unbroken
	480	−1	100	...	...	10 710 900	unbroken
	761	−1	100	...	...	10 200 000	rupture

TABLE 6—*Fatigue test results obtained from Superelso S70 specimens.*

Condition	Specimen Number	Stress Ratio (R)	Stress Range N/mm^2	Cycles to Through-Thickness Cracking	Surface Crack Length, mm	Cycles to Failure	Criterion of Failure
As-welded	490	0.67	100	864 600	47	969 900	rupture
	486	0.67	50	4 175 000	45	4 975 500	rupture
	494	0.5	150	236 000	42	283 200	rupture
	492	0.5	100	564 560	54	644 520	rupture
	491	0,5	75	1 418 500	48	1 668 600	rupture
	487	0.5	50	6 241 000	44	7 085 000	rupture
	496	−1	200	142 360	33	219 000	rupture
	493	−1	150	275 780	48	363 200	rupture
	495	−1	100	622 500	50	947 900	rupture
	489	−1	75	1 407 000	42	2 063 100	rupture
	498	zero-compression	200	246 500	42	400 000	70 mm crack
	499	zero-compression	150	373 300	62	500 000	70 mm crack
	488	zero-compression	100	527 300	46	600 000	65 mm crack
	640	zero-compression	75	2 787 000	44	3 100 000	75 mm crack
Stress-relieved	505	0.67	125	360 600	45	409 700	rupture
	507	0.67	100	690 500	47	802 100	rupture
	503	0.67	75	1 885 000	41	2 237 400	rupture
	504	0.67	50	8 274 500	43	9 306 300	rupture
	500	0.5	150	267 600	45	310 200	rupture
	506	0.5	100	663 700	45	771 00	rupture
	501	0.5	75	1 565 000	43	1 836 500	rupture
	509	−1	200	247 300	44	370 200	rupture
	508	−1	150	569 670	46	928 800	rupture
	502	−1	100	. . .	. . .	9 422 100	unbroken

TABLE 7—*Fatigue test results obtained from QT445A specimens.*

Condition	Specimen Number	Stress Ratio (*R*)	Stress Range, N/mm^2	Cycles to Through-Thickness Cracking	Surface Crack Length, mm	Cycles to Failure	Criterion of Failure
As-welded	523	0.67	100	723 200	70	755 700	rupture
	512	0.67	75	1 500 500	48	1 863 000	rupture
	516	0.67	50	4 256 000	42	5 150 900	rupture
	519	0.5	150	206 400	54	240 400	rupture
	517	0.5	100	580 800	69	621 600	rupture
	510	0.5	75	1 174 400	44	1 453 900	rupture
	524	0.5	50	5 796 800	42	6 461 600	rupture
	520	−1	200	92 800	45	184 500	rupture
	511	−1	150	277 900	45	504 400	rupture
	522	−1	100	2 212 400	44	2 854 600	rupture
	515	−1	75	1 603 200	66	1 833 000	rupture
	571	zero-compression	450	31 000	48	55 000	77 mm crack
	574	zero-compression	300	82 500	43	120 000	73 mm crack
	518	zero-compression	200	232 800	44	473 000	78 mm crack
	521	zero-compression	150	438 300	49	1 346 100	80 mm crack
	570	zero-compression	100	1 032 700	46	1 138 500	71 mm crack
	513	zero-compression	75	1 800 000	...	2 028 000	72 mm crack
Stress-relieved	529	0.67	100	637 400	50	753 500	rupture
	527	0.67	75	3 168 600	50	3 447 000	rupture
	526	0.67	50	5 250 300	46	5 950 400	rupture
	534	0.5	150	216 600	47	262 600	rupture
	533	0.5	100	655 100	44	770 500	rupture
	531	0.5	75	1 918 300	44	2 193 100	rupture
	525	0.5	50	...	...	12 495 000	unbroken
	532	−1	150	272 700	47	476 200	rupture
	530	−1	100	588 900	44	1 756 600	rupture
	575	−1	75	...	...	10 738 000	unbroken

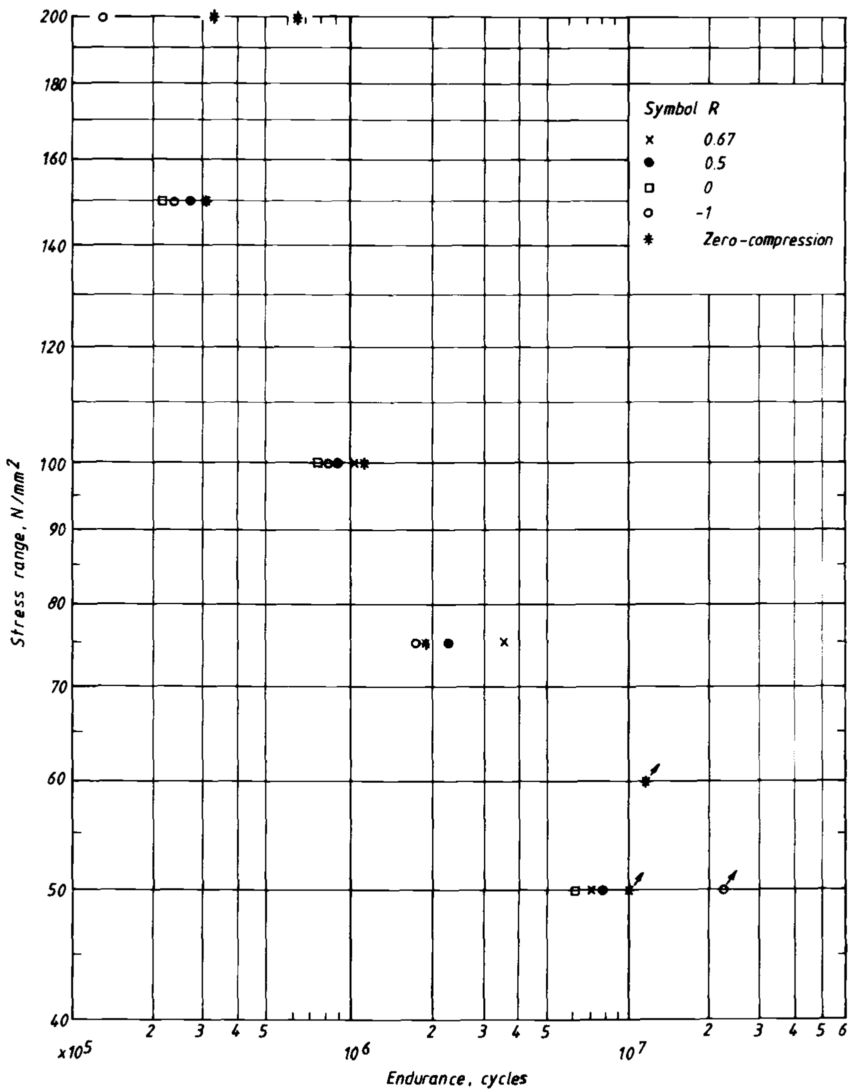

FIG. 4—*Fatigue test results for as-welded BS 4360 Grade 50B specimens.*

in Fig. 12. The surface crack length 2*a* is plotted; 2*a* was usually 40 to 50 mm when a crack had grown through the thickness, as noted in Tables 4 to 7. Fracture surface marks indicated that fatigue cracks were 2 to 3 mm deep when they were first detected, at which time 2*a* was on the order of 20 mm. As will be seen, under compressive loading the crack growth rate decreased rapidly as the through-thickness crack propagated away from the weld, indicating that the residual stresses were very small or still compressive, as in the original distribution (Fig. 2*b*), after redistribution resulting from the presence of the crack.

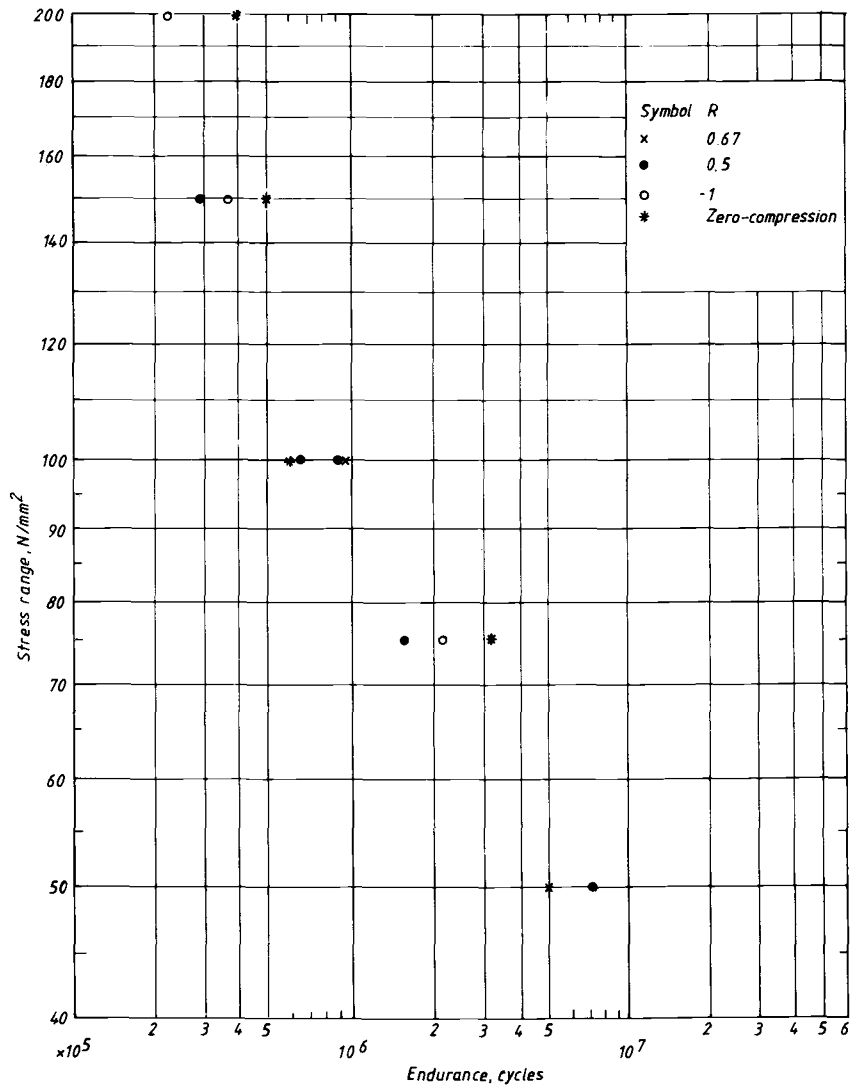

FIG. 5—*Fatigue test results for as-welded Superelso S70 specimens.*

The results obtained partly or fully in tension do not appear to have been influenced by the varying residual stress field. This is confirmed by comparing results obtained under the same loading conditions from "as-welded" and stress-relieved specimens (Fig. 12). As will be seen, the main difference in crack growth rate arose before through-thickness cracking occurred. This may have been due to differences in rates of part-through-thickness crack growth or, more likely, to slight differences in initial conditions at the weld toe—that is, the differences which lead to scatter in fatigue test data.

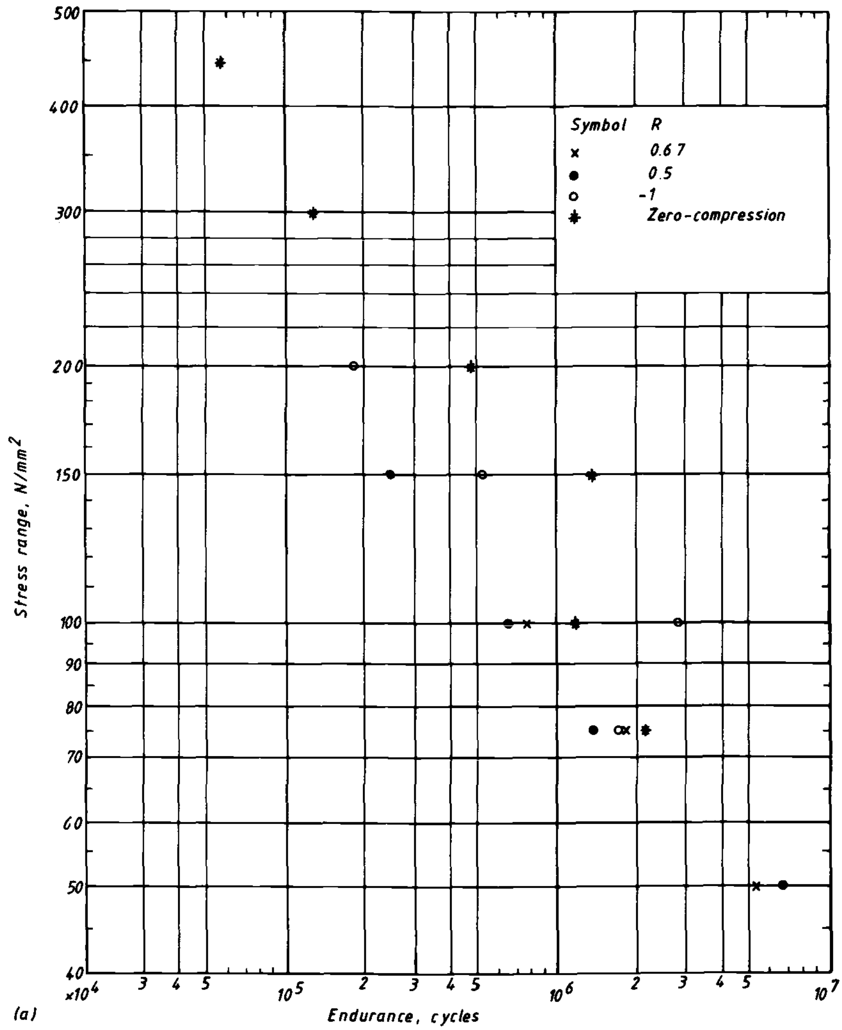

FIG. 6*a*—*Fatigue test results for as-welded QT445A specimens.*

In view of the above behavior, the choice of "failure" criterion in tests carried out in compression is clearly very important, particularly when the results are to be compared with others obtained in tension. The criterion used in the present tests was that the rate of crack propagation started to decrease. This usually occurred when $2a$ was approximately 80 mm, which was fairly typical of the crack size at which fracture occurred in specimens tested in tension. However, it should be noted that it was often difficult to establish precisely when this condition was satisfied, and so some scatter in the test results must be expected. Another possible criterion of failure, perhaps a more suitable one, would be the attainment of a through-thickness crack, since during this stage of the fatigue life the tensile residual stress field should be reasonably uniform. Also, tolerance of

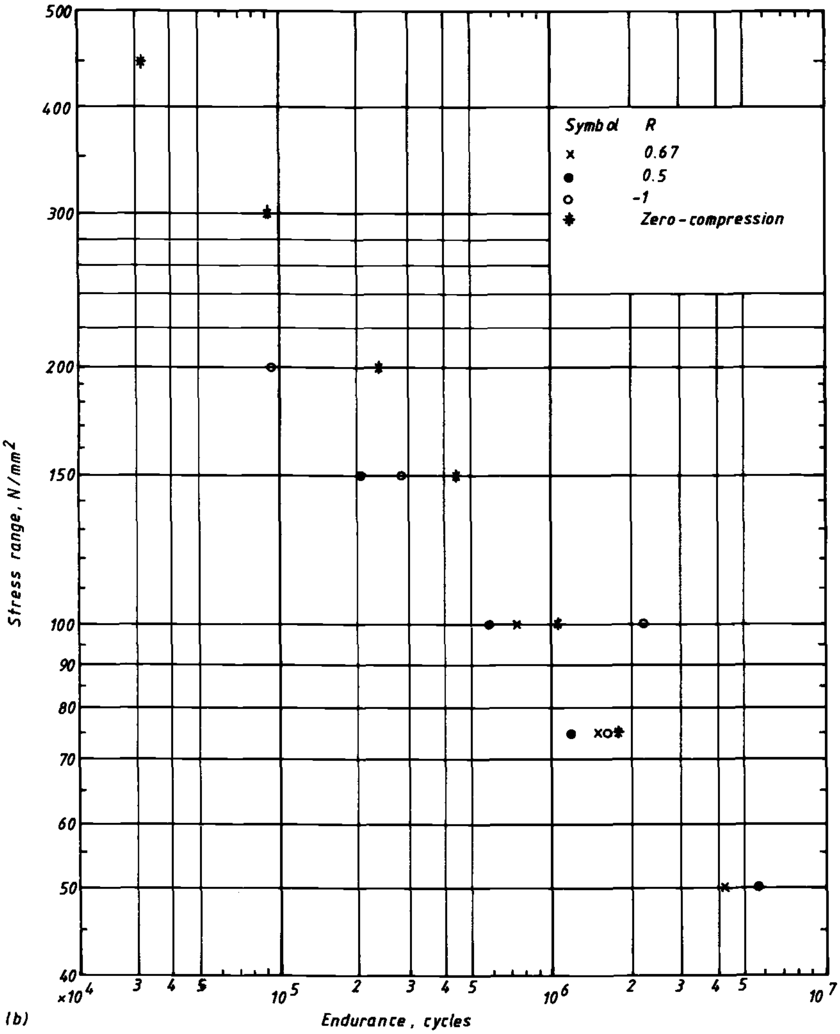

FIG. 6*b* —*Fatigue test results for as-welded QT445A expressed in terms of cycles to produce through-thickness crack.*

a through-thickness crack is a convenient criterion on which to base fracture toughness requirements in joints designed to avoid fracture. The number of cycles required to produce through-thickness cracking is noted in Tables 4 to 7. It is found that plotting the test results in terms of that endurance reduces the scatter, as illustrated for high-strength QT445A specimens in Fig. 6*b*.

Effect of Stress Ratio

As-Welded Joints —The results obtained for as-welded joints are plotted in Figs. 3 to 6. It will be seen that in general there is no consistent influence of stress

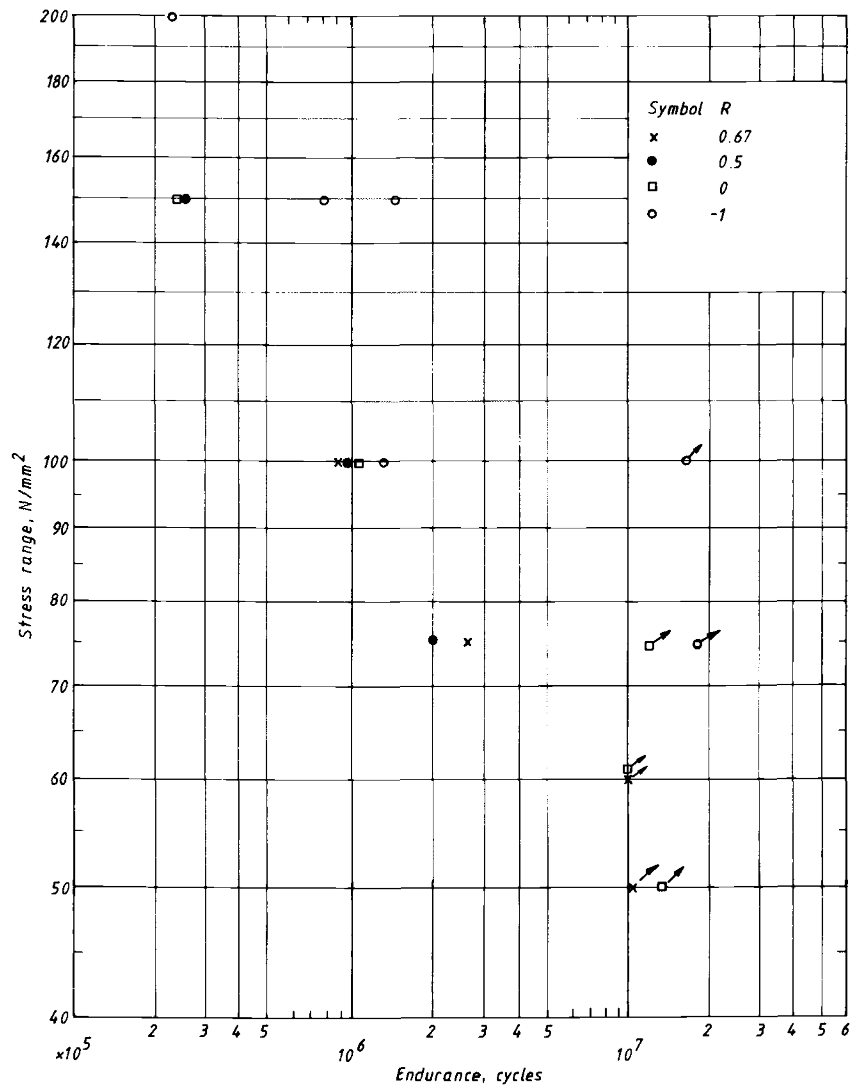

FIG. 7—*Fatigue test results for stress-relieved mild steel specimens.*

ratio, except that results obtained under zero-compression loading usually, but not always, lie near the upper limits of scatter. The same may also be seen from a consideration of the crack propagation results. For example, the results obtained for a stress range of 100 N/mm² are given in Figs. 12 to 15. Apart from the results which refer to long cracks in specimens tested in compression, any large differences between the results generally occurred before cracks were detected, possibly as a result of delayed crack initiation or because, for the joint concerned, the initial weld toe defects were unusually small.

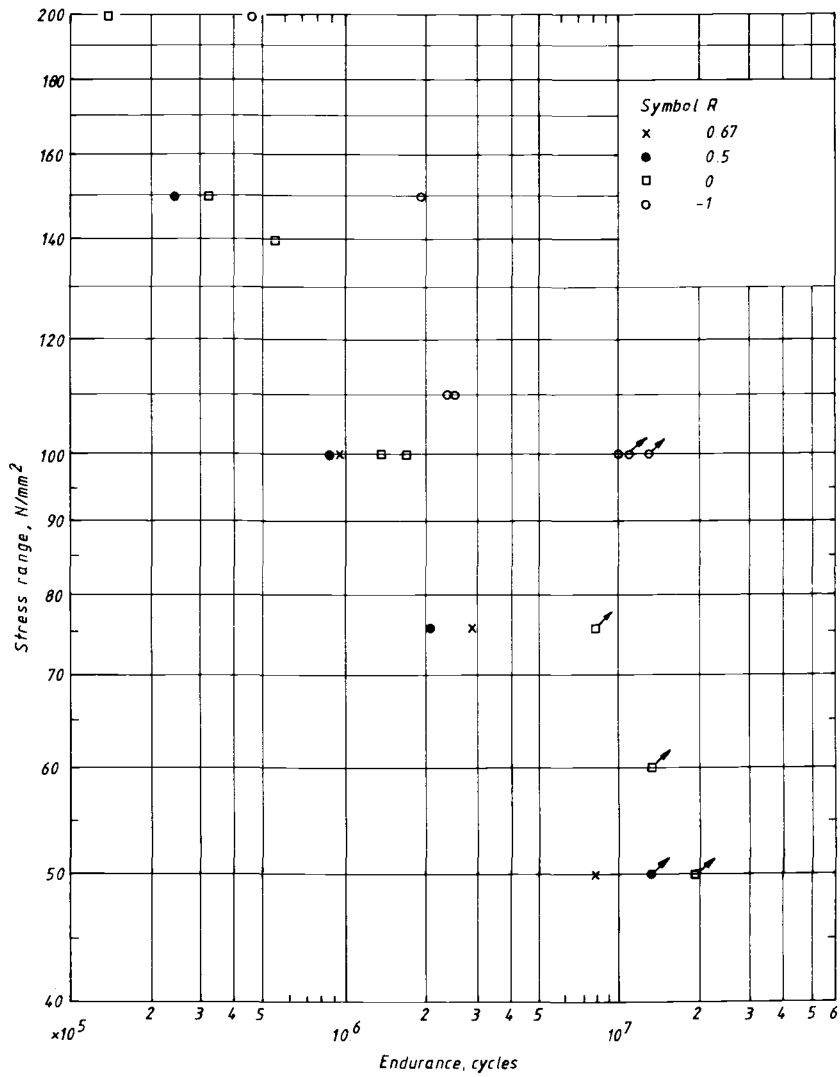

FIG. 8—*Fatigue test results for stress-relieved BS 4360 Grade 50B specimens.*

From the practical point of view, the present results confirm that the proposed method of designing as-welded joints on the basis of applied stress range regardless of applied stress ratio is reasonable for part-or-fully-tensile loading, even for very high R-values, and for fully compressive loading if the occurrence of through-thickness cracking is considered as critical. However, in joints in which a through-thickness fatigue crack propagates away from a weld and its residual stress field, it may be possible to relax the design rules, although of course other consequences of having large but dormant cracks in the structure must be considered.

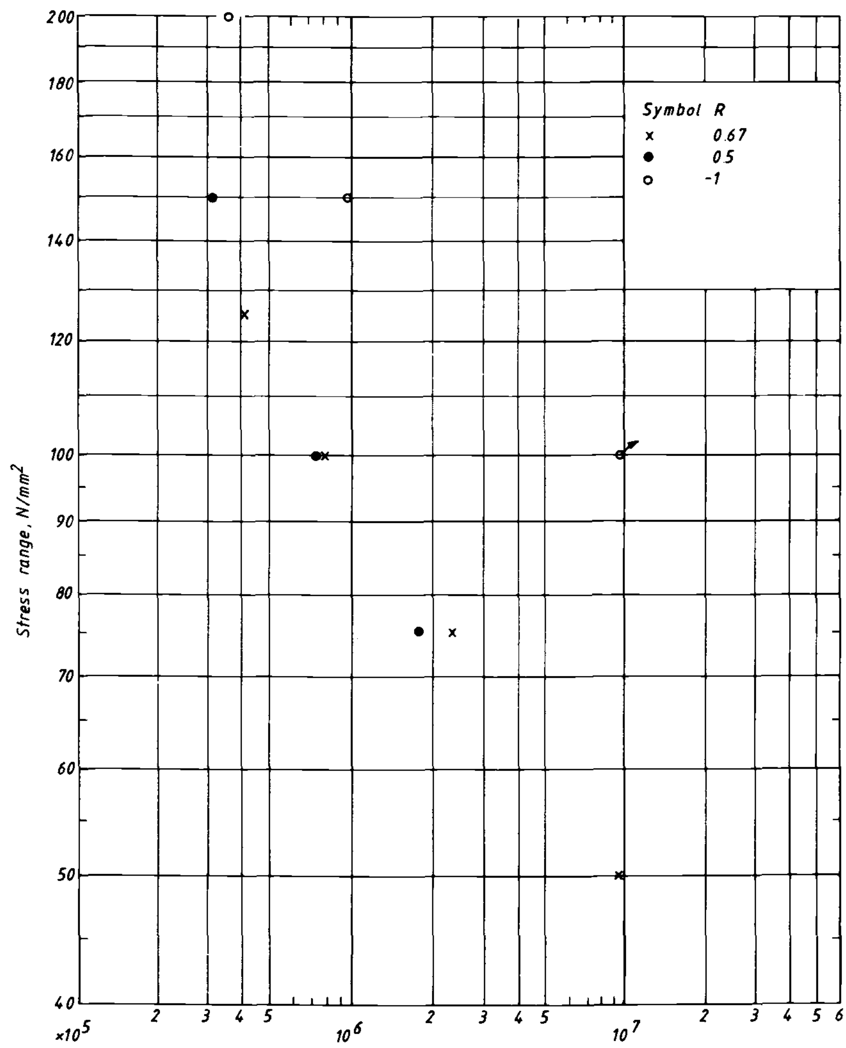

FIG. 9—*Fatigue test results for stress-relieved Superelso S70 specimens.*

Stress-Relieved Joints—The results obtained from stress-relieved joints are plotted in Figs. 7 to 10. It will be seen that, apart from a possible increase in the fatigue limit, there is no consistent influence of R for positive values. This conforms with the results obtained from "as-welded" joints loaded in tension and also with fatigue crack propagation results obtained for structural steels [*11*] which exhibited little effect of R for positive values. The results obtained from stress-relieved joints loaded with $R = -1$ were generally higher than those obtained in tension. The fatigue limit also seemed to be higher. The crack propagation results referred to above [*11*] may be used to assess the likely

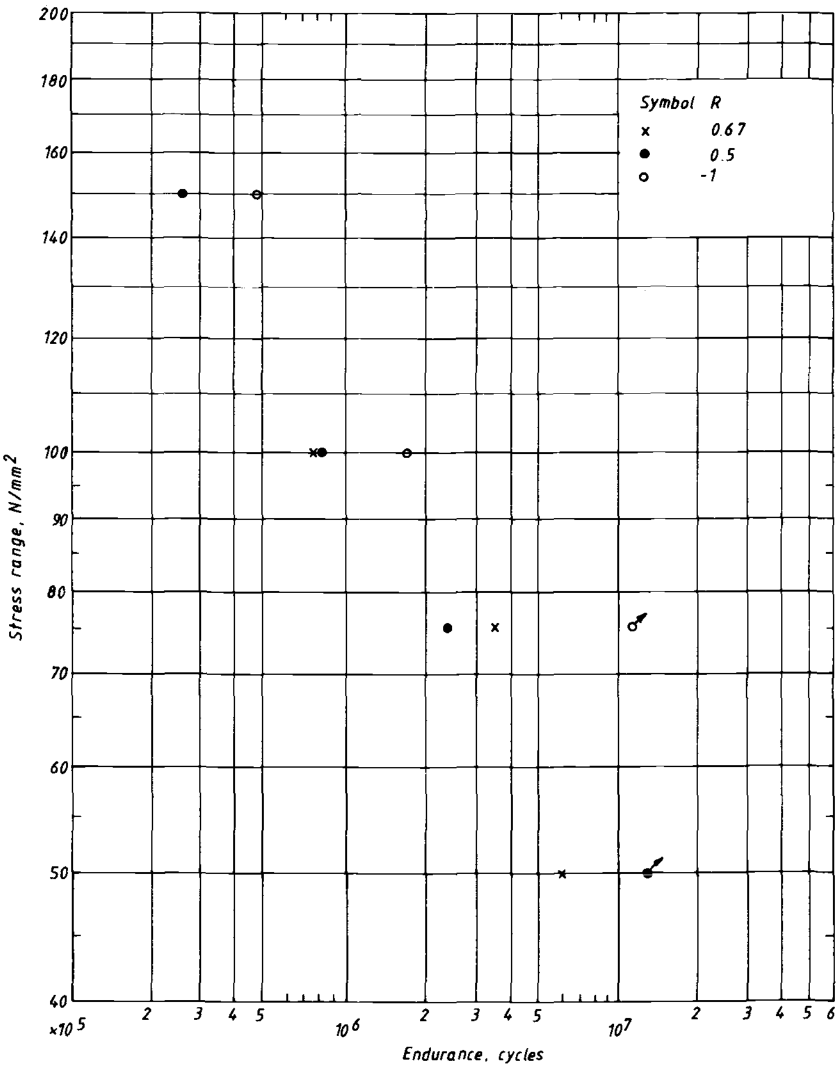

FIG. 10—*Fatigue test results for stress-relieved QT445A specimens.*

influence of R in stress-relieved joints subjected to alternating loading, particularly in relation to the level of residual stress left after stress relief. In the present case, tensile residual stresses ranging from 0 to 124 N/mm^2 were measured in stress-relieved specimens. For the former extreme, the applied stress ratio would be the same as the effective value. Under such circumstances crack propagation results indicate that fatigue lives obtained under alternating loading ($R = -1$) may be expected to be up to ten times greater than those obtained under $R = +0.67$. Such a variation was obtained in the present investigation, particularly in BS 4360 Grade 50B and Superelso S70 joints (Figs. 8 and 9). In the

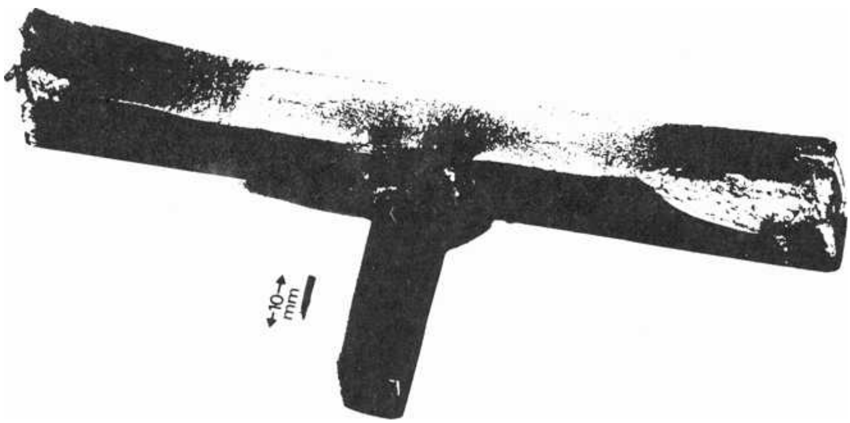

FIG. 11—*Fracture surface of failed specimen.*

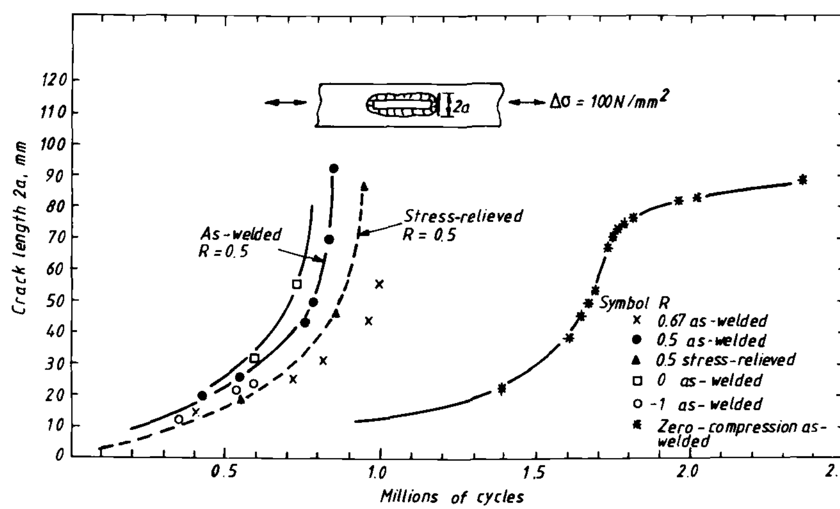

FIG. 12—*Fatigue crack propagation results obtained from mild steel specimens under stress range of 100 N/mm*^{2}.

presence of a tensile residual stress the effective stress ratio is not the same as the applied value. For a residual stress of 124 N/mm^2 an alternating stress of, for example, ± 100 N/mm^2 becomes $+24$ to $+224$ N/mm^2, giving $R \simeq +0.1$. Crack propagation results indicate that there may be no difference between fatigue lives obtained under $R = 0.1$ and $R = 0.67$; however, a variation of lives of up to two may occur. Again this is consistent with the present results, particularly those obtained from QT445A joints (Fig. 10), the joints in which the highest residual stresses after stress relief were measured. Thus it seems reason-

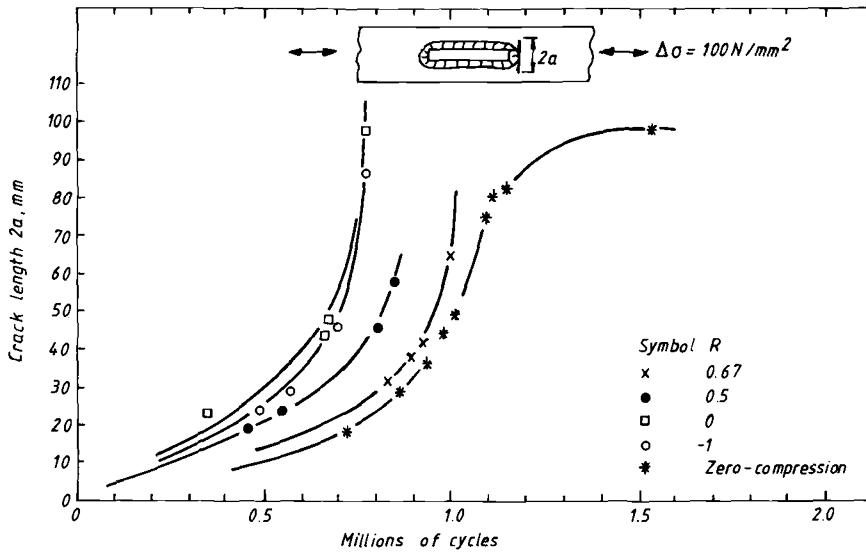

FIG. 13—*Fatigue crack propagation results obtained from as-welded BS 4360 Grade 50B specimens under stress range of 100 N/mm^2.*

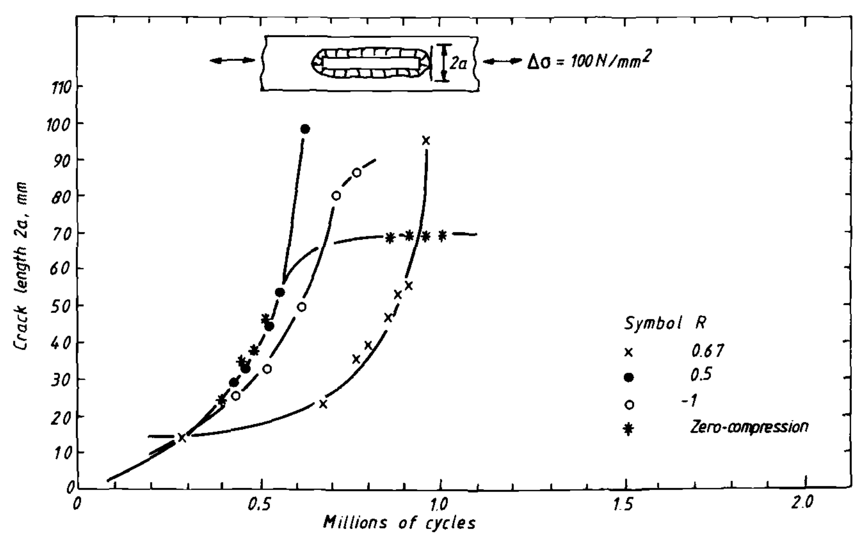

FIG. 14.—*Fatigue crack propagation results obtained from as-welded Superelso steel under stress range of 100 N/mm^2.*

able to suppose that the differences between the results obtained under $R = -1$ and those obtained under positive R-values are attributable to differences in the magnitude of residual stresses left in the specimens after stress relief.

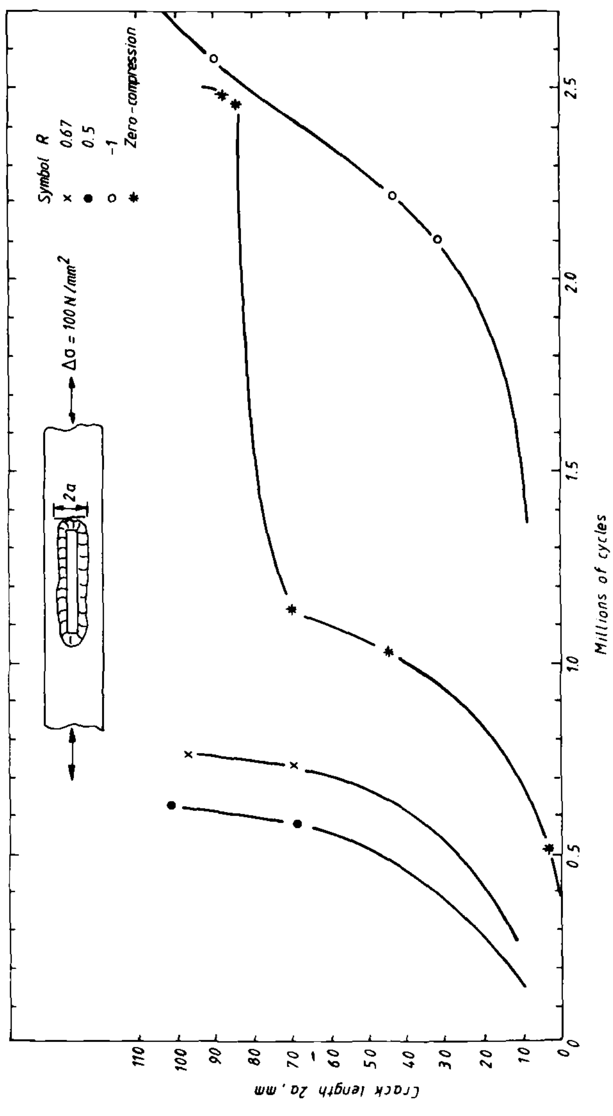

FIG. 15—*Fatigue crack propagation results obtained from as-welded QT445A steel specimens under stress range of 100 N/mm².*

Effect of Tensile Strength

As-Welded Joints—In order to consider the effect of tensile strength on the fatigue strength of the as-welded joints, all the results have been plotted together in terms of the applied stress range and are presented in Fig. 16. Combining the results in this way is justified on the basis of the conclusion reached earlier that for as-welded joints containing high tensile residual stresses the applied stress ratio had little influence on their fatigue strengths. It can be seen in Fig. 16 that in spite of scatter, which is mainly attributable to the results obtained under zero-compression loading, as discussed earlier, there is no consistent influence of the material on the fatigue strengths obtained. For comparison, the 95 percent

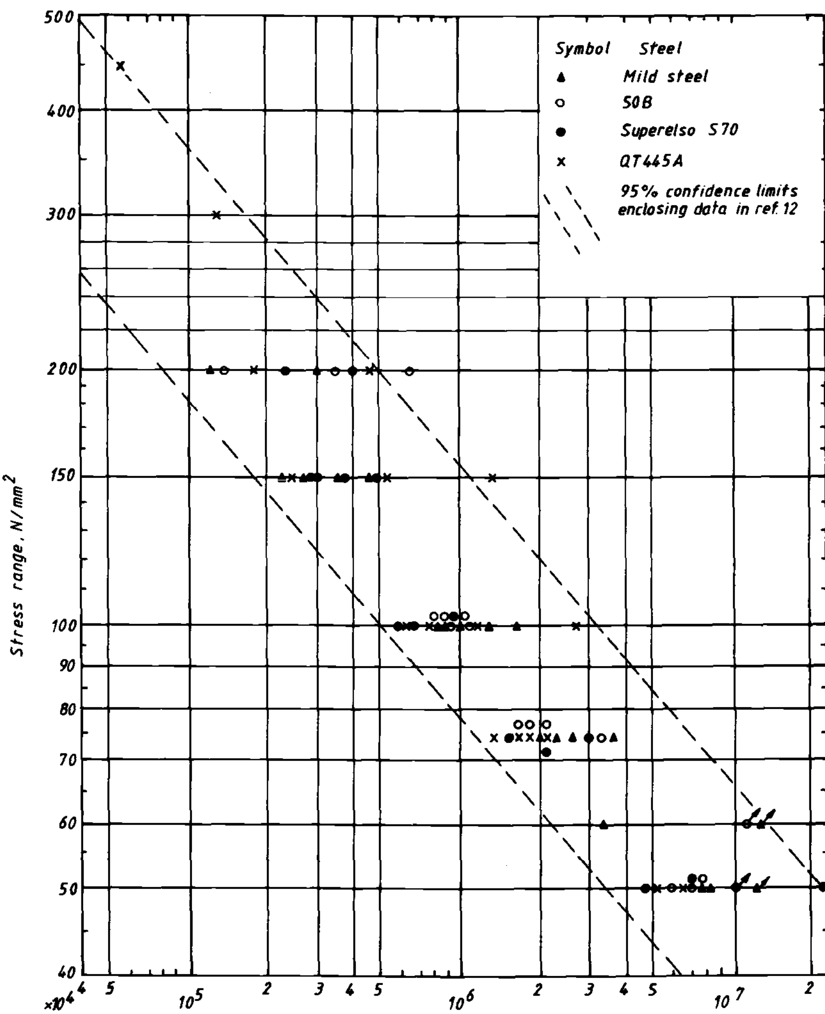

FIG. 16—*All fatigue test results obtained from as-welded specimens.*

confidence limits enclosing results presented in Ref *12* for the same type of joint as that used in the present work are shown. These results were obtained from a number of steels with yield strengths covering approximately the range in the present investigation tested under $R = 0$. As can be seen, there is good agreement between the results. There was no influence of material strength in the results given in Ref *12*.

Thus it may be concluded that fillet welded joints in any of the steels considered should be assumed to have the same fatigue strength. This result is not altogether surprising, since, from the point of view of residual stresses, the present specimens made from high tensile steels did not contain proportionally higher residual stresses than those in specimens made from the lower strength steels.

The relatively low residual stresses in the high-strength steel specimens precluded the investigation of the effect of material strength on the value of the limiting applied compressive stress S above which no further reduction in fatigue life would occur, as discussed in the opening remarks. However, it is interesting to see, particularly from the results for QT445A in Fig. 6, which extended to relatively high stresses, that the value of S for the present specimens was considerably higher than the value of 160 N/mm^2 found by Gurney [*6*] for a lower fatigue strength weld detail, namely a weld on the edge of a stressed member. This perhaps reflects the lower stress concentration factor associated with the present weld detail.

Stress-Relieved Joints — In order to consider the effect of tensile strength on the fatigue strengths of stress-relieved joints, all the results obtained under tensile applied stresses are presented in Fig. 17. Combining the results in this way is justified on the basis of the conclusion reached earlier that the fatigue strength of stress-relieved joints was not dependent on applied stress ratio for positive values. Although there was some justification for including the results obtained under alternating loading, since they were widely scattered they are considered separately and are presented in Fig. 18. It can be seen in Figs. 17 and 18 that, as was the case with as-welded joints, there is no consistent influence of the type of material on fatigue strength. Again this is not surprising in the light of previous work which has shown that tensile strength does not influence the fatigue strength of fillet welded joints in steel [*6,12*].

Effect of Stress Relief

In order to consider the effect of stress relief on the fatigue strength of the fillet welded joints tested, all the test results obtained under tensile loading are presented in Fig. 19. No distinction is drawn between different applied stress ratios or different materials, in view of the conclusions reached above that neither of these variables influences the fatigue strengths of either as-welded or stress-relieved joints when subjected to tensile loading. The results obtained under alternating loading, the only other stress ratio investigated for both as-welded and stress-relieved joints, are again considered separately in view of the scatter

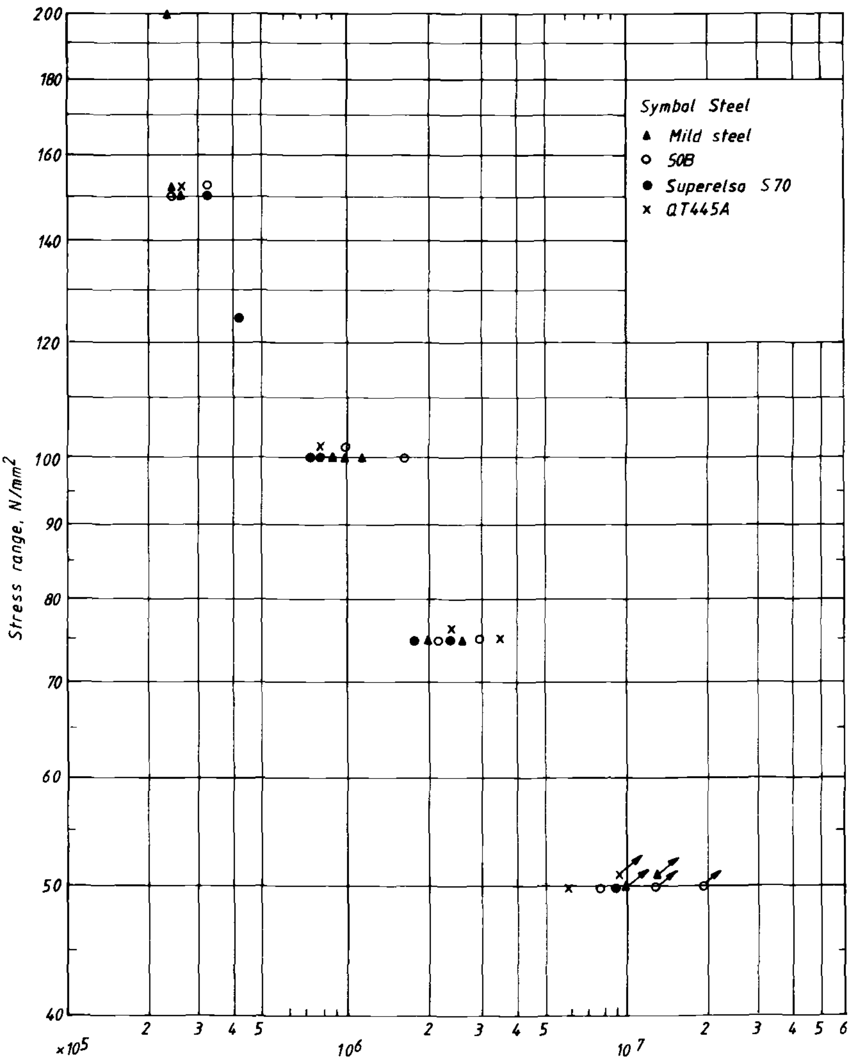

FIG. 17—*Fatigue test results obtained from stress-relieved specimens under positive stress ratios (that is,* R = *0, 0.5, and 0.67).*

obtained. Those results are given in Fig. 20. It can be seen in Fig. 19 that there was no consistent influence of stress relief on the fatigue behavior of the welded joints. This is compatible with fatigue crack propagation data for steels [*11*], as noted earlier. Thus, on the basis of the present results, it must be assumed that stress-relieved welded joints subjected to tensile loading have the same fatigue strengths as as-welded joints. However, it is recognized that this may not always be the case. For example, results reported by Gurney [7] suggest that there may

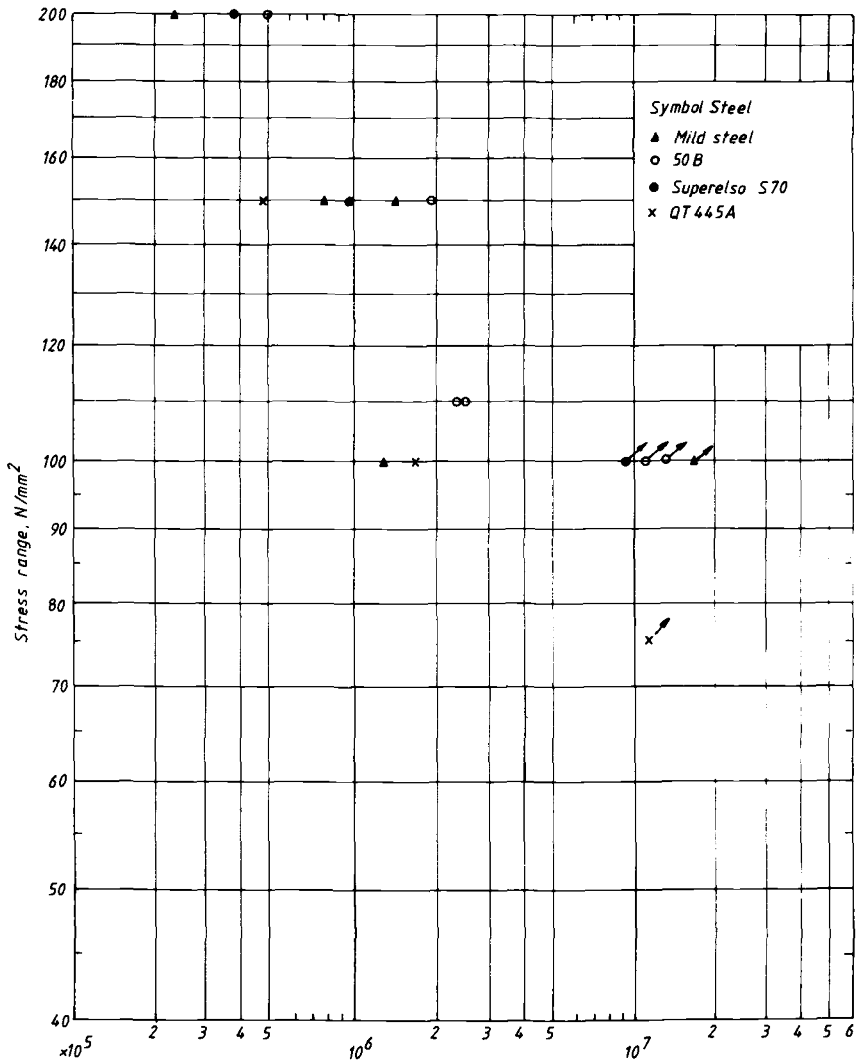

FIG. 18—*Fatigue test results obtained from stress-relieved joints under alternating loading* (R = *−1*).

be some benefit from stress relief for joints subjected to fully tensile loading, such that the *S-N* curve for stress-relieved joints is rotated with respect to the curve for as-welded joints. Clearly, further work is required before any general conclusions can be drawn.

It can be seen in Fig. 20 that, in general, stress-relieved joints gave longer fatigue lives than as-welded joints when subjected to alternating loading ($R = -1$). However, there is some overlap and, as noted earlier, it is believed

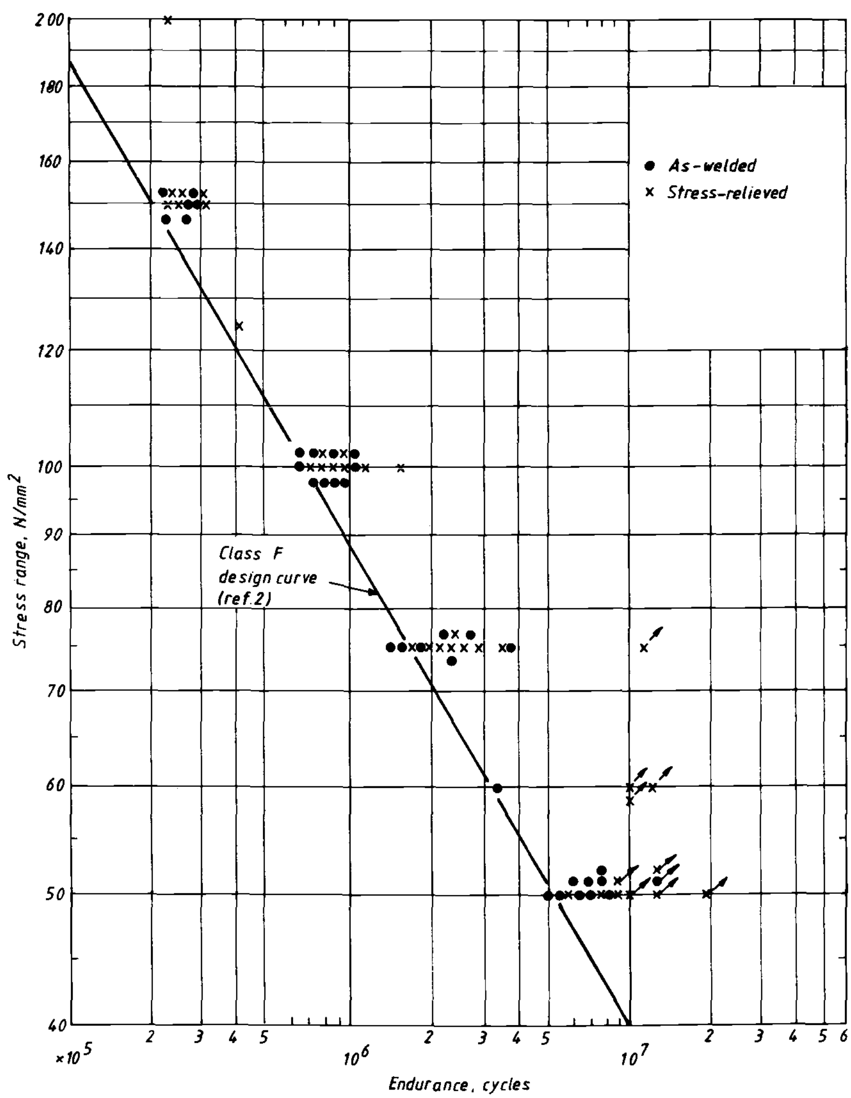

FIG. 19—*Fatigue test results obtained from as-welded and stress-relieved specimens under positive stress ratios (that is,* R = *0, 0.5, and 0.67).*

that scatter in the results obtained from stress-relieved joints is largely attributable to differences in the magnitude of residual stresses left after stress relief, such that the lowest results obtained reflect the presence of relatively high residual stresses after stress relief.

A practical point which should be considered when assessing the present results is that stress relief of real structures is likely to be even less effective than it was in the present specimens. Unless there is good reason to suppose that stress

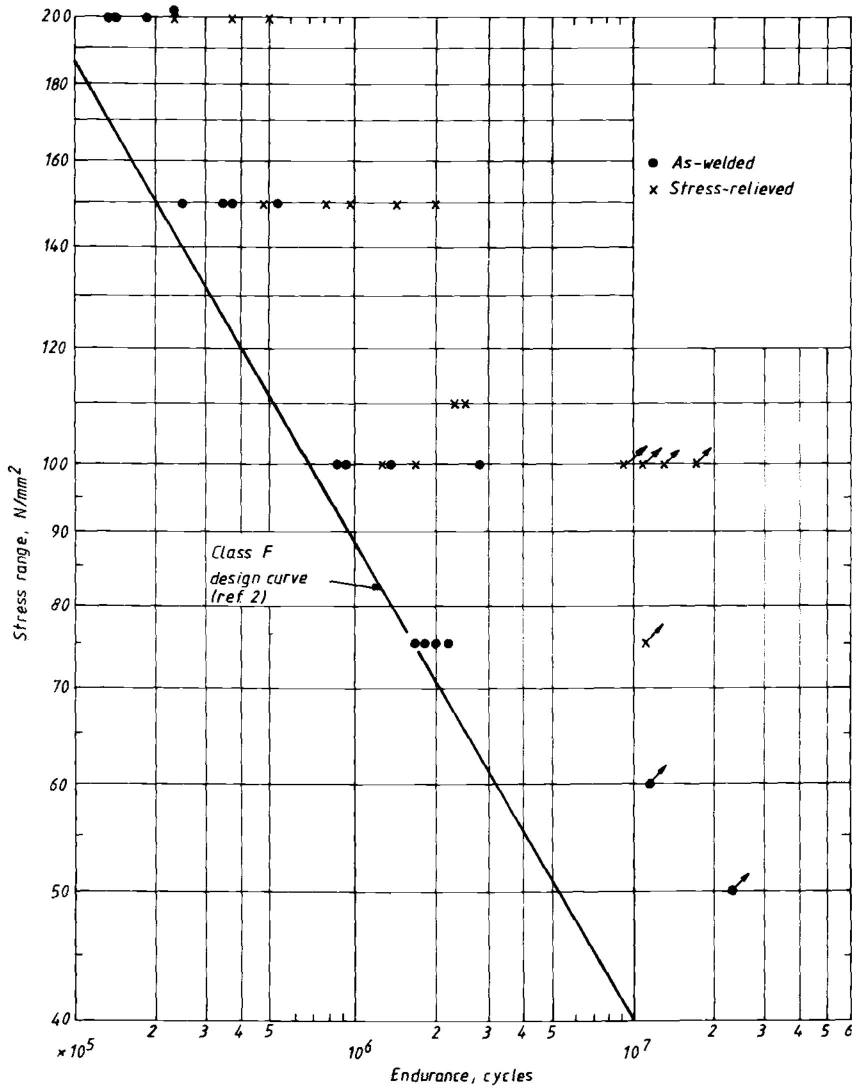

FIG. 20—*Fatigue test results obtained from as-welded and stress-relieved specimens under alternating loading* (R = *−1*).

relief of a structure was fully effective, it is suggested that the assumption is made that tensile residual stresses, perhaps on the order of 80 N/mm^2, will remain after stress relief. Under such circumstances any loading in which the compressive component was up to 80 N/mm^2 (for example, alternating loading giving a stress range of 160 N/mm^2 or less) would produce an effective tensile stress cycle; therefore joints subjected to such conditions should be designed as if they were loaded in tension. If, however, the loading was predominantly compressive and part of the effective stress cycle was compressive, then stress relief could be regarded as being beneficial from the fatigue viewpoint and higher design stress than those for as-welded joints would be justified. Further results are needed to define such design stresses. However, for the present it is believed that the conservative assumption should be made that stress relief offers no benefit from the fatigue point of view to joints subjected to $R \geqslant -1$. The same design rules could, of course, be used for lower R-values, but then they would usually be over-conservative. The appropriate design S-N curve in European Codes [*2 – 4*] for the weld detail tested in the present work, Class F, is shown, for comparison with the present results, in Figs. 19 and 20. The curve provides a good approximation to the lower limits of scatter in both cases and, referring to Fig. 20, is certainly not unduly conservative for considering stress-relieved joints subjected to alternating loading.

Finally, as noted earlier, the present results indicate that stress relief may be beneficial from the point of view of the fatigue limit, especially in joints loaded with $R = -1$, but too few results were obtained to quantify the effect. More convincing evidence was presented in Ref *7*; the fatigue limit of specimens similar to those used in the present investigation, tested under zero-tension loading, was raised from 30 to 50 N/mm^2 by stress relief. However, it should be noted that the comments made earlier about the effectiveness of stress relief still apply in relation to the fatigue limit and in fact are of particular significance in that context since relatively low applied stresses are concerned. Thus there is still a need to establish the effect on the fatigue limit of the presence of residual stresses of a level which would be expected to be present in stress-relieved welded structures.

Future Work

Work aimed at validating the stress range approach to fatigue design of welded steel structures has been carried out under constant amplitude loading and yet, in practice, the design rules are usually applied to structures subjected to random loading. There is an urgent need to investigate the behavior of welded joints which contain high tensile residual stresses under random loading to ensure that the approach is still valid. In particular, it will be necessary to investigate the possibility that residual stresses will be changed by the loading and that currently used cycle-counting techniques, for breaking-down a complex waveform into cycles, are applicable when high tensile residual stresses are present.

Conclusions

On the basis of fatigue tests carried out under stress ratios ranging from zero-compression to $R = +0.67$ on non-load-carrying fillet welded joints in the "as-welded" (actually spot-heated to induce high tensile residual stresses as found in as-welded structures) and stress-relieved conditions, in four steels of yield strengths from 332 to 727 N/mm^2, the following conclusions were drawn:

1. For the present specimens, the level of tensile residual stress in as-welded joints was no higher in the high tensile steels than in the lower strength steel joints; values ranged from 256 to 448 N/mm^2.

2. The tensile strength of the steel did not affect the fatigue strength of the as-welded or stress-relieved joints.

3. The fatigue strength of as-welded joints containing high tensile residual stresses, subjected to stress ratios ranging from zero-compression up to $R = 0.67$, was not strongly dependent on R, and results were reasonably correlated in terms of applied stress range. In the case of joints subjected to compressive loading it was important to consider only that part of the fatigue life during which the fatigue crack growth rate was increasing since, as a result of the varying residual stress field, it was found that fatigue cracks slowed down as they propagated away from the weld.

4. For positive applied stress ratios, the fatigue strengths of as-welded and stress-relieved joints were the same.

5. For alternating loading, the stress-relieved joints generally gave higher fatigue lives than the as-welded joints, apparently depending on the magnitude of residual stresses left after stress relief.

6. Because stress-relieved welded structures are likely to contain higher tensile residual stresses than those measured in the present stress-relieved specimens, it was proposed that designers should assume that stress relief has no effect on fatigue life for joints subjected to $R > -1$. However, there was some evidence to suggest that stress relief may increase the fatigue limit.

Acknowledgments

The author is glad to acknowledge the work of the Fatigue Laboratory staff under Mr. R. A. Males. The work presented in this report was financed jointly by Research Members of The Welding Institute and the Engineering Materials Requirements Board.

References

[1] "Structural Welding Code—Steels," American Welding Society, 1979.
[2] BS 5400, "Steel, Concrete and Composite Bridges," Part 10 Code of Practice on Fatigue, British Standards Institution, 1980.
[3] *Rules for the Design Construction and Inspection of Offshore Structures*, Det norske Veritas, 1977.
[4] *Department of Energy Offshore Installations: Guidance on Design and Construction*, HMSO, London, 1977.
[5] "Comparative Study of Fatigue Design Rules for Welded Structures," ECSC Report No. 7210KD/305, European Coal and Steel Community, 1981 (to be published).
[6] Gurney, T. R., *Fatigue of Welded Structures*, Cambridge University Press, 2nd ed., 1980.
[7] Gurney, T. R., "Some Recent Work Relating to the Influence of Residual Stresses on Fatigue Strength," in *Proceedings*, Conference on Residual Stresses in Welded Construction and Their Effects, The Welding Institute, 1977, pp. 151-164.
[8] Gurney, T. R. and Maddox, S. J., *Welding Research International*, Vol. 3, No. 4, 1973, pp. 1-54.
[9] Satoh, K., *Transactions of the Japan Welding Society*, Vol. 3, No. 1, April 1972, pp. 135-142.
[10] Beaney, E. M., *Strain*, Vol. 12, No. 3, July 1976, pp. 99-106.
[11] Maddox, S. J., Gurney, T. R., Mummery, A. M., and Booth, G. S., "An Investigation of the Influence of Applied Stress Ratio on Fatigue Crack Propagation in Steel," Welding Institute Research Report 72/1978/E, Sept. 1978 (to be published).
[12] Harrison, J. D., "Programmed Load Fatigue Tests on Fillet Welded Joints in Five High Strength Steels," in *Fatigue Performance of Welded High Strength Steels*, The Welding Institute Report Series, 1974.

L. P. Pook[1]

Fatigue Crack Growth in Cruciform-Welded Joints under Nonstationary Narrow-Band Random Loading

REFERENCE: Pook, L. P., "**Fatigue Crack Growth in Cruciform-Welded Joints under Nonstationary Narrow-Band Random Loading,**" *Residual Stress Effects in Fatigue, ASTM STP 776,* American Society for Testing and Materials, 1982, pp. 97-114.

ABSTRACT: Fatigue tests were carried out in air at zero mean load on unstress-relieved cruciform-welded steel joints. The load history used consisted of four different levels of stationary narrow-band random loading arranged in rising and falling sequence, with an overall block length of 100 000 cycles. The fracture surfaces had program markings corresponding to the load blocks. Analysis of these showed that for medium crack depths residual stresses and the level of the maximum load have little effect on fatigue crack growth rate, which can be predicted fairly accurately from constant-amplitude data using linear summation. Crack growth rates for shallow (<1.5 mm) cracks are strongly influenced by tensile residual stresses, and events within this region dominate the overall life. Analysis of two specimens tested in seawater with cathodic protection showed that crack growth was significantly slower than in air.

KEY WORDS: fatigue, welded joints, random loading, fatigue crack growth rate, fracture mechanics, Miner's rule, residual stress

Nomenclature

a	Crack length or depth
C,m	Constants in Eq 1
K_I	Opening mode stress intensity factor
K_{rms}	Root-mean-square value of K_I
ΔK_I	Range of K_I in fatigue cycle
ΔK_{th}	Threshold value of ΔK_I for fatigue crack growth
k,n	Constants in Eq 3
ℓ_o	Short crack length correction
N	Number of cycles
N_i	Number of cycles for failure at ith load level
n_i	Number of cycles at ith load level
S	Stress

[1] Senior Principal Scientific Officer, National Engineering Laboratory, East Kilbride, Glasgow, Scotland.

S_T/σ Clipping ratio
$P(S/\sigma)$ Probability that a peak exceeds S/σ
σ Root-mean-square value of stress

NOTE: For consistency with Ref *12* stress is given in N/mm^2(=MPa) and stress intensity factor in $N/mm^{3/2}(=1000^{1/2} \times MN/m^{3/2})$.

Fatigue tests have recently been carried out [*1,2*] on unstress-relieved cruciform-welded joints made from a medium-strength structural steel.[2] Both constant-amplitude and nonstationary narrow-band random (NBR) tests were carried out in air at zero mean load. The NBR load history used consisted of four different levels of stationary NBR loading arranged in rising and falling sequence, with an overall block length of 100 000 cycles. The fracture surfaces of the NBR loading specimens had program markings corresponding to the loading blocks, similar to those produced [*3*] when different levels of constant-amplitude loading are used. Various fracture mechanics calculations were made in an attempt to rationalize the observed crack growth rates. Two specimens, which had been tested at zero mean load in seawater with cathodic protection, also had program markings, and these were also analyzed.

The original fatigue tests were carried out as part of the United Kingdom Offshore Steels Research Project [*4*], which was set up to obtain fatigue and fracture data relevant to tubular structures in the North Sea. The NBR load history used [*5*] was intended to be representative of wave loading on North Sea structures. However, the fractographic observations and fracture mechanics analysis are felt to be of wider interest and significance.

Fatigue Test Method and Results

Details of the specimens and test techniques used are given in Refs *1* and *2* and outlined below. The specimens were cruciform-welded full-penetration joints of the types shown in Fig. 1; they are all class F joints [*6,7*]. All were manufactured from medium-strength carbon-manganese structural steel plate to British Standard BS 4360-1979, Specification for Weldable Structural Steels, grade 50D (modified) by using manual metal arc welding; they were not stress-relieved after welding. Type A specimens were made from 25-mm plate, and had a tensile strength of 536 N/mm^2 and a 0.2 percent proof stress of 383 N/mm^2; they were loaded axially. Type B specimens were made from 38-mm plate, and had a tensile strength of 538 N/mm^2 and a 0.2 percent proof stress of 370 N/mm^2; they were tested in 4-point bending. Type C specimens were also made from the 38-mm plate, and were tested in seawater with impressed current cathodic protection at a potential of -0.85 V. The test frequency was 0.167 Hz, which corresponds to the predominant wave passing frequency in the North Sea. The nonstationary NBR loading load history used is shown in Fig. 2.

[2] The italic numbers in brackets refer to the list of references appended to this paper.

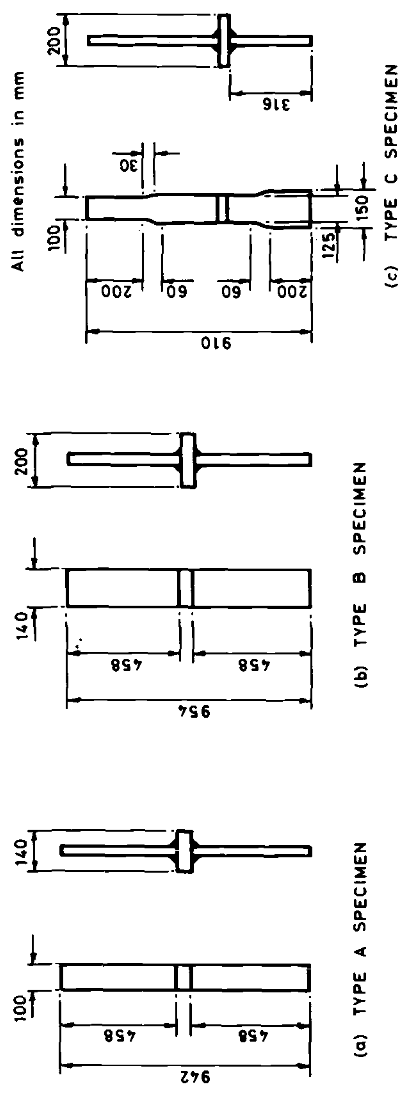

FIG. 1—*Specimen dimensions.*

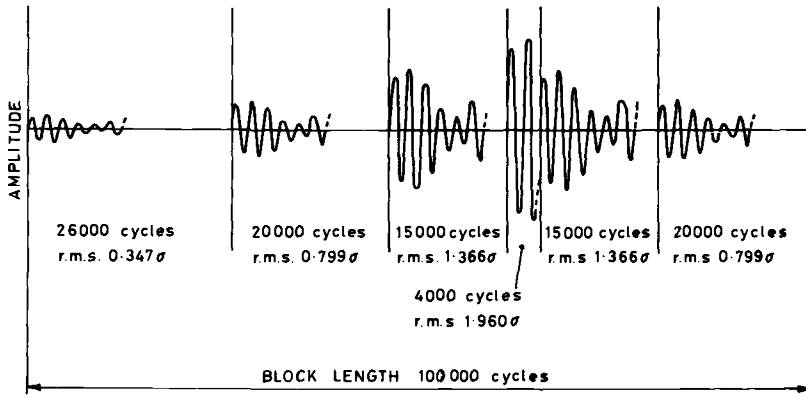

FIG. 2—*Nonstationary narrow-band random load history.*

The results obtained are shown in Tables 1 and 2 and Figs 3 and 4. For the non-stationary NBR tests the nominal clipping ratio, S_T/σ, which is the ratio of maximum load to the root mean square (rms) load, was 7.7; actual values are shown in Table 2. All specimens failed by crack growth in the parent plate at the weld toe. Stresses quoted are nominal direct or bending stresses at the failure site.

Preliminary Analysis

In full-penetration welded joints, fatigue cracks can be expected to originate at small crack-like flaws at the weld toe [*8*], with virtually the whole fatigue life occupied by fatigue crack growth. Crack propagation behavior may be described by the Paris equation

TABLE 1—*Fatigue life of specimens tested under constant-amplitude loading.*

Specimen	Mode of Testing	Alternating Stress, MN/m^2	Life Cycles to Failure
A1/1	axial	232	3.11×10^4
A1/4a	axial	170	1.050×10^5
A1/2	axial	116	2.404×10^5
A1/3	axial	77	7.467×10^5
A1/5	axial	62	1.156×10^6
A1/6	axial	54	1.567×10^6
A1/4	axial	46	1.533×10^7 (unbroken)
A1/7	axial	42	2.405×10^7 (unbroken)
B1/4	4-point bending	147	9.36×10^4
B1/8	4-point bending	127	2.240×10^5
B1/2	4-point bending	93	4.841×10^5
B1/3	4-point bending	72	1.380×10^6
B1/5	4-point bending	56	2.267×10^6
B1/6	4-point bending	45	9.711×10^6
B1/7	4-point bending	39	3.232×10^7 (unbroken)

TABLE 2—*Fatigue life of specimens tested under nonstationary narrow-band random loading.*

Specimen	Mode of Testing	Root-Mean-Square Stress, MN/m^2	Life Cycles to Failure	Clipping Ratio
A2/2	axial	35.4	1.796×10^6	6.8
A2/3	axial	27.8	3.329×10^6	7.6
A2/5	axial	25.6	4.798×10^6	7.6
B2/1	4-point bending	27.6	3.370×10^6	6.1
B2/2	4-point bending	25.8	5.772×10^6	6.1
B2/3	4-point bending	34.0	2.059×10^6	6.3
B2/4	4-point bending	52.3	6.506×10^5	5.0
B2/5	4-point bending	43.7	9.651×10^5	5.8
B2/6	4-point bending	21.1	8.077×10^6	3.8
C5/1	cantilever bending	48.2	8.532×10^5	8.4
C5/2	cantilever bending	58.3	2.647×10^5	8.5

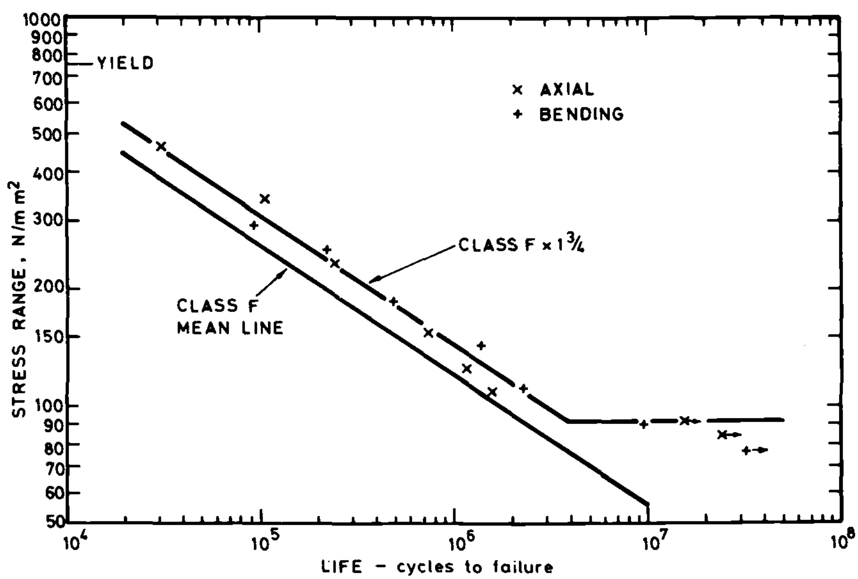

FIG. 3—*Fatigue life under constant-amplitude loading.*

$$\frac{da}{dN} = C(\Delta K_I)^m \tag{1}$$

where ΔK_I is the range of the opening mode stress intensity factor, K_I, in the fatigue cycle, and C and m are material constants. Crack growth does not take place [*9*] unless ΔK_I exceeds a threshold value ΔK_{th}. For a structural steel m is usually about 3. It is easily shown [*8-10*] that this implies that the slope of the constant-amplitude *S-N* curve should be $-1/m$; various standards [*7,11,12*]

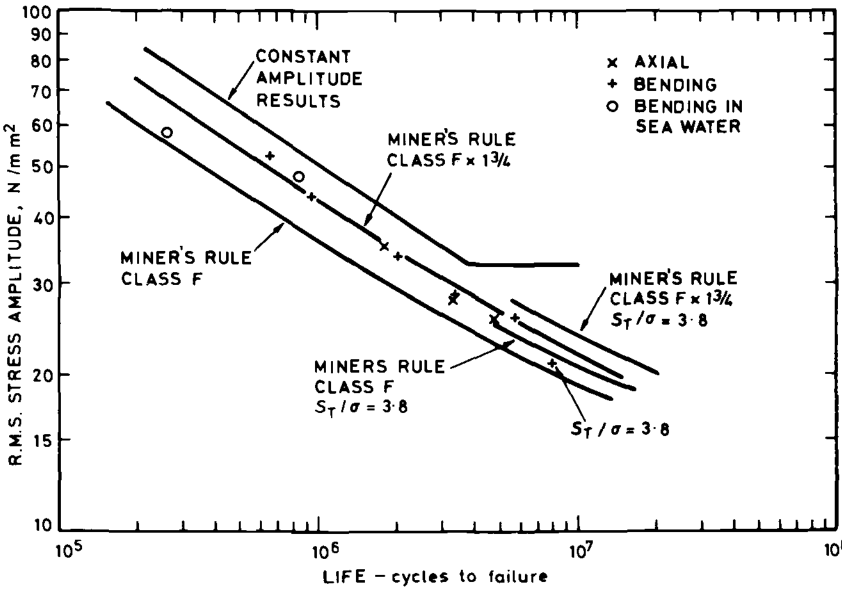

FIG. 4—*Fatigue life under nonstationary narrow-band random loading.*

use a value of −⅓. The fatigue limit corresponds to the fatigue crack growth threshold.

Since compressive stresses simply close a crack, only tensile stresses would be expected to be damaging when the load cycle passes through zero. However, in unstress-relieved joints the presence of tensile residual stresses, usually assumed to be of yield-stress magnitude [*8*], means that the crack is always open; thus the whole of the load cycle must be regarded as tensile and therefore damaging.

When plotted on a stress range basis (Fig. 3) the constant-amplitude results are quite close to the class F mean line [*6,7*], which is the mean *S-N* line obtained from the analysis of a large amount of fatigue test data for unstress-relieved class F joints; thus confirming that virtually the whole of the stress range must have been damaging. There is no significant difference between the two types of joint, and a line with a life 1¾ times the mean class F line gives a reasonable fit in the finite life region. The stress range at the fatigue limit is about 92 MN/m². This is low for tests at zero mean load [*9*], and suggests the presence of tensile residual stresses.

Miner's rule [*9*] states that under variable-amplitude loading failure takes place when

$$\sum \frac{n_i}{N_i} = 1 \tag{2}$$

where n_i is the number of cycles at the ith load level and N_i is the life under constant-amplitude loading at the ith load level. Despite its well-known shortcomings, which have recently been reviewed [*13*], Miner's rule has been found useful in practical applications and is recommended in various standards [7,11,12]. The nonstationary NBR results (Fig. 4) fall above a Miner's rule summation based on the class F mean line, so that design calculations based on this line would be conservative. However, they fall below a summation based on a line through the constant-amplitude results. As a consequence an attempt to forecast the nonstationary NBR results from the constant-amplitude results was unsuccessful [14], even though it was felt that the behavior of welded joints under NBR loading was fairly well understood.

In both the summations S_T/σ was taken as 7; taking it as 5 or 9 made very little difference for the endurances shown. More sophisticated calculations [10] based on a fracture mechanics extension to Miner's rule also made little difference.

In general there is no significant difference between the different types of joint, and for the one test where comparison is possible immersion in seawater with cathodic protection has no effect. The specimen with an unusually low clipping ratio of 3.8 falls below a Miner's rule summation based on this clipping ratio and the class F mean line.

Fractography

Typical examples of fracture surfaces of specimens tested under nonstationary NBR loading are shown in Figs. 5 and 6. The general appearance is similar to program markings observed [3] on specimens where the individual levels are constant amplitude. Multinucleation was observed in all specimens, and the crack

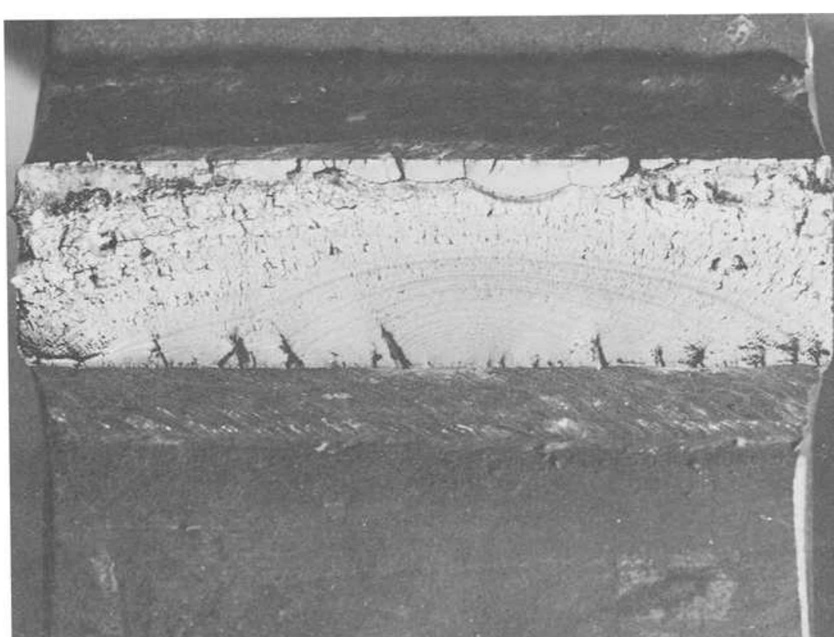

FIG. 5—*Fracture surface of Specimen A2/3.*

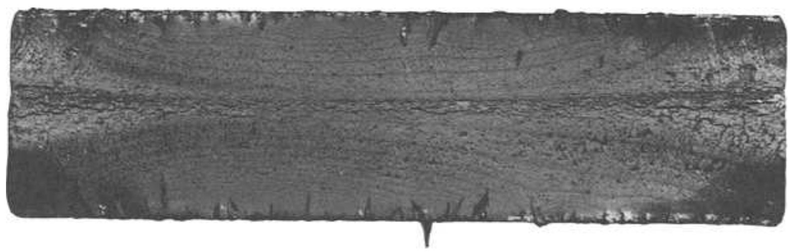

FIG. 6—*Fracture surface of Specimen B2/2.*

aspect ratio (ratio of surface length to depth) was always large in the regions used in the analysis. Examination in a scanning electron microscope revealed striations [9], their irregular spacing reflecting the NBR loading used.

Crack growth data were obtained by measuring the program marking spacing using a toolmaker's traveling microscope capable of being read to 0.01 mm. Measurements were made along a line passing through one of the multiple origins and at or near the greatest crack depth. Few data were obtained for crack depths of less than 1 mm because of mechanical damage to the fracture surfaces, presumably during the compressive part of the load cycles. The raw data are shown in Figs. 7 to 9, with results for different sides of the same specimen distinguished by different symbols.

The actual appearance of the markings was critically dependent on the lighting used, so except for Specimen C5/2 it was not possible to assign a particular part of a marking unambiguously to a particular load level; thus the position of markings on the life axes cannot be precisely determined. The convention adopted was to place the last measurement at the end of the last completed load block. Crack growth rates on each side of a specimen are generally similar, even where the total amount of crack growth is very different.

Fracture Mechanics Analysis

Expressions for stress intensity factors and fatigue crack growth data recommended by Det norske Veritas [12] were used to construct estimated crack depth

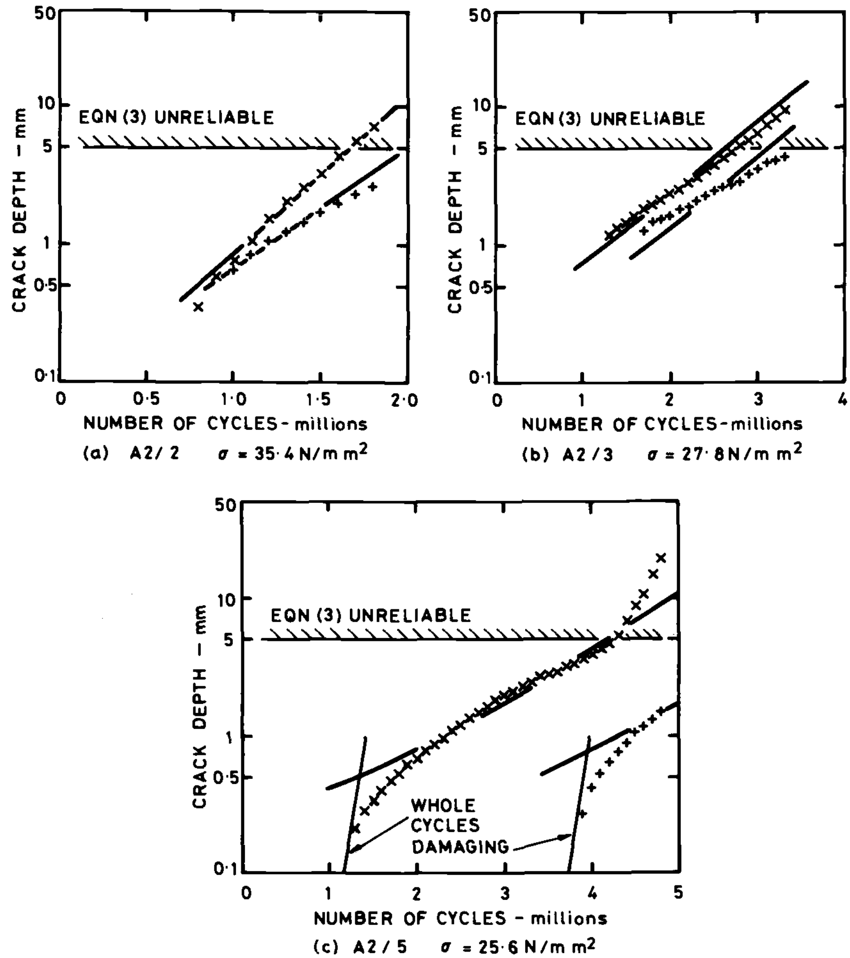

FIG. 7—*Crack growth data for axial specimens.*

versus number of cycles curves for comparison with the measured data. The opening mode stress intensity factor, K_I, for a crack at a weld toe is given by

$$K_I = Ska^n \tag{3}$$

where S is applied stress, a is crack depth, and k and n are parameters which depend on joint geometry. Values for various configurations are given in Ref *12*. Here $n = 0.30$ and k is 3.41 (N, mm units) for the axial specimens and 3.69 for the bend specimens. This two-dimensional approach is appropriate for the high aspect ratio cracks involved. A power law representation of K_I is particularly convenient [*10*] for welded joint calculations. The relationship of Equation 3 to more usual expressions for K_I may be seen by writing it in the form

$$K_I = YSa^{1/2} \qquad Y = ka^{n-1/2} \tag{4}$$

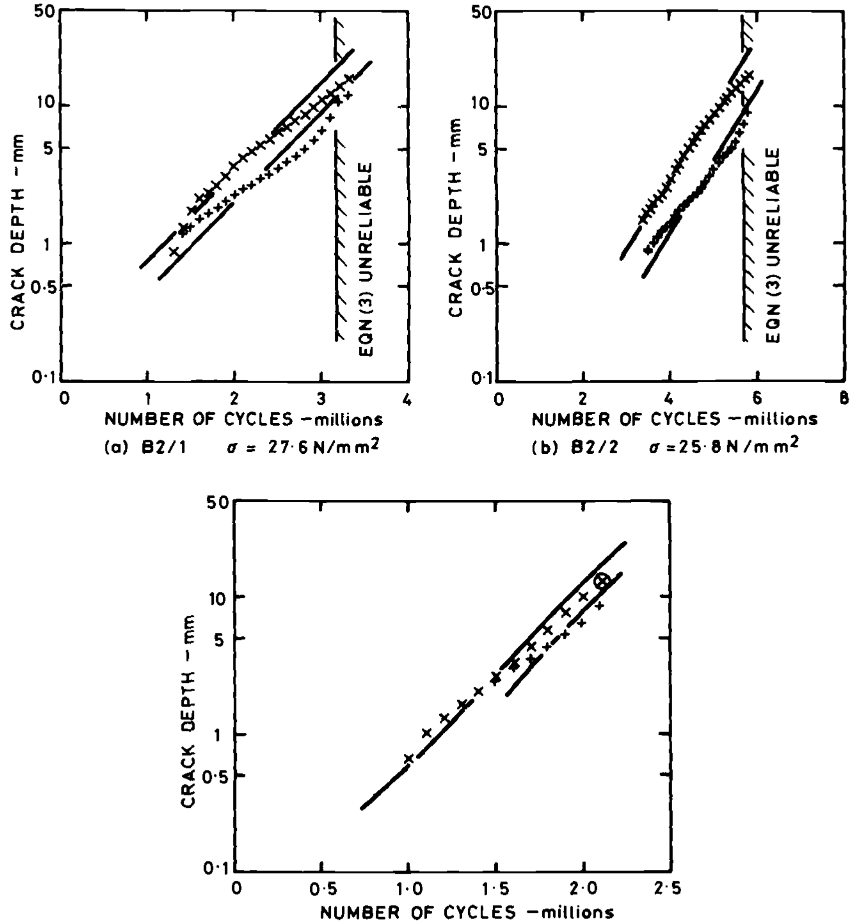

FIG. 8—*Crack growth data for 4-point bend specimens.*

For variable-amplitude loading crack growth may be estimated by assuming that the amount of crack growth due to each load level is the same as if it were part of a constant-amplitude loading; load levels below the fatigue crack growth threshold make no contribution to crack growth. This linear summation neglects 'interaction' effects which can occur when load levels are changing. However, for NBR loading, interaction effects may be modeled [*15*] by using linear summation, and taking into account elevation of the threshold due to the prior loading at the highest loads in the history.

The load history shown in Fig. 2 is a practical realization [*5*] of a calculated wave-loading distribution given by

$$P(S/\sigma) = \exp\{-0.8594(S/\sigma)^{1.2715}\} \tag{5}$$

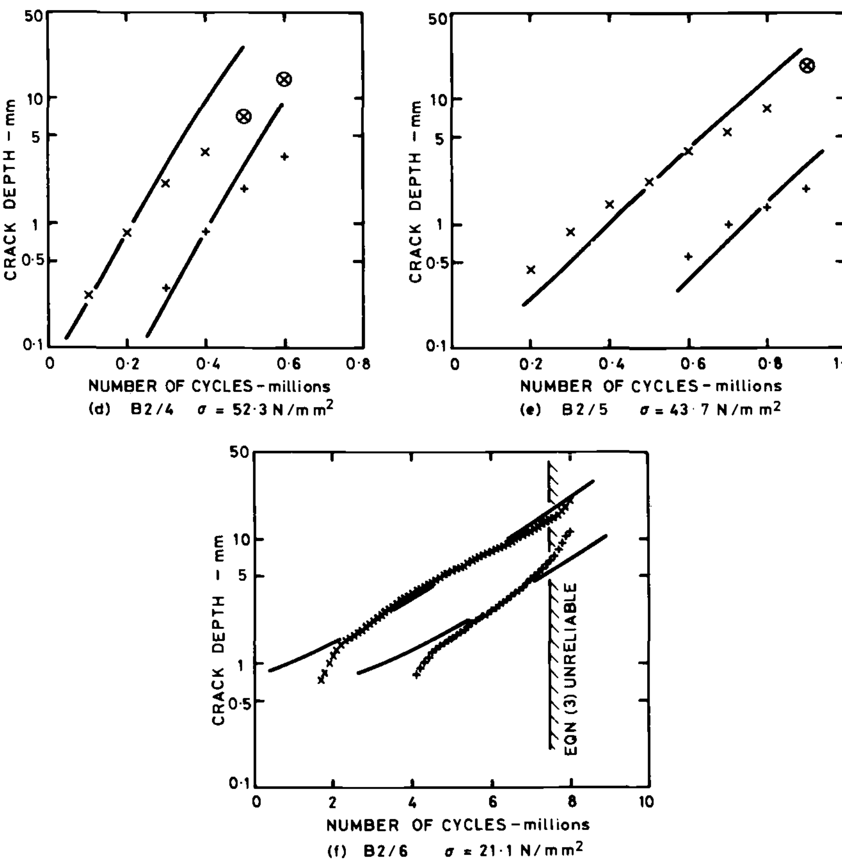

FIG. 8—*(continued)*.

where σ is the rms stress amplitude of the process and $P(S/\sigma)$ is the probability that a peak exceeds S/σ. The history shown in Fig. 2 is slightly more damaging than that described by Eq 5 and was used in conjunction with Eqs 1 and 3 to estimate fatigue crack growth by the numerical integration method described in Ref *15*. It was assumed that only the positive part of each load cycle contributed to crack growth. As recommended [*12*] for a structural steel in air, m was taken as 3.1 and C as 2×10^{-13} (N, mm units), and a typical [*9*] threshold value of 200 N/mm$^{3/2}$ was used. The clipping ratio was taken as 7, except for Specimen B2/6 where the actual value was used. For one side of Specimen A2/2 the weld toe angle was 30 deg rather than 45 deg as specified, so k was taken as 3.17.

This prediction method treats the nonstationary load history used as if it were stationary. Different crack growth rates for different parts of the load history are therefore averaged, but the method does correctly predict the amount of crack growth between corresponding points in different load blocks even when this distance is not small compared with the crack depth.

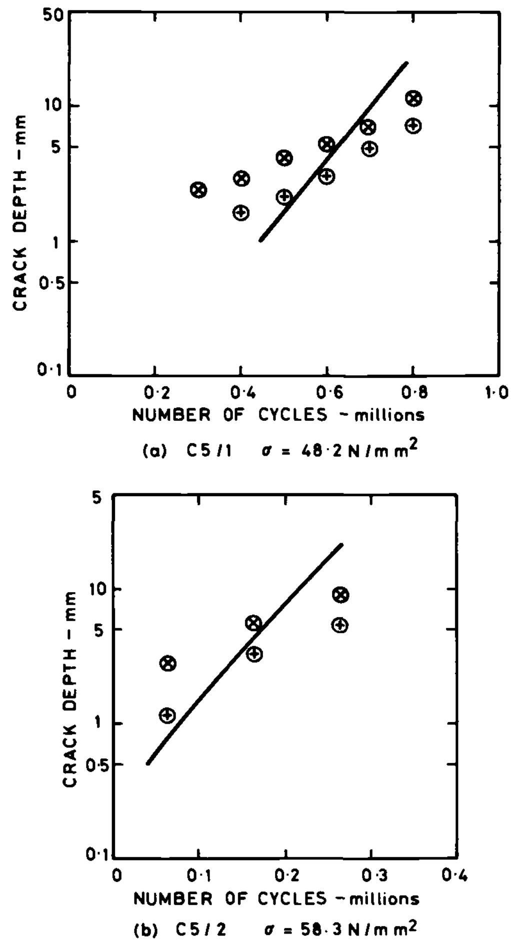

FIG. 9—*Crack growth data for cantilever bend specimens in seawater with cathodic protection.*

Predicted crack growth rates are compared with the experimental data in Figs. 7 to 9. They are not particularly sensitive to either the value of S_T/σ (within the range of 5 to 9) or ΔK_{th}, but are sensitive to the values of C and m. The predicted lives are nearly straight lines on the log-linear scales used; for medium crack depths the fairly good fits could be improved by making relatively small adjustments (within the normal spread of experimental data) to C and m. If this is done it is immediately clear that crack growth rates are underestimated for some shallow (<1.5 mm) cracks, and for some deep cracks. However, it is clear that for medium depth cracks only the tensile part of the load cycles contributes to crack growth, at least to a first approximation. This does not appear to be true for shallow cracks, and for Specimen A2/5 (Fig. 7*c*), for which most shallow crack points were obtained, the results approach a prediction assuming that the whole range of the cycles must be taken into account.

Det norske Veritas [12] suggest that Eq 3 can be used up to the full plate thickness. However, the increase in crack growth rates for the axial specimens for crack depths of greater than 5 mm suggests that it underestimates the stress intensity factor for crack depths greater than one fifth of the plate thickness.

The derivation of Eq 3 assumes that for a bend specimen any crack on the compressive side remains closed. However, if the central uncracked ligament is too small such a crack can open partially [16]. When this occurs the stress intensity factor for the crack on the tension side is affected and crack growth takes place on the compressive side. This probably accounts for inflections at deep crack sizes in some of the bend specimen data. Equation 3 should therefore be regarded as unreliable when either crack depth is greater than the uncracked ligament. The unreliability of Eq 3 for deep cracks is unimportant because of the relatively small proportion of total life involved.

Stress intensity factors only provide a fully valid basis [9] for the analysis of fatigue crack growth data if the maximum nominal net section stress does not exceed 80 percent of the yield (taken as 0.2 percent proof stress). A somewhat less restrictive limit of the yield stress is sometimes satisfactory [17]. Data still have some meaning when the yield criterion is not met, but crack growth rates are usually faster than for valid data. Check calculations showed that underestimation of crack growth rates for regions where Eq 3 appears to be reliable was associated with nominal net section stresses in excess of the yield stress. Data affected are indicated by ringed symbols in Figs. 7 to 9.

The markings were also used to derive fatigue crack growth rate data. The fatigue crack growth rate da/dN was taken as the average between adjacent markings. The value of K_{rms} (root mean square value of K_I) was calculated for the point midway between adjacent markings by using Eq 3. Figure 10 shows results for medium depth cracks (1.5 mm deep to the onset of net section yield); Fig. 11 shows results for cracks outside these limits. Data for regions where Eq 3 apppears to be incorrect, as noted earlier, were discarded. The prediction line shown used the same data and assumptions as before. Some points are omitted from crowded areas for clarity.

The data for the medium depths cracks are tightly grouped and are somewhat conservative compared with the prediction line. Plotted separately there was no noticeable difference between the axial and 4-point bending data. The deep crack data are about the same as the medium crack data. A noticeable feature is that crack growth rates in sea water with cathodic protection are distinctly slower than in air. This contrasts with constant-amplitude fatigue crack growth data for the same steel and conditions, where faster crack growth was observed [18]. The prediction line seriously underestimates the shallow crack data, as would be expected. However, a prediction line based on the whole load cycles is conservative for all the shallow crack data.

The behavior of Specimen B2/6 (Fig. 12), which was tested using a much lower clipping ratio than the other specimens, is generally similar to them, except that there is perhaps some tendency towards faster crack growth rates, especially at lower rates of crack growth. A prediction line based on $S_T/\sigma = 3.8$ is dis-

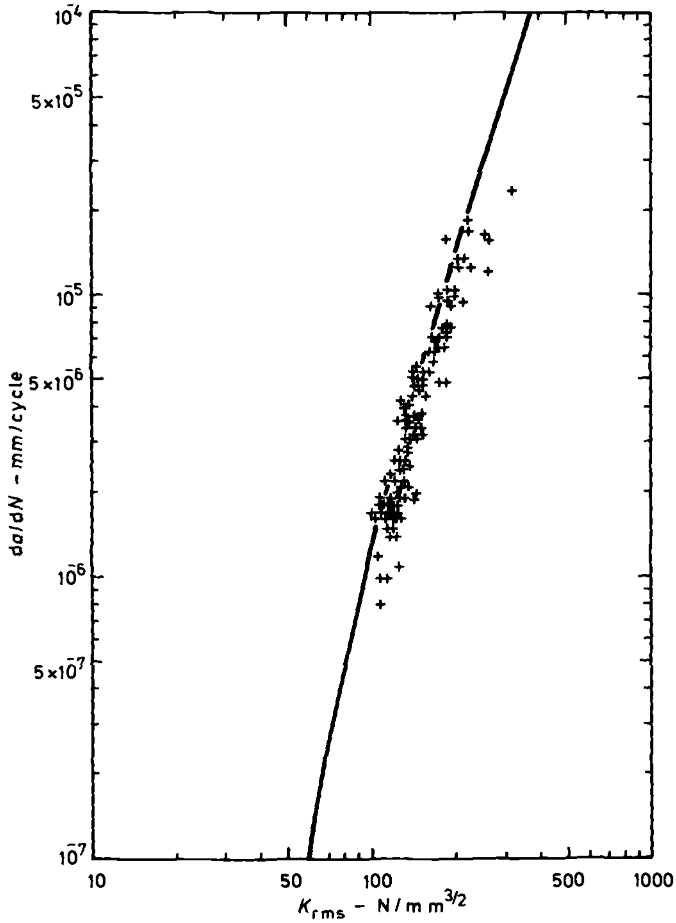

FIG. 10—*Fatigue crack growth data for medium depth cracks.*

placed by a factor of 1.04 on the K_{rms} axis compared with the line based on $S_T/\sigma = 7$, so the difference is barely significant.

Various investigators have found that fatigue crack growth rates for short cracks are greater than those for long cracks. For example, El Haddad et al [*19*] found that if short crack data were corrected by adding a material constant, ℓ_0, to the physical crack length when calculating the stress intensity factor, they agreed with long crack data. Using their method ℓ_0 was estimated to be 0.18 mm for BS 4360 steel; however, their correction provided only about a quarter of the adjustment needed to bring the shallow crack data into agreement with the medium crack data.

Discussion

Any analysis of fatigue crack growth in residual stress fields is complicated by the difficulty of calculating accurate stress intensity factors, even when the

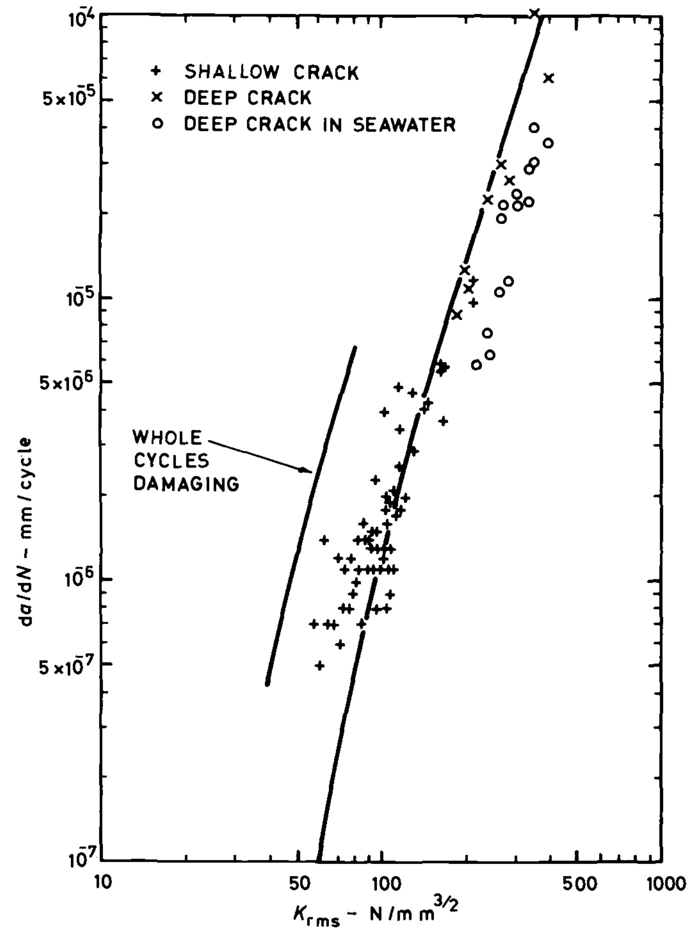

FIG. 11—*Fatigue crack growth data for shallow and deep cracks.*

residual stress distribution is known [*20*]. For the unstress-relieved cruciform-welded joints it can only be inferred through its effect on crack growth behavior. For crack depths of over 1.5 mm the effect of residual stress has died away, so tensile residual stresses must be concentrated near the surface.

Unfortunately, detailed consideration of crack growth within 1.5 mm of the surface is complicated, both by the paucity of data and the inevitable irregularity of the surface of a welded joint (Fig. 13), which make Eq 3 of doubtful accuracy. Nevertheless, it is clear for two reasons that there must be high tensile residual stresses near the surface. Firstly short crack corrections are insufficient to account for the crack growth rates observed, and secondly the observed specimen fatigue strengths are much lower than would be expected for stress-relieved joints where only the tensile half cycles would be damaging [*8*].

Although crack growth rates on each side of a specimen are very similar at medium crack lengths, the number of cycles to reach a crack depth of 1.5 mm

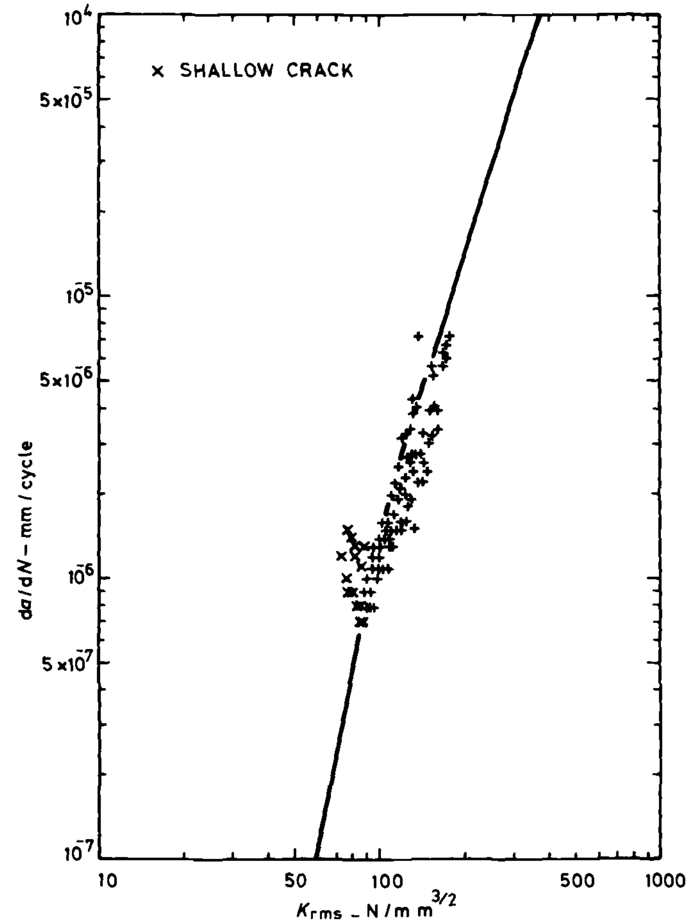

FIG. 12—*Fatigue crack growth data for Specimen B2/6.*

can differ markedly. Figure 14 shows data on fatigue life to this crack depth for the axial and 4-point bend specimen. The scatter band is greater than the scatter band for total life (Fig. 4). Cracks are probably present at the weld toes on the unbroken side of the cruciform. If data from these were added the scatter could be expected to be further increased. Cruciform-welded joints are notorious for scatter in fatigue tests [*6*]. It is clear that this is associated with events within 1.5 mm of the weld surface, which emphasizes the importance of the precise weld quality achieved.

The actual clipping ratio used appears to have little influence on fatigue crack growth rates at medium crack lengths, but this does not mean that it has little effect at short crack lengths and hence on overall life.

Conclusions

The conclusions apply only to the particular load history and specimens used. At medium crack depths residual stress and clipping ratio have little effect on

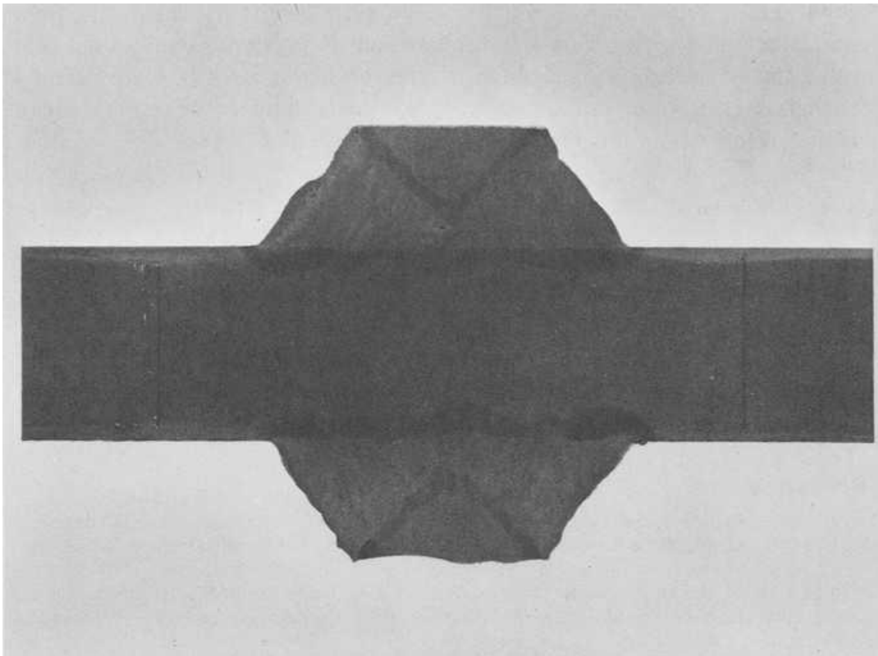

FIG. 13—*Cross section through a constant-amplitude specimen.*

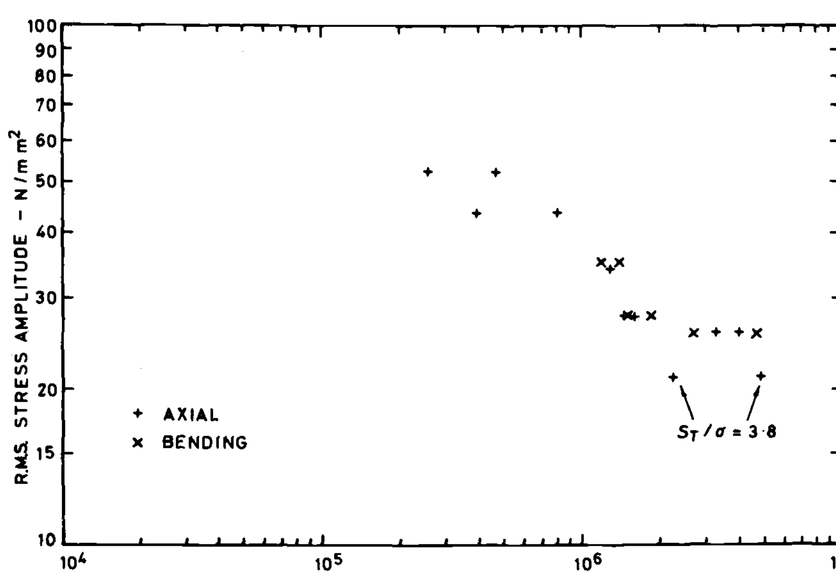

FIG. 14—*Fatigue life to a crack depth of 1.5 mm under nonstationary narrow-band random loading.*

fatigue crack growth rates, which can be predicted fairly accurately from constant-amplitude data using linear summation. Crack growth rates in seawater with cathodic protection are significantly slower than in air. Crack growth rates for shallow (<1.5 mm) cracks are strongly influenced by tensile residual stresses, and events within this region dominate the overall life.

Acknowledgments

This paper is published by permission of the Director, National Engineering Laboratory, U.K. Department of Industry. It is British Crown copyright. The fatigue tests were carried out by Mr. R. Holmes and Mr. J. K. Sharples as part of the United Kingdom Offshore Steels Research Project. The remainder of the work was supported by the Engineering Materials Requirements Board of the U.K. Department of Industry.

References

[1] Holmes, R., "Fatigue and Corrosion Fatigue of Welded Joints under Random Load Conditions," in *Proceedings, European Offshore Steels Seminar, 1978*, The Welding Institute, Cambridge, for U.K. Department of Energy, 1980.

[2] Holmes, R., "The Fatigue Behavior of Welded Joints under North Sea Environmental and Random Loading Conditions," OTC Paper No. 3700, 12th Offshore Technology Conference, Houston, 1980.

[3] Ryman, R. J., *Aircraft Engineering*, Vol. 34, No. 396, 1962, pp. 34-42.

[4] "Description of U.K. Offshore Steel Research Project: Objective and Current Progress," Reference MAP 015G (1)/20-2, U.K. Department of Energy, 1974.

[5] Pook, L. P., *Journal of the Society of Environmental Engineers*, Vol. 17-1, 1978, pp. 22-23, 25-28, 31-35.

[6] Gurney, T. R., *Welding Institute Research Bulletin*, Vol. 17, No. 5, 1976, pp. 115-124.

[7] BS 5400: Part 10: 1980, *Steel, Concrete and Composite Bridges, Part 10, Code of Practice for Fatigue*, British Standards Institution, 1980.

[8] Gurney, T. R., *Fatigue of Welded Structures*, 2nd ed., Cambridge University Press, 1979.

[9] Frost, N. E., Marsh, K. J., and Pook, L. P., *Metal Fatigue*, Clarendon Press, Oxford, 1974.

[10] Pook, L. P., "Some Features of Fatigue Behaviour in the Presence of Crack-Like Flaws," NEL Report No. 624, National Engineering Laboratory, East Kilbride, Glasgow, 1977.

[11] DD55: 1978, *Draft for Development, Fixed Offshore Structures*, British Standards Institution, 1978.

[12] *Rules for the Design, Construction, and Inspection of Offshore Structures, Appendix C—Steel Structures*, Det norske Veritas, Hovik, Norway, 1977.

[13] Schütz, W., *Engineering Fracture Mechanics*, Vol. 11, No. 2, 1979, pp. 405-421.

[14] Pook, L. P. and Holmes, R., "Forecasting the Fatigue Life of Welded Joints under Narrow-Band Loading," in *Advances in Fracture Research*, D. François, Ed., Pergamon Press, Oxford, Vol. 5, pp. 2079-2091, 1981.

[15] Pook, L. P. and Greenan, A. F., *International Journal of Fatigue*, Vol. 1, No. 1, 1971, pp. 17-22.

[16] Paris, P. C. and Tada, H., *International Journal of Fracture Mechanics*, Vol. 11, No. 6, 1975, pp. 1070-1072.

[17] Pook, L. P., "Fatigue Crack Propagation," in *Developments in Fracture Mechanics—1*, G. G. Chell, Ed., Applied Science Publishers, London, 1979, pp. 183-220.

[18] Johnston, R., Bretherton, I., Tomkins, B., Scott, P. M., and Sylvester, D. R. V., "The Effect of Sea-Water Corrosion in Fatigue Crack Propagation in Structural Steel," in *Proceedings, European Offshore Research Seminar, 1978*, The Welding Institute, Cambridge, for U.K. Department of Energy, 1980.

[19] El Haddad, M. H., Dowling, N. E., Topper, T. H., and Smith, K. N., *International Journal of Fracture Mechanics*, Vol. 16, No. 1, 1980, pp. 15-30.

[20] Underwood, J. H., Pook, L. P., and Sharples, J. K. in *Flaw Growth and Fracture, ASTM STP 631*, American Society for Testing and Materials, 1977, pp. 402-415.

S. Berge[1] *and O. I. Eide*[1]

Residual Stress and Stress Interaction in Fatigue Testing of Welded Joints

REFERENCE: Berge, S. and Eide, O. I., "**Residual Stress and Stress Interaction in Fatigue Testing of Welded Joints,**" *Residual Stress Effects in Fatigue, ASTM STP 776*, American Society for Testing and Materials, 1982, pp. 115-131.

ABSTRACT: Longitudinal non-load-carrying fillet welds in a structural steel were tested in axial tension. In constant-amplitude loading, the stress range approach was verified. In variable-amplitude block loading, stress interaction effects were observed. In general, interaction effects were beneficial or, in one case, only slightly detrimental to the fatigue life as compared to the Miner Palmgren summation index. For $R = 0$, interaction caused a significant delay in crack growth as compared to constant-amplitude loading, particularly with small cycles in the load spectrum. For $R = -1$, delay effects were small, and dependent on the sequence of peak/trough in each load cycle. Stress-relieved, as compared to as-welded specimens, exhibited a larger delay at $R = 0$, and a slight acceleration of crack growth at $R = -1$. Increasing the mean stress from 0 to 25 MPa gave only small changes, as did randomization of the block sequence.

KEY WORDS: fatigue testing, welded joints, cumulative damage, constant amplitude testing, block program testing, residual stress

Nomenclature

- D Miner-Palmgren summation index
- n_i Number of load cycles at stress range $\Delta\sigma_i$
- N_i Number of cycles to failure at stress range $\Delta\sigma_i$
- R Stress ratio $\sigma_{min}/\sigma_{max}$ in one load cycle
- σ_m Mean stress
- σ_r Residual stress
- $\sigma_{c\ell}$ Stress due to bending caused by clamping a specimen
- $\Delta\sigma$ Stress range
- S-N Constant amplitude (-data, -loading, etc.)

Fatigue design procedures for welded structures take into account the effects of residual stresses by assuming a "stress range philosophy" [*1,2*].[2] The fundamental of this is that residual stresses are tensile and large; hence fatigue test data for assessment of design curves are considered accordingly [*3*].

[1] Senior Lecturer and Research Assistant, respectively, Division of Marine Structures, The Norwegian Institute of Technology, Trondheim, Norway.

[2] The italic numbers in brackets refer to the list of references appended to this paper.

For stress-relieved structures loaded partly in compression, this procedure may be overly conservative [*4*]. A recent recommendation for fatigue design gives design *S-N* curves for stress-relieved structures, in which there is a considerable increase in design stresses for negative stress ratios [*5*]. These design criteria have been derived from constant-amplitude (*S-N*) tests of welded joints, for which there are a fair amount of data in the as-welded and in the stress-relieved conditions [*6*].

In comparison, little data are available on the effects of residual stresses on cumulative damage of welded joints, except for test results in which residual stresses are an intrinsic, and unquantified, feature.

Residual stresses in variable-amplitude loading may be expected to exhibit at least the following characteristics: (*1*) relaxation of residual stresses throughout the loading history, due to local yielding during peak loads; and (*2*) interaction effects, which are largely dependent on local stresses at the crack tip, and may therefore be dependent on the residual stress level [*7*].

One main problem in discussing residual stresses in welded structures is the somewhat enigmatic nature of these stresses. A brief discussion on this will therefore be given.

Residual stresses in structures may be separated into two types (Fig. 1):

1. *Short-range stresses* exist only in and close to a weld, and are self-balanced over the cross section of one member. The cause of these stresses is the thermal contraction of parts of the cross section, under restraint from the cooler portions. Stresses will generally be large, at or above yield magnitude, and with large through-thickness gradients. Due to the short range, the stresses will be associated with small end displacements. Hence, they may fairly easily be reduced by heat treatment, or by local yielding caused by peak loads.
2. *Long-range stresses* are uniform throughout a structural member, and are self-balanced within the structure. Their origin is from the procedure of assembling a monolithic structure from pre-fabricated components, whereby welding shrinkage and the use of local heating, mechanical restraints, brute force, etc., in the process of fitting the pieces together, may cause significant locked-in stresses. Long-range stresses are generally small compared with the yield stress, with small gradients. However, the associated end displacements, and hence the stored strain energy, may be large. As a consequence, these stresses are not easily relaxed by ordinary heat-treatment procedures, nor are they affected very much by peak load conditions and local yielding.

Very little is known about residual stresses in marine structures, their magnitude, through-thickness variation, and variations through service life. In one particular investigation on welds in a ship's deck, the residual stresses were found to be far in excess of stresses from applied loads. Long-range stresses were approximately 25 percent of the short-range stresses [*8*].

In the present investigation, the effects of short-range residual stresses were investigated in constant-amplitude and variable-amplitude block-loading testing.

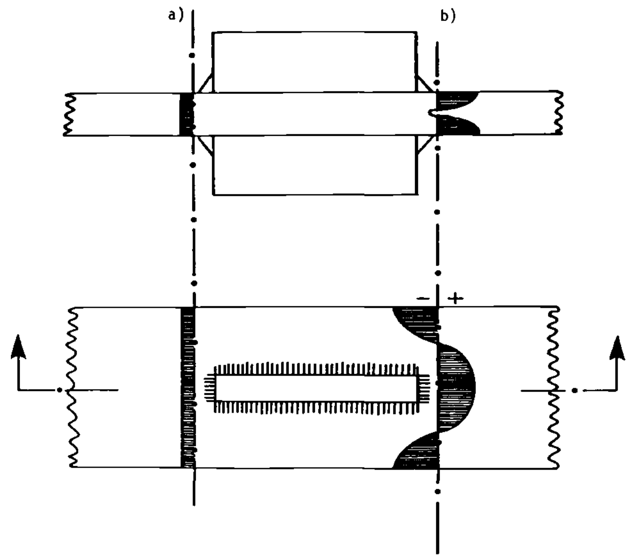

FIG. 1—*Residual stresses (schematic).* (a) *Long-range stresses.* (b) *Short-range stresses.*

Test Procedure

Fatigue tests, particularly with variable-amplitude loading, may be performed and interpreted in a number of ways. For that reason, the fundamentals of the test procedure will be briefly summarized.

The constant-amplitude test data were assumed to follow a log-linear relationship (S-N curve). A standard procedure of analysis was applied in accordance with ASTM Practice for Statistical Analysis of Linear or Linearized Stress-Life (S-N) and Strain-Life (ε-N) Fatigue Data (E 739), in which a constant variability along the median line is assumed.

Cumulative damage was analyzed using the Miner-Palmgren summation index

$$D = \sum \frac{n_i}{N_i} \tag{1}$$

Although formulated on a heuristic basis, Eq 1 with fracture criterion

$$D = 1 \tag{2}$$

may be shown to be consistent with fracture mechanics analysis of fatigue based on a Paris-Erdogan type crack growth rate equation [9]. Thus, in the absence of interaction effects and disregarding scatter, Eqs 1 and 2 conform with the more basic principles of linear-elastic fracture mechanics.

In constant-amplitude testing there will generally be a fatigue limit. In variable-amplitude loading, however, cycles below the fatigue limit will be damaging, due to the gradual growth of the crack. In Eq 1, the Gurney model of cumulative damage was applied—that is, linear extrapolation of the S-N curve to 2×10^7 cycles [*10*].

Specimen

The specimen was chosen to fulfill the following requirements: (*1*) fatigue load capacity less than 500 kN, (*2*) realistic weld geometry and weld procedure, and (*3*) three-dimensional crack growth, simulating crack growth from a weld in a large structural member. The longitudinal fillet-welded attachment shown in Fig. 2 complied with most of these requirements. In addition, this specimen has been used in many other laboratories, so that much background material exists [*11*].

The material was a structural carbon-manganese steel with yield stress $\sigma_y \approx 300$ MPa. The welding process was manual in the flat position with low-hydrogen electrodes. All specimens were produced by the same welder; scatter was thereby decreased considerably as compared to what is normally experienced in fatigue testing of weldments. It is therefore emphasized that the scatter should not be taken as a measure of the variability in the fatigue capacity of welded structures in general.

Stress-relieving was accomplished by heating in an oven to 850 K, with a subsequent slow cool-down.

Residual Stresses

Residual stresses in the vicinity of a weld are extremely hard to measure, due to large gradients and an irregular geometry. In this case, residual stresses were measured by strain gages attached approximately 5 mm from the weld toe (Fig. 2). The specimen was cut by a cold-saw in the plane of crack growth, and the change of strain as recorded by the gages was taken as a measure of the residual stresses acting across the crack plane. The strains were interpreted as elastic, and the Poisson ratio effect was taken into account.

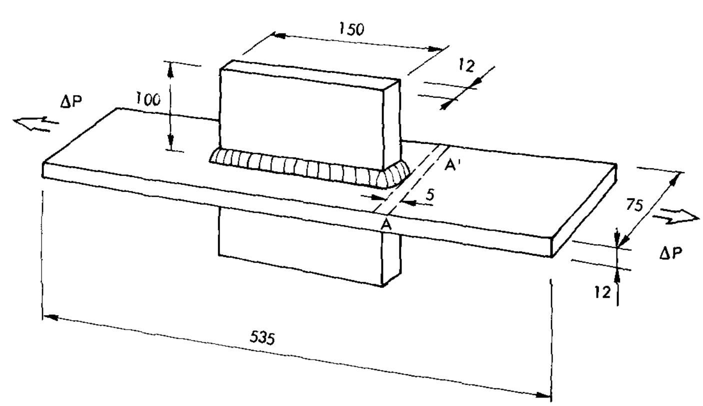

FIG. 2—*Dimensions of specimen (millimetres).*

Results from a series of residual stress measurements, performed on several specimens, are shown in Fig. 3 for as-welded and stress-relieved specimens. For as-welded specimens, the measured residual tensile stresses are shown to reach a maximum of approximately 200 MPa, that is, 0.7 σ_y.

Figure 4 shows measurements along the center-line in front of the weld at various distances from the weld toe. By extrapolation, the stress at the weld toe must be close to σ_y.

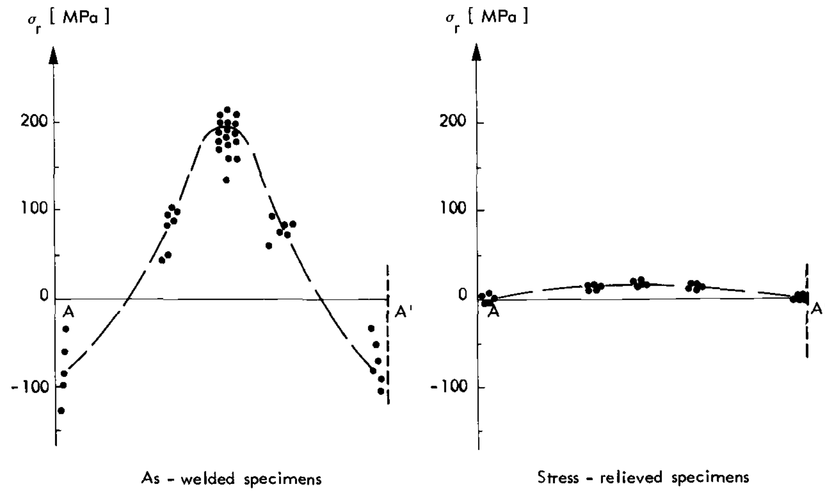

FIG. 3—*Residual stresses transverse to the crack plane measured across the specimen 5 mm from the weld toe (cf. Fig. 2).*

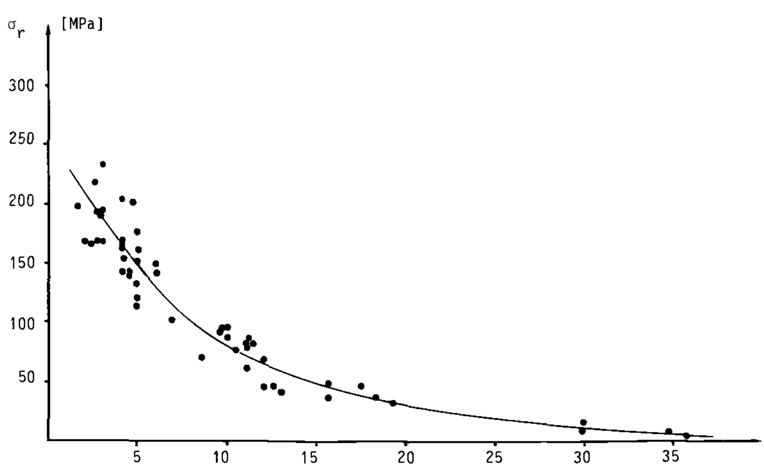

FIG. 4—*Residual stresses measured along the center-line of the specimens at varying distance from the weld toe; as-welded specimens.*

Although the method of measurements was crude, the following facts were established:

1. Residual stresses at the toe of the weld, where fatigue cracks are initiated, were of yield magnitude.
2. At some distance from the weld, across the crack growth plane, the stresses were compressive, typical of structural welds.
3. In the stress-relieved specimens, residual stresses were very small ($\sigma_r \lesssim 0.1\ \sigma_y$).

Through-thickness variations of the residual stresses could not be measured in a reliable manner. In this case, however, with attachment welds on relatively thin plate, the stresses may be assumed to be constant through the thickness.

In variable-amplitude loading, relaxation of residual stresses due to overloads and subsequent plastic strains, may be important. In order to investigate this, specimens were cycled at $R = 0$ through 10^3 to 10^4 cycles in constant-amplitude loading, and then examined for residual stresses as described above. Due to slight welding distortions, clamping the specimens in the grips of the testing machine would cause some bending. Therefore, bending moments induced by clamping were recorded in all the tests.

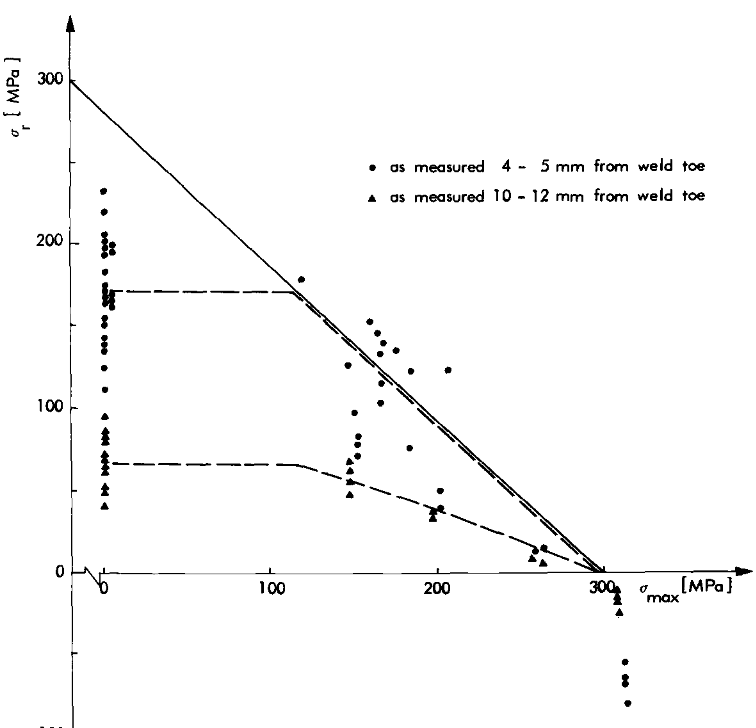

FIG. 5—*Relaxation of residual stresses following cycling through 10^3 to 10^4 cycles at* R = *0 and* σ_{max} *as measured 10 mm in front of the weld toe; as-welded specimens.*

Results are plotted in Fig. 5 as residual stresses σ_r versus σ_{max} where

$$\sigma_{max} = \sigma_{c\ell} + \Delta\sigma$$

where $\sigma_{c\ell}$ are bending stresses due to clamping. $\Delta\sigma$ was taken as measured 10 mm from the weld toe.

As shown in Fig. 5, there is a significant relaxation of the residual stresses. Assuming $\sigma_r = 300$ MPa in the as-welded condition and an ideal elastic-plastic material behavior, the solid line would describe the relaxation process. For residual stresses less than yield, the dashed curves are appropriate.

However, this interpretation is too simplistic, for two main reasons:

1. From hardness tests, it may be inferred that the yield stress in the heat-affected zone was approximately 465 MPa (HV 5 $\simeq$ 450), whereas at a distance more than about 3 mm from the weld toe, the yield stress was 310 MPa (HV 5 = 300). (HV 5 indicates Vickers Hardness with 5 kgf applied load).
2. At the weld toe, there is a local stress concentration. Depending on weldment shape, the concentration factor is in the range of 2 to 3.

Hence the elastic-plastic material behavior at the weld toe is extremely difficult to describe. In a qualitative manner, however, it may be concluded that there is a relaxation following peak loads, which in the limit of yield magnitude local stresses tends to completely eliminate the residual stresses. For stresses exceeding yield, the residual stresses become compressive, most probably due to the elastic action of the remote parts of the specimen (Fig. 2).

It should be noted that the findings reported here, refer to one particular geometry, and one particular stress field, and should be generalized only with great care. In particular, the behavior of long-range residual stresses may be entirely different from what has been observed with short-range stresses.

Constant-Amplitude Tests

S-N curves were established for as-welded and stress-relieved specimens, applying loads with stress ratios $R = 0$ and $R = -1$. In order to investigate the effects of cumulative damage, the *S-N* curves have to be extrapolated in the long endurance region [*10*]. Hence uncertainty in the determination of the slope should be minimized. This was achieved by testing at high and low stresses in the linear region. For each *S-N* curve, 20 specimens were tested. The results with scatterbands ($\pm$ two standard deviations) are shown in Figs. 6 to 9 and summarized in Fig. 10.

Clearly, the "stress range philosophy" for as-welded specimens is verified—as expected. The stress-relieved specimens tested at $R = -1$ exhibit a larger scatter, a somewhat shallower slope, and a 20 to 30 percent increase in fatigue strength. The scatter is particularly pronounced in the low end of the curve. These observations may be explained by the influence of static bending moments from clamping the specimens. Bending stresses were measured to be in the range of 0 to 30 MPa. These stresses would cause random shifts in the

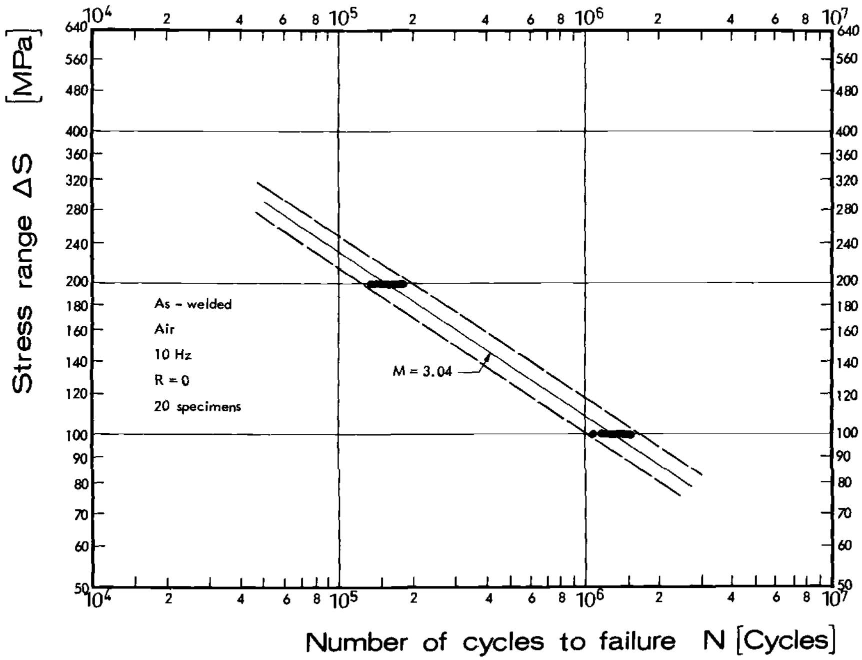

FIG. 6—S-N *data*.

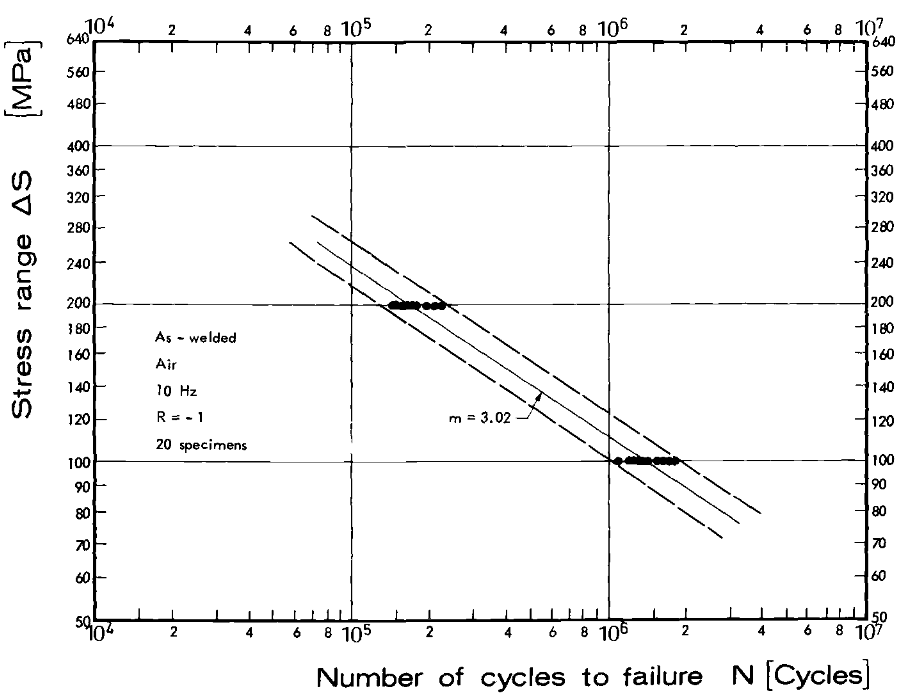

FIG. 7—S-N *data*.

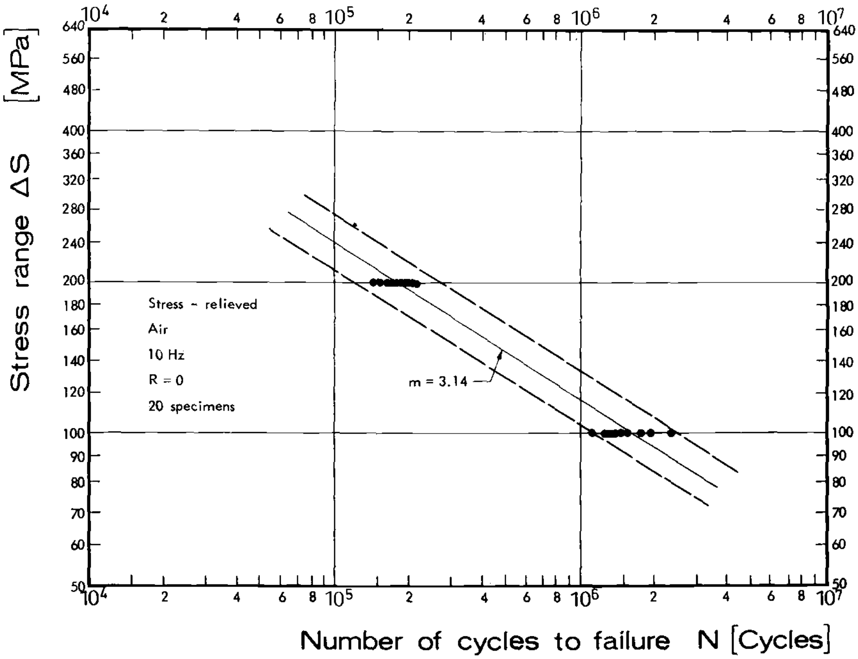

FIG. 8—S-N *data*.

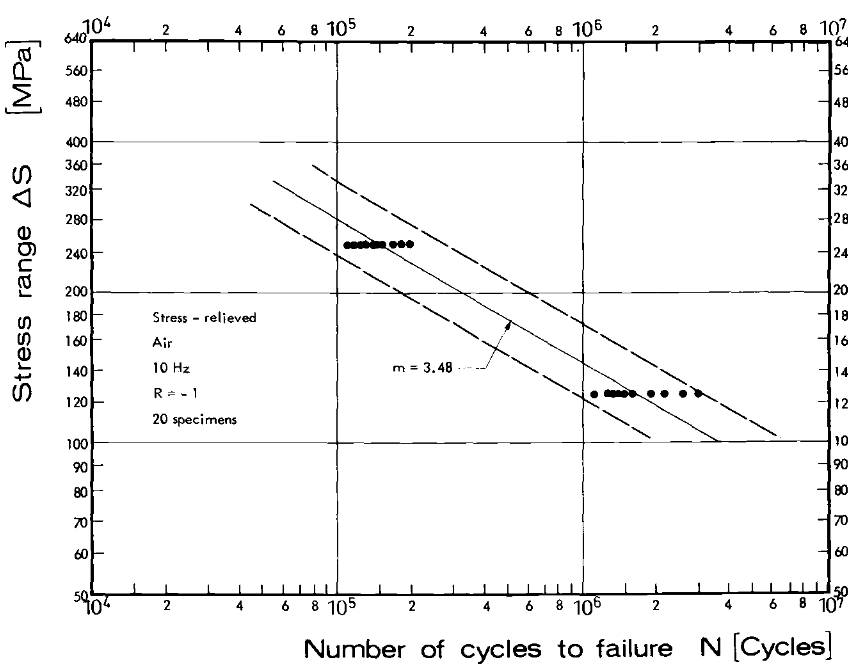

FIG. 9—S-N *data*.

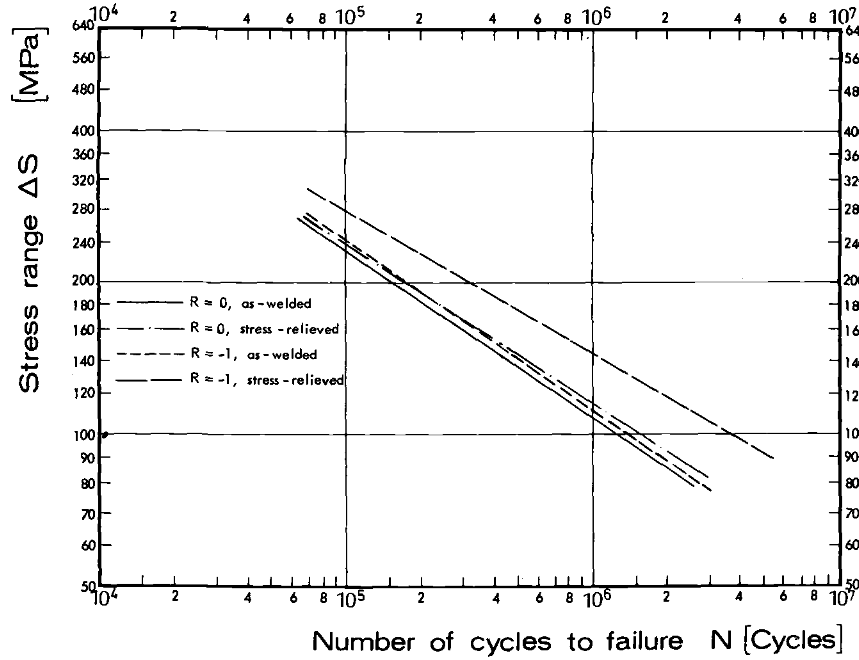

FIG. 10—S-N *curves, summarized.*

R-ratio, and thereby an overall decrease in fatigue strength and an increased scatter due to threshold effects.

Block-Program Testing

A block program was designed to resemble the general shape of stress spectra for marine structures (Figs. 11 and 12). The block levels were chosen so that the peak load would occur once in each period, and each period would have to be repeated at least 100 times in order to give a Miner-Palmgren sum of unity. Thus the loading could be assumed to be stationary. The effects of peak loads with a more rare occurrence than once in each period are not included in this program.

In order to avoid excessive testing duration, the spectrum was truncated in the lower end. Several cut-off levels corresponding to constant-amplitude endurances close to or below the fatigue limit were used (Table 1).

As shown in Fig. 10, there were slight differences between regression lines for the *S-N* data found under different conditions of stress ratio and heat treatment. The peak levels of the corresponding stress spectra, keeping the abscissa intercept at 2×10^8 cycles, were adjusted accordingly in order to give a Miner sum of unity.

Furthermore, the stress levels of each block were adjusted slightly in order to obtain a digital number of cycles in each period of blocks. These adjustments in

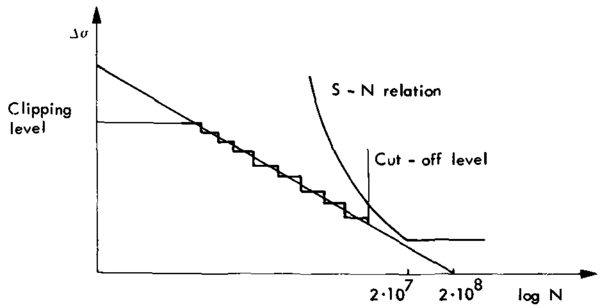

Fig. 11—*Stress spectrum typical of marine structures with block approximation; clipping and cut-off levels illustrated. Also shown is* S-N *relation (linear axis of ordinates).*

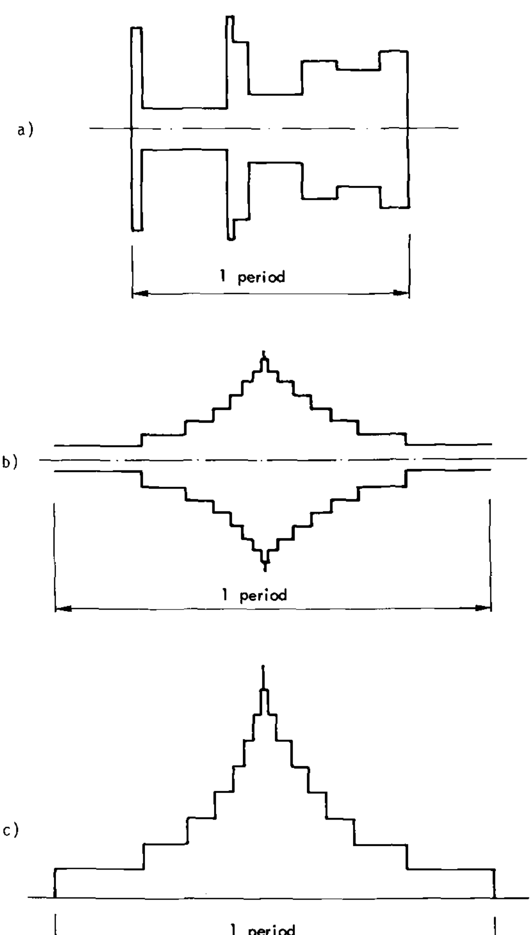

FIG. 12—*Block program.* (a) *randomized at* R = *−1.* (b) *Ascending/descending at* R = *−1.* (c) R = *0.*

TABLE 1—*Stress spectra for block loading.*

Spectrum No.	R	σ_m, MPa	$\Delta\sigma$ (Clipping Level), MPa	$\Delta\sigma$ (Cut-off Level), MPa	No. of Stress Levels (Blocks)	No. of Cycles per Period	Block Sequence within each Period	Specimen
1a	0	...	183.5	56.3	9	20 000	ascending/descending	as-welded
1b	−1	0	189.7	58.3	9	20 000	ascending/descending	as-welded
2a	0	...	183.5	71.1	8	6 000	ascending/descending	as-welded
2b	−1	0	189.7	73.3	8	6 000	ascending/descending	as-welded
3a	0	...	197.5	76.3	8	6 000	ascending/descending	stress-relieved
3b	−1	0	261.1	100.9	8	6 000	ascending/descending	stress-relieved
4	—	25	189.7	73.3	8	6 000	ascending/descending	as-welded
5	−1	0	189.7	73.3	8	6 000	randomized	as-welded

TABLE 2—*Details of block loading.*

$R = 0$			
Block No.	No. of Cycles	Stress Range, as-welded	Stress Range, stress-relieved
1	1	177.5	191.0
2	4	163.9	176.4
3	12	149.3	160.7
4	40	135.0	145.3
5	122	120.8	129.9
6	400	106.6	114.6
7	1 300	92.2	99.1
8	4 120	77.8	83.6
9	14 000	63.3	67.9
$R = -1$ and $\sigma_m = 25$ MPA			
Block No.	No. of Cycles	Stress Range, as-welded	Stress Range, stress-relieved
1	1	183.7	252.6
2	4	169.5	233.3
3	12	154.4	212.5
4	40	139.7	192.2
5	124	124.9	172.1
6	400	110.2	151.7
7	1 300	95.4	131.3
8	4 240	80.4	110.7
9	13 880	65.4	90.0

effect made the test conditions in terms of cumulative damage identical for each series of specimens.

The details of the test spectra are given in Tables 1 and 2. Results from the block program testing are shown in Tables 3 to 8 and will be discussed briefly.

In the absence of interaction effects, and assuming fracture to occur by crack growth according to a Paris-Erdogan type growth relation, the Miner-Palmgren summation index (Eq 1) will be unity at fracture (disregarding scatter). Deviation from unity is taken as a measure of interaction.

Table 3 compares the effects of small stress cycles at $R = 0$. Clearly, cycles below the fatigue limit are less effective than prescribed by the Gurney model. Whether that is due to a shortcoming of that model, or an increased interaction effect, may be open to discussion.

Table 4 shows results for stress-relieved specimens, tested under conditions equal to the spectrum 2a tests in Table 3. The delay effects are seen to be greater for stress-relieved specimens. In light of the popular Wheeler model [7], this seems surprising, because retardation is assumed to depend on the maximum stress intensity. One explanation could be that although retardation is caused by a peak stress, the main effect is on the small amplitudes—for example, through crack closure. If so, that could explain the trend shown in Table 3 comparing the effect of small cycles. It is noteworthy that the Miner-Palmgren index is very conservative for $R = 0$ loading.

TABLE 3—*Results from block-program testing at* R = *0; as-welded specimens.*

	Block Program No.	N_{Miner}	N_{test}	D	$\bar{D}$	Comments
a)	1a)	3.548.000	8.380.000	2.36	···	···
		3.548.000	>10.740.000	>3.03	···	run-out
		···	9.880.000	2.79	>2.89	···
		···	>10.820.000	>3.05	···	run-out
		···	>11.380.000	>3.21	···	run-out
b)	2a)	2.039.500	2.946.000	1.44	···	···
		2.039.500	3.684.000	1.81	···	···
	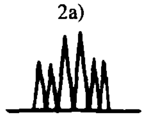	2.039.500	2.370.000	1.16	1.60	···
		2.039.500	3.402.000	1.67	···	···
		2.039.500	3.924.000	1.92	···	···

TABLE 4—*Results from block-program testing at* R = *0; stress-relieved specimens.*

Block Program No.	N_{Miner}	N_{test}	D	$\bar{D}$
3a)	1.951.220	3.744.000	1.92	···
	···	5.480.000	2.81	···
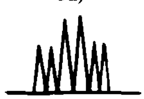	···	3.990.000	2.05	2.25
	···	3.564.000	1.83	···
	···	5.106.000	2.62	···

TABLE 5—*Results from block-program testing at* R = *−1; as-welded specimens.*

	Block Program No.	Amplitude Sequence	N_{Miner}	N_{test}	D	$\bar{D}$
a)	1b)		3.566.000	3.489.710	0.98	···
			···	4.560.000	1.28	···
			···	3.960.000	1.11	1.09
			···	3.620.000	1.02	···
			···	3.760.000	1.05	···
b)	2b)		2.026.300	1.458.000	0.73	···
			···	2.328.000	1.15	···
			···	2.304.000	1.14	0.99
			···	1.956.000	0.97	···
			···	1.920.000	0.95	···
c)	2b)		2.026.300	3.024.000	1.49	···
			···	2.454.000	1.21	···
			···	2.538.000	1.25	1.39
			···	3.624.000	1.79	···
			···	2.478.000	1.22	···

Table 5 shows results for conditions similar to those of Table 3, but with $R = -1$. Clearly, the interaction effects are much smaller at $R = -1$. Moreover, a significant effect of the sequence of peak and trough is observed. In Tables 5 to 8, the last load excursion in each block is encircled, showing the particular sequence for each test series. With one block ending with a peak, there is some interaction, whereas if the block ends with a trough, interaction is

TABLE 6—*Results from block-program testing at* R = *−1; stress-relieved specimens.*

Block Program No.	Amplitude Sequence	N_{Miner}	N_{test}	D	$\bar{D}$
3b)		1.644.355	1.358.000	0.82	...
		...	1.218.000	0.73	...
		...	918.000	0.55	...
		...	834.000	0.50	...
		...	1.434.000	0.86	0.81
		...	1.304.000	0.78	...
		...	1.053.000	0.63	...
		...	2.070.000	1.24	...
		...	2.063.788	1.24	...
		...	1.194.180	0.72	...

TABLE 7—*Results from block-program testing;* σ_m = *25 MPa; as-welded specimens.*

Block Program No.	Amplitude Sequence	N_{Miner}	N_{test}	D	$\bar{D}$
4	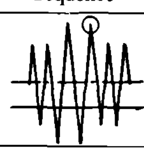	2.026.300	2.784.000	1.36	...
		...	2.514.000	1.24	...
		...	2.124.000	1.05	1.12
		...	2.070.000	1.02	...
		...	1.836.000	0.91	...

TABLE 8—*Results from block-program testing at* R = *−1; as-welded specimens.*

Block Program No.	Amplitude Sequence	N_{Miner}	N_{test}	D	$\bar{D}$
5	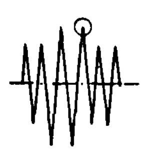	2.026.300	1.896.000	0.94	...
		...	1.843.000	0.91	...
		...	1.519.000	0.75	...
		...	2.107.000	1.04	1.09
		...	3.078.000	1.52	...
		...	2.706.000	1.34	...
		...	2.256.000	1.11	...

negligible. This is in qualitative agreement with findings from single overload tests [*11*].

Table 6 shows results with $R = -1$ for stress-relieved specimens. Contrary to what was found at $R = 0$, stress-relieving seems not only to reduce the effect of retardation, but to cause acceleration of the fatigue damage. No ready explanation for this can be given.

Table 7 shows results for conditions similar to those in Table 5c, but with a mean stress of 25 MPa. As shown, the retardation is somewhat decreased.

Table 8 shows results with $R = -1$ and a randomized block sequence. By this, the retardation effects are also decreased, as compared to Table 5c.

Conclusions

The aims of this project were to assess the significance of residual welding stresses in constant and variable amplitude fatigue. Only short-range residual stresses were considered. The following observations were noted:

1. In constant-amplitude testing, there was no difference in fatigue capacity for as-welded specimens tested at $R = 0$ and $R = -1$, and stress-relieved specimens tested at $R = 0$. Thus the "stress range philosophy" was verified for these conditions. At $R = -1$, stress-relieved specimens had an increased strength of 20 to 30 percent.
2. In variable-amplitude loading, short-range residual stresses are relaxed due to local yielding at peak loads. With the particular specimens employed, the residual stresses were eliminated by peak stresses of yield magnitude.
3. Except in one case—stress-relieved specimens tested at $R = -1$—interaction effects were beneficial; that is, the crack growth was retarded as compared to constant-amplitude behavior.
4. At $R = 0$, stress interaction effects (retardation) were large, particularly for small cycles in the spectrum. Stress-relieved specimens showed a greater effect of retardation than as-welded specimens.
5. At $R = -1$ or with $\sigma_m = 25$ MPa, interaction effects were generally small. At $R = -1$, stress-relieved specimens experienced an accelerated crack growth.
6. The sequence of peak and trough in each cycle was important for interaction effects at $R = -1$. A peak/trough sequence gave negligible interaction, whereas trough/peak gave some interaction. These results conform with what is observed with single overloads.
7. Randomizing the blocks caused a small reduction in the interaction effects as compared to an ascending/descending sequence.
8. The data are believed to be extremely useful for testing of analytical models of stress interaction.

Acknowledgments

This work is a part of the coordinated Norwegian research on fatigue and fracture of offshore steels. Financial support from the Norwegian Council for Scientific and Technical Research (NTNF) is gratefully acknowledged.

References

[1] *Steel, Concrete and Composite Bridges, Part 10. Code of Practice, BS 5400:1980*, British Standards Institution.
[2] *Structural Welding Code D1.2-77*, American Welding Society.
[3] Gurney, T. R. and Maddox, S. J., "A Re-Analysis of Fatigue Data for Welded Joints in Steel," Report E/44/72, The Welding Institute.
[4] Gurney, T. R., "Some Recent Work Relating to the Influence of Residual Stresses on Fatigue Strength," in *Residual Stresses in Welded Constructions and their Effects*, The Welding Institute, 1977.
[5] *Guidance on Some Methods for the Derivation of Acceptance Levels for Defects in Fusion Welded Joints, PD 6493:1980*, British Standards Institution.

[6] Olivier, R. and Ritter, W., *Catalogue of* S-N *Curves of Welded Joints in Structural Steels*, Deutscher Verlag für Schweisstechnik, 1979–81.
[7] Broek, D. and Smith, S. R., *Engineering Fracture Mechanics*, Vol. 11, 1979, pp. 123-141.
[8] Leide, N., "The Significance of Residual Stresses—Some Experimental Results and Practical Experience in a Shipyard," *Residual Stresses in Welded Construction and their Effects*, The Welding Institute, 1977.
[9] Frost, N. E., Marsh, K. J., and Pook, L. P., *Metal Fatigue*, Clarendon Press, Oxford, 1974.
[10] Gurney, T. R., "Cumulative Damage Calculations Taking Account of Low Stresses in the Spectrum," The Welding Institute Report 2/1976.
[11] Garwood, S. J. and Boulton, C. F., "Cumulative Damage to Welded Steel Structures," British Steel Corporation Report FR 97-782, 1979.

R. C. Rice,[1] *B. N. Leis,*[1] *and M. E. Tuttle*[1]

An Examination of the Influence of Residual Stresses on the Fatigue and Fracture of Railroad Rail

REFERENCE: Rice, R. C., Leis, B. N., and Tuttle, M. E., **"An Examination of the Influence of Residual Stresses on the Fatigue and Fracture of Railroad Rail,"** *Residual Stress Effects in Fatigue, ASTM STP 776,* American Society for Testing and Materials, 1982, pp. 132-157.

ABSTRACT: Fatigue cracks in rails can be the source of failures and subsequent derailments. The present paper examines the effect of residual stresses on the fatigue and fracture resistance of rail steel materials and the probable influence of residual stresses on the fatigue performance of rails in service. The magnitudes of residual stresses in rails were measured as a part of this study. Tensile and compressive residual (mean) stresses are shown to have a significant effect on the fatigue resistance of rail steels through tests using cylindrical smooth and compact tension specimens (free of inherent residuals) over a range of mean stress conditions. Fatigue and fatigue crack growth rate data developed are analyzed using specific damage parameters to consolidate the effect of mean stress. These data are then used in combination with measured residual stresses on rails to estimate the influence of service/fabrication induced, residual stresses in actual rail.

KEY WORDS: fatigue, crack initiation, crack propagation, residual stresses, rail steel, mean stresses, periodic overstrain

Nomenclature

a	Crack length
B	Specimen thickness
C	Crack growth rate intercept
CT	Compact tension
da/dN	Crack growth rate
E	Elastic modulus
FEC	Florida East Coast
j, k	Subscripts denoting specific cycle intervals, stress intensity levels, and crack growth rates
K	Stress intensity factor
ΔK	Stress intensity factor range
K_{max}	Maximum stress intensity factor

[1]Principal Research Scientist, Senior Research Scientist, and Research Scientist, respectively, Battelle Columbus Laboratories, Columbus, Ohio 43201.

K_c	Plane stress fracture toughness
K_{th}	Threshold stress intensity factor
K_t	Theoretical stress concentration factor
LT	Long transverse
m	Exponent in equivalent strain parameter
MGT	Million gross tons
n	Crack growth rate exponent
N	Fatigue cycles
N_i	Fatigue cycles to crack initiation
NEC	North East Corridor
P	Applied load
R	Ratio of minimum to maximum stress
$\overline{R}$	A special form of R; $= R$ for $R > 0.0$; $= 0$ for $R < 0.0$
SEN	Single edge notched
SP	Southern Pacific
W	Specimen width
ε_{eq}	Equivalent strain parameter
$\Delta\varepsilon_t$	Total stable strain range
θ_1	Orientation of σ_1 with respect to the x-axis
σ_1, σ_2, σ_3	Principal stresses
σ_m	Mean stress
σ_{max}	Maximum stable stress
σ_{res}	Residual stress
σ_x, σ_y, σ_z	Orthogonal stress components in the lateral, vertical, and axial directions of the rail
τ_{xy}	Shear stresses in the lateral plane of the rail

Since fatigue cracks in rails can be a source of failures and subsequent derailments, prevention of such failures and design against cracking are of paramount concern to both government and industry. Often, the bulk of the service life of a rail is spent nucleating cracks at highly stressed locations and sharpening existing manufacturing/processing defects. Once such microcracks have fully developed, their growth as macrocracks carries them to sizes which can be reasonably detected, and ultimately to failure when the critical crack size is reached. Today, unfortunately, crack nucleation, microcrack growth, and macrocrack growth cannot be characterized by a single mathematical model that is internally consistent with phenomenological observations. Government and industry interest in (*1*) design against cracking and (*2*) preventing derailment by inspection and removal of growing macrocracks, therefore, cannot be served by the same analysis procedure. For this reason, separate models for crack initiation and growth must be developed to explore the sensitivity of rail performance to variables such as train make-up and rail weight.

This paper addresses defect development and growth in rails with specific reference to the probable influence of residual stresses on the fatigue and fracture resistance of rails in-service. Residual stress effects on rail steels were examined in the laboratory using cylindrical smooth and compact tension specimens (free of inherent residuals). These specimens were tested at different mean stresses to simulate the combined action of service/fabrication induced residual stresses and mean service stresses in a rail head. Constant amplitude fatigue and fatigue crack growth rate data that were developed are analyzed in this paper using specific damage parameters to consolidate the effect of mean stress. In turn, fatigue data generated on specimens tested under variable strain and load amplitude conditions are predicted using these damage parameters. The constant amplitude data are also then used to estimate the influence of measured, service/fabrication induced, residual stresses in actual rail. Finally, the significance of residual stresses as compared to other factors believed to control the fatigue resistance of rails is discussed.

Problem Definition and Approach

Railroad engineers are faced with two questions: (*1*) Which factors have a first-order influence on rail life and safety? and (*2*) How can these factors be controlled to achieve optimum performance? The process becomes one of balancing control parameters such as speed, wheel load, road-bed quality, and inspection interval against traffic volume and economics. The process has not been quantitative; rather, this qualitative procedure has been based on slowly accumulated experience. The purpose of the present study, funded by the Federal Railroad Administration as part of their Track Performance Improvement Program, is to develop analytical models that incorporate train and track service parameters and to perform a correlative study of system performance as a function of these control parameters. Part of this study is reported here. Specifically, the influence of residual stress on service life and its relative influence on performance is considered as compared to other parameters believed to influence service life. The approach has been to develop rail specific models of crack nucleation and macrocrack growth, the details of which are reported elsewhere [*1–4*].[2]

Residual Stresses in Rails

During fabrication and subsequent use in the field, a rail section is subjected to various loadings that cause plastic deformation of the rail material, both along the length of the tread surface and through the rail cross section. These plastic deformations cause residual stresses in the rail—stresses which remain after the external loads have been removed. Residual stresses, coupled with the cyclic operational stresses, constitute an important driving force affecting the development and growth of cracks. Detailed knowledge of the residual stresses existing in rail is therefore essential for any analysis that attempts to investigate fatigue and fracture of rail.

[2] The italic numbers in brackets refer to the list of references appended to this paper.

The stresses that exist in a rail *in situ* are the result of a variety of factors, including the effects of the manufacturing/fabrication processes, the constraints and/or loadings due to the total track structure (for example, those due to temperature changes, joints, tie plates, ballast, etc.), and the "live" loads imposed during passage of a train. Although *in situ* plastic deformation is normally associated with live loads, loadings induced by the track structure can combine to produce high stresses, possibly contributing to plastic deformation of the rail.

For the purpose of this discussion, the term "residual stresses" will be used to denote those stresses existing in the rail after removal from the track structure, when all external loads have been removed. As such, these residual stresses are the result of the loads induced by the manufacturing/fabrication process, the total track structure, and the live loads. Some stresses, such as thermal stresses, are lost upon removal of the track from service, and they are not part of the residual stress pattern considered.

Residual Stress Measurement

The procedure used in this program to determine the three-dimensional stress state in a rail is a two-step process. First, residual strain measurements are obtained using a special slicing technique in which the rail specimen is destructively sliced or cut. These data are then used to determine the residual stress state, using a closed form, point-by-point calculation procedure.

Both the slicing technique and the analysis are subject to the following assumptions:

1. The residual stresses σ_x, σ_y, σ_z, and τ_{xy} are not functions of z (the position along the rail). The coordinate system used is defined in Fig. 1.
2. The residual stresses that originally exist in the rail are not increased by plastic deformation during cutting, and all residual stresses are relieved elastically.
3. The rail material is everywhere homogeneous, linearly elastic during stress relief, and orthotropic. For simplicity during this discussion, however, the rail material will be considered isotropic.

The details of the slicing technique and subsequent analytic point-by-point calculations are not presented here. A detailed presentation is given in Ref 5.

Analysis and Typical Results

Residual stresses have been measured in sections of tangent and curved rail, although the majority of work to date has been completed on tangent track. Although the number of specimens examined to date is not large enough to form a sound statistical basis, a distinctive pattern of residual stress buildup in rails has begun to emerge. Typical results for a 136 lb/yd rail are shown in Figs. 2 to 4. Figure 2 shows the axial residual stress pattern across the head of the rail. The interior portions of the rail head are generally in tension, although occasionally there is a small "island" of compressive axial stresses near the center of the rail

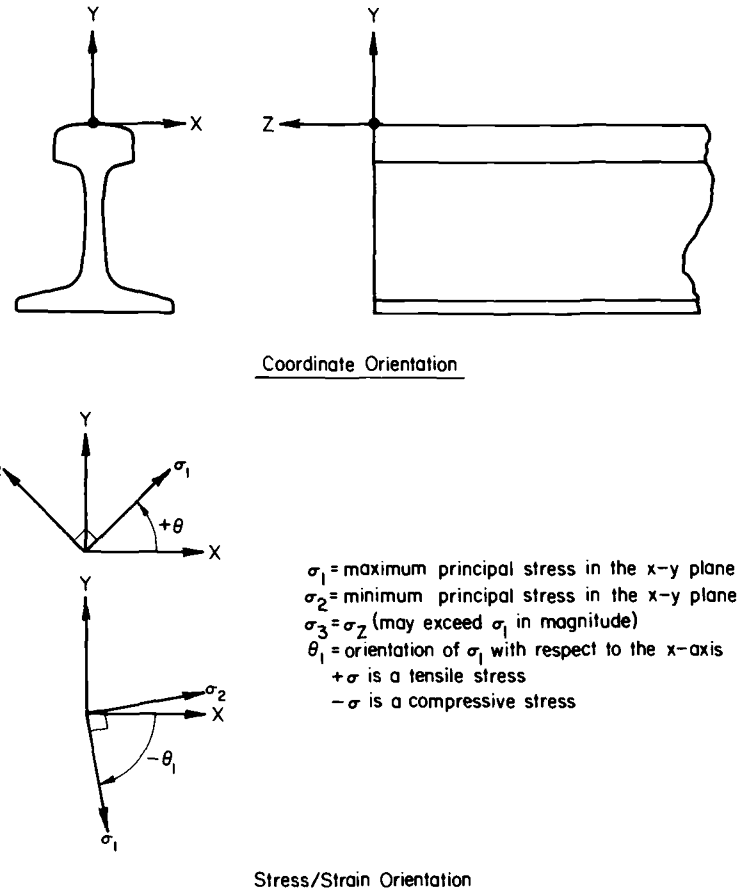

FIG. 1—*Orientation and sign conventions.*

head, as in Fig. 2. The tensile region extends in "fingers" towards both upper corners of the cross section. Compressive axial stresses are normally found around the periphery of the cross section. The only atypical result for this specimen is the small "knot" of high compressive stresses in the lower right corner of the cross section. This knot has not been found in other test pieces, and perhaps is an artifact from the manufacturing process.

Figure 3 shows the in-plane tensile stress contours; Figure 4 shows the in-plane compressive stresses. The magnitude and orientation of the in-plane principal stresses are shown in Fig. 5. A very high compressive stress is found at the gage-side surface, just below the flange wear pattern.[3] Only the very center of the rail head experiences completely tensile residual stresses.

[3] In a few of the rail specimens studied, these high compressive stresses were in excess of the material's typical tensile strength. It is suspected that in these cases the rail material was plastically deformed during removal of the material, causing artifically high strain readings. These stresses were assumed to be acting in the direction indicated, with a magnitude somewhere between yield and ultimate.

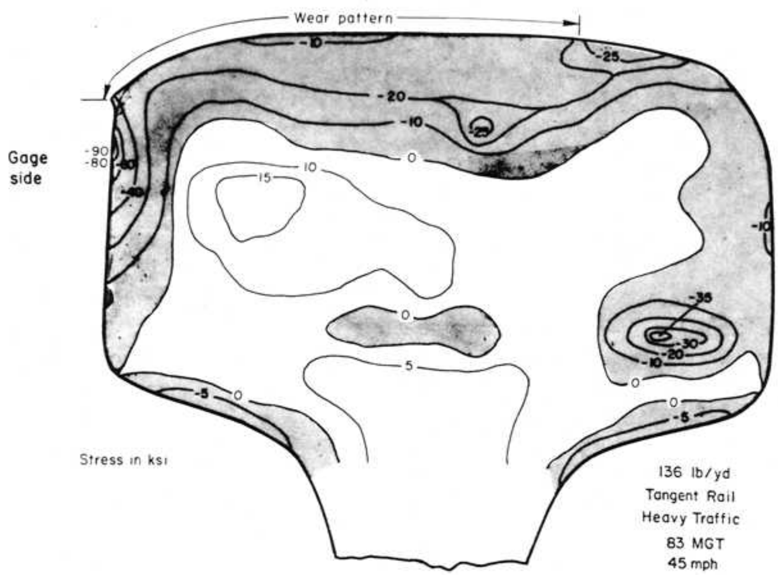

FIG. 2—*Axial residual stress pattern—Specimen 1.*

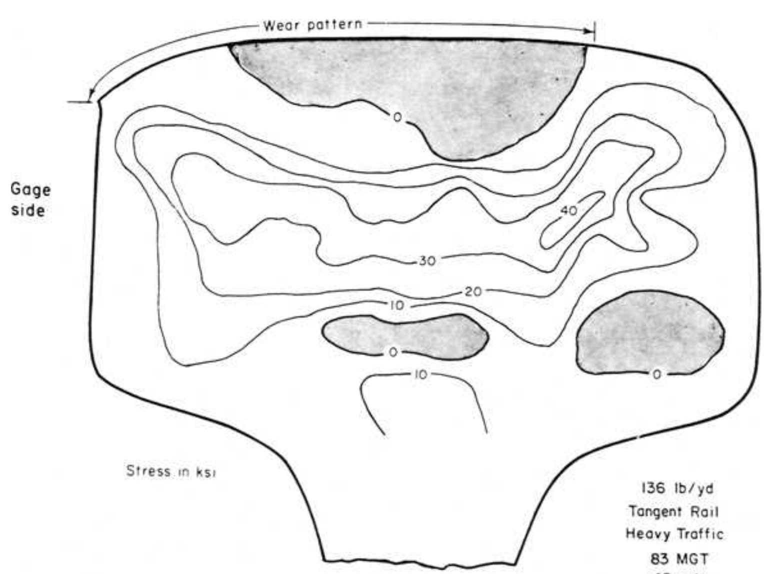

FIG. 3—*Specimen 1 in-plane tensile stress magnitude contours.*

The results presented in Figs. 2 to 5 indicate the general pattern of stress distribution found thus far in tangent rail. The surface and near subsurface compressive stresses are highest in magnitude, and the transverse compressive

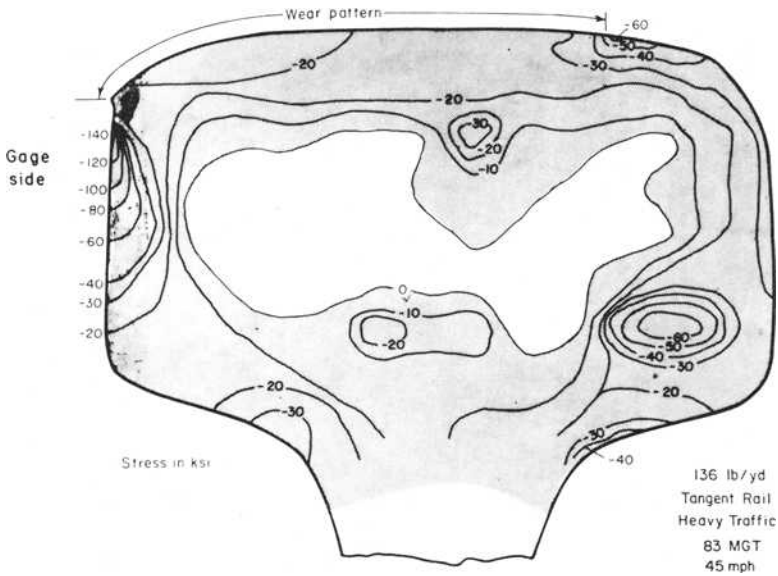

FIG. 4—*Specimen 1 in-plane compressive stress magnitude contours.*

stresses are higher than the axial compressive stress. The tensile stress components are also higher in the transverse plane than in the axial direction.

Before initiation of this program, it was thought that a "shakedown" condition (in which the residual stress magnitudes would develop towards a stable, unchanging level) might occur with increased tonnage. Based upon the limited data obtained to date, this does not appear to be the case. In all cases involving rails which had seen different amounts of similar traffic severity, the residual stress distributions were very similar, but the stress magnitudes changed with increased usage.

Mean Stress Influence on Rail Material Fatigue Resistance

Extensive laboratory experiments have been completed to quantify the crack initiation and crack growth characteristics of rail steel material for a range of mean stress conditions. These data have been reported in detail in Refs *1* to *4*. The data pertinent to this discussion of mean stress effects are summarized in the following sections.

Data on the rail steel alloy composition and tensile properties are provided in Table 1. Extensive microstructural characterization of rail steel materials has been presented in Ref *6*.

Crack Initiation Resistance

Constant Amplitude Experiments—Over 200 constant amplitude crack initiation experiments were completed in this program. Of this total about one third

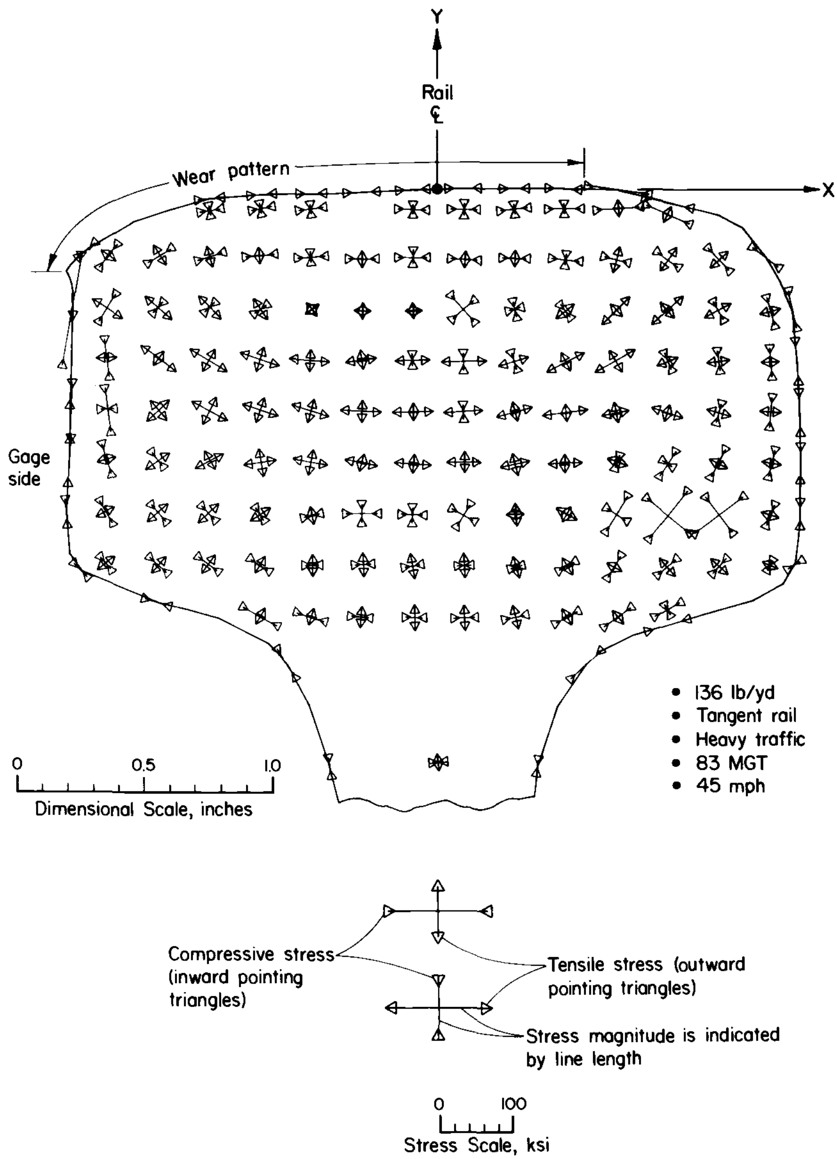

FIG. 5—*Magnitude and orientation on in-plane principal stress—Specimen 1.*

were strain-controlled experiments involving positive, negative, and zero mean strains. The remainder were load control experiments conducted by Boeing Commercial Aircraft Company (BCAC) [*3*]. These experiments involved positive and zero mean stresses.

In order to account for differences in control mode and effects of mean stress/strain on crack initiation behavior, an equivalent strain parameter was

TABLE 1—*Rail steel alloy composition and tensile properties.*

Alloy Composition				
	Nominal Weight, lb/yd			
Element, %	61 to 80	81 to 90	91 to 120	121 and over
Carbon	0.55 to 0.68	0.64 to 0.77	0.67 to 0.80	0.69 to 0.82
Manganese	0.60 to 0.90	0.60 to 0.90	0.70 to 1.00	0.70 to 1.00
Phosphorus, max	0.04	0.04	0.04	0.04
Silicon	0.10 to 0.23	0.10 to 0.23	0.10 to 0.23	0.10 to 0.23

Tensile Properties[a]				
Mechanical Property	Mean Value	Maximum	Minimum	Standard Deviation
Yield strength, ksi[b]	73.4	83.3	59.9	4.93
Ultimate strength, ksi	133.1	141.5	111.5	5.53
Elongation, %	11.8	17.0	9.0	1.78
Reduction in area, %	19.7	42.3	13.2	4.73
Young's modulus, 10^3 ksi	30.6	34.8	26.5	1.85
True fracture stress, ksi	156.4	185.3	119.8	8.67
True fracture ductility	0.112	0.157	0.086	0.016

[a] Based on 65 rail samples.
[b] 1 ksi = 6.89 MPa.

employed. This parameter is similar in form to that originally developed by Walker [*7*], but it was modified in an earlier study [*8*] along the lines suggested by Smith et al [*9*]. Equivalent strain was thereby defined as

$$\varepsilon_{eq} = (\Delta\varepsilon_t)^m (\sigma_{max}/E)^{1-m} \tag{1}$$

where

$\Delta\varepsilon_t$ = total stable strain range,
σ_{max} = maximum stable stress,
E = elastic modulus, and
m = constant for the material.

For the strain-controlled experiments, $\Delta\varepsilon_t$ was controlled and σ_{max} was measured after the stress response had stabilized. An average E was obtained from several monotonic stress-strain curves. In the load control tests, σ_{max} was controlled, but $\Delta\varepsilon_t$ was not measured. The strain range for these experiments had to be estimated from the cyclic stress-strain response of the material.

A value for the material constant m in Eq 1 was found through an examination of the load control data generated at three stress ratios. The maximum stress levels which provided nearly identical fatigue lives at different stress ratios were identified and Eq 1 was solved for a series of different m-values until a value of m was found which provided equal equivalent strain values. A value of $m = 0.60$ gave the best overall consolidation of the data. All the raw data are presented in Refs *3* and *4*. Crack initiation was considered to occur at the point where a crack approximately 0.76 mm (0.030 in.) deep had formed. Crack depth was not monitored routinely, but was correlated with a load drop from the stable load of about 2 percent. Using this procedure, the ratio of initiation cycles to total failure cycles ranged from about 0.85 to 0.95 on 13 specimens tested at several different strain ranges.

The grouped and consolidated crack initiation data are presented in Fig. 6. Load control data are identified with solid symbols, while strain control data are identified as open symbols. Numbers above a symbol denote the number of replicates used to establish the plotted average crack initiation life. For the most part the equivalent strain parameter consolidated the load and strain control data well. The only deviation from the general trend was with the very low, stable stress ratio, strain control data. The equivalent strain parameter appears to over-predict fatigue lives for these low maximum stress cases. However, more data of this type must be generated before any definite conclusions can be drawn regarding the applicability of the equivalent strain parameter in this regime. The general trends of the replicate data were well represented by a double-log-linear relationship between equivalent strain and crack initiation life, defined as

$$N_i = A_1 \varepsilon_{eq}^{n_1} + A_2 \varepsilon_{eq}^{n_2} \tag{2}$$

Variable Strain Amplitude Experiments—All variable amplitude testing was done in strain control. Periodic overstrain experiments were the simplest variable strain amplitude experiments performed, detailed discussion of which is presented elsewhere [*3*]. The insertion of infrequent overstrain cycles in an otherwise constant amplitude history dramatically reduced the apparent fatigue limit for the material (Fig. 7). This phenomenon has been observed previously [*10,11*] and is noted here, since this behavior must be accounted for in predicting the variable amplitude fatigue resistance.

Three different spectra were used in the variable amplitude experiments. These spectra were derived from cumulative probability curves of wheel rail loads

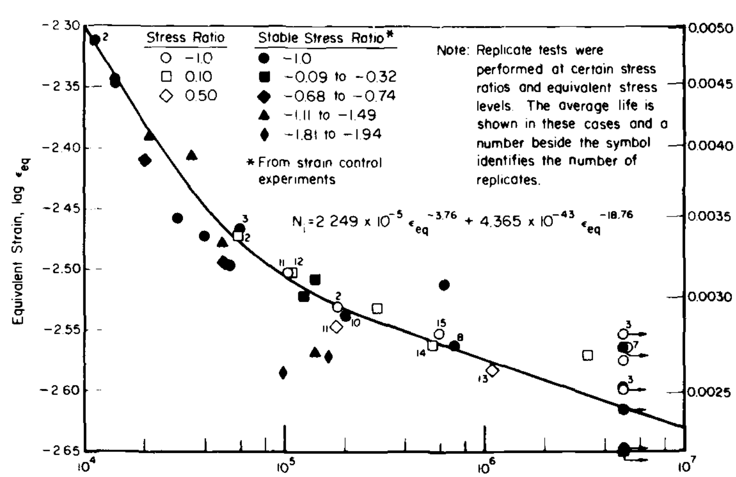

FIG. 6—*Consolidation of load and strain controlled crack initiation data generated at stress ratios ranging from −1.94 to 0.50.*

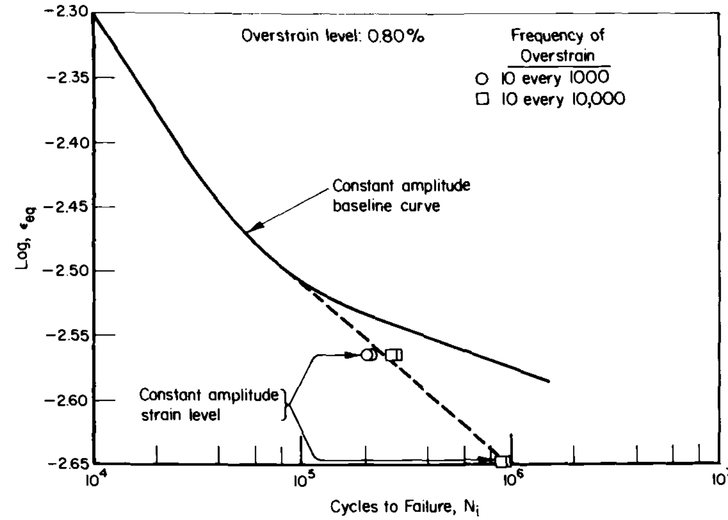

FIG. 7—*Periodic overstrain fatigue test results.*

measured for four different railroads [*12*]. These curves are shown in Fig. 8. The most severe spectrum used in this program was based on the North East Corridor (NEC) wheel rail loads, while the least severe was based on the Southern Pacific (SP) wheel rail loads. The third spectrum used in this program was based on a combination of the Union Pacific (UP) and Florida East Coast (FEC) wheel rail load distributions; it fell intermediate to the NEC and SP spectra. Note that all these railroads are rated Class 4 or higher, representing some of the better tracks in this country and relatively low rail failure rates.

The maximum strain levels in each test were held constant to simulate a residual tensile strain within the rail head, while the magnitudes of the negative strain excursions from that maximum strain were selected to achieve long-life but nonrunout fatigue crack initiation conditions.

Three different representations of the combined FEC/UP spectrum were tested. Only the simplest (unit train) representation was used for the NEC and SP spectra. The unit train history was a continuously repeated 8-level, high-to-low, block loading history. It was designed to represent an average or unit train. A total of 170 unit trains (1 MGT) contained the same number of cycles at each strain level as the same number of trains in the more complex spectra.

The history of intermediate complexity was a train-by-train loading pattern which consisted of an 11-level series of high-to-low block loadings, the exceedance spectra for which are shown in Fig. 9. This history was made up of six different trains, the composition of each being selected more or less arbitrarily. However, each resembled actual trains in size and load content. The mixture of trains was established in such a way that the heavy and light trains were not grouped together. A 170 train history made up of the 6 train types was repeated during the tests.

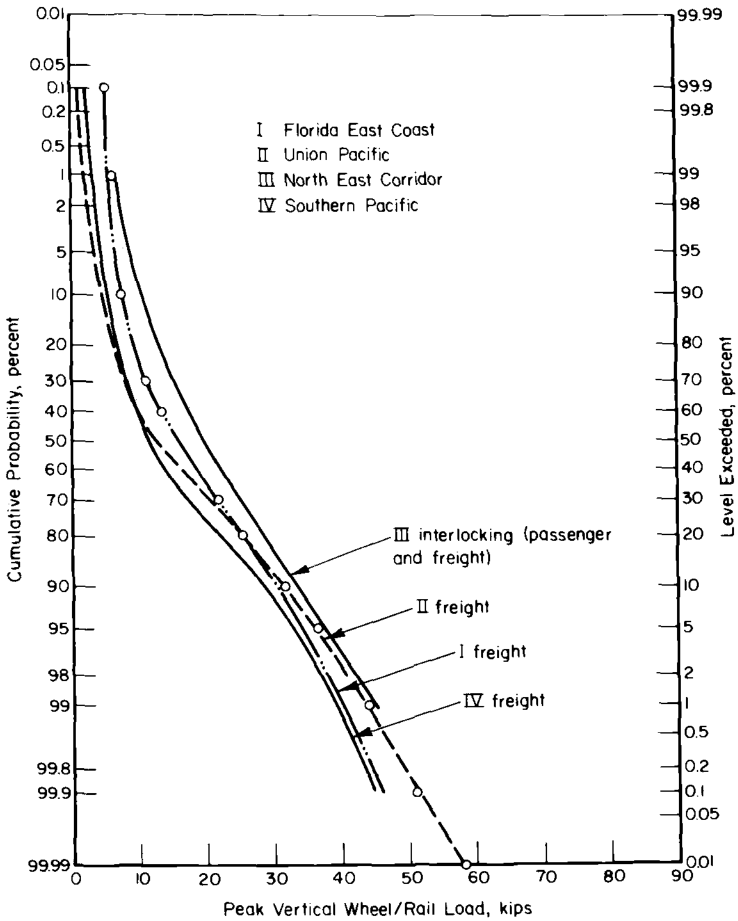

FIG. 8—*Load probability diagram.*

The most complex history was random in nature with the 11 strain range levels within each train randomized and the six different train types within the history also randomized. Different maximum strain levels were imposed for each spectra to simulate different residual stress conditions. A total of 17 variable amplitude strain control experiments were performed, resulting in fatigue lives ranging from 127 000 to 6 480 000 cycles. The mean stress effects displayed in these experiments are reviewed in the section on Crack Initiation Life Prediction.

Crack Propagation Resistance

The results of constant and variable amplitude fatigue crack growth experiments to determine the effects of stress ratio/mean stress are presented in this section. Data developed at the same time on the effects of cycling frequency, test temperature, and crack orientation are included in Ref *1*.

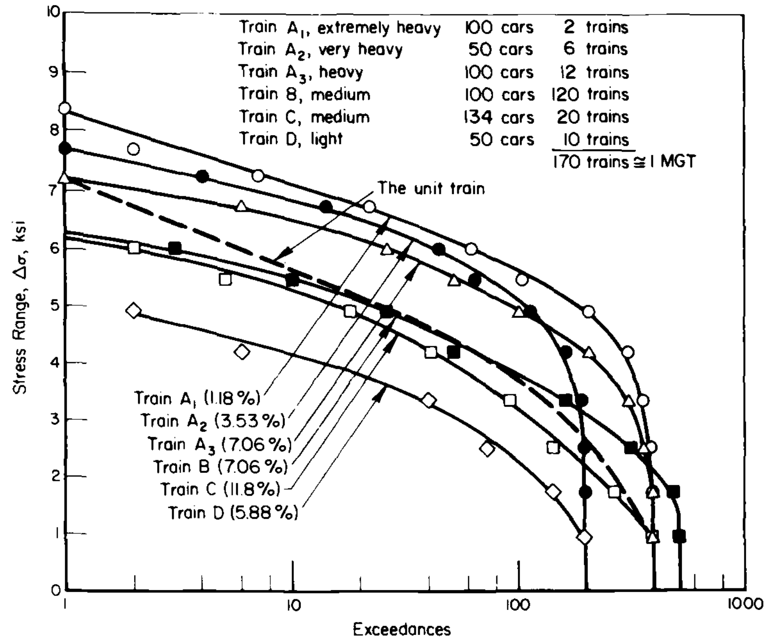

FIG. 9—*Exceedance spectra for six types of trains.*

Constant Amplitude Experiments—To evaluate the effects of stress ratio on the crack-growth behavior of rail-steels in the LT orientation (Fig. 10), a series of constant amplitude fatigue crack growth experiments at $R = 0.0$, -1.0, and 0.50 were performed on 18 SEN-type specimens. In addition, in order to verify that specimen geometry did not influence test results, three experiments at $R = 0.0$ were performed on a CT-type specimen. The resultant crack length-cycles data were analyzed using the 3-point divided difference method. The effect of specimen geometry on crack growth behavior was found to be negligible.

The overall data trends for the room-temperature crack growth experiments on LT orientation specimens are shown in Fig. 11. Three distinct bands are formed for each stress ratio when the data are plotted versus the stress intensity range ΔK. Note that negative stresses are included in the stress intensity calculation of the stress intensity range for $R < 0$. Each band has an average slope of approximately 4 in the logarithmically-linear range of data.

Experiments were also completed to develop estimates of threshold stress intensity levels. The zero and positive stress ratio conditions were evaluated using CT specimens. Negative stress ratio threshold conditions were examined with SEN specimens. Significant variability between and within specimens was evident, but trends did follow previously established trends at higher crack growth rates.

The effects of R-ratio displayed in Fig. 11 were partially accounted for by simply considering crack growth rate as a function of maximum stress intensity

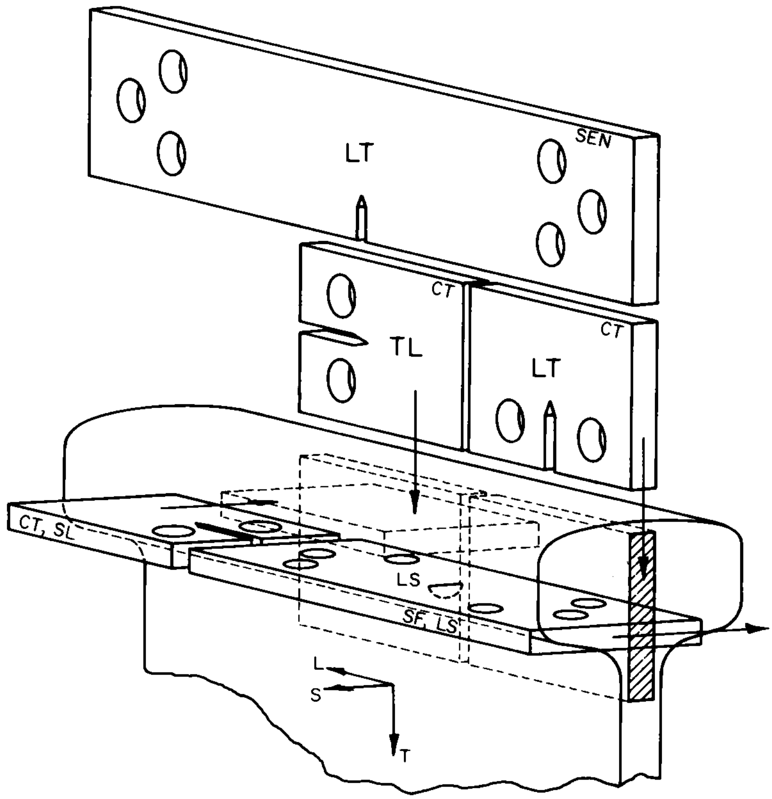

FIG. 10—*Orientation of specimens.*

K_{max}, rather than ΔK. When such a plot is constructed the $R = 0.0$ and -1.0 data bands nearly overlap for all values of K_{max}, which effectively means that negative loads are insignificant factors in the propagation of cracks in rail steels (at least for constant amplitude loading conditions). The $R = 0.5$ data band does not coincide with the lower R-ratio bands, which indicates that some combination of K_{max} and ΔK is necessary to accurately represent the effects of positive R-ratios on crack-growth rates.

In order to more accurately account for stress ratio effects, the Forman equation [*13*] was evaluated. It did not adequately condense the data. A variation on the Forman equation did work well, however. The variant expression is given as

$$da/dN = C(1 - \overline{R})^2 \frac{K_{max}^{n+2}}{K_c - K_{max}} \tag{3}$$

where

$\overline{R} = R$ (stress ratio) for $R > 0.0$, and
$= 0$ for $R \leq 0.0$.

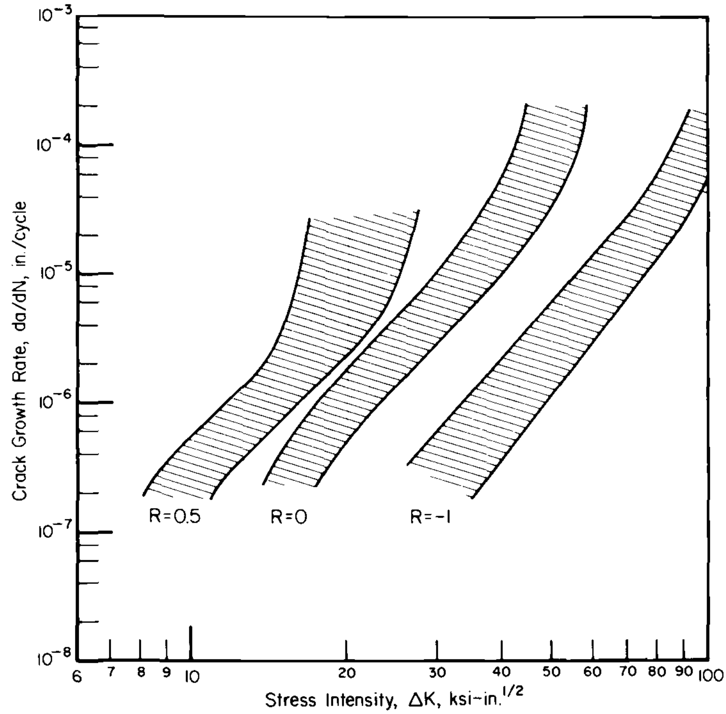

FIG. 11—*Bands of data variability for LT orientation rail samples at room temperature.*

A more involved form of Eq 3 was also devised, which accounted for threshold effects in addition to stress ratio. It is expressed as

$$da/dN = C(1 - \overline{R})^2(K_{max}^2 - K_{th}^2)\frac{K_{max}^{n-1}}{K_c - K_{max}} \qquad (4)$$

where

$K_{th} = 13.5 \text{ ksi}\sqrt{\text{in.}}$,
$C = 4.27 \times 10^{-9}$, and
$n = 2.13$.

To illustrate the quality of fit obtained with Eq 4, the expression is plotted in Fig. 12 in comparison to the mean crack growth curves for the LT orientation data (the variability bounds on these data were shown in Fig. 11). In Eq 4, K_{th} is assumed constant for different stress ratios. This assumption implies that regardless of the ΔK, crack growth in a rail would not be expected unless the residual stress were high enough to cause K_{max} to exceed K_{th}. As yet, this assumption has not been verified with carefully controlled crack growth experiments on actual rails.

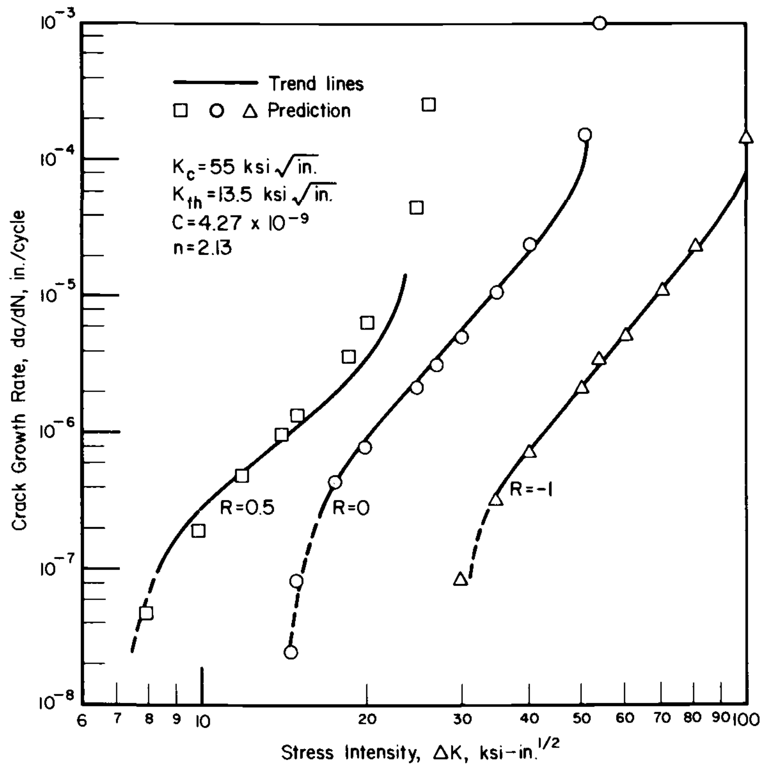

FIG. 12—*Applicability of crack growth equations, LT orientation, room temperature.*

Variable Load Amplitude Experiments —Three types of variable load amplitude crack growth experiments were conducted: periodic overload, simple history, and service simulation. The periodic overload experiments were conducted to evaluate potential load interaction effects that could grossly influence fatigue crack propagation rates [*14,15*]. Crack growth retardation caused by periodic overloads was not found to be significant.

The simple history tests were conducted to examine rail crack growth under load patterns similar to those seen by an element of material in the rail head during passage of a set of railroad car wheels. From these tests it was determined that the actual complex load variation pattern experienced by a rail during passage of a railroad car could be simplified with almost no change in crack growth trends, to only 4 cycles, the maximum stress of each cycle being representative of a residual stress.

Service simulation experiments were based on the wheel rail load probability diagram (Fig. 8). The same types of histories were examined as previously discussed for the crack initiation studies. It was concluded, from an experimental point of view, that the complexity of the stress history was of secondary importance if seven or more load levels were used. Even the unit train history provided comparable results, on the average, to the random history. There was a significant mean stress effect, however, which was reflected in the different average lives for the different service histories.

Assessment of Residual Stress Effects on Rail Fatigue Resistance

The influence of residual stresses on rail fatigue life is quite significant, as is demonstrated in the following paragraphs. The relative effects on crack initiation and propagation are similar, although there are some differences that will become apparent in the separate treatments of the two phases of the damage process which follow.

Crack Initiation Life Prediction

It has been speculated that the rapidity with which a transverse defect or detail fracture nucleates in a rail head is related to the magnitude of the residual stress field which has developed at that specific location in the head. This argument is supported by accurate life predictions on rail material specimens that had been tested in the laboratory under a variety of simulated service histories involving several different maximum strain levels which were selected to represent different residual stress levels. The argument is also supported by fatigue damage calculations made on a simulated rail head that include typical residual stresses and which correctly indicate one of the more common sites for crack initiation. (In this context, crack initiation may be the formation of a transverse defect from a shell below the rail running surface.)

Analysis of Laboratory Samples Subjected to Simulated Service—The residual stress crack initiation fatigue model was assessed in terms of its ability to reconcile fatigue lives of unnotched specimens tested under simulated service conditions. Three different methods of computing damage based on the equivalent strain model were examined. Since strain was controlled in these spectrum tests, the various levels of strain range, $\Delta\varepsilon_t$, were known and the maximum stable stress, σ_{max}, was necessarily measured or calculated. Where σ_{max} was computed, the cyclic stress-strain curve for the material was used in an expression of the form $\sigma_{max} = A\varepsilon_{max}^n$. The individual methods of linear damage calculation involved the variables shown in Table 2. Obviously, then, the differences in the methods relate to the basis for (*1*) the damage calculation—the fatigue curve—and (*2*) the value of the maximum stress.

Method 1 overestimated actual crack initiation lives in nearly every case, in an unconservative manner—an obvious indication that at least some of the small amplitude strain ranges in the history were damaging. Methods 2 and 3 provided comparable results, so Method 3 was selected for further study since maximum stresses are almost never measured in a practical situation. As shown in Fig. 13, Method 3 consolidated the data well for all test histories and simulated residual stress conditions. Converting from cycles to millions of gross tons (MGT) of traffic, it is important to note that the fatigue lives obtained in the variable

TABLE 2—*Variables considered in linear damage calculations.*

Method	Fatigue Curve	Maximum Stress
1	constant amplitude	actual
2	periodic overstrain	actual
3	periodic overstrain	computed

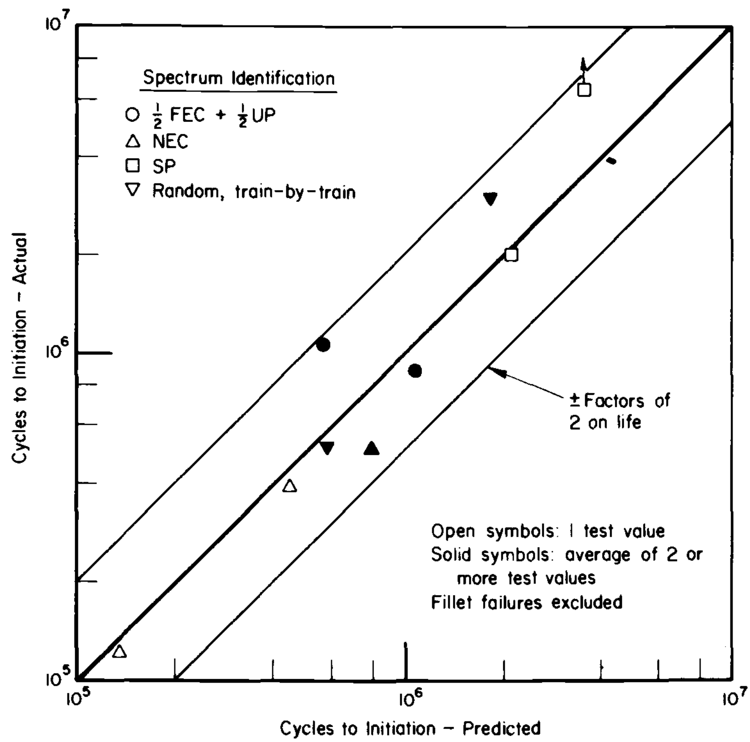

FIG. 13—*Actual versus predicted crack initiation lives by using a linear damage analysis and periodic overstrain baseline fatigue data.*

amplitude experiments performed in this study represented roughly 10 to 100 MGT of traffic. Most rail failures occur in the 100 to 1000 MGT range, so it is not clear whether the analysis method would accurately predict the very high service life failures often seen in the field. However, it can be said that most of the laboratory service histories which were used represented only the relatively heavy cars in a rails history. Many smaller amplitude cycles caused by lighter cars were clipped from the laboratory history based on experimental evidence that these smaller cycles were minor damage contributors. These lighter cars are counted in accumulating a rails MGT history, even though they probably contribute very modestly to a rail's failure. Thus it can be said that simulations for shorter lived laboratory histories represent the much longer lived field situations.

Prediction of Crack Initiation in Rails — The prediction of crack initiation in rails was handled parametrically to attempt to establish the relative influence of a wide variety of loading variables and rail system tradeoffs. From the outset it was recognized that life predictions would be qualitative, rather than quantitative, because only typical stress histories and material properties were considered, while in practice nearly all fatigue-induced rail failures occur at sites of extreme stress or inferior material.

The approach taken was straightforward. Axial residual strains were computed from axial residual stresses reported in Ref *5* for 26 sites in each rail cross section.[4] (Figure 2 was an example axial residual stress map.) Since wheel loads induce compressive axial strains in the head,[5] the residual strain constituted a constant maximum axial strain that served as the origin for negative strain excursions caused by wheel loading. On a cycle-by-cycle basis the maximum and bending strains were combined to compute an equivalent strain. Using the periodic overstrain equivalent strain curve defined as follows for $\varepsilon_{eq} < 0.0035$:

$$N_i = 3.02 \times 10^{-13} \varepsilon_{eq}^{-6.99} \quad (5)$$

a linear damage sum was accumulated until a damage fraction of unity was obtained which indicated crack initiation. Equation 5 was used rather than Eq 2 because it adequately reflects the reduced low strain range fatigue resistance of the rail steel material when subjected to periodic overstrains, over the range of strains considered.

Using this uniaxial stress model, it was possible to project relative damage at different sites in the head of the rail. Over 40 parametric combinations of rail weight, lateral load, wheel-rail contact point, track modulus, and rail wear severity were examined. For example, one of the parametric cases involved a 136 lb/yd rail, no lateral load, on center wheel contact, 8000 lb/in.^{2} track modulus and no wheel wear. Results from that analysis are shown in Fig. 14. This figure shows an estimate of the relative criticality at various sites in the rail cross section in terms of crack initiation. This result is very interesting because it accurately predicts the situation which is seen where transverse defects or detail fractures are found subsurface in the rail head. Note that crack initiation is not predicted at the top of the rail where compressive bending stresses are highest; that is because sizable compressive residual stresses are found there and the damage model being used is set up to exclude crack initiation damage for negative maximum stress cycles.

Crack Propagation Life Prediction

As with crack initiation, crack propagation rates in railroad rails are substantially influenced by residual stresses. Again, this argument is supported by

[4] Axial residual stresses were assumed to be constant with increased rail usage in order to simplify the analysis. Experimental measurements suggest this is not strictly true.

[5] Small amplitude tensile axial strains are also produced in the rail head in front of and behind the wheel. These smaller amplitude tensile strain excursions caused by "upbending" of the rail were ignored in this analysis.

Significant Parameters

- 136 lb rail
- No lateral load
- Centerline loading
- 8000 lb/in.^{2} track modulus
- No rail wear

Zone	Relative Service Life*
1	1
2	10
3	100
4	∞

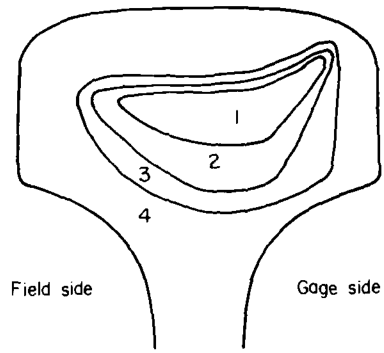

* Zone 1 predicted service lives vary from 300 MGT to 10^6 MGT depending on severity of rail traffic

FIG. 14—*Relative crack initiation life estimates for a rail head.*

accurate life predictions on rail material specimens subjected to service simulation histories that included simulated service residual stresses. Predictions on the growth rate of transverse defects in rail heads also show dramatic residual stress effects.

Analysis of Laboratory Specimens Subjected to Simulated Service—Predictions of the experimental results were made by means of linear integration. Since retardation was not a consideration, a cycle-by-cycle integration was not necessary. Therefore the integration was completed in increments of 0.5 MGT. The integration went stepwise through the load levels and occurrences for 0.5 MGT, calculating the new crack size after each load block. Crack extension during N_j-cycles at stress intensity level k was simply integrated as $N_j \cdot (da/dN)$.

The stress intensity factor was calculated by the use of the following expression for the SEN-type specimens:

$$K = \frac{P}{BW}\sqrt{a}\left\{1.99 - 0.41\left(\frac{a}{W}\right) + 18.7\left(\frac{a}{W}\right)^2 - 38.48\left(\frac{a}{W}\right)^3 + 53.85\left(\frac{a}{W}\right)^4\right\} \qquad (6)$$

Crack growth rates were than obtained by using Eq 4. Using this approach, predicted average fatigue lives were resolved to within ±35 percent of actual test results, which was nearly optimum considering the significant variability in crack growth lives to failure for virtually identical test conditions.

Prediction of Crack Propagation in Rails—Prediction of crack propagation in rails is complex because the stress distribution is uneven and the geometry is nonuniform. The implication is that crack growth rates will be different at different locations along the crack front so that the crack will change shape as it grows. The rail also experiences shear stresses which cause Mode II and III stress intensities, in addition to the commonly considered opening Mode I stress intensity.

Since the wheel loads cause predominantly compressive axial stresses in the rail, and cracks do not grow in Mode I compression, inherent tensile residual stresses are likely to be important contributors to crack growth in rails. The growth rate of transverse defects, in particular, is probably very sensitive to the magnitude of axial residual stresses in the rail. Figure 15 shows the result of crack growth predictions for a transverse defect considering three different residual stress magnitudes. Obviously, relatively minor changes in residual stress magnitude are predicted to have great impact on the service life to failure.

Discussion of Factors Controlling Rail Fatigue Resistance

Railroad rails have been failing by fatigue for years and they still do today. Some of the primary reasons for failure have changed over the past 30 years, however. Up to about 20 years ago, it was not uncommon to find rail failures that initiated at the center of the head where hydrogen flakes remained from improper heat treatment. As is shown in Fig. 16, the influence of moderately flat inclusions, relative to the long axis of the rail is expected to be substantial, with a factor of 100 difference in crack initiation life predicted between an elongated inclusion (which is sometimes seen in today's rails) as compared to a flattened inclusion such as a hydrogen flake.

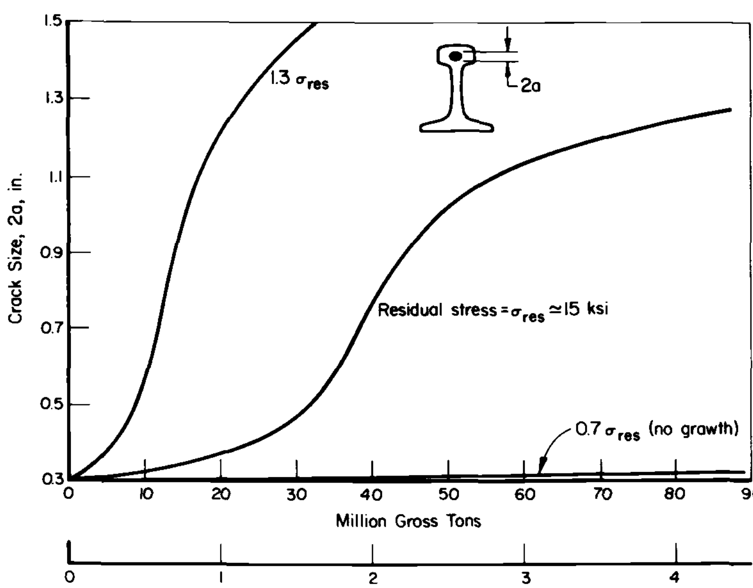

FIG. 15—*Effect of residual stress level on growth of transverse fissure.*

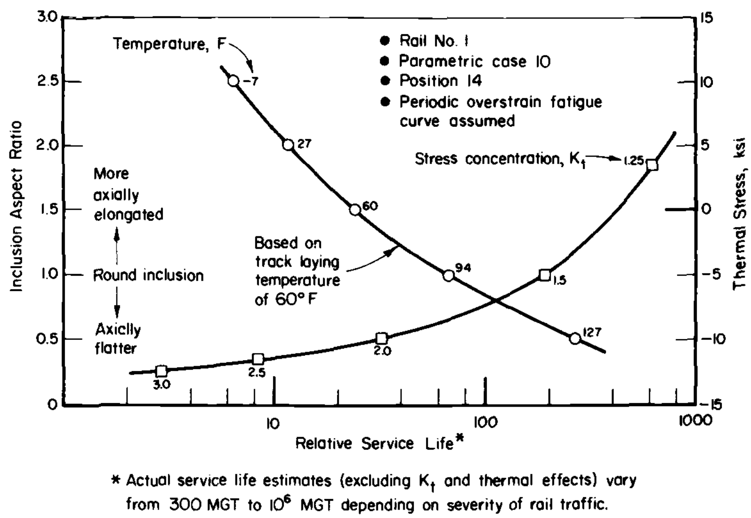

FIG. 16—*Effect of thermal stresses and inclusion shape on crack initiation.*

Thermal stress effects also have been modeled analytically. The results, depicted in Fig. 16, are based on the assumption that thermal stresses add directly to internal residual stresses to give the combined steady-state stresses in the rail head. These combined stresses have been estimated for cold-temperature conditions to be in excess of 207 MPa (30 ksi) in tangent track and 414 MPa (60 ksi) in curved track. These high residual stresses are most likely to develop in welded rail and in rails installed in very hot weather.

The effect of a residual stress on crack initiation would appear to be greatest for the small compressive axial strain amplitudes most commonly generated in field rails. A rail that repeatedly sees a compressive axial strain range of 0.20 percent superimposed on a tensile residual stress of 207 MPa (20 ksi) is expected (based on the present model) to fail approximately 5 times sooner than a similar rail which sees the same compressive axial strain but no residual stress. The difference in life is expected to be somewhat less for rails subjected to larger axial strains. These trends are shown in a relative sense for two strain ranges as a function of mean stress in Fig. 17.

In terms of life prediction, the use of periodic overstrain data as a baseline damage analysis (as compared to the more usual constant amplitude results) is as important as properly accounting for residual stresses. As Fig. 18 illustrates, fatigue life to crack initiation of an element of rail material is predicted to be about a factor of 10 longer using constant amplitude data (circles) versus periodic overstrain data (squares). In contrast, predictions without the influence of a 207 MPa (20 ksi) mean stress (open circles and squares) are about a factor of 4 longer than the corresponding results with the mean stress (solid circles and squares). Clearly then, while residual stress is an important factor in the damage process, it is not nearly as significant as history effects in the present case.

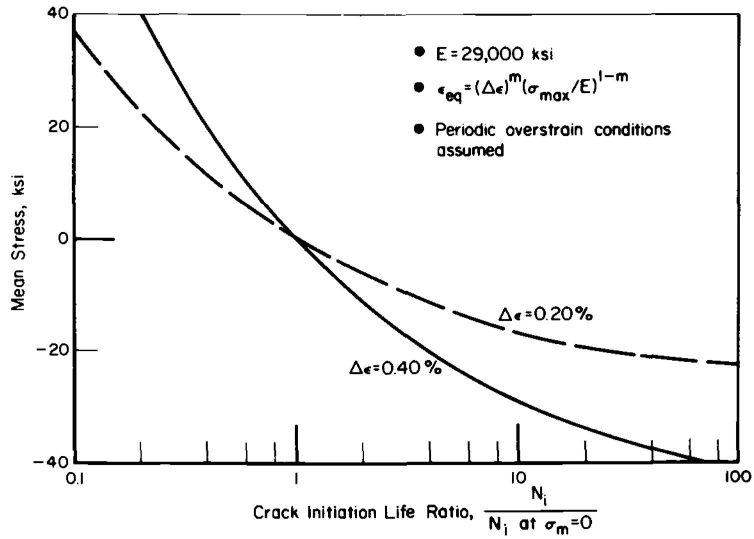

FIG. 17—*Relative crack initiation life versus mean stress.*

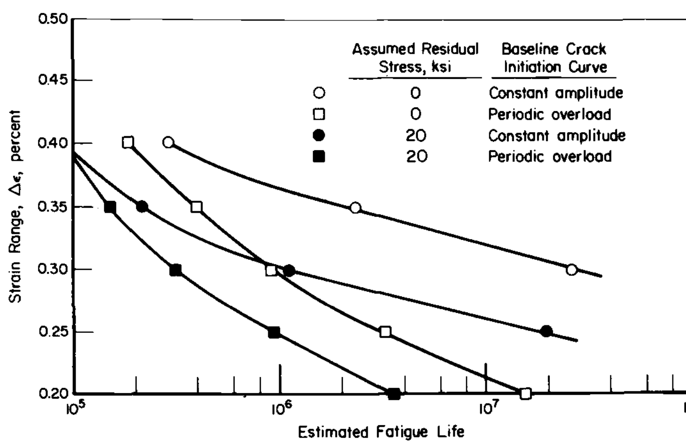

FIG. 18—*Effect of assumed residual stress and choice of baseline crack initiation curve on life estimates.*

Crack initiation appears to occupy the largest fraction of time in the total damage process in most rail head failures. This appears to be true despite the apparent sensitivity of crack initiation to largely compressive strain cycles that are not damaging in terms of crack propagation. This may be rationalized if one considers the sharp transition region from compressive to tensile residual stresses that is typically seen in a rail head at the point just below the plastically deformed rail surface. This stress gradient may act much like a stress concentration site for crack initiation, especially since this region has the highest bending strain ranges, which drive crack initiation. Then, once the crack has formed and progressed downward into the high tensile residual stress field, the axial strains are pulled upward into tension where they are effective drivers for crack propagation.

The transition region between crack initiation and propagation in a rail head is probably a region in which microcrack growth is driven both by compressive strain excursions and tensile residual stresses. A pending fractographic study of rail head failures will provide further insights regarding the causes of crack initiation, and the relative contribution of microcrack progression and macrocrack growth to the total life of a railroad rail before failure.

Several areas of uncertainty remain. Particularly significant in this regard is the influence of wear, a factor now being incorporated in the simulation scheme. The effect of the triaxial state of residual stress in the rail has not been considered. It is anticipated, however, that the introduction of in-plane residual stresses would increase the severity of a three-dimensional equivalent strain parameter and reduce the anticipated crack initiation lives below those computed for the uniaxial case. The effect of subsurface versus surface crack initiation and propagation has also not been considered. Cracks initiating and growing in a vacuum generally do so at a somewhat reduced rate from that observed in laboratory environments, but a quantitative statement regarding the magnitude of this effect in rail steels cannot be made at this time.

Summary and Conclusions

Residual stresses in railroad rails can be quite large, and are one of the major contributors to crack initiation and growth in railroad rails. A method has been outlined for the measurement of residual stresses in rails. While the residual stress pattern appears to stabilize with increased rail use, the stress magnitudes do not appear to do so. For the tangent rail specimens studied thus far, stress magnitudes have been found to vary widely, within the matrix of a characteristic stress pattern. Apparently, shakedown does not occur.

Experimental data showing the influence of mean stresses on crack initiation and crack growth in rail steel material have been discussed and analytical predictions of residual stress influences on crack initiation and growth in rails have been presented.

There are many factors which influence the magnitude of residual stresses in a section of track, and there is no accurate nondestructive means of identifying internal residual stresses. Even if all other uncertainties could be resolved, it is doubtful that even a very sophisticated analysis, beyond that conducted in the referenced studies, would be useful for quantitative prediction of the service life of a specific piece of rail. Fortunately, however, representative and near-worst case conditions can be analytically simulated, and the results of these studies can be used to set up meaningful inspection intervals and retirement periods.

Acknowledgments

This research was sponsored by the U. S. Department of Transportation under Contracts DOT-TSC-1051, 1076, 1426, and 1663. The early work was monitored at the Department of Transportation by Dr. Roger Steele. More recently, Dr. Oscar Orringer has served as technical project monitor. Their inputs and guidance in this work have been valuable.

In addition, numerous Battelle staff and former staff have contributed to these studies, and this paper is indirectly a result of their efforts. Specifically, Dr. David Broek was a leader in much of the early fatigue and crack growth work, while Mr. Jack Groom led the residual stress measurement and analysis activities. Mr. Donald Ahlbeck was responsible for much of the in-field wheel/rail load measurement and analysis, while Dr. James Kennedy was responsible for the generation of all the finite-element rail stress data. Dr. Sam Sampath supervised the most recent DOT program at Battelle, during which the predictions of crack initiation in rails were made. His critical review of this work was helpful and his efforts are appreciated.

Finally, with respect to the laboratory data generation, Messrs. Norman Frey and James Wood of Battelle were key individuals, while Mr. Edward Gonterman of Boeing coordinated the load control fatigue data generation.

References

[1] Broek, D. and Rice, R. C., "Fatigue Crack Growth Properties of Rail Steels," Final Report (Part I) by Battelle Columbus Laboratories to the U. S. Department of Transportation, Contract No. DOT-TSC-1076, July 1977.

[2] Broek, D. and Rice, R. C., "Prediction of Fatigue Crack Growth in Rail Steels," Final Report (Part II) by Battelle Columbus Laboratories to the U. S. Department of Transportation, Contract No. DOT-TSC-1076, Sept. 1977.

[3] Rice, R. C. and Broek, D., "Fatigue Crack Initiation Properties of Rail Steels," Final Report by Battelle Columbus Laboratories to the U. S. Department of Transportation, Contract No. DOT-TSC-1426, Sept. 1979.

[4] Leis, B. N. and Laflen, J. H., "Cyclic Inelastic Deformation and Fatigue Resistance of a Rail Steel: Experimental Results and Mathematical Models," Interim Report on Item 11 of DOT-TSC-1076, June 1977.

[5] Groom J. J., "Task 2. Determination of Residual Stresses in Rails," Final Report to the U. S. Department of Transportation by Battelle Columbus Laboratories, Contract No. DOT-TSC-1426, 26 Nov. 1979.

[6] Buchheit, R. D. and Broek, D., "Microstructural and Fractographic Characterization of Fatigue-Tested Rail Steels," Final Report (Part III) by Battelle Columbus Laboratories to the U. S. Department of Transportation, Contract No. DOT-TSC-1076, Oct. 1977.

[7] Walker, E. K. in *Effects of Environment and Complex Load History on Fatigue Life, ASTM STP 462*, American Society for Testing and Materials, 1970, pp. 1-14.

[8] Rice, R. C., Davies, K. B., Jaske, C. E., and Feddersen, C. E., "Consolidation of Fatigue and Fatigue-Crack-Propagation Data for Design Use," NASA Contractor Report, NASA CR-2586, Oct. 1975.

[9] Smith, K. N., Watson, P., and Topper, T. H., *Journal of Materials and Testing*, Vol. 5, No. 4, Dec. 1970, pp. 767-778.

[10] Brose, W. R. et al, "Effect of Periodic Large Strain Cycles on the Fatigue Behavior of Steels," SAE Paper No. 740221, 1974.

[11] Conle, A. and Topper, T. H., *International Journal of Fatigue*, Vol. 2, No. 7, July 1980, pp. 130-136.

[12] Ahlbeck, D. R., Harrison, H. D., Tuten, J. M., and Johnson, M. R., "Wheel/Rail Load Data — A Statistical Characterization," Interim Report submitted by Battelle Columbus Laboratories to the U. S. Department of Transportation, Contract No. DOT-TSC-1051, Jan. 1979.
[13] Forman, R. G., Kearney, V. E., and Engle, R. M., *Journal of Basic Engineering, Transactions of ASME*, Vol. 89D, 1967, p. 459.
[14] Broek, D., *Elementary Engineering Fracture Mechanics*, Noordhoff International Publishing, Leyden, The Netherlands, 1974, pp. 241-256.
[15] Rice, R. C. and Stephens, R. I. in *Progress in Flaw Growth and Fracture Toughness Testing*, *ASTM STP 536*, American Society for Testing and Materials, 1973, pp. 95-114.

J. B. Kohls,[1] *J. T. Cammett,*[1] *and A. W. Gunderson*[2]

Effects of Multiple Shot-Peening/Cadmium-Plating Cycles on High-Strength Steel

REFERENCE: Kohls, J. B., Cammett J. T., and Gunderson, A. W., **"Effects of Multiple Shot-Peening/Cadmium-Plating Cycles on High-Strength Steel,"** *Residual Stress Effects in Fatigue, ASTM STP 776,* American Society for Testing and Materials, 1982, pp. 158-171.

ABSTRACT: A study was made of the effects of multiple shot-peening and cadmium plating operations on high-strength AISI 4340 steel used in aircraft landing-gear applications. No detrimental effects were observed on surface microstructure and tensile properties or on fatigue and unnotched stress corrosion resistance in high-humidity air. An apparent degradation in stress corrosion life of fatigue precracked specimens was observed after four and five peening and plating operations.

KEY WORDS: shot-peening, cadmium plating, fatigue, stress corrosion, tensile, high-strength steel

High-strength steels are used widely for load-bearing components in aircraft landing gear. Typically, such components are shot-peened after machining, then are plated with cadmium and chromium followed by painting, all to enhance resistance to fatigue and corrosion. Overhaul rework procedures for such components include stripping platings, inspecting for cracks, build-up and remachining of worn areas, followed by shot peening and plating as for the original finishing sequence. Landing-gear components typically are subjected to several such overhaul procedures during their service life.

The objective of this program was to establish the effects of the original and overhaul rework peening and plating cycles on fatigue and stress corrosion resistance of high-strength AISI 4340 steel which is commonly employed in aircraft landing-gear components. Experimental evaluations involved metallography and tension testing in addition to fatigue and stress corrosion testing in high-humidity environments. The remaining sections of this paper are devoted to descriptions of material and specimen preparation, test procedures, results obtained, and interpretation thereof.

[1] Metcut Research Associates Inc., Cincinnati, Ohio 45209.
[2] U. S. Air Force, AFWAL/MLLX, Wright-Patterson Air Force Base, Ohio 45433.

Procedure

Material and Specimen Preparation

The material employed in this work was vacuum-melted AISI 4340 steel per requirements of MIL-S-8844. This material, heat-treated nominally to a 1790 to 1830 MPa ultimate strength level, was used in landing gear of many earlier aircraft. The material was procured in the form of forgings 25 by 108 by 1829 mm. Each forging was cut into eight specimen blanks approximately 12 by 102 by 460 mm. Specimens were rough machined about 4 mm oversize prior to heat treatment. The geometries of tension, fatigue, and stress corrosion specimens are shown in Fig. 1. Following rough machining, all specimens were heat-treated.

The heat treatment consisted of oil quenching from 1085 K and tempering at 480 K. The resulting hardness was 52 to 54 Rc. The average results from tension tests were 2070 MPa ultimate tensile strength, 1397 MPa 0.2 percent yield strength, 51 percent reduction of area, and 12.4 percent elongation (25 mm gage length). After heat treatment, the specimens were finish machined. The final 0.5 mm of material was removed from all surfaces by a controlled low-stress grinding procedure [*1*].[3] This introduces low-level compressive stresses at the surface and within about 0.1 mm beneath the surface. Further, this grinding procedure does not produce any overtempering or re-transformation of the martensitic surface microstructure. After finish grinding, the edges of the specimen gage sections were radiused to about 1 mm and hand polished through 600 grit SiC paper to a surface roughness of about 0.2 μm AA.

Shot-Peening

Following heat treatment and machining, specimens other than those tested in the baseline condition (no shot-peening or cadmium plating) were shot-peened per MIL-S-13165B. Specimens were clamped in a vertical position and rotated at 10 to 15 rpm. Six nozzles were used to propel the shot simultaneously at the specimen. These nozzles oscillated during peening to ensure consistent overall coverage of the surface. After peening for 3 min, each specimen was flipped end for end and then peened for an additional 3 min. Peening was performed with hardened size 230 steel shot. Coverage was 200 percent. The resulting Almen strip intensity was 6A to 8A.

Cadmium Plating

Cadmium plating was performed per MIL-C-8837, Type II. The procedure involves vacuum deposition of cadmium followed by a supplementary chromate treatment to form a protective oxide film. Specimens were cleaned in a solvent and were lightly dry-blasted prior to insertion in the vacuum chamber to ensure

[3] The italic numbers in brackets refer to the list of references appended to this paper.

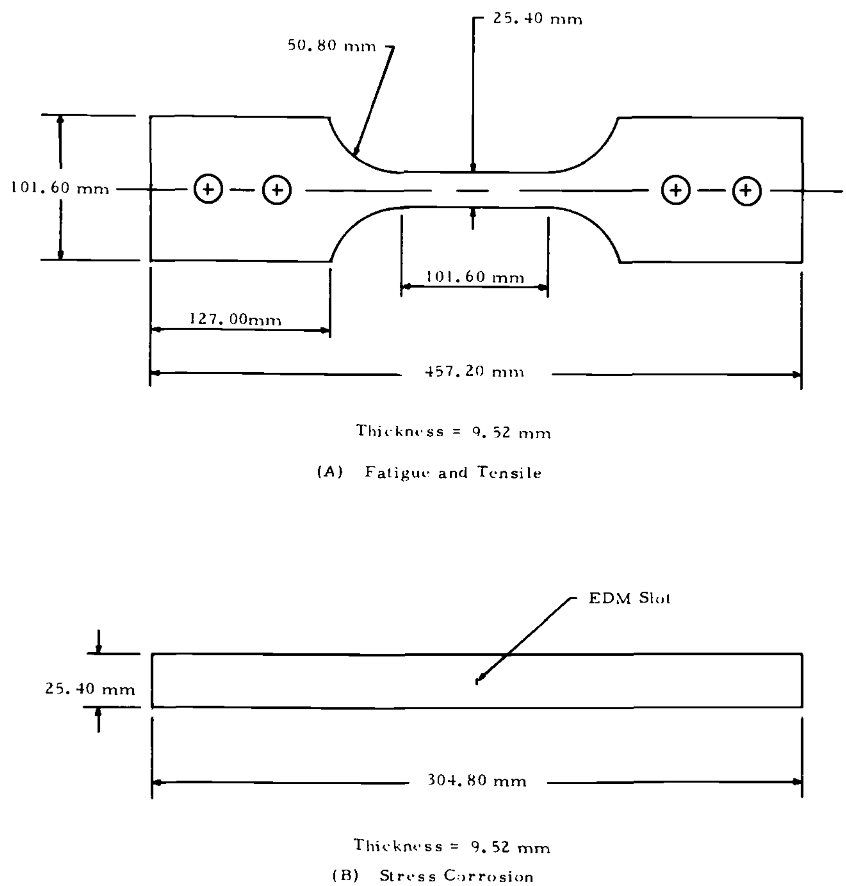

FIG. 1—*Specimen geometries.*

cleanliness of surfaces. The blasting did not roughen the surface beyond the finishes specified in Fig. 1. The plating on specimens selected for multiple shot-peening and plating cycles was stripped between each cycle.

Tension and Fatigue Testing

Tension and fatigue tests were performed on a servocontrolled closed-loop hydraulic universal test machine. The load cell and all support equipment were calibrated immediately before and after this program using secondary standards whose calibrations were traceable to the National Bureau of Standards. The loading grips and associated fixtures were aligned using a strain gaged specimen of the same geometry as the test specimen.

Tension tests were performed per ASTM Methods of Tension Testing of Metallic Materials (E 8) in ambient air at about 293 K and 50 percent relative humidity.

The strain rate for all tests was 0.005 min^{-1} to failure. Strain measurement was performed via an LVDT extensometer attached to the specimen gage section over a 25 mm gage length.

Fatigue tests were conducted under constant load amplitude conditions at stress ratio $R = 0.1$ and -0.3 in a high-humidity air environment. The environment was maintained by bubbling compressed air slowly through a column of water and then passing the air into a plastic jacket surrounding the specimen gage section. All testing was performed at a frequency of 2 to 4 Hz using a sinusoidal load-time waveform. Tests were terminated after 10^6 cycles if fracture had not occurred beforehand.

Stress Corrosion Testing

Stress corrosion testing was performed per ASTM Practice for Preparation and Use of Bent-Beam Stress-Corrosion Test Specimens (G 39) with the exception that tests were conducted under constant load rather than constant displacement in four-point bending. Testing was conducted in deadweight-loaded test frames, commonly used for creep and stress rupture testing. The frames were outfitted with four-point bend fixturing specially designed for this program. The constant bending moment test section of each specimen was the central 75 mm of its 300 mm length.

The test environment was 293 K air at 80 to 100 percent relative humidity produced by slowly bubbling compressed air through a water reservoir and then passing it into a plastic bag surrounding the specimen test section. Both unnotched and fatigue precracked specimens were tested. The fatigue precracked specimen had been manufactured with 1.2 mm wide by 0.6 mm deep electrically discharge machined (EDM) notch in the geometric center of one surface. These specimens were fatigue precracked before any shot-peening or plating cycles. Fatigue precracking was performed in ambient air under three-point bend loading at a frequency of 30 Hz and a stress ratio R of about 0.1. Fatigue cracks were initiated at a calculated maximum surface stress of 100 ksi and were permitted to grow until the total surface notch plus crack length reached 2.5 mm.

Results and Discussion

Residual Stresses

No residual stress measurements were included in the scope of this work. In previous work, however, Metcut Research Associates performed residual stress measurements on quenched and tempered AISI 4340 (50 Rc) [*1*]. Residual stress results from that work, characterizing surface and subsurface residual stresses parallel to the grinding direction, are shown in Fig. 2. Please note that this figure, reproduced from Ref *1*, is in customary English units rather than the SI units used otherwise throughout this paper. As can be seen, the gentle grinding produced relatively low compressive stresses to a depth of less than 0.05 mm (0.002 in.), while the shot-peening produced relatively large compressive stresses to a depth

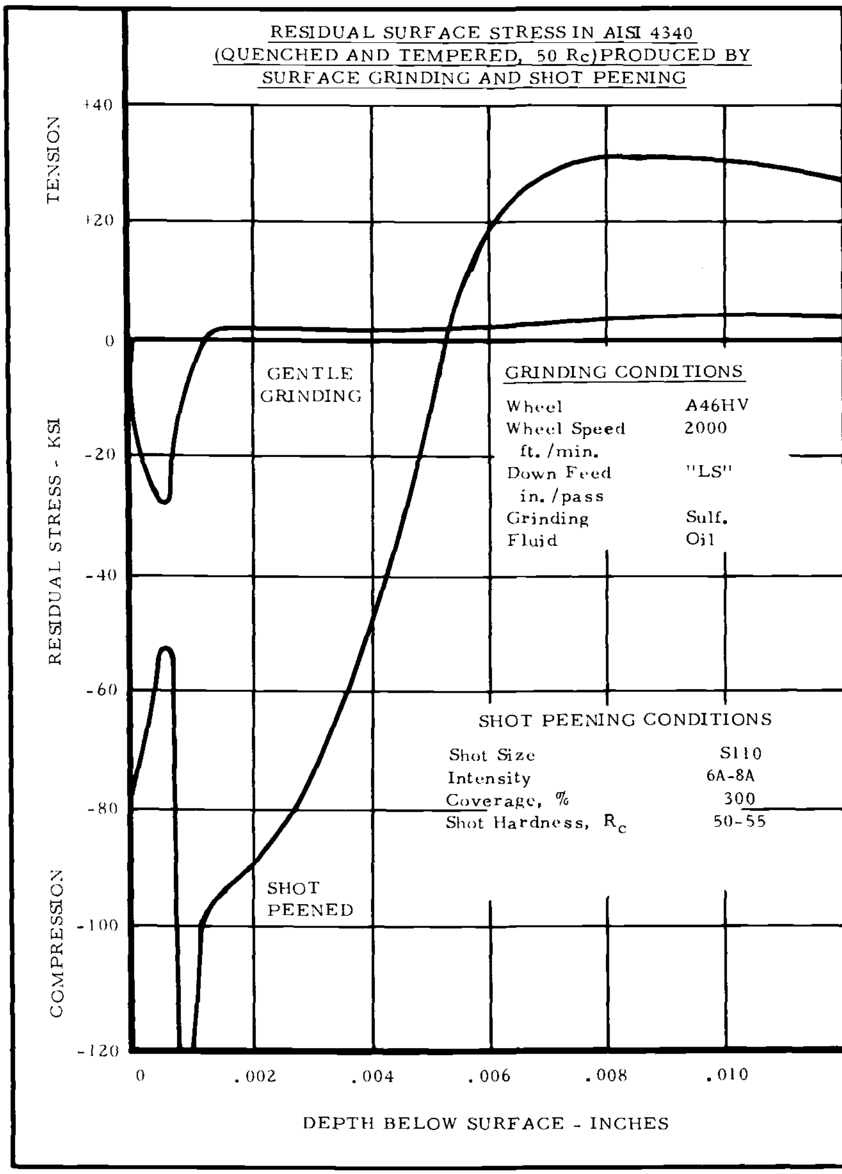

FIG. 2—*Residual stress data for AISI 4340 steel, 50 Rc (1 ksi = 6.9 MPa; 1 in. = 25.4 mm)* [1].

in excess of 0.1 mm. It is believed that the residual stress data shown in Fig. 2 are representative of residual stresses created in the AISI 4340 steel employed in the current study, since the same grinding and shot-peening parameters were used.

Tension Test Results

Tension test results from baseline specimens (as-heat-treated and gently ground) and from specimens subjected to from one to five shot-peening and plating cycles are summarized in Fig. 3. As can be seen, no degradation of tensile strength, yield strength, or elongation occurred as a result of shot-peening and plating cycles.

Fatigue Test Results

Fatigue testing was performed axially at maximum stress levels of 1170 and 1380 MPa at stress ratios R of 0.1 and −0.3. Results representing each combination of stress level and stress ratio are presented in Fig. 4. It is evident that the

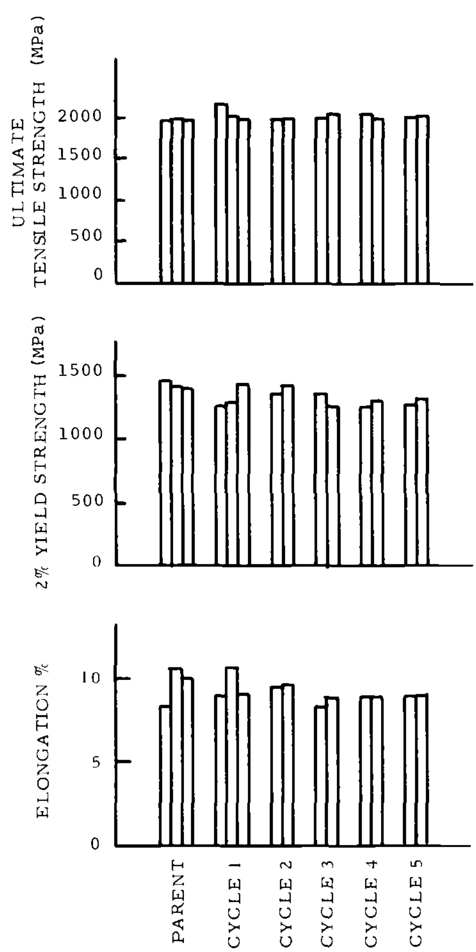

FIG. 3—*Tension test results.*

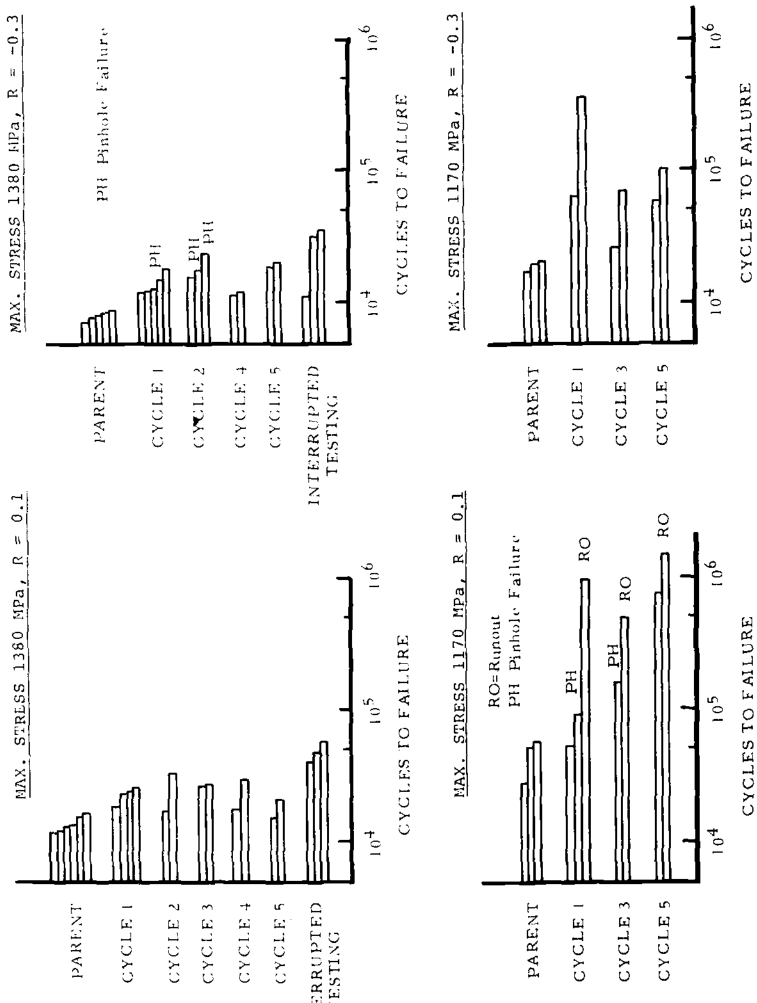

FIG. 4—*Fatigue test results.*

average fatigue lives of specimens subjected to one to five shot-peening plus plating cycles exceeded the average lives of all baseline specimens tested at the same stress level and stress ratio. This effect, however, was greater for specimens tested at the lower stress level (1170 MPa) than for specimens tested at the higher stress level (1380 MPa).

The greater fatigue life after shot-peening is consistent with the residual stress patterns presumed to be in the specimens, since previous work by Metcut has shown a strong correlation between peak residual stress and fatigue strength in AISI 4340 steel [2]. It is believed further that the effect of shot-peening is less pronounced for the higher testing stress level (1380 MPa) because this is close to the magnitude, though opposite in sense, of shot-peening residual stresses presumed to be in the surface and subsurface layers.

It is also evident from the results in Fig. 4 that fatigue lives of specimens subjected to from three to five shot-peening and plating cycles were generally lower than lives of specimens subjected to one or two such cycles. Determination of the reason for this was beyond the scope of this investigation. It is believed, however, that the observed behavior resulted either from an over-peening effect or from hydrogen accumulation with repeated stripping, peening, and plating operations. It is re-emphasized, however, that fatigue lives of shot-peened and plated specimens generally exceeded those of baseline specimens regardless of the number of shot-peening and plating cycles.

Also shown in Fig. 4 are fatigue results from "interrupted testing" wherein specimens were cycled in fatigue between successive shot-peening and plating cycles. The number of fatigue cycles applied after each shot-peening and plating cycle was one fourth the average fatigue life of specimens tested at the same stress level and stress ratio to failure after just one shot-peening and plating treatment. After three such increments of fatigue cycling and four cycles of shot-peening and plating, the specimens were tested to failure. It is evident that the lives of specimens thus treated exceeded those of all baseline specimens and generally exceeded those of specimens subjected to from one to five shot-peening and plating cycles without intermittent fatigue cycling.

Stress Corrosion

A total of 24 stress corrosion tests were performed, 14 on smooth specimens and 10 on fatigue precracked specimens. All multiple shot-peening and plating cycles were performed on individual specimens prior to stress corrosion testing. All precracking of notched specimens was performed prior to shot-peening and plating cycles.

Initially, the maximum bending stress level for testing was chosen to be equal to the 0.2 percent offset yield stress (1415 MPa) for the material. This level subsequently was increased to 1655 MPa when no specimen failures were observed at the lower stress level. Therefore the surface stress level as reported here is a pseudo-elastic stress level calculated per simple beam theory rather than an actual stress level. Specimens were held at load in the moist air environment for at least 200 h or until fracture, whichever occurred first.

Stress corrosion results for smooth specimens are presented in Table 1. These results are inconclusive with respect to the influence of shot-peening and plating on stress corrosion resistance, since no stress corrosion failures occurred. Visual examination of specimens after testing revealed neither any cracking nor any general corrosion on the specimens.

Stress corrosion results from notched and fatigue precracked specimens are presented in Table 2. It is evident that lives of specimens subjected to four or five shot-peening and plating cycles were lower than for baseline specimens or those subjected to a lesser number of such cycles. As was mentioned previously in discussion of fatigue results, it is believed that this behavior resulted either from an over-peening effect or from hydrogen accumulation during successive stripping, peening, and plating operations. The extent of fatigue precracking in specimens so prepared greatly exceeded the depth to which any shot-peening would have influence. Therefore the belief is favored that hydrogen accumulation was responsible for the observed behavior.

Metallography

The metallographic specimens prepared for this program were oriented parallel and perpendicular to the machining lay. The specimens were mounted in epoxy material embedded with aluminum oxide pellets for optimum edge retention. They were polished by conventional means and examined in the unetched and etched conditions at magnifications of up to approximately ×1000. The etchant used was a 2 percent Nital solution.

Baseline 4340 samples and five groups of samples with varying number of shot-peening and plating cycles were examined. Surface structural features are briefly described and characterized by photomicrographs shown in Fig. 5. Traces of a thin white layer were observed on the surfaces of the peened samples. These

TABLE 1—*Stress corrosion results—smooth specimens.*

Specimen Number	No. of Shot-Peening and Plating Cycles	Nominal (Pseudo-Elastic) Surface Stress, MPa	Test Duration, h	Result[a]
11	none	1415	258	N
12	none	1415	257	N
13	none	1415	279	N
14	none	1415	279	N
16	1	1415	259	N
23	1	1415	259	N
18	2	1655	214	N
21	2	1655	209	N
19	3	1655	209	N
24	3	1655	213	N
17	4	1655	215	N
22	4	1655	215	N
15	5	1655	200	N
20	5	1655	200	N

[a]N = No cracking observed; test terminated.

TABLE 2—*Stress corrosion results—fatigue precracked specimens.*[a]

Specimen Number	No. of Shot Peening and Plating Cycles	Nominal (Pseudo-Elastic) Surface Stress, MPa	Nominal Surface Stress Intensity Factor,[b] $MPa \cdot m^{1/2}$	Test Duration, h	Result[c]
9	none	1415	46	266	N
10	none	1415	46	266	N
9[d]	none	1550	50	216	N
10[d]	none	1655	54	214	F
7	1	1655	54	362	N
8	1	1655	54	350	F
6	2	1655	54	213	N
3	3	1655	54	233	N
5	3	1655	54	204	F
1	4	1655	54	42	F
2	5	1655	54	97	F
4	5	1655	54	2.2	F

[a] Precracked nominal crack length = 2.5 mm.

[b] Calculated per A. F. Grandt, Jr., and G. M. Sinclair, *Stress Analysis and Growth of Cracks, ASTM STP 513*, American Society for Testing and Materials, 1972, pp. 37-58.

[c] N = No crack extension observed (precracked specimens); test terminated. F = specimen fractured.

[d] Retest of a specimen from a terminated test at a lower stress.

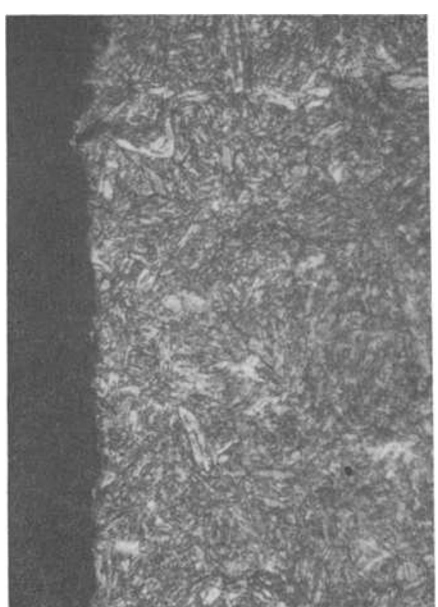

Baseline: As-Ground

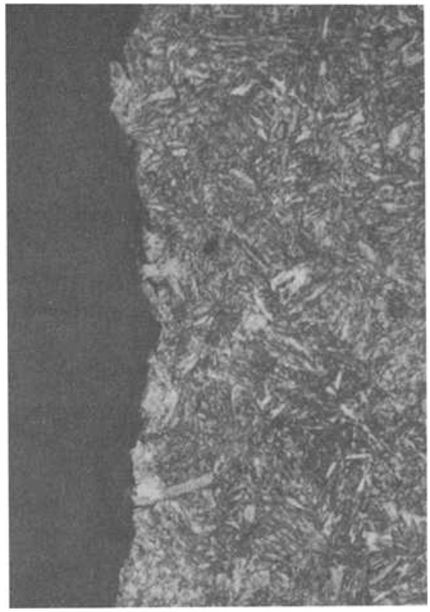

After One Shot Peening/Plating Cycle

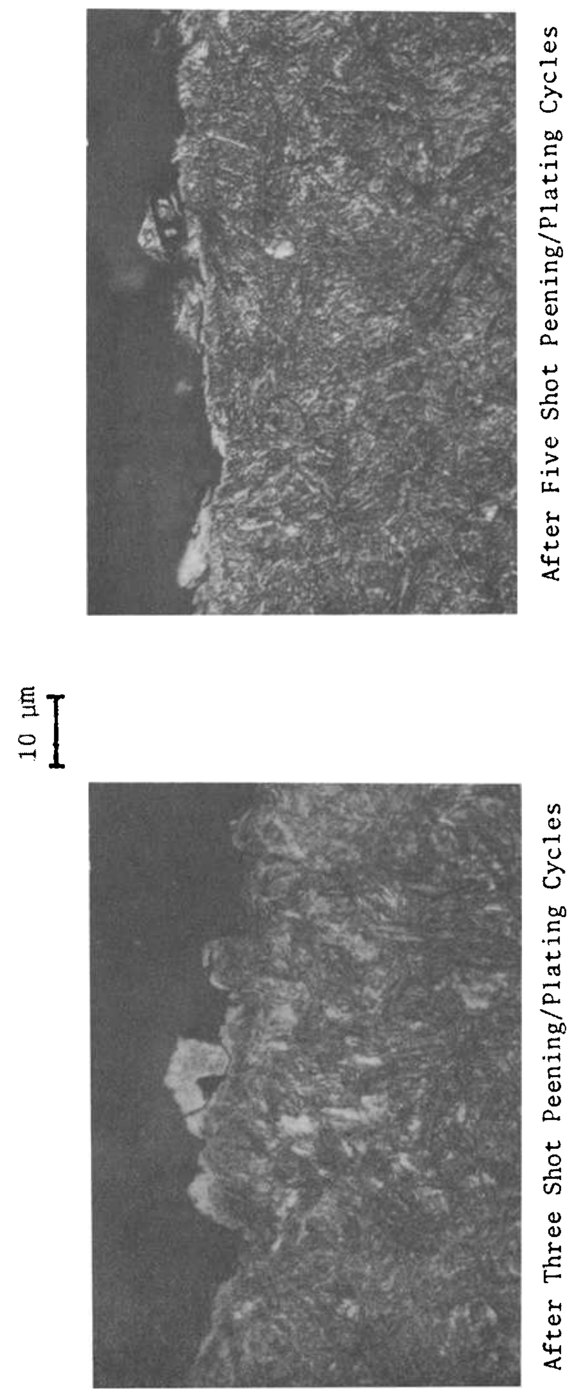

FIG. 5—Metallographic sections through AISI 4340 steel specimen surfaces; all sections parallel to grinding direction.

white or light etching layers and stringers may be attributable to a high degree of surface plastic deformation. The thin layers probably represent highly deformed material rather than untempered martensite, which has a similar appearance.

In addition to the preceding general characterization of surface features, a metallographic study was performed on several failed test specimens in an attempt to ascertain whether or not the observed white layer influenced the failure process. The specimens selected for this study represented parent or baseline material and extremes in test life for various fatigue and stress corrosion test conditions.

Before proceeding with metallographic examination of the test specimens, a test blank and the two baseline specimens were macro-etched to investigate whether or not any significant grinding burn had occurred. This was done in order to resolve the issue of whether the presence of a white layer could be traceable to machining in the manufacture of the specimens. The three specimens were etched by a multi-step procedure widely used in industry, which consisted of a dilute solution of 4 percent nitric acid in water and a solution of 2.5 percent hydrochloric acid in acetone. One of the parent specimens was also etched with a 2 percent Nital solution. None of these etching techniques revealed the presence of grinding burn on the specimens.

The test specimens were first examined on a binocular microscope at magnifications of up to approximately ×40 in order to locate failure origins. Examination of the fatigue specimens revealed that failure origins were located either at one of the corners of the specimen or on the sides of the specimen. Failures in the stress corrosion specimens initiated from the pre-existing fatigue crack that was introduced at the bottom of the EDM notch.

Metallographic sections were made approximately through the center of each failure initiation site and examined in the unetched and etched conditions at magnifications up to approximately ×1200. Observations indicated that the white layer was not associated exclusively with the initiative area of specimens exhibiting the lowest fatigue lives. Fatigue initiation was apparently also influenced by other forms of surface degradation, such as microcrack and slivers, and by specimen geometry (that is, the corner areas).

Conclusions

Specific conclusions from experimental results were as follows:

1. Shot-peening/cadmium-plating cycles up to five in number had no influence on tensile properties relative to those from as-heat-treated material.

2. Fatigue resistance in high humidity air at stress ratios R of 0.1 and −0.3 was enhanced by shot-peening/cadmium-plating cycles up to five in number. The increase was most noticeable after one to three such cycles.

3. Stress corrosion results from unnotched specimens in high-humidity air were inconclusive since both as-heat-treated and shot-peened/cadmium plated specimens survived 200-h exposure at up to a 1650 MPa elastic surface stress level without cracking.

4. Fatigue precracked stress corrosion specimens subjected to four and five shot-peening/cadmium-plating cycles exhibited shorter lives than as-heat-treated specimens and specimens subjected to fewer shot-peening/cadmium-plating cycles. All specimens were fatigue precracked to a surface crack length of about 2.5 mm after heat treating, prior to any shot-peening/plating cycles. Stress corrosion testing of precracked specimens was performed in 293 K, 80 to 100 percent relative humidity air at a pseudo-elastic surface stress level of 1650 MPa.

5. No microstructural changes of significance relative to mechanical properties were observed to result from shot-peening/cadmium-plating cycles. White stringers observed metallographically at the surface tended to increase in prominence with increasing cycles. These stringers were believed to be an etching phenomenon related to plastic deformation in the peened surface layers.

Acknowledgments

Sponsorship of this work by the Air Force Wright Aeronautical Laboratories/Material Laboratory, AFWAL/MLSA, under Contract F33615-78-C-5201 is gratefully acknowledged. One of the co-authors, A. W. Gunderson, of the Materials Integrity Branch, Systems Support Division, served as project monitor. Also acknowledged are the contributions of various Metcut Research Associates personnel, in addition to the co-authors, who were instrumental in performance of the experimental work: W. J. Stross, Tensile and Fatigue Testing; L. R. Gatto, Metallography; and T . E. Arnold, Stress Corrosion Testing.

References

[1] Koster, W. P. et al., "Surface Integrity of Machined Structural Components," AFML-TR-70-11, March 1970.

[2] Koster, W. P. et al., "Surface Integrity of Machines Materials," AFML-TR-74-60, April 1974.

D. V. Nelson[1]

Effects of Residual Stress on Fatigue Crack Propagation

REFERENCE: Nelson, D. V., "**Effects of Residual Stress on Fatigue Crack Propagation,**" *Residual Stress Effects in Fatigue, ASTM STP 776,* American Society for Testing and Materials, 1982, pp. 172-194.

ABSTRACT: Experimental results on the effects of compressive and tensile residual stresses on Mode I fatigue crack growth are briefly reviewed. Prediction methods that attempt to account for the observed effects are compared. Current limitations of the methods and their relative advantages and drawbacks for use in design analysis are discussed. The possible role of residual stress re-equilibration on growth behavior, caused by crack extension itself, is also discussed.

KEY WORDS: crack propagation, crack closure, fatigue of metals, fracture mechanics, residual stress, superposition method

Machine parts and structural components often contain residual stresses from forming and joining processes and from heat treatments. Residual stresses may also develop in service if loadings cause localized plastic straining. It is well known that regions of compressive residual stress retard fatigue crack growth rate (or arrest cracks), while tensile residual stress regions produce the opposite effect.

A growing fatigue crack will also generate its own residual stress field, both in front of and in the wake of its tip. The compressive residual stresses left in the wake cause the crack closure phenomenon, which has provided an explanation for such effects as crack growth retardation caused by periodic high tensile loads and transient acceleration caused by low-to-high load transitions.

The purpose of this paper is to compare and discuss existing approaches for predicting the influence of residual stress on fatigue crack growth. Two approaches will be considered: (*1*) superposition of the respective stress intensity factors for the residual stress field and for the applied stresses, and (*2*) a simplified crack closure model. Current limitations of the approaches and their relative advantages and drawbacks for use in design analysis will be discussed. Except as otherwise noted, only the behavior of Mode I through-thickness cracks (>1 mm) will be considered.

[1] Assistant Professor, Mechanical Engineering Department, Stanford University, Stanford, Calif. 94305.

Superposition Approach for Existing Residual Stress

To quantify the influence on crack growth of residual stresses existing from fabrication, the following items are needed: (*1*) an accurate estimate of the original residual stress field (both magnitude and distribution in depth); (*2*) a method for expressing the influence of residual stress on growth rate, preferably in a linear elastic fracture mechanics format so that existing da/dN–ΔK data may be utilized; and (*3*) knowledge of how the residual stress fields may be altered by service loadings before a crack starts and as it grows.

Initial residual stress fields caused by nonuniform plastic straining have been computed with closed-form solutions for geometries such as cold-worked holes [*1*] and overstrained cylinders [*2*], or may be estimated by finite-element analyses for more complicated geometries.[2] X-ray diffraction and destructive measurements are used to determine residual stresses caused by processes such as welding and induction hardening.

The approach employed most frequently to account for the effect of residual stress on crack growth involves superposition of the respective stress intensity factors for the initial residual stresses and for the applied stresses. The K_I for the residual stress field is obtained by loading the crack faces with the residual stresses which exist normal to the plane of potential crack growth in the uncracked body. Such residual stress intensity factors, K_{res}, have been computed for a number of different crack types and crack face stress distributions [*3-7*].

An "effective" stress intensity is then taken as $K_{eff} = K_{res} + K_{applied}$. The superposition approach is illustrated schematically in Fig. 1 for an edge crack growing through a compressive residual stress field which decreases linearly from a maximum value at the surface to zero at some depth a_0. For constant-amplitude, zero-to-maximum tension ($R = 0$) loading, growth rate can be correlated in terms of the range of ΔK_{eff} above zero (ΔK_a shown in Fig. 1) by using basic da/dN–ΔK data. Good predictions have been achieved by using this type of approach, with appropriate K_{res} factors, for cracks emanating from cold-worked holes [*8,9*], at least for crack lengths greater than 1 mm. (For shorter cracks, growth rate was significantly higher [*8*] than predicted by this approach.) For surface flaws under $R = 0$ loading, reasonably good predictions have also been obtained for bluntly notched bend specimens [*10*] with compressive residual stresses produced by various means (for example, tensile overload and swaging) and for shot-peened dogbone specimens [*11*]. In these studies, it was assumed that K_{res} could be calculated by correcting K_{res} relations for through-thickness edge cracks with shape factors for semi-elliptical surface flaws.

Growth rate can also be correlated in terms of $\Delta K_{eff} = \Delta K_b$ shown in Fig. 1 and an "effective" R-ratio given by $(K_{eff,min}/K_{eff,max})$. Since ΔK_b equals $\Delta K_{applied}$, slower growth is attributed to the influence of negative R_{eff}. This type of approach has also produced good predictions of growth rate in the region of compressive residual stress surrounding holes in sheet specimens that had been given a tensile

[2] The italic numbers in brackets refer to the list of references appended to this paper.

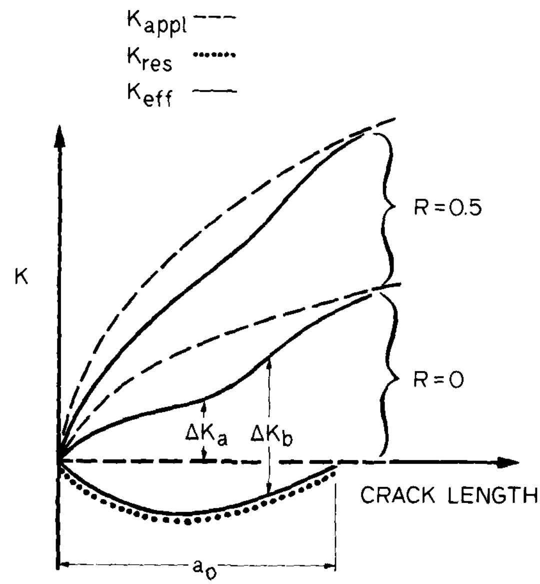

FIG. 1—*Schematic variation of effective stress intensity (based on superposition) for crack growth through a region of compressive residual stress, with constant stress range applied at two mean stress levels.*

pre-load and then tested under $R = 0.1$ loading [*12*]. Use of this approach requires da/dN–ΔK data for different R-ratios or an empirical relation which predicts such mean stress effects.

In the above cases, $R \simeq 0$ loading was used. If the applied loading were to have a significant tensile mean level, such as the $R = 0.5$ loading shown in Fig. 1, the influence of compressive residual stress would only be to lower R_{eff}. The ΔK_{eff} would be the same as $\Delta K_{applied}$ (unless K_{res} were very large and $\Delta K_{applied}$ small). Thus the beneficial effect of compressive residual stress may be diminished, depending on the influence of R-ratio on the crack growth behavior of a given metal.

The effect of tensile residual stress on K_{eff} is depicted schematically in Fig. 2. For constant amplitude loading from zero to maximum compression, use of $\Delta K_{eff} = \Delta K_a$ shown in this figure (with appropriate K_{res} factors) has successfully predicted growth rate of cracks in regions of tensile residual stress surrounding sharp center notches in sheet specimens [*13,14*]. The residual stresses were produced by the first application of maximum compression.

When the applied loading has a tensile mean bias, the tensile residual stress raises R_{eff} above R of the applied loading, but $\Delta K_{eff} = \Delta K_b$ shown in Fig. 2, which is the same as $\Delta K_{applied}$. Glinka [*15*] has investigated growth rate in center-cracked sheet specimens, through regions of tensile and accompanying compressive residual stress produced by transverse and longitudinal butt welds. Constant amplitude loading was applied at R-ratios between 0.35 and 0.5. He

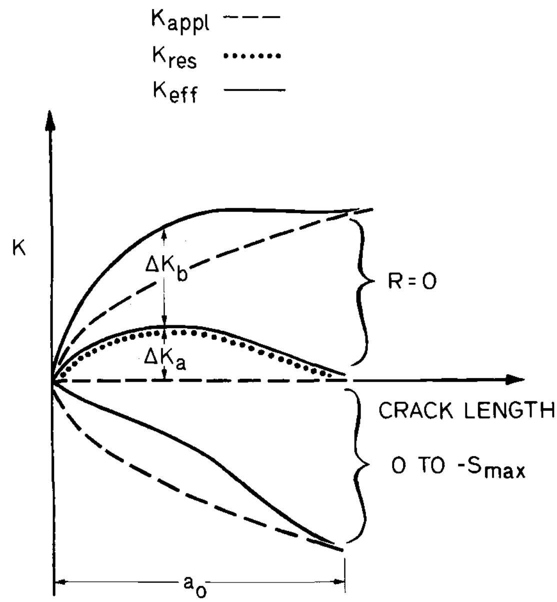

FIG. 2—*Schematic variation of effective stress intensity (based on superposition) for crack growth through a region of tensile residual stress, with constant stress range applied at two mean stress levels.*

obtained reasonably good predictions of growth rate in terms of $\Delta K_{eff} = \Delta K_b$ shown in Fig. 2 and R_{eff}, so long as cracks were within the regions of tensile residual stress. Higher growth rate was attributed to R_{eff} being larger than applied R. The Forman relation [*16*] was used to predict the influence of R_{eff} on growth rate.

A more detailed consideration of the use of the superposition approach to predict crack growth behavior will be presented later.

Crack-Generated Residual Stress and the Closure Approach

For through-thickness cracks in "plane stress" specimens under constant amplitude loading, the magnitude and distribution of crack-generated residual stress components normal and parallel to the plane of growth have been determined photoelastically [*17,18*] and by X-ray diffraction [*19,20*]. Such residual stresses have also been estimated by elastic-plastic analyses [*21,22*] and dislocation mechanics [*18*]. Little is known quantitatively about the distribution of residual stress through the thickness or about the distribution surrounding a growing surface crack.

The significance of crack-generated residual stress was pointed out by Elber [*23*], who observed that the residual tensile displacements left in the wake of a crack would cause it to close before tensile load was removed (under $R \geq 0$

loading) and thus generate compressive residual stresses in the wake. The crack would not open until a certain level of tensile loading was applied to overcome the crack opening stress resulting from the compressive residual stresses. By correlating crack growth rate with only that portion of the cyclic stress intensity when the crack was fully open, and by noting how the crack opening stress varied with applied mean stress and load sequence, Elber was able to provide a plausible physical explanation for R-ratio effects and retardation caused by tensile overloads.

In general, it is necessary to conduct elastic-plastic finite-element analyses [*21,24*] to keep track of changes in crack-opening stress under variable amplitude loadings. Simpler methods [*25-27*] for computing crack closure stress, based on the Dugdale model, are now available; however, their applicability is limited to through-thickness cracks in plane stress specimens. Recently, Newman [*28,29*] has extended the applicability of a Dugdale type of crack closure model to investigate the influence of plane stress versus plane strain, mean stress, and ratio of maximum stress-to-yield strength on crack-opening stress under constant amplitude loading. The model also provided excellent predictions of crack growth behavior for a variety of load sequence effects in variable amplitude load histories applied to center-cracked specimens.

To summarize, the superposition approach has been used primarily to predict growth rate under constant amplitude loading of cracks in existing residual stress fields. The closure model has been used to predict load sequence and mean stress effects in specimens with crack-generated residual stress fields.

Detailed Evaluation of Approaches

Crack Growth Initially Through Residual Tension

It is interesting to examine more closely Glinka's study of crack growth through residual tension and then into residual compression. Specimen details are shown in Fig. 3, and corresponding residual stresses in Fig. 4. (Residual stresses were determined in randomly selected P and L specimens by sectioning, and averaged distributions reported.)

To simplify the calculation of K_{res}, Glinka used a rectangular distribution to approximate the actual distribution, as shown by the dashed lines in Fig. 4. Kanazawa's relation [*30*] for K_{res} was used; that is,

$$K_{res} = \int_{-a}^{a} \sigma_{res}(x) \left[\frac{2 \sin \dfrac{\pi(a+x)}{W}}{W \sin \dfrac{2\pi a}{W} \sin \dfrac{\pi(a-x)}{W}} \right]^{1/2} dx \qquad (1)$$

where a = crack half-length, W = plate width, x = the distance from the plate centerline, and $\sigma_{res}(x)$ = residual stress.

The variation of K_{res} with x was not shown in Glinka's paper. Computations were performed here to determine this variation for the L specimen, and the

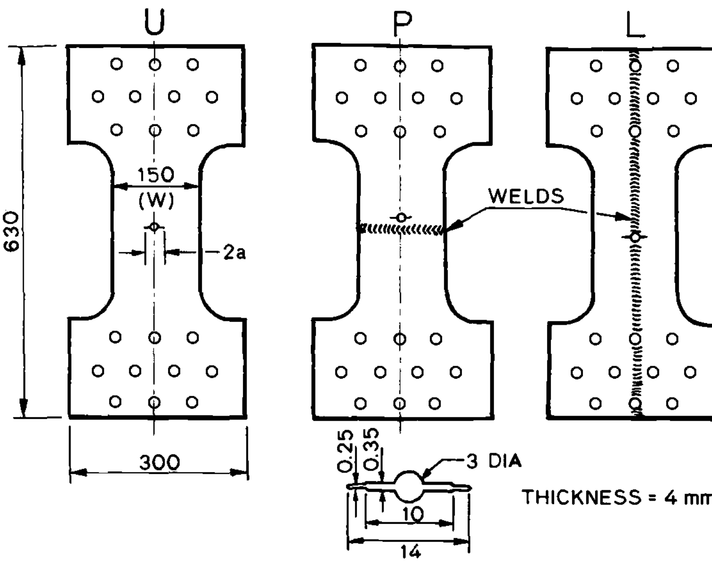

FIG. 3—*Crack growth specimens used in Glinka's tests* [15].

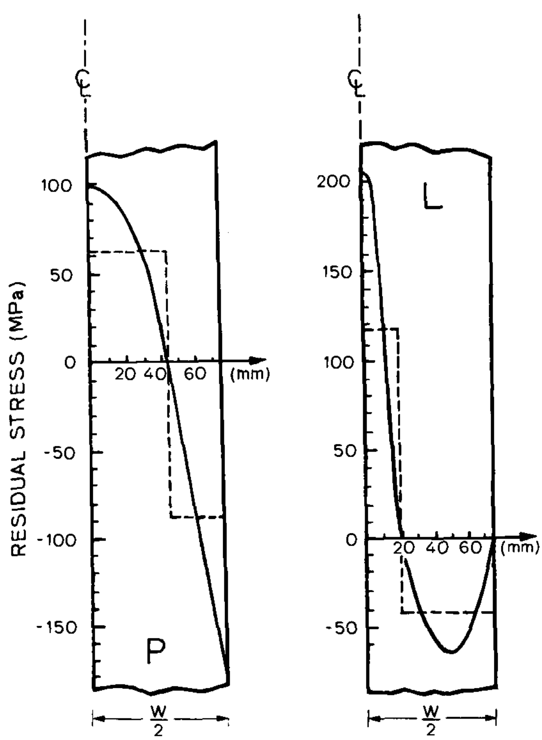

FIG. 4—*Initial residual stress normal to the plane of crack growth for the specimens shown in Fig. 3.*

results are shown in Fig. 5 for the rectangular distribution. (Use of a somewhat different relation [31] for the K_{res} of a center crack in a residual stress field also produced values similar to those from Eq. 1.)

A comparison of crack growth rate based on the superposition approach with representative test data from Glinka's paper is shown in Fig. 6. For the P specimens, the K_{res} values are lower than in the L specimens, thus resulting in a relatively lower R_{eff} and lower predicted growth rate in the region of tensile residual stress. In the P specimens, cracks grew through residual tension until fracture, and the predicted growth rate agrees reasonably well with data over the entire range of applied ΔK. In the L specimens, the K_{res} approach overestimates the growth rate in the manner shown in Fig. 6. The sharp drop in predicted growth rate occurs when the computed K_{res} starts to decline as the crack grows into the region of original compressive residual stress, causing computed R_{eff} to drop correspondingly and approach the applied R-ratio. The predicted drop in growth rate is not observed experimentally. Instead, a shift towards that of the U specimens occurs. The predicted drop is not associated with the use of a rectangular residual stress distribution, since calculations of K_{res} based on the actual distribution are quite similar at the transition between tensile and compressive residual stress. The drop is inherent to the K_{res} approach used. It is also significant to note that the observed growth rate in both L and P specimens for

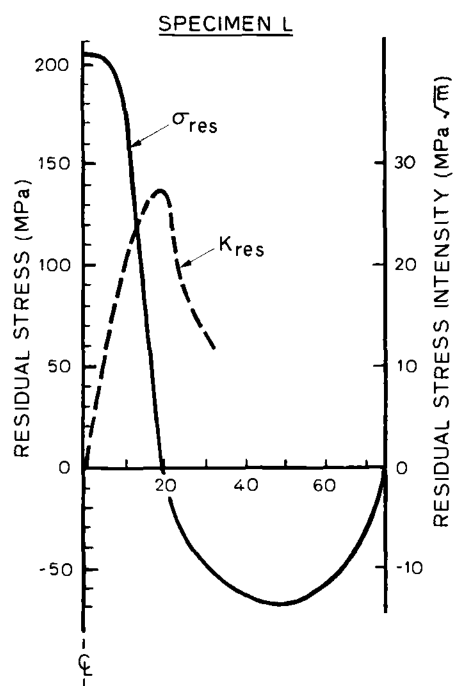

FIG. 5—*Residual stress and residual stress intensity distributions for L-type specimens.*

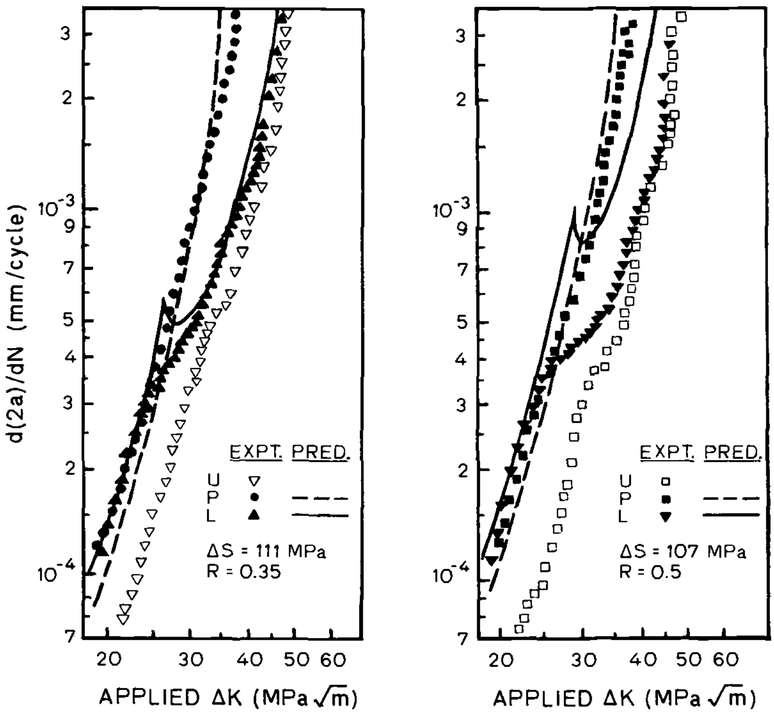

FIG. 6—*Comparison of representative crack growth rate data* [15] *with predictions using a superposition approach.*

$\Delta K_{\text{applied}} \leq 25$ MPa$\sqrt{\text{m}}$ is essentially the same, in spite of the fact that growth is occurring through initial tensile residual stress fields of quite different magnitude and distribution and thus different K_{res}.

The observed growth rate behavior in the L specimens may be caused by re-equilibration of the residual stresses as the crack grows. When a crack reaches a half-length of about 20 mm (see Fig. 4), it has released the original tensile residual stresses. In turn, the compressive residual stresses must also be released to maintain equilibrium. Thus, when a crack is at the transition between original tensile and compressive residual regions, it may behave in effect as an initial, "fresh" crack of that length with minimal surrounding residual stress.

The crack closure phenomenon may provide a reasonable explanation for the observed growth rate behavior in both L and P specimens. For a center-cracked specimen under constant amplitude loading without pre-existing residual stress, Newman [29] has shown analytically that the crack-opening stress level, S_{op}, is nearly constant over a substantial range of crack length and equal to a fraction of the maximum applied stress; that is, $S_{\text{op}} = qS_{\text{max}}$. In Fig. 7, this level is depicted schematically for postivie R-ratio loading of the type used in Glinka's tests. For a crack growing through a tensile residual stress region, the crack-opening stress should be lowered well below this level. Thus the effective ΔS for growth, as shown in

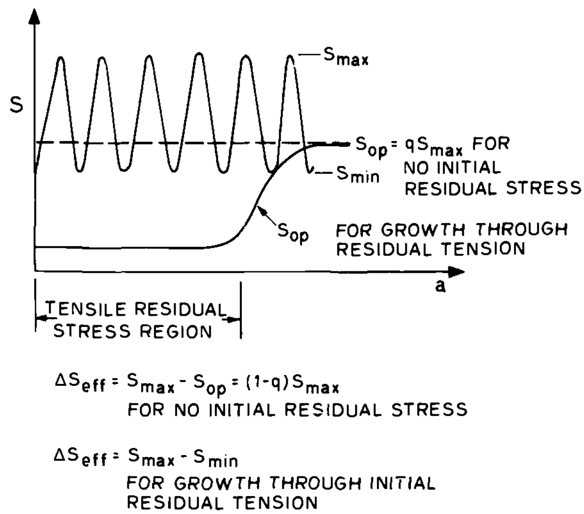

FIG. 7—*Simple crack closure model for crack growth initially through residual tension.*

Fig. 7, increases from $(1 - q)S_{max}$ to the applied $(S_{max} - S_{min})$, and ΔK_{eff} increases correspondingly. When a crack reaches the transition between initial tensile and compressive residual stress, the self-generated crack-opening stress should start to recover to the level for specimens without pre-existing residual stress. This model predicts that the growth rate should be the same in both L and P specimens in the zone of tensile residual stress, since the magnitude of tensile residual stress should have little influence on ΔK_{eff} so long as it is large enough to cause the crack-opening stress to drop below applied S_{min}.

In order to investigate this approach, values of q were taken from Newman's analysis [*29*] as a function of applied R-ratio and (S_{max}/σ_{yield}), for plane stress conditions. It was assumed that these values of q would approximately apply to crack growth in Glinka's unwelded specimens (4 mm thick). For each applied R-ratio, crack growth rate data in the unwelded specimens were correlated in terms of

$$da/dN = C(\Delta K_{eff})^n = C[(1 - q)K_{max}]^n \qquad (2)$$

The same relation was used to predict growth rate in the welded specimens, except that ΔK_{eff} increases from $(1 - q)K_{max}$ to $(K_{max} - K_{min})$ in the zone of tensile residual stress. The resulting predictions of growth rate are shown in Figs. 8 and 9. The cross-hatched region indicates the range of crack half-length (18 to 20 mm) for L specimens in which original tensile and compressive residual stresses are likely to have been released and in which crack-opening stress and ΔK_{eff} are postulated to start recovering to values which would exist in specimens without pre-existing residual stress.

Through consideration of re-equilibration of residual stress caused by crack growth and use of a crude crack closure model, observed crack growth rate

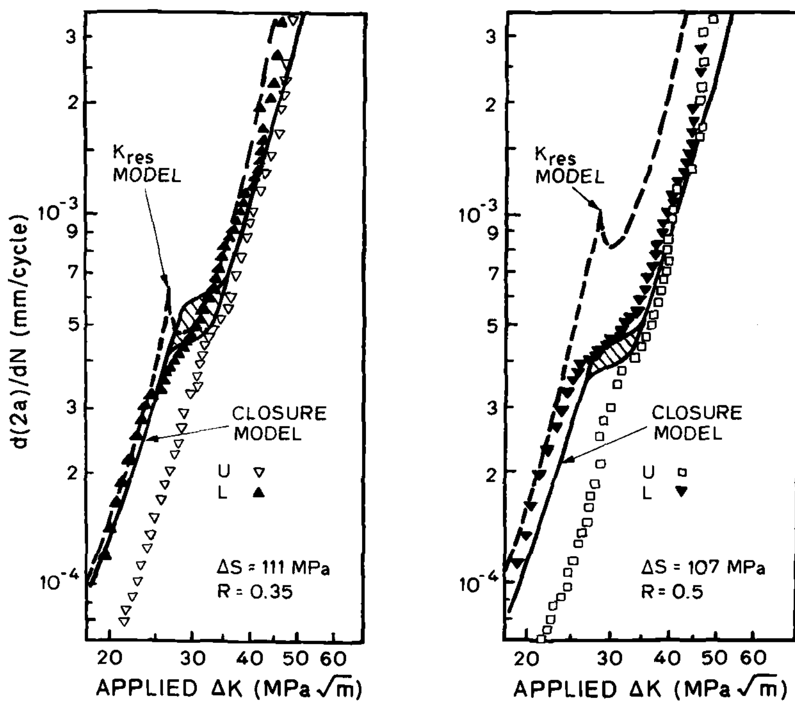

FIG. 8—*Comparison of crack growth rate behavior predicted by a superposition approach and by a simple closure model with data* [15] *for applied* R*-ratios of 0.35 and 0.50.*

behavior is predicted more realistically than by the superposition approach used in this case.

Crack Growth Initially Through Residual Compression

It is also interesting to examine in more detail the results of Liu [*12*], who studied crack growth under $R = 0.1$ loading through residual stress fields induced by tensile pre-loading of sheets with central holes, as cited previously. Figure 10 shows the residual stress distribution (computed by finite elements) and the variation of K_{res} with distance from the hole. The corresponding variation in predicted K_{eff} and R_{eff} is given in Fig. 11 for a typical specimen. K_{res} and R_{eff} are computed to be negative well into the zone of original tensile residual stress; they start to asymptotically approach zero for (a/r) ratios greater than about one, which corresponds to crack lengths of 6 to 10 mm, depending on the size of holes used. Thus, the crack growth rate is expected to be lower than the rate in specimens without preload, but to gradually approach that rate as the influence of K_{res} diminishes.

The observed growth rate behavior for a representative specimen is shown in Fig. 12. Growth rate is lower initially, as expected, but then exceeds the baseline $R = 0.1$ rate. This faster growth rate is not anticipated and occurs at (a/r)

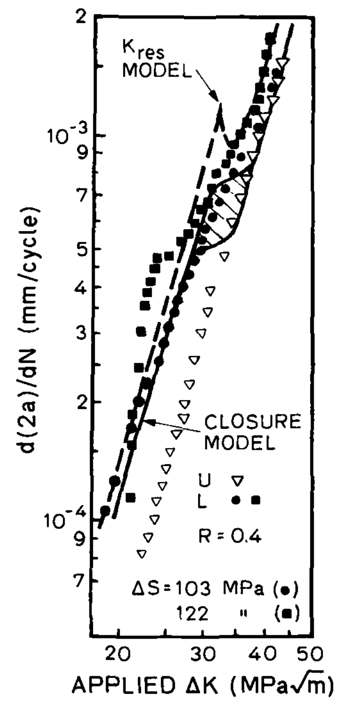

FIG. 9—*Comparison of crack growth rate behavior predicted by a superposition approach and by a simple closure model with data* [15] *for an applied* R*-ratio of 0.40.*

between 1.2 and 1.4, depending on applied stress level and hole size. These (a/r) values were computed from knowledge of applied stress and the experimentally observed $\Delta K_{applied}$ at which the "cross-over" in growth rate behavior occurs (Fig. 12). Referring to Fig. 10, the (a/r) values also correspond to the region where cracks have penetrated most of the original tensile residual stress field. Similar behavior was seen in several specimens with cold-worked holes [*8*].

A possible explanation for the growth rate being higher than the baseline rate involves re-equilibration of residual stresses caused by crack growth. When a crack is within the region of initial compressive residual stress, the overall residual stress pattern should not change appreciably, since the presence of a crack does not prevent compressive residual stresses from being carried through the material. However, as the crack extends beyond the residual compression, it severs material that would otherwise be in residual tension. As release of tensile residual stress occurs, the residual compression which balanced the tension will also be relaxed. As a result, the crack-opening stress may vary schematically as shown in Fig. 13. In the compressive residual stress region, the opening stress should develop to a maximum value and then decline as a crack penetrates residual tension. If the opening stress drops below the stabilized value that would exist in the absence of any pre-existing residual stresses, faster growth in the

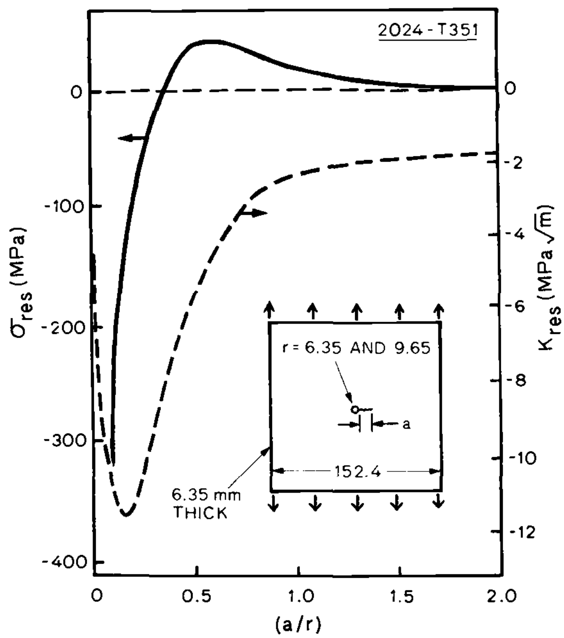

FIG. 10—*Residual stress and residual stress intensity distributions for a tensile pre-load stress of 250 MPa* [12].

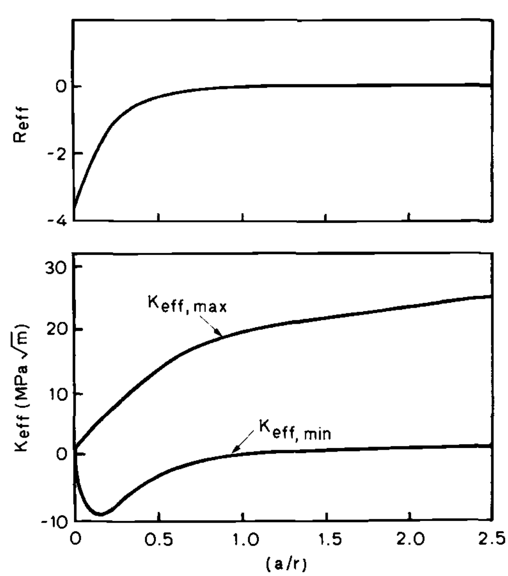

FIG. 11—*Variation of effective stress intensity and effective* R*-ratio (based on superposition) for the specimen of Fig. 10 cycled between 16.6 and 166 MPa* [12].

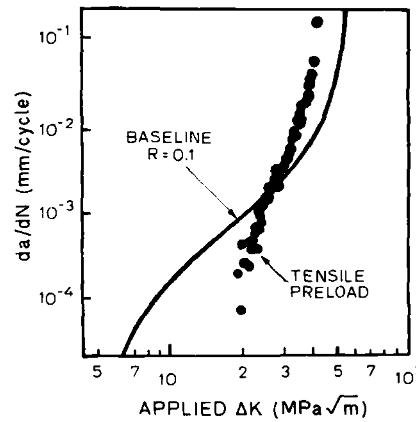

FIG. 12—*Crack growth rate in a representative specimen with a tension pre-loaded hole compared with that determined in specimens with no initial residual stress* [12].

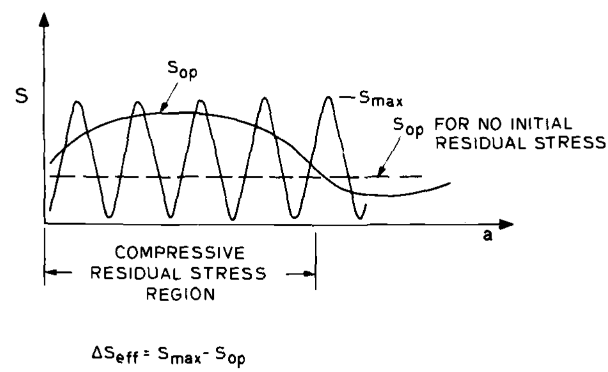

FIG. 13—*Expected variation of crack-opening stress for growth initially through residual compression and on into residual tension.*

region of residual tension would be expected. To estimate the extent of the drop would require use of Newman's computer analysis [*29*], modified to account for the presence of the original residual stress field. Experimental measurements of opening load for a crack growing through a qualitatively similar residual stress field at a cold-worked hole have been made [*9*] with a laser interferometric technique. For a heavily cold-worked specimen, the opening load appeared to drop below the stabilized value for a hole without cold-work when the crack was in the tensile residual stress region. However, since measurements were reported for only one specimen and since the observed drop could have been within experimental uncertainty, it is difficult to know if such behavior actually does occur. Further study of this postulated behavior seems warranted.

Elber [*11*] has also studied the behavior of cracks growing first through residual compression and then into residual tension. The cracks were semicircular surface flaws (initial shape) and the residual stresses were produced by shot-peening. The residual stress distribution estimated by Elber is shown in Fig. 14. A superposition method was used to predict crack growth rate under $R = 0$ loading. K_{res} was computed to be negative for crack depths less than 1.3 mm and positive thereafter. Thus, for depths greater than 1.3 mm, growth rate higher than in specimens without initial residual stress is expected. The depths at which higher growth rate actually did occur were estimated here (from applied stress levels and $\Delta K_{applied}$ at which the higher rates were observed). These depths are shown in Fig. 14; note that they decrease with higher applied stress level. This behavior was also seen in Ref *12*. In Elber's study, the superposition approach gave a conservative estimate of depth for higher growth rate. It also predicted the *rate* of growth reasonably well, but tended to somewhat underestimate that rate in the tensile residual stress region.

Unlike through-thickness cracks growing in residual stress fields in thin sheets, surface cracks such as studied by Elber should relieve only neighboring parts of the overall tensile residual stress field. It is thus uncertain how the accompanying compressive residual stress field would also be altered, owing to the three-dimensional nature of the problem. Analysis of how residual stress fields are affected by surface crack growth and, in turn, how the altered fields influence growth behavior certainly presents a challenging problem, of considerable practical importance.

Summary and Discussion

Based on studies to date, the superposition approach appears to adequately predict growth rate when a crack is growing first through the compressive portion

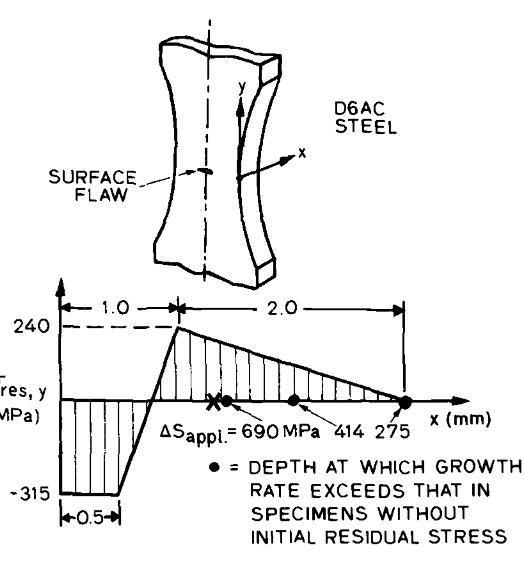

FIG. 14—*Estimated residual stress distribution due to shot-peening* [11].

of a residual stress field or first through the tensile portion of a field. In several cases, though, discrepancies between predicted and observed growth rate have occurred when growth extended into regions of accompanying residual stress of opposite sign.

Any assessment of the predictive ability of the superposition approach must be done with caution, since apparent success or lack thereof depends on accurate knowledge of the initial residual stress field, which is often a source of considerable uncertainty in itself. In any case, since most of the crack growth life is usually expended before a crack grows into residual stress of opposite sign, predicted total life may not be seriously affected by such discrepancies.

Most tests investigating the superposition approach have been made under applied $R = 0$, constant amplitude loading. Tests at different R-ratios, with different residual stress distributions, are needed to further support the approach.

The superposition approach has the distinct advantage for use in design analysis of requiring only calculation of stress intensities by using established methods of linear elastic fracture mechanics. However, since it is based on elastic analysis, it lacks the ability to account for the influence of possible changes in residual stress fields induced by service loadings, before a crack starts and as it grows.

The crack closure approach provides the mechanics to account for the influence of pre-existing residual stress fields on growth behavior, including changes in fields due to service loadings and crack growth, but has not been used much for that purpose. It has furnished a basis for predicting the influence of load sequence on crack growth, and an extension of that basis to cases of pre-existing residual stress fields should also be feasible.

A simplified crack closure model that considers residual stress re-equilibration with crack extension provided somewhat better predictions of crack growth behavior than Glinka's method for cracks growing first through residual tension, and on into residual compression. It may also be able to better explain the growth behavior of cracks that grow from residual compression into residual tension, but this must be investigated.

The primary drawback of the crack closure approach is that it usually requires elastic-plastic finite-element analysis, which must be repeated as a crack grows. Simplified closure models (for example, based on the Dugdale model) are available to reduce that computational burden, but their applicability is currently limited to simpler crack geometries, such as center-cracked sheets.

Most fatigue cracks start at notches. If there is a pre-existing residual stress field below the notch (for example, due to cold-working) or if residual stresses develop in service (for example, due to an overload), subsequent service loads may alter the residual stress distribution before a crack starts. For instance, residual stresses near the notch surface may be relaxed by localized cyclic plastic straining, but the re-equilibrated distribution in depth may still have a significant influence on subsequent crack growth behavior. Very little is known about this problem. The formation and growth of small cracks under such conditions needs study in order to assist development of improved life prediction methods.

References

[1] Hsu, Y. C. and Forman, R. G., *Journal of Applied Mechanics, Transactions of ASME*, Vol. 42, No. 2, 1975, pp. 347-352.

[2] Davidson, T. E., Barton C. S., Reiner, A. N., and Kendall, D. P., "Overstrain of High Strength Open-End Cylinders of Intermediate Diameter Ratio," in *Proceedings of First International Congress on Experimental Mechanics*, Society for Experimental Stress Analysis, 1961, pp. 335-352.

[3] Underwood, J. H. and Throop, J. F. in *Part-Through Crack Fatigue Life Predictions, ASTM STP 687*, American Society for Testing and Materials, 1979, pp. 195-210.

[4] Grandt, A. F., *International Journal of Fracture*, Vol. 14, No. 4, 1978, pp. R221-R229.

[5] Bueckner, H. F., "Field Singularities and Related Integral Representations," in *Methods of Analysis and Solutions of Crack Problems*, Noordhoff International Publishing, Leyden, The Netherlands, Chapter 3, 1972.

[6] Barenblatt, G. I., "The Mathematical Theory of Equilibrium Cracks in Brittle Fracture," in *Advances in Applied Mechanics*, Vol. 7, Academic Press, New York, 1962.

[7] Jones, A. T. and Callabresi, M. L., *Engineering Fracture Mechanics*, Vol. 11, No. 4, 1979, pp. 675-688.

[8] Cathey, W. H. and Grandt, A. F., Jr., *Journal of Engineering Materials and Technology, Transactions of ASME*, Vol. 102, No. 1, 1980, pp. 85-91.

[9] Chandawanich, N. and Sharpe, W. N., Jr., *Engineering Fracture Mechanics*, Vol. 11, 1979, pp. 609-620.

[10] Underwood, J. H. and Throop, J. F., "Residual Stress Effects on Fatigue Cracking of Pressurized Cylinders and Notched Bending Specimens," paper presented at Fourth International Congress on Experimental Mechanics, Society for Experimental Stress Analysis, May 1980.

[11] Elber, W. in *Fracture Toughness and Slow-Stable Cracking, ASTM STP 559*, American Society for Testing and Materials, 1974, pp. 45-58.

[12] Liu, A. F., "The Effect of Residual Stress on Crack Growth from a Hole," Report NOR-79-74, Northrop Corporation, Hawthorne, Calif., August 1979.

[13] Hubbard, R. P., *Journal of Basic Engineering, Transactions of ASME*, Vol. 91, No. 4, 1969, pp. 625-631.

[14] Saal, H., "Fatigue Crack Growth in Notched Parts with Compressive Mean Load," Paper No. 71-MET-Z, American Society of Mechanical Engineers, 1971.

[15] Glinka, G. in *Fracture Mechanics, ASTM STP 677*, American Society for Testing and Materials, 1979, pp. 198-214.

[16] Forman, R. G., Kearney, V. E., and Engle, R. M., *Journal of Basic Engineering, Transactions of ASME*, Vol. 89, No. 3, 1967, pp. 459-464.

[17] Cheng, Y. F. and Brunner, H., *International Journal of Fracture Mechanics*, Vol. 6, 1970, pp. 431-434.

[18] Tirosh, J. and Ladelski, A., *Engineering Fracture Mechanics*, Vol. 13, 1980, pp. 453-461.

[19] Tanaka, K., *Journal of Strain Analysis*, Vol. 10, No. 1, 1975, pp. 32-41.

[20] Kunz, L., Knesl, Z., and Lukas, P., *Fatigue of Engineering Materials and Structures*, Vol. 2, No. 3, 1979, pp. 279-287.

[21] Newman, J. C., Jr., in *Mechanics of Crack Growth, ASTM STP 590*, American Society for Testing and Materials, 1976, pp. 281-301.

[22] Rice, J. R. in *Fatigue Crack Propagation, ASTM STP 415*, American Society for Testing and Materials, 1967, pp. 247-311.

[23] Elber, W. in *Damage Tolerance in Aircraft Structures, ASTM STP 486*, American Society for Testing and Materials, 1971, pp. 230-242.

[24] Socie, D. F., *Engineering Fracture Mechanics*, Vol. 9, 1977, pp. 849-865.

[25] Dill, H. D. and Saff, C. R. in *Fatigue Crack Growth under Spectrum Loads, ASTM STP 595*, American Society for Testing and Materials, 1976, pp. 306-319.

[26] Budiansky, B. and Hutchinson, J. W., *Journal of Applied Mechanics, Transactions of ASME*, Vol. 45, June 1978, pp. 267-276.

[27] Fuhring, H. and Seeger, T., *Engineering Fracture Mechanics*, Vol. 11, 1979, pp. 99-122.

[28] Newman, J. C., Jr., "Prediction of Fatigue Crack Growth under Variable Amplitude and Spectrum Loading Using a Closure Model," NASA Technical Memorandum 81942, Langley Research Center, Jan. 1981.

[29] Newman, J. C., Jr., "A Crack Closure Model for Predicting Fatigue Crack Growth under Aircraft Spectrum Loading," NASA Technical Memorandum 81941, Langley Research Center, Jan. 1981.
[30] Kanazawa, T., Oba, H., and Mahida, S., *Society of Naval Architects of Japan Journal*, No. 109, 1961, pp. 359-369.
[31] Vaidyanathan, S. and Finnie, I., *Journal of Basic Engineering, Transactions of ASME*, Vol. 93, No. 2, 1971, pp. 242-246.

DISCUSSION

A. P. Parker[1] *(written discussion)*—I have serious doubts on the validity of the author's arguments for rejecting the superposition technique as applied to fatigue crack growth in residual stress fields. The superposition technique is covered in detail by Parker,[2] the important facets being the incorporation of K_{res} into both ΔK (the stress intensity factor range) to produce ΔK_{eff} (an effective ΔK), and R (the nominal stress ratio) to produce R_{eff}. Glinka's model is based on the superposition approach,[3] allied with Forman's crack growth law,[4] and is examined in detail by the author. From a superposition viewpoint the only flaws in Glinka's approach are an over-idealized representation of the residual stress field (and hence K_{res}) and an attempt to employ Forman's crack growth law in a form that does not match the available crack growth rate data at high R-values.

The author implies that he has recalculated K_{res} based on the accurate residual stress distribution and that they "are quite similar at the transition between tensile and residual stress". Figure 15 is based on the author's Fig. 5 and shows σ_{res} as calculated by Glinka, the idealized distribution employed by Glinka, K_{res} as calculated by the author on the basis of Glinka's idealized distribution, and K_{res} calculated on the basis of the actual stress distribution, using an available Green's function.[5] We note that the author's comment on the similarity of the K_{res} values at the 20-mm point is correct, but misleading in that the K_{res} predictions based on the actual and idealized distribution disagree by a factor of almost two at short crack lengths. Furthermore, the peak value of K_{res} cannot be associated with the transition between tensile and residual stress, as emphasized by Parker.[2] Also shown in Figure 15 is the variation in R_{eff} for the 'L' type specimens subjected to a nominal R-value of 0.35.

Figure 16 is based on the author's Fig. 8, which is in turn based upon Glinka's Fig. 6.[3] It indicates Glinka's crack growth rate predictions and results for 'L' type

[1] Materials Branch, Royal Military College of Science, Shrivenham, Swindon, Wiltshire, England.
[2] Parker, A. P., this publication, pp. 13-31.
[3] Glinka, G. in *Fracture Mechanics, ASTM STP 677*, American Society for Testing and Materials, 1979, pp. 198-214 (Ref *15* in Nelson's paper).
[4] Forman, R. G., Kearney, V. E., and Engle, R. M., *Journal of Basic Engineering, Transactions of ASME*, Vol. 89, No. 3, 1967, pp. 459-464 (Ref *16* in Nelson's paper).
[5] Tada, H., Paris, P. C., and Irwin, G., "The Stress Analysis of Cracks Handbook," Del Research Corp., Hellertown, Pa., 1973.

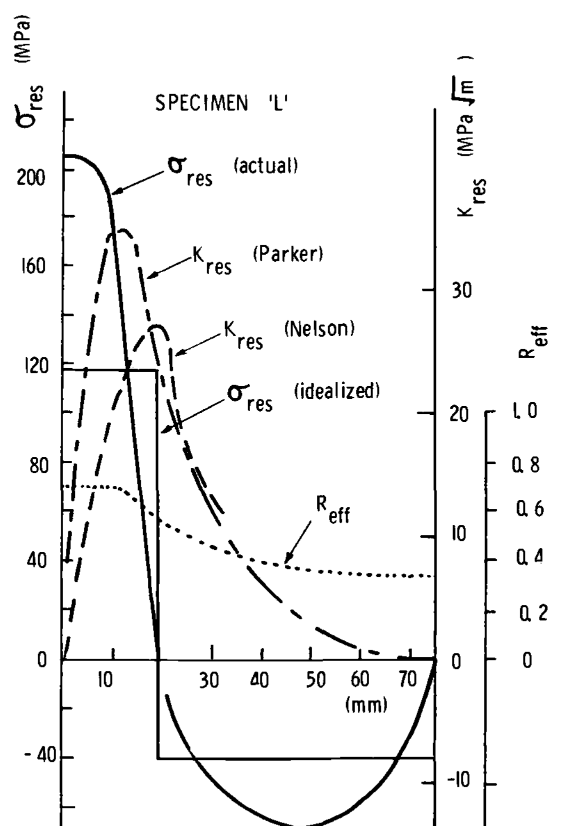

FIG. 15—*Residual stress, residual stress intensity, and effective stress ratio.*

specimens at a nominal R-value of 0.35. The author states that the predicted drop in crack growth rate "is not associated with the use of a rectangular residual stress distribution . . . The drop is inherent to the K_{res} approach used". Using the corrected K_{res} values and Forman's crack growth rate expression (Eq 5 in his paper), with the appropriate constants given in Glinka's earlier paper,[6] a revised prediction curve is obtained (Fig. 16). This curve again exhibits a drop in predicted crack growth rates in the region where the value of R_{eff} is reducing rapidly from 0.7.

After inspecting Glinka's data for the effect of stress ratio on fatigue crack growth rate in the base material (Fig. 3 in Glinka's paper) and comparing them with the predictions from Eq 5, it appears that the crack growth constants and material properties employed by Glinka[6] considerably overestimate crack growth rates at higher R-values. By ignoring the Forman expression, and extracting crack growth rates directly from Figs. 3 and 4a in Glinka,[3] it is a straightforward

[6] Glinka, G., "Fatigue Crack Growth in a Residual Stress Field," in *Seventh Polish Symposium on Experimental Studies in Mechanics of Solids*, Warsaw, 28-29 Sept. 1976 (in Polish).

procedure to predict the variation in crack growth rates. This is shown as an additional curve in Fig. 16. The agreement appears to be excellent over the whole range of ΔK. Thus it appears that the drop in Glinka's crack growth rate predictions, described by the author as "inherent to the K_{res} approach", is actually a result of an inappropriate selection of parameters for use in Forman's law, and is not inherent to the superposition.

My conclusions are (*1*) that for the most extensive experimental work quoted by the author, the argument for rejecting the superposition approach is not valid; and (*2*) that the proper use of a rapid superposition technique gives crack growth rate estimates that are superior to those obtained from the crack closure model.

D. V. Nelson (author's closure)—The author did not reject the superposition approach. To the contrary, as noted throughout the paper, the approach has produced good predictions of crack growth life and is a useful method. The author did raise some questions about the discrepancies between predicted and observed crack growth behavior in Glinka's study. This was not meant, of course, to be an argument for rejecting the approach. In the author's description of Glinka's predictions, the phrase "inherent to the K_{res} approach used" refers to the particular approach used by Glinka and should not be condensed as in the latter part of

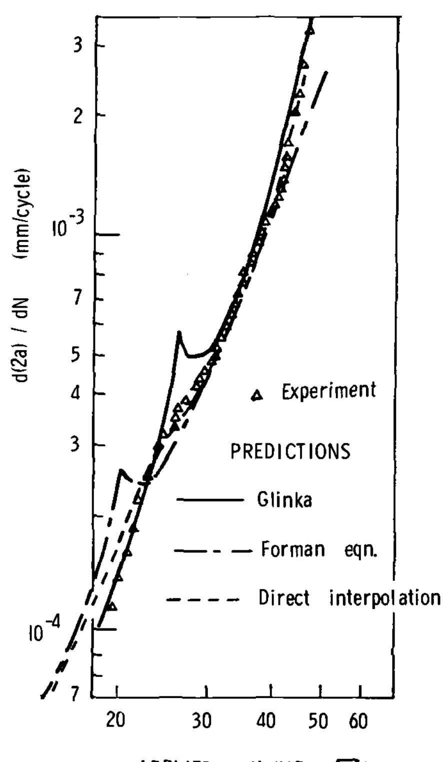

FIG. 16—*Crack growth rates—experimental results and predictions (Specimen L).*

the discussion to "inherent to the K_{res} approach," which implies a generalization not intended.

The author did note that in Glinka's 'L' type specimen, K_{res} reached a peak near the transition from tensile to compressive residual stress, when K_{res} is computed based on Glinka's rectangular distribution for σ_{res}. The author is aware that this is not the case in general, but appreciates the discusser's reminder.

The discussion concentrates on the drop in growth rate predicted by Glinka, showing that it appears to vanish when K_{res} for the actual σ_{res} distribution is used in conjunction with values of growth rate interpolated from Glinka's R-ratio data. These data are shown in Fig. 17, which was taken from the preprint and used in original, enlarged form by the author in preparing both the paper and this closure. Figure 18 compares representative interpolated values reported in the discussion

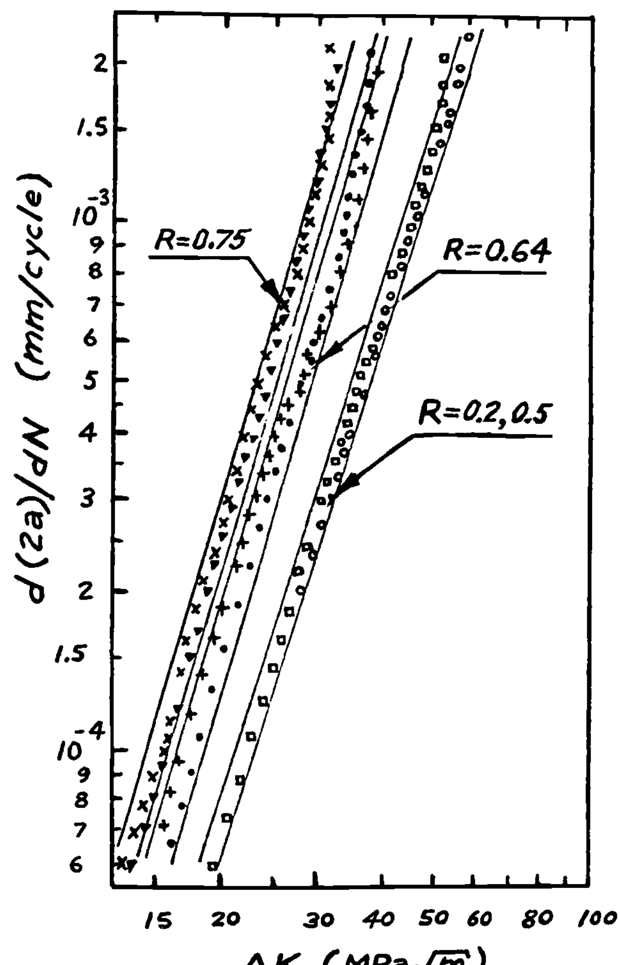

FIG. 17—*Glinka's* R*-ratio data.*

with data from Fig. 17. The interpolated values were obtained by the author from the "direct interpolation" curve of Fig. 16 at values of ΔK (which are the same as ΔK_{eff} in Glinka's study) for different crack lengths and the ΔS = 111 MPa loading considered in the discussion. The corresponding R_{eff} for a given ΔK was obtained from the crack length at that ΔK, the relation between "actual" K_{res} and length, which is shown in Fig. 15, and the known applied K_{min} and K_{max} values. R_{eff} is then the ratio $(K_{min} + K_{res})/(K_{max} + K_{res})$, providing values to be used with R-ratio data to predict da/dN at a given ΔK. The author carried out this evaluation over a range of applied ΔK from approximately 20 to 34 MPa$\sqrt{m}$. At ΔK of 20.5 MPa$\sqrt{m}$ and corresponding R_{eff} of 0.7, the interpolated value seems rather low, as shown in Fig. 18. It would be in better agreement with the data at R = 0.64. This can also be seen directly by reference to Fig. 17. Over a range of ΔK from 20 to approximately 29 MPa$\sqrt{m}$, the author's evaluation indicates that all interpolated values appear somewhat low. At R = 0.64, where test data exist, and thus interpolation is not really needed, the interpolated value is still on the low side. At ΔK-values greater than about 29 MPa$\sqrt{m}$, the interpolated values become higher than their trend at lower ΔK.

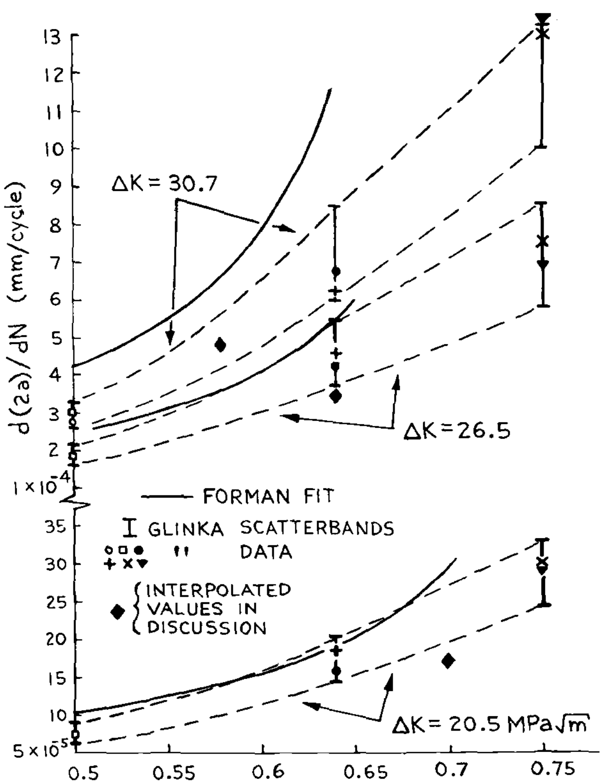

FIG. 18—*Comparison of interpolated values from discussion with* R*-ratio data.*

Figure 18 also shows the Forman fit based on Glinka's constants. The discusser is correct in pointing out that the Forman relation tends to overestimate the influence of R-ratio at higher values of R. The overestimation also worsens for higher ΔK.

Figure 19 shows growth rate predicted using K_{res} for the actual σ_{res} distribution and values interpolated by the author for a given ΔK, R_{eff} combination as midway between dashed lines such as shown in Fig. 18. This interpolation was carried out over a range of R_{eff} from approximately 0.57 to 0.7, and may also be open to question because of the difficulty in establishing any relation between da/dN, ΔK, and R based on limited data; however, it does seem more defensible than the discusser's interpolations. A drop in growth rate is still predicted, but it is diminished relative to what the Forman fit would predict, as expected.

Use of the discusser's interpolated values, which seem low for ΔK between points a and b on the curve of Fig. 19, and which become relatively higher thereafter, does indeed cause a lower curve between a and b, making a later drop disappear.

The drop in growth rate in Glinka's study appears to be caused by two competing effects. Over a certain small region of ΔK where R_{eff} is declining, the increase in da/dN due to higher ΔK with crack growth is more than offset by the reduction in da/dN caused by lower R, the net result being a temporary drop in

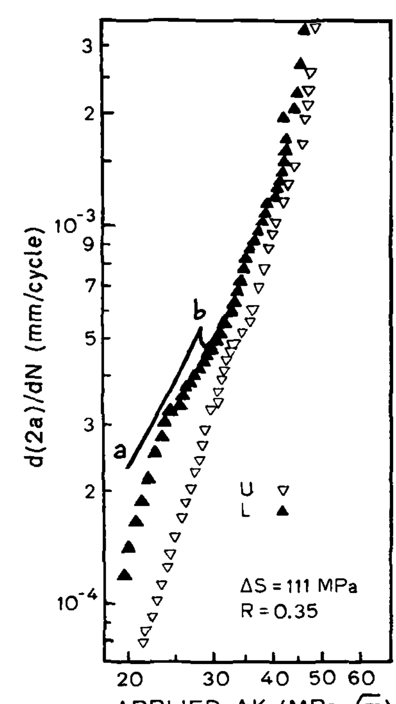

FIG. 19—*Predicted growth rate based on author's interpolations.*

predicted da/dN. This drop may not occur in other metals with different R-ratio effects or for different test conditions, and the author does not intend that it be construed as a general feature of the superposition method. Preparation of this closure does suggest that it would be interesting to see how sensitive the superposition method, as well as other methods, are to differences in R-ratio data representations and to differences in K_{res} computed for various representations of σ_{res} distributions. After all, residual stress distributions are rarely known with precision for most components, and comprehensive R-ratio data for the numerous metals used in structure are often lacking.

In the same paragraph of the paper which mentions the drop in Glinka's predicted growth rate, another observation is made—namely, the growth rate in 'L' and 'P' type specimens is essentially the same for ΔK less than about 25 MPa$\sqrt{m}$, even though the specimens have quite different σ_{res} distributions and thus different K_{res} values. For example, at a crack half length of $a = 10$ mm, K_{res} values for the 'L' and 'P' specimens are 35 and 17 MPa$\sqrt{m}$, respectively, based on the use of the actual σ_{res} profiles and the relation [*31*]

$$K_{res}(x) = \frac{2\sqrt{a}}{\sqrt{\pi}} \int_0^a \frac{\sigma_{res}(x)\,dx}{\sqrt{a^2 - x^2}}$$

(The value for the 'L' specimen agrees well with that shown in Fig. 15). For the applied $\Delta S = 111$ MPa and $R = 0.35$ loading considered in the discussion, the corresponding R_{eff} values in the 'L' and 'P' specimens are 0.69 and 0.58, respectively. The growth rate in the 'L' specimen would then be predicted to be about 70 percent higher than in the 'P' specimen at that crack length; yet the rate is virtually the same. Again, this type of discrepancy is not intended to be a rejection of the superposition approach. The drop in growth rate and this discrepancy are effects not much stronger than possible scatter in growth rate behavior. They did serve to make the author seek another possible explanation for the observed behavior—that is, a highly simplified crack closure model.

To further explore the influence of residual tension on crack growth, tests could be performed using a metal that is relatively insensitive to R-ratio effects over a certain range of da/dN and R. The steel (unwelded) tested by Glinka, for example, had essentially the same growth rate for applied R-values between 0.2 and 0.5 and da/dN between 5×10^{-5} and 10^{-3} mm/cycle. Suppose that tests were conducted with that steel using a combination of applied R, ΔK, and σ_{res} which would produce R_{eff} varying between 0.2 and 0.5 during growth through residual tension. In that case, no significant influence of residual tension would be predicted by the superposition approach. It would be interesting to see if growth rate was still affected by the residual tension.

My conclusions are that: (*1*) both the superposition and crack closure methods are useful, with respective advantages and limitations; and (*2*) additional analyses and experiments are needed to investigate some of the questions raised by the author in the paper.

S. M. Kudva[1] *and D. J. Duquette*[1]

Effect of Surface Residual Stresses on the Fretting Fatigue of a 4130 Steel

REFERENCE: Kudva, S. M. and Duquette, D. J., **"Effect of Surface Residual Stresses on the Fretting Fatigue of a 4130 Steel,"** *Residual Stress Effects in Fatigue, ASTM STP 776,* American Society for Testing and Materials, 1982, pp. 195-203.

ABSTRACT: Fretting fatigue is defined as the fatigue of a material caused by the presence of a rubbing contact with a relative displacement of less than 100 micrometres. The presence of fretting results in a lowering of the fatigue life of the material. The relative displacement, also known as the slip amplitude, has a considerable effect on the life of the specimens that were investigated. Different surface microstructures were studied in order to investigate the effect of slip amplitude on the fatigue life. These treatments, namely carburization and decarburization, also induced surface residual stresses which were instrumental in causing the changes that were observed in the fatigue life.

Effects of residual stress on fretting fatigue were studied using three kinds of heat-treated specimens of a medium carbon steel. Two sets of experimental specimens were respectively decarburized and carburized to induce residual stresses on the surface. A set of control specimens of tempered martensite was used to compare results. All three structures showed a minimum in life versus the slip amplitude; the carburized specimens exhibited longer lives in general and the opposite was true for the decarburized specimens. In all cases, transverse cracks initiated on the surface, at the interface between the contacting and free surfaces, and propagated inwards, perpendicular to the loading axis. An attempt is made to explain the observed phenomena using residual stress arguments.

KEY WORDS: residual stresses, carburizing, decarburizing, fretting, fatigue, debris, slip, normal load, cyclic stress, fatigue cracks, martensitic

It is well known that residual stresses are present in many components. These stresses may be intentional or unintentional, depending on the thermal and mechanical history of the component. It is generally acknowledged, however, that compressive surface residual stresses aid in prolonging the fatigue life of components by reducing the surface tensile stress felt by the components [*1*].[2] Thermo-chemical treatments such as shot peening, hammer peening, etc., have been widely used in order to induce compressive residual stresses on and below the surface.

In many of the above situations, fatigue is accompanied by a form of cyclic wear known as fretting. A general fretting situation comprises two contacting

[1] Instructor and Professor, respectively, Materials Engineering Department, Rensselaer Polytechnic Institute, Troy, N.Y. 12181

[2] The italic numbers in brackets refer to the list of references appended to this paper.

surfaces having a relative oscillatory motion of small amplitudes, usually less than 100 micrometres [2]. The ensuing wear itself is capable of resulting in an undesirable loss of material from the surface in the form of metallic or oxidized debris. However, the main deleterious effect of fretting on fatigue is a reduction in the fatigue life of the component, resulting from an increased number of surface cracks initiated by fretting [*3-5*]. The latter phenomenon, termed fretting fatigue, is observed in a wide range of engineering applications and in a variety of metals. Although the fretting fatigue life in general has been observed to be lower than the fatigue life under the same loading conditions, the analysis of the situation is complicated by the fact that the extent to which the life is reduced depends on several variables such as normal load and degree of relative motion [*6,7*]. This study emphasizes not only the effect of surface residual stresses on fretting fatigue, but the effect of a few other important variables as well.

Fretting Fatigue

A fretting fatigue situation consists of a component under loading in contact with one or more surfaces. The contact surfaces impose a load normal to the instantaneous load on the surface of the component. The normal load causes a tangential load on the surface of the component, the extent of which is dependent on the nature of the interface between the two surfaces. The relative motion between the two surfaces is termed slip. The magnitude of slip is referred to as the slip amplitude and is dependent on several factors, including the modulus of the respective materials, the cyclic stress, and the normal stress. The resistance to slip is often represented by a coefficient of friction, which is the tangential force divided by the normal force.

The effects of various fretting parameters on fatigue life have been reported by several investigators. Waterhouse [*6*] reported a general decline in fatigue life under fretting conditions. The fretting fatigue limit increased with an increase in compressive mean stress and declined with an increase in tensile mean stress. When normal stress was increased, the fretting fatigue life was observed to decline until it saturated at some level beyond which no further degradation in life occurred [*6,7*]. Nishioka and Hirakawa [*8-10*] studied the effect of slip amplitude at a constant normal load and observed that the stress required to initiate fatigue cracks lessened with an increase in slip amplitude. Waterhouse [*6*] reported an increase in fretting fatigue strength with a decrease in slip amplitude. Plate-like debris indicating surface delamination has been revealed by surface damage studies [*11-13*]. Spherical wear particles were also observed in some cases [*3,14*].

In fretting, the time required to initiate a fatigue crack was observed to decline when compared with tests performed in the absence of fretting. An equation developed by Nishioka and Hirakawa [*8*] for the initiation of fretting fatigue cracks in flat fatigue specimens fretted by cylindrical pads is

$$\sigma_{\text{fwl}} = \sigma_{\text{wl}} - 2\mu Po[1 - \exp(-s/k)] \tag{1}$$

where σ_{fwl} is the alternating stress necessary to initiate fretting fatigue cracks, σ_{wl} is the alternating stress necessary to initiate cracks in the absence of fretting, μ is the coefficient of friction, Po is the peak Hertzian normal stress, s is the relative slip, and k is a constant depending on the material and the surface condition.

Although Eq 1 was developed for a specific geometry, it is not unreasonable to assume that an equation of the same general form would apply to other geometries. Also, since compressive surface residual stresses reduce the apparent tensile stresses on the surface and delay crack initiation, the same mechanism might be expected to operate in the case of fretting fatigue. Hence, according to Eq 1, any treatment that causes an increased fatigue life will also increase the life under fretting fatigue.

Experimental Procedure

A 4130 steel was chosen because of the ease of controlling residual stresses by thermo-chemical as well as mechanical means. It is worth noting that the thermo-chemical treatments alter the surface hardness and the surface microstructure in addition to inducing surface residual stresses, whereas the mechanical treatments such as shot peening may be used to induce to compressive surface residual stresses without much change in surface hardness. Some of the relevant information on the steel used in the investigation are shown in Table 1.

Specimens were cut out of a sheet 0.254 cm thick with the longitudinal axis along the rolling direction. The dimensions of the specimen are shown in Fig. 1.

TABLE 1—*Chemical composition of the 4130 steel (weight percent).*

C	Mn	Si	Cr	Mo	P	S	Fe
0.3	0.44	0.30	0.94	0.23	0.008	0.018	balance

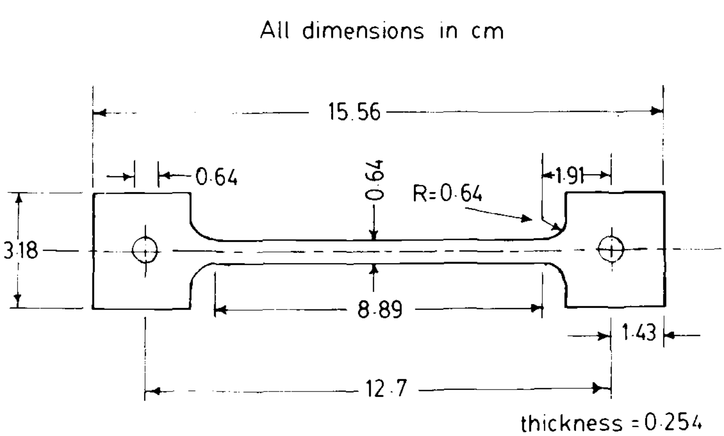

FIG. 1—*Dimensions of specimen.*

Carburization and decarburization were chosen as surface treatments for inducing surface residual stresses. The heat-treatment details are shown in Table 2. Specimens were polished with 600 grit paper after heat-treatment and cleaned with acetone in an ultrasonic cleaner before testing. It is worth mentioning that the X-ray strain measurements were made after the final polishing.

The testing was done in a 130-MN Instron dynamic loading machine. Tension-tension mode was used and the tests were conducted at 15 Hz with a maximum tensile stress of 400 MPa. The minimum tensile stress was maintained at a small positive value of 22 MPa. A sinusoidal waveform was used for the tests.

A drawing of the fretting fatigue apparatus is shown in Fig. 2. The apparatus was designed to allow independent control of the fretting variables while maintaining rigidity and ease of handling. Normal stress was applied by means of two martensitic (65 R_c) cylindrical pads of 4130 steel with a curved tip radius 1.58 cm to avoid edge effects. Two sets of spring washers were used to apply a precise normal load on the specimen. The whole assembly was then bolted rigidly to the stationary grip of the testing machine. Since the cyclic load was applied by the bottom grip, it is evident that the cyclic displacement increases as the distance from the top (stationary) grip increases. Thus, for a given normal load,

TABLE 2—*Heat treatment details for the 4130 steel.*[a]

Treatment	Austenitizing Temperature and Atmosphere	Post-Quench Treatment
Quench and temper	950°C in Ar, 20 min	temper at 450°C, 1 h
Decarburization	950°C in wet H_2, 30 min	temper at 450°C, 1 h
Carburization	950°C in H_2/CH_4 mixture, 2 h	temper at 450°C, 1 h

[a] Post-treatment yield strength ~1000 MPa.

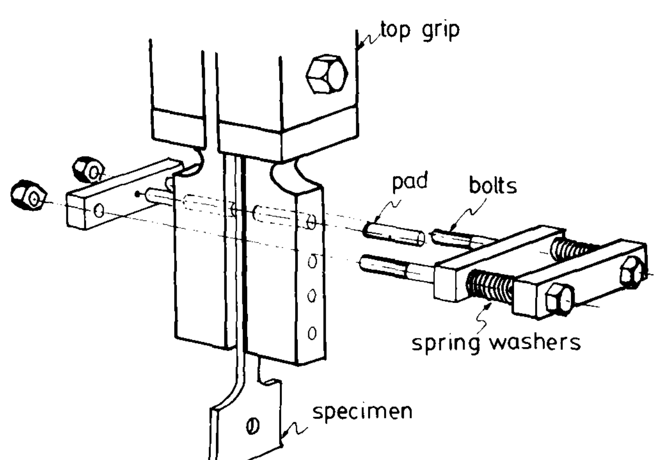

FIG. 2—*Fretting fatigue apparatus.*

slip can be controlled by changing the position of the pads on the gage length of the specimen. It was also observed that the slip amplitude decreased linearly as the normal load increased, and this fact was used to vary the slip amplitude in the experiments.

The slip amplitude was measured both by direct and indirect methods. The direct method used was as follows: A 2500 mesh transmission electron microscope grid (10 microns between lines) was attached to one of the nonfretting sides of the specimen, between the two fretting pads. A paper marker was attached to one of the fretting pads, so as to point at the grid. Once the experiment started, the relative motion between the marker and the grid was "frozen" by using a variable frequency strobe light, and the displacement was measured through a microscope by counting the number of lines on the grid the marker traversed. In the indirect method, strain gages were mounted on the posts of the fretting fatigue apparatus to measure the strain in the posts. The output of the strain gages was displayed on an oscilloscope screen. The peak-to-peak measurement of this strain waveform was found proportional to the actual slip amplitude, as measured by the direct method. Thus the slip amplitude could be measured indirectly to a reasonable degree of accuracy.

Results

Specimens were tested at various levels of slip amplitude until failure occurred by specimen separation, and their fatigue lives were plotted against the slip amplitude. The slip amplitude was observed to remain fairly constant throughout the experiment. However, to avoid discrepancies, slip amplitudes at regular intervals were noted and time-averaged to obtain a single value of the slip amplitude for the entire life of each specimen. Since the slip amplitude was found to vary inversely with the normal load, the plot in Fig. 3 also indirectly represents the variation of fretting fatigue life with normal load. The lines drawn through the points highlight the trends observed in the experiments.

It can be seen that although the maximum alternating stress was well below the fatigue limit, most of the specimens failed under 10^6 cycles.

The trend lines show a minimum in their fatigue lives. The minimum for the carburized specimens, which have the least compressive surface residual stress, occurs at a lower slip amplitude than the other two. In short, the minimum occurs at a higher level of slip amplitude with a higher compressive surface residual stress.

All three minima appear to occur around the same number of cycles-to-failure.

Figure 4 shows a schematic drawing of the cracks that were found on the fretted specimen and the one which propagated to failure. Cracks that led to failure in all the specimens were found to initiate below the fretting pads. Cracks, both parallel and transverse, were found under the fretting region but did not propagate to failure.

Oxide debris were observed at slip amplitudes of greater than 50 microns, regardless of surface treatment.

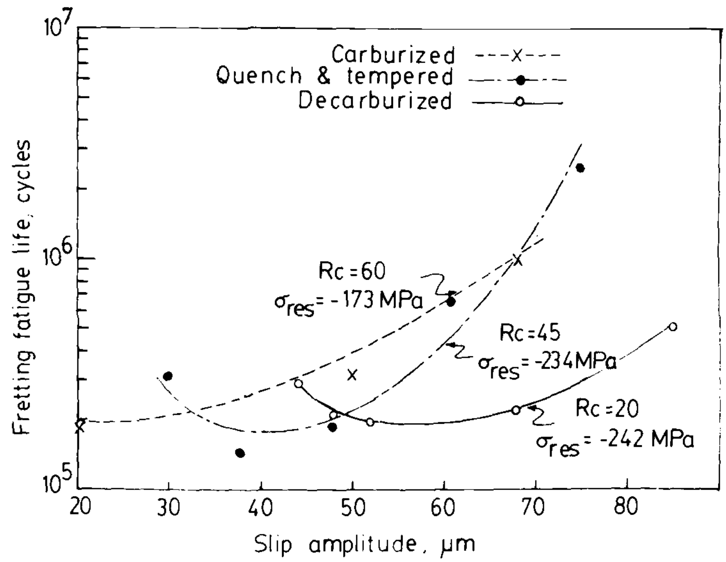

FIG. 3—*Fatigue lives plotted against slip amplitude.*

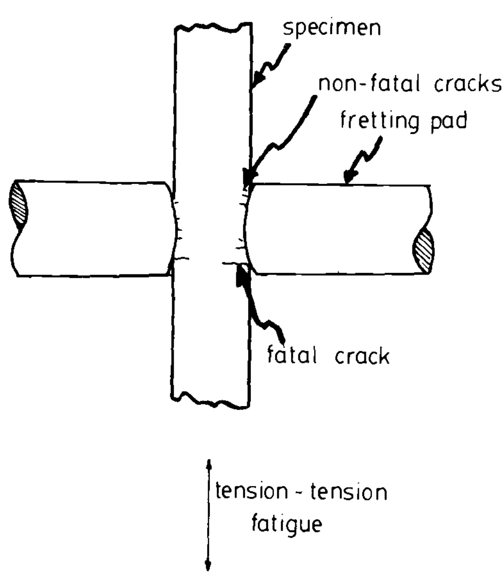

FIG. 4—*Schematic of cracks found on the fretted specimen and the crack which propagated to failure.*

Discussion

It is evident from the results shown that the presence of fretting in fatigue has a deleterious effect. Of all the measurable variables, the relative movement or the slip amplitude has the most pronounced effect on the fatigue life. The trend observed in the change in fatigue life with the slip amplitude can be attributed to two competing phenomena. According to Sproles and Duquette [*14*] the wear mechanism in fretting fatigue involves creation of subsurface cracks in the initial stages, parallel to the specimen surface. These cracks eventually connect with transverse cracks and surface delamination occurs. The delaminated debris are oxidized in a favorable environment. However, at very low slip amplitudes no debris were observed, leading the authors to conclude that the relative motion was too small to create enough subsurface cracks or transverse cracks. Thus it can be inferred that initiation of fatigue cracks under fretting increases with increasing slip amplitude and the fatigue life can be expected to diminish. By the same argument, at higher slip amplitudes, a large amount of wear and debris removal can be expected and the fatal cracks can be expected to be shortened or eliminated by wear. This crack elimination or stunting through material removal has a favorable effect on the fatigue life and increases as the slip amplitude increases. A hypothesis based on the above argument is proposed in the following paragraph.

Figure 5 schematically demonstrates the difference in trends between a carburized and a decarburized specimen. The figure has been divided into two regions. In Region I, the carburized specimens have shorter lives than the decarburized specimens and vice versa in Region II. In Region I, the surface of the carburized material provides easy subsurface crack initiation owing to its low plasticity and low energy absorption capacity. The wear rate at this point is not high enough, however, to remove the cracks. The lower compressive residual stresses allow the fatal crack to open up sooner than in the decarburized material. A decarburized material in the same region will deform plastically before any of the cracks can actually initiate. The depth of deformation, however, is higher owing to high ductility of the surface material. In Region II, the carburized material tends to delaminate, thus wearing away any candidate for a fatal crack. Subsurface cracks coalesce and join the transverse cracks to form platelets which eventually get removed from the fretting region. The lower compressive residual stress permits more transverse cracks to open up and aids in wearing away cracks that might eventually be fatal. In a decarburized material, at high slip amplitudes, the surface work hardens to a greater depth and although material removal is higher, the cracks are too deep to be worn out and failure results when one of the cracks reaches critical length.

The difference in hardness shown in Fig. 3 has not been taken into account in the discussion above. Further work needs to be done to separate the effects of residual surface stresses from the effects of surface hardness variation, and tests intended to isolate the effects are being prepared.

Readers may note that in Table 3 the surface residual stress for the carburized material is less compressive than for the other two, which is contrary to common belief. This can be explained, however, by the following argument: Surface residual stresses due to cooling are compressive in nature [*15*] regardless of the surface treatment. However, martensitic transformation results in a tensile stress on the surface, and the net effect of both cooling and martensitic transformation

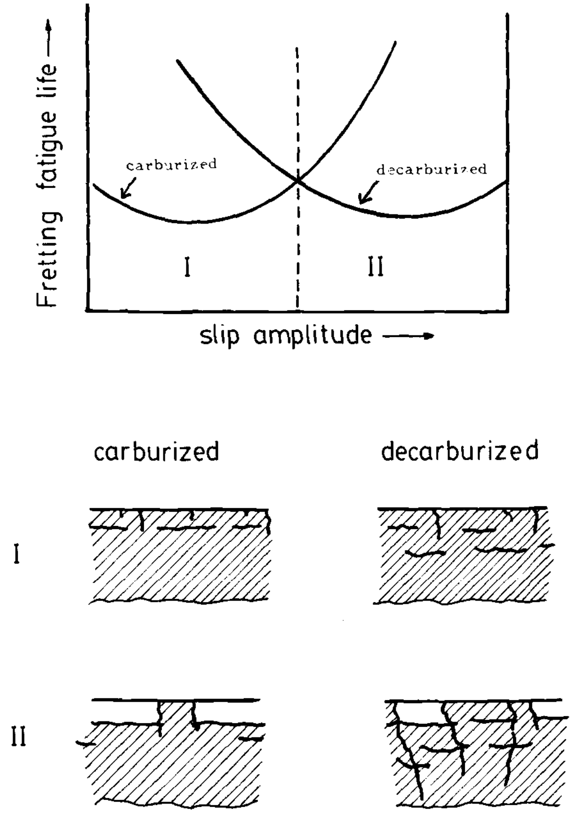

FIG. 5—*Difference in trends between a carburized and a decarburized specimen.*

TABLE 3—*Characterization of surface treatments.*

Treatment	Case Hardness, Rockwell C	Core Hardness, Rockwell C	Case Depth, microns	Surface Residual Stress, MPa
Quench and temper	45	45	...	−234
Decarburization	20	45	80	−242
Carburization	60	45	125	−173

results in less compressive net surface stress for the *carburized* specimen than for the other two conditions.

Readers may also note that the graph in Fig. 3 shows trend lines drawn from individual data points. Because of the high amount of scatter at this stress level, the trends need to be confirmed with further experimentation. Similar trends for a quench and tempered 4130 steel have been observed by Gaul [*3*] after considerable amount of experimentation. Work is currently under way to confirm the above trends with statistical analysis.

Conclusion

Effects of residual stresses on fretting fatigue are complex. Thermo-chemical treatments used in this study further complicate the problem by introducing surface hardness as an additional variable. The isolation of surface stress as a variable (for example, by using shot-peened specimens) will shed better light on the problem and a study is currently under way. Here an explanation of the observed phenomena using combined residual stress and surface plasticity arguments has been presented. One of the important observations was that all the treatments examined showed a lowering in fatigue lives in the presence of fretting, and an explanation is offered which takes into account the different surface treatments and stress states.

References

[1] Almen, J. O. and Black, P. H., *Residual Stress and Fatigue in Metals*, McGraw-Hill, New York, 1963.
[2] Gordelier, S. C. and Chivers, T. C., *Wear*, Vol. 56, 1979, pp. 177-190.
[3] Gaul, D., "Fretting Fatigue of a 4130 Steel," Master's thesis, Materials Engineering Department, Rensselaer Polytechnic Institute, Troy, N. Y., 1976.
[4] Waterhouse, R. B. and Saunders, D. A., *Wear*, Vol. 53, 1979, pp. 381-386.
[5] Endo, K. and Goto, H., *Wear*, Vol. 48, 1978, pp. 347-367.
[6] Waterhouse, R. B. in *Proceedings*, International Conference on Corrosion and Fatigue, University of Connecticut, Storrs, 1971, p. 608.
[7] Hoeppner, D. W. and Goss, G. L. in *Proceedings*, International Conference on Corrosion and Fatigue, University of Connecticut, Storrs, 1971, p. 617.
[8] Nishioka, Kunio and Hirakawa, Kenji, *Bulletin of JSME*, Vol. 12, No. 2, 1969, pp. 692-697.
[9] Nishioka, Kunio and Hirakawa, Kenji, *Bulletin of JSME*, Vol. 12, No. 50, 1969, pp. 180-187.
[10] Nishioka, Kunio and Hirakawa, Kenji, *Bulletin of JSME*, Vol. 12, No. 51, 1969, pp. 397-407.
[11] Goss, G. L. and Hoeppner, D. W., *Wear*, Vol. 24, 1974, pp. 77-95.
[12] Reeves, R. K. and Hoeppner, D. W., *Wear*, Vol. 48, 1978, pp. 87-92.
[13] Hurricks, P. L., *Wear*, Vol. 27, 1974, pp. 319-328.
[14] Sproles, E. S. and Duquette, D. J., *Wear*, Vol. 49, 1978, pp. 339-352.
[15] Waterhouse, R. B. and Taylor, D., *Wear*, Vol. 17, 1974, p. 141.

J. E. Hack[1] *and G. R. Leverant*[1]

Influence of Compressive Residual Stress on the Crack-Opening Behavior of Part-Through Fatigue Cracks

REFERENCE: Hack, J. E. and Leverant, G. R., "**Influence of Compressive Residual Stress on the Crack-Opening Behavior of Part-Through Fatigue Cracks,**" *Residual Stress Effects in Fatigue, ASTM STP 776,* American Society for Testing and Materials, 1982, pp. 204-223.

ABSTRACT: Direct observations of the surface crack opening displacement (SCOD) of surface and corner fatigue cracks were made on samples of Ti-6Al-4V under both cyclic and static loading conditions. The experiments were conducted *in situ* in a scanning electron microscope. Results show that surface residual stresses can significantly affect crack opening behavior—thus crack growth behavior—even when the crack has grown well beyond the zone of residual stress. An analytical approach was developed and used to predict SCOD for Mode I part-through cracks based on crack geometry and the boundary integral technique. Correlation with independent results for macrocracks and values for microcracks measured in this program are excellent for the case of zero residual stress. The analytical approach is currently being extended to more accurately account for the presence of residual stress gradients.

KEY WORDS: residual stress, fatigue, part-through crack, crack-opening displacement, stress intensity, titanium

Residual stresses are introduced in metal surfaces by many common mechanical and thermal processes. Their introduction can be intentional, as in the case of shot-peening, or inadvertent, as in the case of differential contraction between weld metal and base material during solidification and cooldown. The affected region caused by shot-peening is generally quite thin with a maximum depth of 125 to 250 μm, while welding-induced residual stresses can extend to significant depths in the material. Since fatigue crack initiation usually occurs at or near a free surface and initial growth rates are very low ($\approx 10^{-6}$ mm/cycle), fatigue cracks spend a significant portion of their lifetimes under the influence of the surface residual stress state. Although several studies [*1-3*] have been conducted to evaluate the effects of surface condition on fatigue behavior in both ferrous and nonferrous alloys, the fundamental relationship between surface condition and fatigue crack initiation and growth remains to be defined.[2]

[1] Senior Research Metallurgist and Assistant Director, respectively, Department of Materials Science, Southwest Research Institute, San Antonio, Tex. 78284.

[2] The italic numbers in brackets refer to the list of references appended to this paper.

Data by Leverant et al [*4*] and others [*5*] have shown that surface residual stresses do not significantly alter crack initiation behavior in titanium alloys but that crack propagation can be profoundly affected by their presence. This suggests that residual stresses act to modify crack-opening displacement (COD) behavior by changing the effective stress intensity range [COD $\simeq \Delta K_{\text{eff}}^2/(4E\sigma_y^2)$]. Since COD can be directly related to crack growth [*6,7*], the surface residual stress state could markedly affect propagation behavior without necessarily influencing the number of cycles required for Stage I crack initiation.

The present investigation was undertaken to quantify the effects of surface residual stresses on surface crack opening displacement (SCOD) behavior of part-through cracks. In the context of this paper, SCOD is defined as the crack opening at the central portion of the crack as opposed to the opening at the tip of the crack. Current results of experimental observations are presented which compare SCOD behavior in the absence and presence of a compressive residual stress field. In addition, the initial results of attempts to analytically model SCOD versus load behavior are presented.

Material and Experimental Procedures

The chemical analysis of the Ti-6Al-4V material used in this study is given in Table 1. The material was machined from a pancake forging that was forged at 1241 K in the alpha-beta phase field, annealed for 1 h at 1227 K, water quenched and then aged at 977 K for 2 h. This resulted in a microstructure of primary alpha embedded in a matrix of transformed beta with an average alpha particle size of approximately 14 μm. The microstructure is shown in Fig. 1.

A cantilever beam fatigue specimen was designed to ensure surface crack initiation. Figure 2 shows the tapered gage section which yields a constant stress over the entire gage length. It can be seen that slots are incorporated in the grip sections to allow for fixturing the specimen into the SEM loading stage after the initiation of cracks in a bending rig.

The SEM loading stage is shown in Fig. 3. The stage is capable of cyclically loading a sample in tension-tension at loads up to 3780 N at frequencies ranging from 0 to 5 Hz while maintaining the area of interest within the viewing screen of the SEM and in focus. Crack behavior can be videotaped and replayed for analysis of crack-opening displacement response. In addition, samples can be statically loaded in tension at loads up to 4895 N.

TABLE 1—*Range of analyzed compositions for Ti-6Al-4V material.*

Element	Weight Percent
Al	6.3 to 6.4
V	4.3
Fe	0.10 to 0.18
O	0.17 to 0.18
N	0.013 to 0.015
H	0.005 to 0.006

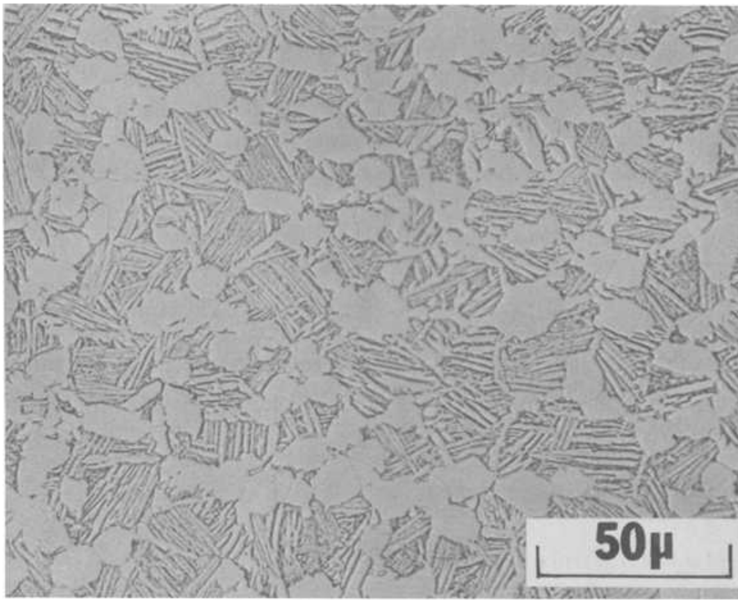

FIG. 1—*Microstructure of the Ti-6Al-4V material used in this study. The microstructure was developed by forging at 1241 K, annealing for 1 h at 1227 K, water quenching and aging for 2 h at 977 K.*

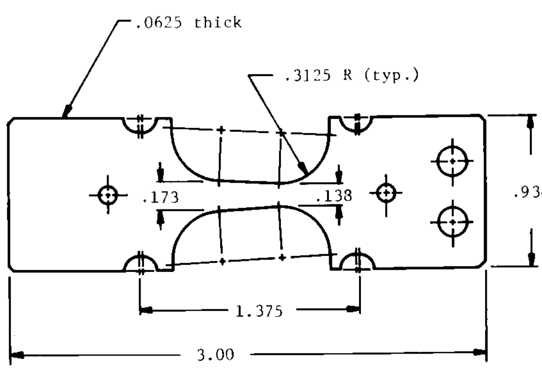

FIG. 2—*Cantilever beam fatigue specimen (dimensions in inches).*

Residual stress was introduced in the specimen surfaces by shot-peening at an intensity of 0.011 A. The samples were then lightly polished by standard metallographic techniques. A final electropolish and light etch (85 H_2O–10 HF–5 HNO_3) were then used to reveal the surface microstructure of the specimens. A total of less than 75 μm of material was removed by this process, which allowed the elimination of the surface roughness induced by the peening without

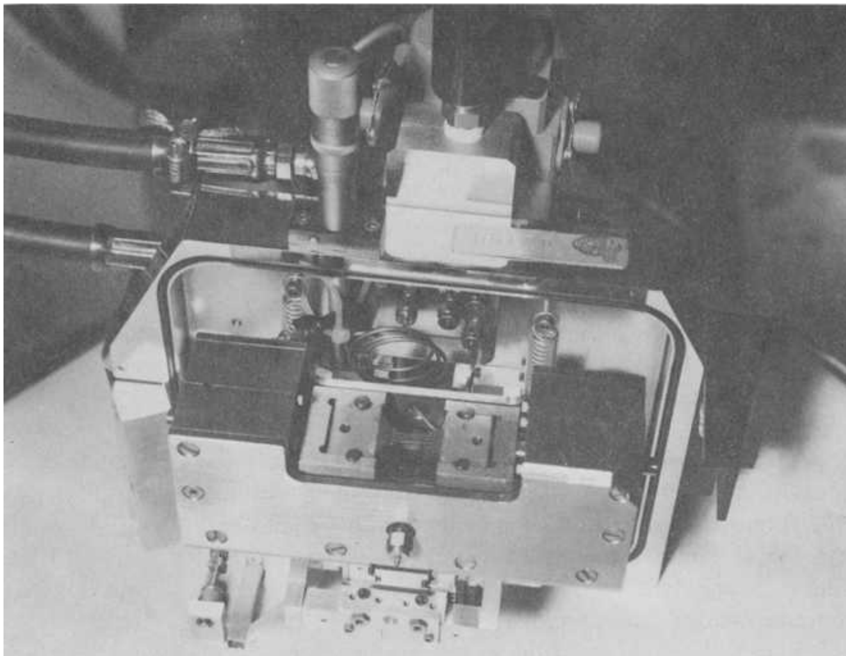

FIG. 3—In situ *loading stage for SEM.*

significant relaxation of the surface residual stress state. Material was removed equally from both sides of the specimen to prevent specimen bowing.

The two-exposure X-ray technique [*8*] was used to measure the surface residual stress on all the samples. A computer program was developed to perform a parabolic curve fit on the intensity versus 2θ data obtained from the X-ray measurements. Enough points were used to define the peaks of interest at $\psi = 0$ and 45 deg, and then the peak positions, peak shift, and residual stress were calculated. A comparison of measurements on a sample with a slight amount of compressive residual stress taken at different times under similar conditions showed that the technique was reproducible to within ± 0.015 deg for peak positions and ± 5.06 MPa in residual stress (Table 2). This is well within the predicted accuracy of the technique [*8*].

Cu K_α radiation was used for all measurements in conjunction with a 0.2-deg receiving slit and a 3-deg primary beam slit. The 3-deg primary beam slit was masked with a 127-μm-thick alpha brass foil to restrict the height of the beam impinging on the sample surface to within the thickness of the gage section. No Soller slits were used and the measurements for all peaks were performed with the detector at the focus position for each peak. A nickel filter was used to ensure a strong Cu K_α peak. The (213) plane of alpha titanium was chosen for the diffracting plane, which has a peak at approximately $2\theta = 141$ deg. The stress constant for these conditions is 5.51 MPa/0.01 deg $\Delta 2\theta$.

TABLE 2—*Comparison of independent X-ray stress measurements on a sample with a slightly compressive surface residual stress.*

Measured Quantity	1st Run		2nd Run	
	Cu $K_{\alpha 1}$ Peak	Cu $K_{\alpha 2}$ Peak	Cu $K_{\alpha 1}$ Peak	Cu $K_{\alpha 2}$ Peak
ψ = 0° peak position (°2θ)	141.96	142.77	141.94	142.75
ψ = 45° peak position (°2θ)	142.16	142.93	142.12	142.90
Residual stress, MPa	−108.33	−91.77	−98.24	−87.99

Residual stress profiles were obtained by alternating X-ray stress measurements and removal of material by electropolishing until the stress became negligible. Profiles were corrected for both beam penetration and stress relaxation due to layer removal.

All samples were precracked to bending within the strain limits of 0.3 ± 0.5 percent at 1 Hz. All testing was performed at room temperature. Prior to examination of the SCOD behavior, the samples were "shaken down" by several hundred cycles under load control in axial tension in the SEM loading stage. Load limits used for the shakedown were 100 to 560 MPa applied at 1 Hz. Both static and dynamic measurements of the SCOD versus load behavior were performed on the three specimens.

Dynamic observations of the cyclic loading were videotaped for real time measurement of SCOD. The samples were also step-loaded to allow for still photographs at each loading increment. SCOD versus load data obtained by these two techniques were compared for consistency. One sample, Ti-6, was stress-relieved subsequent to the initial SCOD measurements and the measurements were then repeated. This allowed a direct observation of the effect of residual stress on crack opening for a particular crack. After all testing was completed, crack geometries were obtained by incremental polishing through the specimen with measurements of crack length taken at each depth.

Results and Discussion

Experimental Procedure

The corrected compressive portions of the residual stress profiles for Samples Ti-2 and Ti-6 are presented in Fig. 4. The profile for Ti-6 was determined on a separate specimen which underwent similar treatment and had a comparable surface stress value in order to allow for stress relief of Ti-6 after the initial SCOD measurements. As can be seen from the data, the two specimens differ in maximum compressive residual stress by approximately 300 MPa, although both samples have a significant amount of compression at their surfaces.

The cracks used for observation in both Ti-2 and Ti-6 were corner cracks with profiles (Figs. 5*a* and 5*b*). It should be noted that the shaded portion represents the extent of the zone of compressive residual stress. The effects of balancing tensile stresses were ignored owing to the fact that they act over a much larger area and will not attain a significant magnitude. Thus most of the crack front in

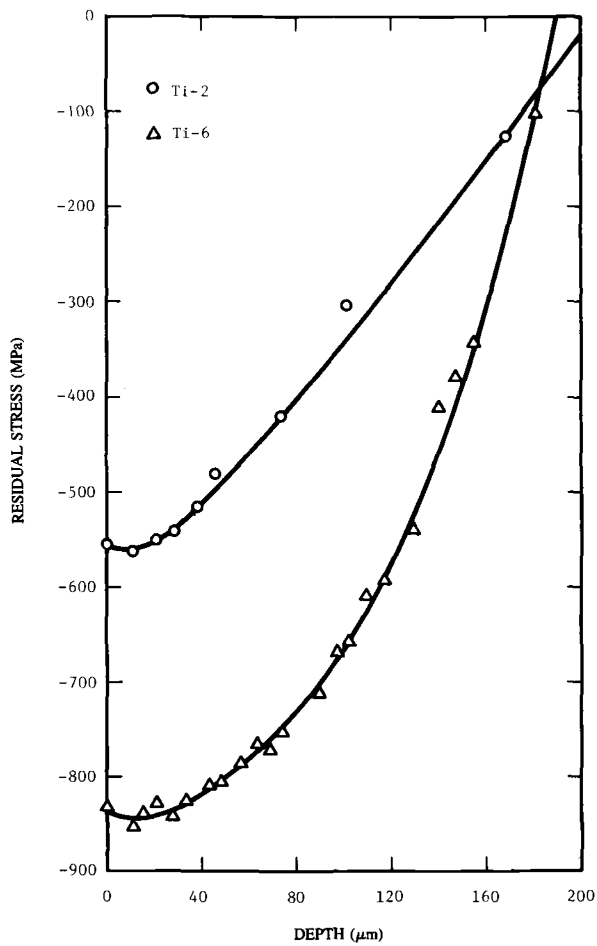

FIG. 4—*Residual stress profile in Samples Ti-2 and Ti-6 (corrected for beam penetration and layer removal).*

both specimens had grown well out of the zone of significant residual stress prior to the SCOD measurements.

At several loads, crack opening was recorded by micrographs and videotape at the center of the crack and at the crack tip on the polished face of each specimen. The measured SCOD values as a function of applied stress are presented for the center of the crack in Fig. 6. Since dynamic and static measurements were extremely close in value, average values were used to draw the graphs. Any effects of residual opening have been subtracted out. In both cases, the crack remains closed until the stress reaches approximately 300 MPa. After that point, the SCOD increases approximately linearly with stress. This is illustrated in the sequence of photographs from Sample Ti-6 (Figs. 7*a* to 7*c*).

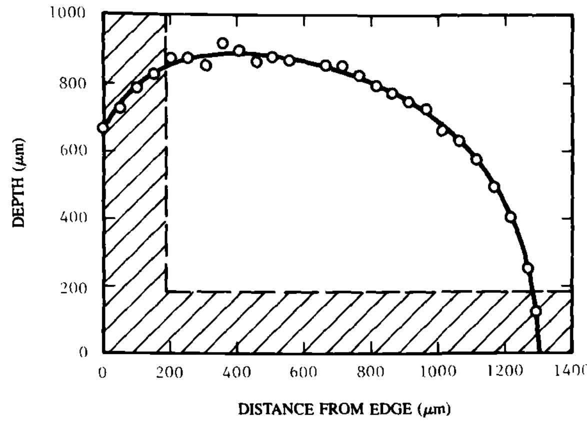

FIG. 5a —*Crack profiles in Sample Ti-2. Shaded area represents region of significant residual compressive stress.*

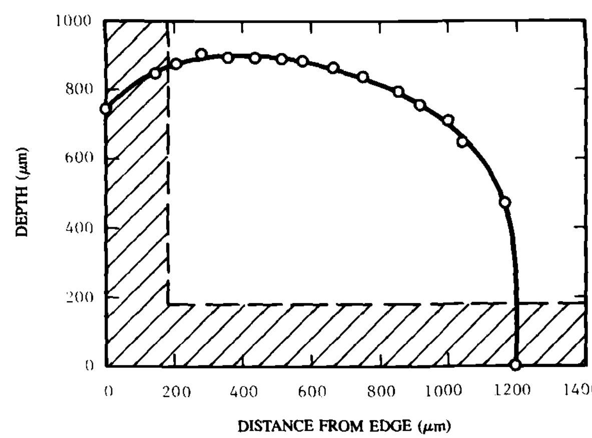

FIG. 5b —*Crack profiles in Sample Ti-6. Shaded area represents region of significant residual compressive stress.*

Figure 8 shows the crack tips away from the edge in both samples at maximum load. The tips have only just begun to open, even at loads approaching 560 MPa. This indicates that the residual compressive stress present at the surface of the two specimens is strongly influencing the surface crack tip opening displacement (CTOD) throughout the entire loading cycle.

Figure 9 presents a comparison of the SCOD versus load behavior of Sample Ti-6 before and after a stress relief heat treatment conducted at 540 °C for 1 h in vacuum. Subsequent to the stress relief treatment, crack opening begins shortly after the application of load. In addition, the opening increases linearly with stress as soon as the crack begins to open.

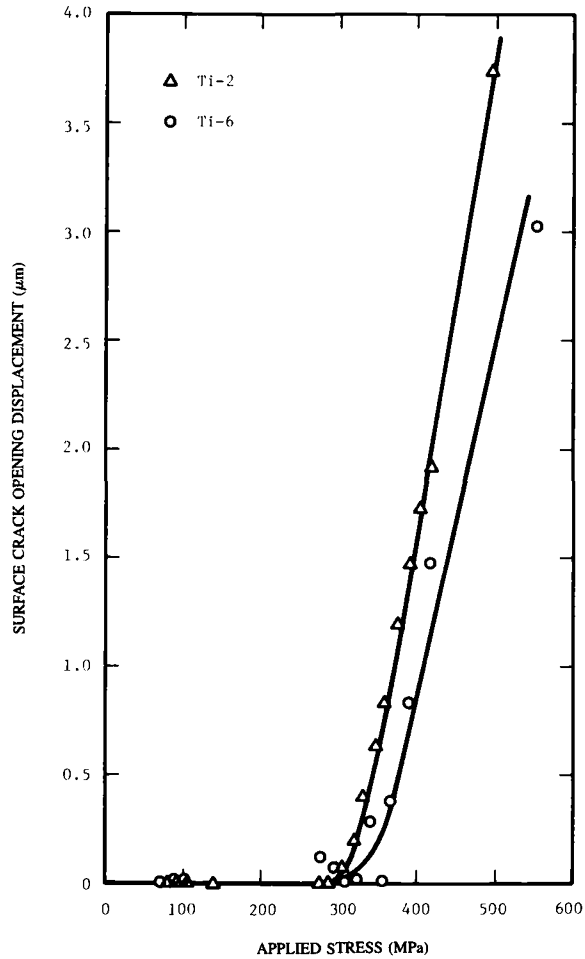

FIG. 6—*SCOD behavior of Samples Ti-2 and Ti-6 with compressive surface stresses.*

Above a stress of approximately 350 MPa, the SCOD versus stress curve for the stress-relieved material becomes nonlinear. This behavior indicates that the crack tip has plastically yawed open. Such opening is apparent in the sequence of photographs in Fig. 10, which contrast the surface CTOD in Sample Ti-6 at two loads before and after the stress relief treatment. The photographs show that while the crack tip in Ti-6 in the shot-peened condition remains closed (or nearly so) throughout the entire loading sequence, the crack tip in the stress-relieved condition begins to open with the onset of nonlinearity in the SCOD versus load curve (Fig. 9). In addition, while no growth occurred during the experiments performed on the two samples in the shot-peened condition, Fig. 10 shows that the crack in Ti-6 did propagate across several grains ($\approx$40 μm) during the course

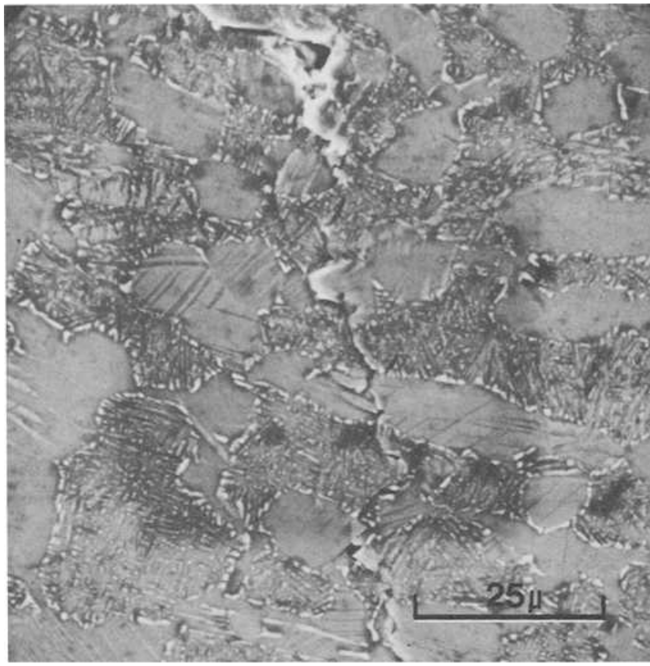

FIG. 7a—*Micrograph of SCOD versus load in Sample Ti-6 with compressive surface residual stresses (103 MPa).*

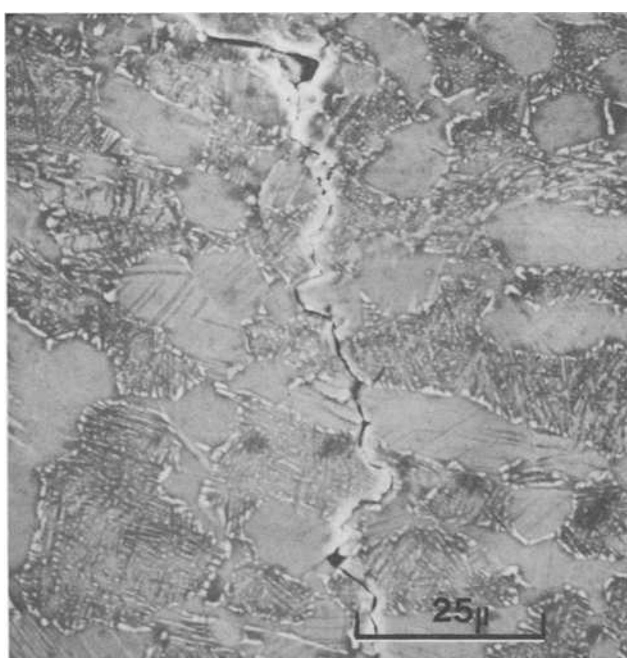

FIG. 7b—*Micrograph of SCOD versus load in Sample Ti-6 with compressive surface residual stresses (354 MPa).*

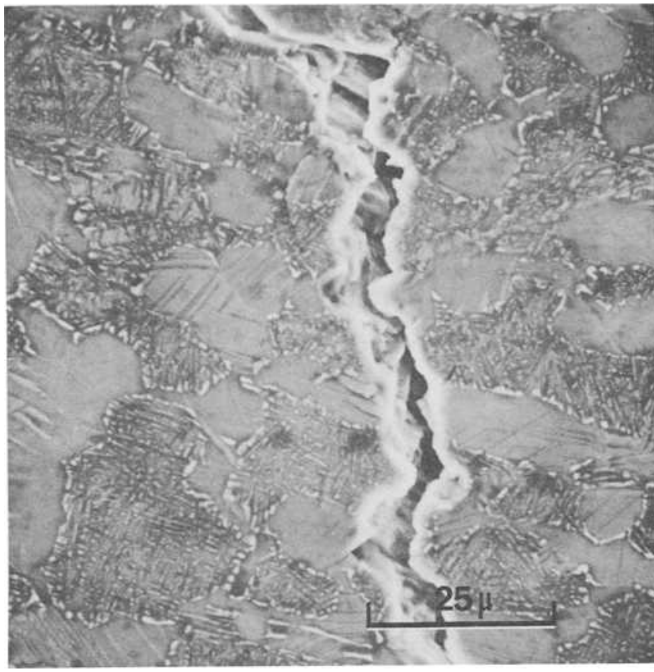

FIG. 7c —*Micrograph of SCOD versus load in Sample Ti-6 with compressive surface residual stresses (552 MPa).*

of the experiment after the stress relief treatment. This crack growth can actually be observed in the videotaped sequences. These results emphasize the strong influence that the surface stresses have on surface crack opening, and thus crack growth, behavior. Even after the majority of the crack has moved out of the residual stress field, the surface opening is still reduced substantially by the compressive surface stress state and, consequently, surface crack growth is reduced. This observation has strong implications with respect to approaches being proposed for component removal from service (for example, retirement-for-cause) based on undestructive inspection and fracture mechanics.

Analytical Prediction of SCOD Behavior

Concurrent with the experimental observations described in the previous section, the development of an analytical approach was initiated to allow for the prediction of SCOD behavior under the influence of residual stress. The approach chosen is based on the stress intensity at the surface crack tip. A general expression for the SCOD of an elliptical crack was derived from the work of Irwin [9], which gives

$$\mathrm{SCOD}(r) = 2\eta = 2\eta_o \frac{\sqrt{r}}{ac}[2ac(a^2 \cos^2\phi + c^2 \sin^2\phi)^{1/2} - r(a^2 \cos^2\phi + c^2 \sin^2\phi)]^{1/2}$$

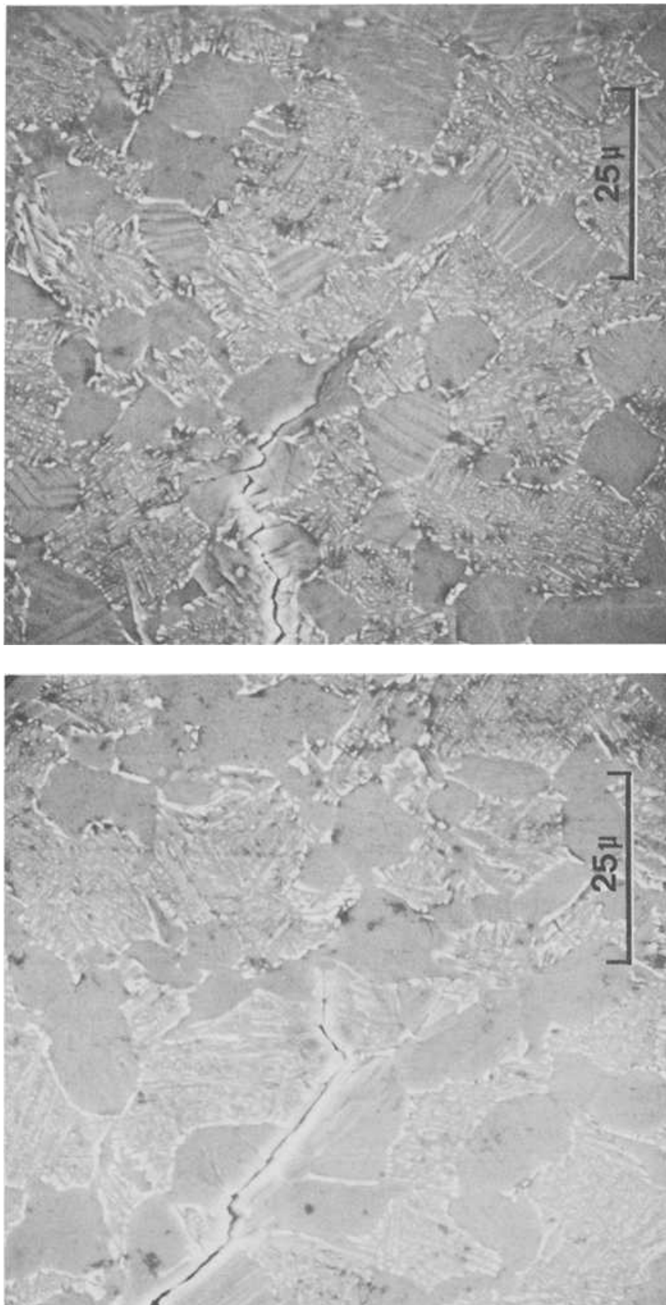

FIG. 8—*Crack tips in Ti-6Al-4V samples under the influence of high residual and applied loads. (left) Crack tip in Ti-2 at 494 MPa. (right) Crack tip in Ti-6 at 559 MPa.*

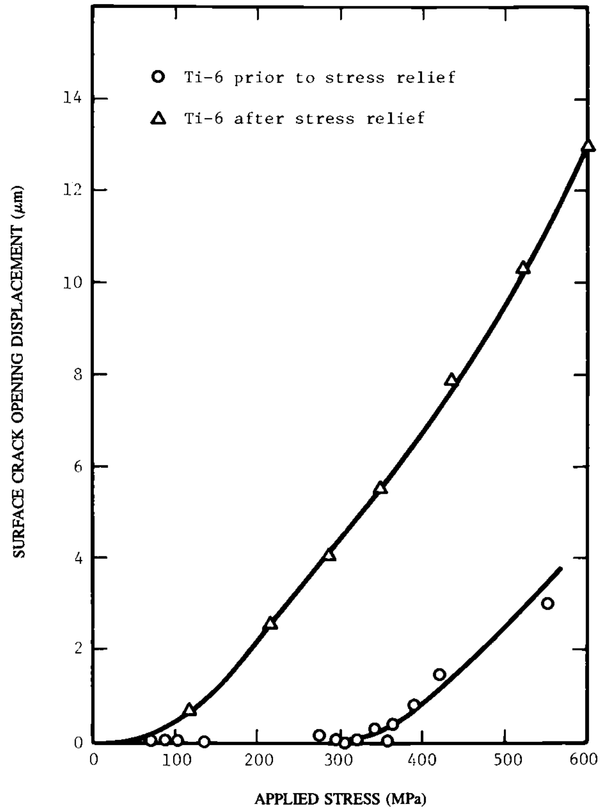

FIG. 9—*Comparison of SCOD behavior in Ti-6 prior to and after stress relief.*

where η is the half crack opening at the point of interest, and r, η_o, a, c, and ϕ are as defined in Fig. 11 and 12.[3] Thus, at $\phi = 0$ and $r = c$, it is found that the SCOD of a surface crack is simply

$$\text{SCOD} = 2\eta = 2\eta_o$$

For the case of the corner cracks studied,[4] where $\phi = 0$ and $r = c/2$,

$$\text{SCOD} = 2\eta = \sqrt{3}\eta_o$$

In these expressions

$$\eta_o = \frac{2(1 - \nu^2)\sigma a\left[1 + 0.12\left(1 - \frac{a}{c}\right)\right]}{E\Phi}$$

[3] It should be noted that ϕ, as defined in Fig. 12, is different from the ϕ defined by Irwin [9]. However, both definitions yield identical solutions in the small r approximation.

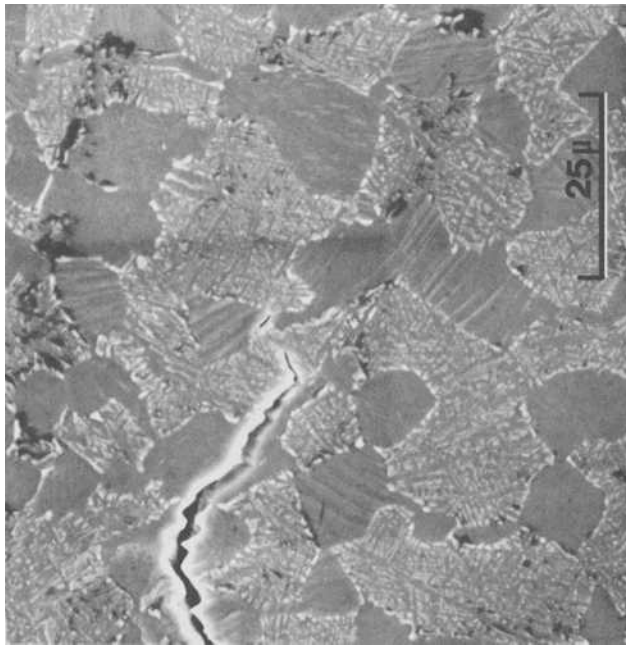
25μ

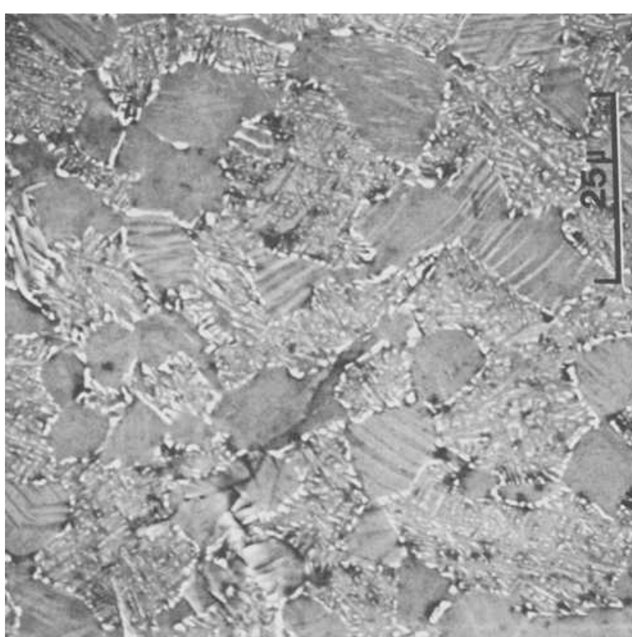
25μ

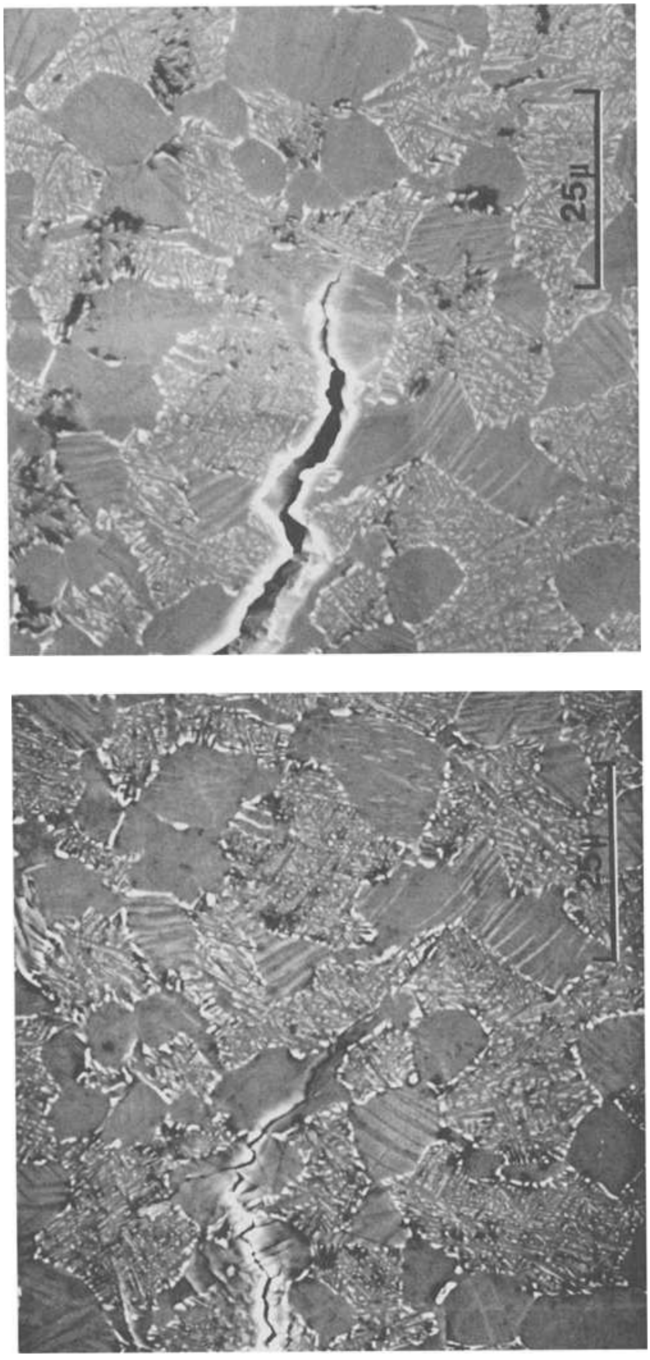

FIG. 10—*Comparison of crack-tip opening in Sample Ti-6 prior to and after stress relief.* (upper left) *Prior to stress relief at 408 MPa.* (upper right) *After stress relief at 408 MPa.* (above left) *Prior to stress relief at 559 MPa.* (above right) *After stress relief at 559 MPa.*

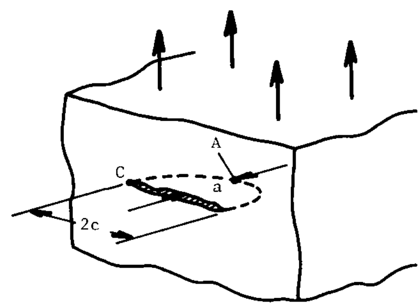

FIG. 11—*Crack geometry used in analytical approach.*

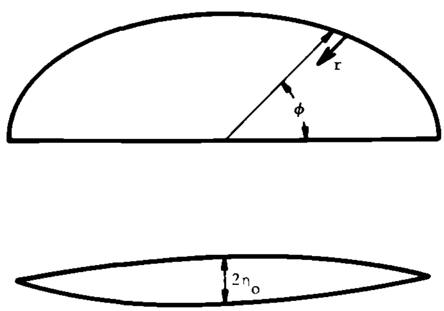

FIG. 12—*Definition of variables used in analytical approach.*

where

ν = Poisson's ratio of the material,
σ = applied stress,
E = Young's modulus of the material, and
Φ = elliptic integral of the second kind:

$$\left(\int_0^{\pi/2}\left[1 - \left(1 - \left[\frac{a}{c}\right]^2\right)\sin^2\phi\right]^{1/2} d\phi\right)$$

Recognizing that the stress intensity at the surface, K_s, is given by[4]

$$K_s = \frac{\sigma}{\Phi}\sqrt{\pi a}\sqrt{\frac{a}{c}}\left[1 + 0.12\left(1 - \frac{a}{c}\right)\right]$$

then

$$\eta_o = \frac{2(1 - \nu^2)\sqrt{c}K_s}{\sqrt{\pi}E}$$

[4] Measurements of SCOD for the corner cracks were taken at the midpoint between the specimen edge and the surface crack tip.

It was desired to maintain complete generality in the analytical approach so that the contributions of a residual stress field could be incorporated for both corner and surface cracks. Consistency among these various cases was attained by obtaining values of K_s from a computer program known as BIGIF [11]. This program calculates values for K_s by the boundary integral technique [12] and is capable of treating the geometry and stress states studied in this program.

As can be seen from the equations, SCOD behavior for a given material is dependent on the surface crack tip stress intensity and the surface crack length. Predictions based on these expressions were compared with independent data on macro surface cracks in Ti-6Al-4V of equivalent microstructure and yield strength gathered by Collipriest [13]. In his work, Collipriest initiated surface cracks in samples and measured SCOD versus load until the behavior became extremely nonlinear (that is, gross plasticity and extension of the crack). Then he fatigued the sample for a short time to mark the end of the first crack extension and repeated his measurements. Figure 13 shows a comparison of SCOD as calculated in the present study to that measured by Collipriest on a 10,000-μm-long surface crack. As can be seen from the figure, the agreement is excellent up to the point where the measured behavior becomes nonlinear.

The applicability of this analytical approach to micro surface cracks was subsequently investigated. Figure 14 shows 50- and 32-μm-long surface cracks in a sample which has been surface ground parallel to the stress axis. The a/c ratios of the 50- and 32-μm cracks were 0.45 and 0.70, respectively. Little or no surface residual stress was present in this specimen. Figure 15 shows a comparison of measured versus predicted behavior for these two cracks. The results of the calculations again give excellent correlation with the experimental observations. It should be mentioned that one would not normally expect linear elastic fracture mechanics to apply when the crack length and depth are on the order of the grain size of the material. It is believed that the extensive degree of cold work in the ground surface causes the near surface material, in which the crack is wholly contained, to act as a continuum. Indeed, experimental results obtained on 7- to 18-μm-long surface cracks in an electropolished surface of Ti-6Al-4V do not agree with predictions based on the present analytical approach [14].

This analytical approach was also evaluated for the experimental data on the two corner cracks that were under the influence of a large compressive residual stress. Comparisons of SCOD at maximum load are given in Table 3. The previously determined residual stress profiles were accounted for where applicable. As can be seen from the data, the correlation between predicted values and experimental values is excellent for the stress relieved case. When a compressive residual stress field is present, the predicted openings are larger than those actually observed.

The source of the latter discrepancy can either be a result of an overestimation of K_s in BIGIF or the failure of the opening expression when a stress gradient is present. In an attempt to resolve this anomaly, another computer program based on the boundary integral technique, 3-D BINTEQ [15], is currently

[5] Another free surface correction must be made for corner cracks, so the term in brackets must be made to read $[1 + 0.2\,(1 - a/c)]$ in this case [10].

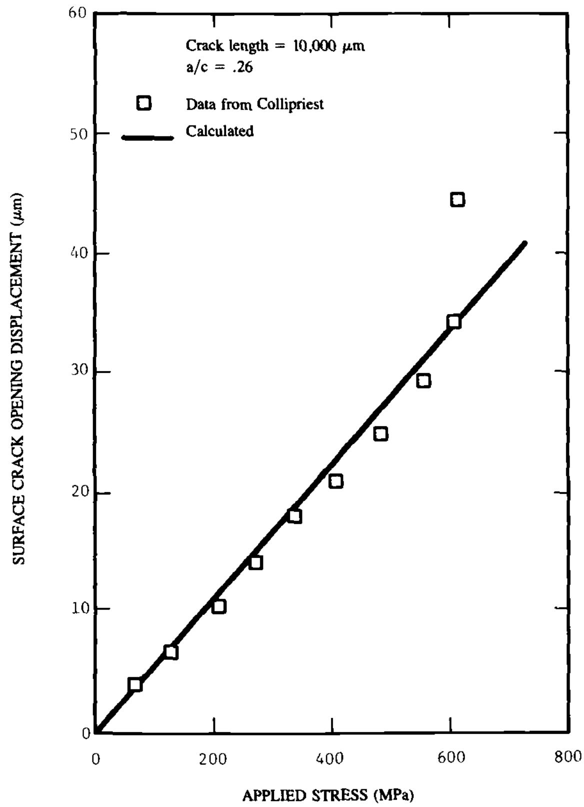

FIG. 13—*Comparison of calculated SCOD behavior and experimental data by Collipriest* [13].

being used to calculate SCOD directly. These results will then be compared with those obtained through the combination of BIGIF and the derived crack opening expression.

Conclusions

1. It has been demonstrated that surface residual stresses exert a significant influence on the surface crack-opening displacement (and, therefore, effective stress intensity) of part-through fatigue cracks in Ti-6Al-4V, even if the majority of the crack front resides outside the zone of residual stress.

2. An analytical approach has been developed for predicting the surface crack opening displacement (SCOD) of part-through Mode I cracks. It has been applied to macrocracks as well as microcracks as small as 20 to 25 μm in depth.

3. In the absence of residual stress, agreement between calculated and measured SCOD is excellent. In the presence of a high level of residual surface compressive stress, the predicted SCOD is somewhat larger than the measured value.

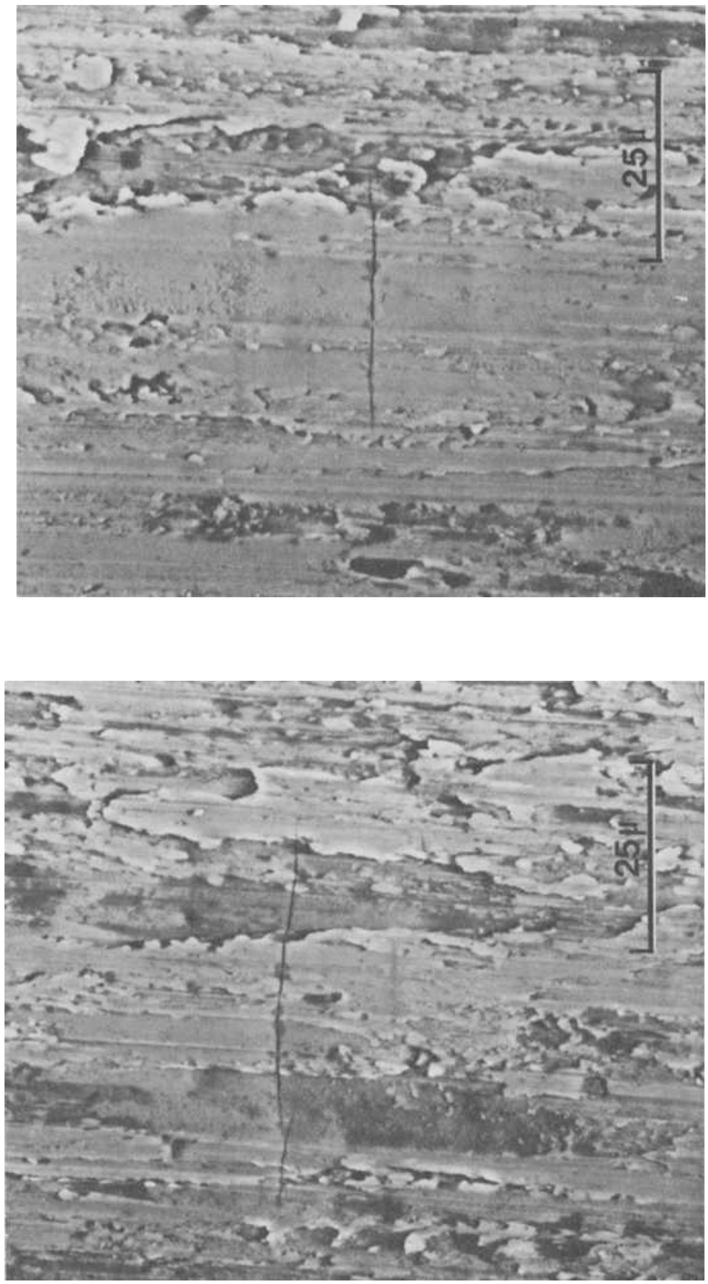

FIG. 14—*Mode I cracks in ground specimen.* (left) *50-μm crack.* (right) *32-μm crack.*

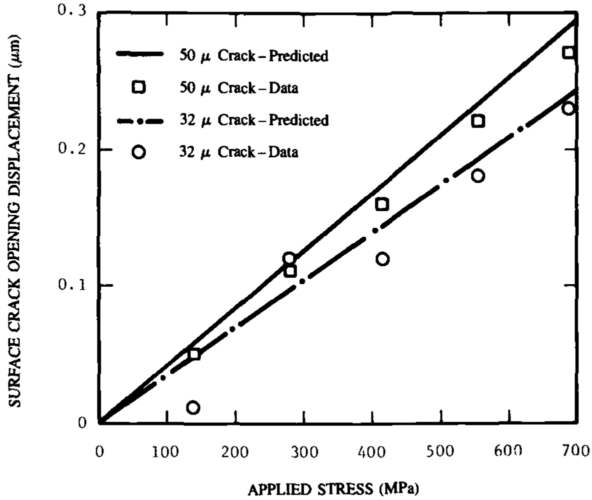

FIG. 15—*Comparison of predicted and measured SCOD behavior of microcracks in ground specimen.*

TABLE 3—*Correlation of measured and predicted Mode I corner crack SCOD at maximum load with a compressive residual stress state.*

Sample	Surface Residual Stress Value, MPa	Maximum Applied Stress, MPa	K_s, MPa$\sqrt{m}$	Predicted SCOD, μm	Measured SCOD, μm
Ti-2	−560	500	10.1	6.0	3.8
Ti-6	−860	560	9.6	5.5	3.1
Ti-6[a]	≈0	560	21.5	11.2	11.3

[a]Stress relieved after initial experiment.

4. The closure of surface cracks due to high compressive stresses may have a significant impact on the ability to detect these cracks by conventional nondestructive inspection methods. This could have significant implications with respect to run/retire decisions for critical components.

Acknowledgments

The authors are grateful for the support of the Office of Naval Research under Contract N00014-78-C-0674.

References

[1] "Surface Integrity of Machined Structural Components," AFML-TR-70-11, March 1970.
[2] Prevey, P. S. and Koster, W. P. in *Fatigue at Elevated Temperatures, ASTM STP 520*, American Society for Testing and Materials, 1973, pp. 522-531.
[3] Williams, D. N. and Wood, R. A., "Effects of Surface Condition on the Mechanical Properties of Titanium and Its Alloys," MCIC-71-01, Aug. 1971.

[4] Leverant, G. R., Langer, B. S., Yuen, A., and Hopkins, S. W., *Metallurgical Transactions*, Vol. 10A, 1979, p. 251.
[5] Burck, L. H., Sullivan, C. P., and Wells, C. H., *Metallurgical Transactions*, Vol. 1, 1970, p. 1595.
[6] McEvily, A. J. and Johnston, T. L., *International Journal of Fracture Mechanics*, Vol. 3, 1967, p. 45.
[7] Garrett, G. G. and Knott, J. F., *Metallurgical Transactions*, Vol. 7A, 1976, p. 884.
[8] Cullity, B. D., *Elements of X-ray Diffraction*, Addison-Wesley, Reading, Mass., 1956, p. 431.
[9] Irwin, G. R., *Journal of Applied Mechanics*, Dec. 1962, p. 651.
[10] Broek, D., *Elementary Engineering Fracture Mechanics*, Noordhoff International Publishing, The Netherlands, 1974, p. 86.
[11] Besuner, P. M., Peter, D. C., and Cipolla, R. C., "BIGIF Fracture Mechanics Code for Structures," Key Phase Report, NP-838 Research Project 700-1, EPRI, July 1978.
[12] Cruse, T. A. in *The Surface Crack: Physical Problems and Computational Solutions*, ASME, 1972, p. 153.
[13] Collipriest, J. E., in *The Surface Crack: Physical Problems and Computational Solutions*, ASME, 1972, p. 43.
[14] Hack, J. E. and Leverant, G. R., "Fatigue Microcrack Behavior under the Influence of Surface Residual Stresses," Interim Report on Contract N00014-78-C-0674, Southwest Research Institute, San Antonio, Tex., 1 Oct. 1980.
[15] Cruse, T. A., "An Improved Boundary-Integral Equation Method for Three Dimensional Elastic Stress Analysis," Interim Report on Contract DA-ARO-D-31-124-72-G3, Carnegie-Mellon University, Pittsburgh, Aug. 1973.

Chongmin Kim,[1] *D. E. Diesburg,*[2] *and G. T. Eldis*[2]

Effect of Residual Stress on Fatigue Fracture of Case-Hardened Steels — An Analytical Model

REFERENCE: Kim, Chongmin, Diesburg, D. E., and Eldis, G. T., **"Effect of Residual Stress on Fatigue Fracture of Case-Hardened Steels — An Analytical Model,"** *Residual Stress Effects in Fatigue, ASTM STP 776,* American Society for Testing and Materials, 1982, pp. 224-234.

ABSTRACT: The influence of residual stress at and near the surface on fatigue life was modeled by utilizing linear elastic fracture mechanics to quantify the stress intensity change due to the residual stress. The initiation and the propagation stages of the fatigue cracking process were distinguished using the concept of the threshold stress intensity amplitude; with a constant load amplitude, the propagation stage commences from the crack length at which the maximum fatigue stress intensity is equal to the threshold value. The influence of residual stress is to increase or decrease the crack length which corresponds to the initiation stage, thereby controlling the fatigue crack initiation life.

KEY WORDS: fatigue, residual stress, crack initiation, threshold fatigue stress intensity, linear elastic fracture mechanics

Fatigue accounts for a significant portion of the failures of case-hardened components. It is known that in bend testing of unnotched steel specimens near the fatigue limit, most of the total fatigue life corresponds to the crack initiation stage [*1*].[3] Residual stress, ever present in a hardened case, has a marked influence on fatigue limit; the greater the compressive stress at and near the case-hardened surface, the higher the fatigue limit [*2*]. Therefore a prerequisite for compositions and heat treatments for case-hardened steels is that they produce compressive residual stress in the case.

Application of fracture mechanics in understanding the influence of residual stress on fatigue fracture has been limited to relatively large initial crack lengths and simple linear stress profiles [*3,4*]. Little effort has been devoted to analyzing the influence of residual stress on crack initiation. In the present paper, a fracture mechanics approach is presented by which the influence of residual stress on stress intensity is quantified. The importance of residual stress in affecting the crack initiation life is demonstrated, and, in the process, a definition of the term

[1] Senior Research Engineer, Metallurgy Department, General Motors Research Laboratories, Warren, Mich. 48090; formerly at Climax Molybdenum Company of Michigan, a subsidiary of AMAX Inc., Ann Arbor, Mich. 48105.

[2] Research Supervisor and Manager of Research, respectively, Climax Molybdenum Company of Michigan, a subsidiary of AMAX Inc., Ann Arbor, Mich. 48105.

[3] The italic numbers in brackets refer to the list of references appended to this paper.

"crack initiation" is obtained by utilizing the concept of threshold stress intensity amplitude.

Influence of Residual Stress on Stress Intensity

Extension by fatigue of a crack having a finite length is determined by stress intensity amplitude. Therefore the influence of residual stress on fatigue can be quantified by analyzing the change in stress intensity due to residual stress. In this paper, the residual stress is assumed to act perpendicular to the surfaces formed by a crack, as was done previously [*3,4*]. It is further assumed that only the residual stress acting across the crack face can influence the stress intensity; residual stress present in the unbroken ligament is assumed to have no effect on the stress intensity. For an infinite body, it has been shown that a stress acting in the ligament contributes zero stress intensity at the crack tip [*5*]. Similarly, for a semi-infinite solid with a point force acting on the back face in the ligament side, the resulting stress intensity is zero [*5*].

The stress intensity caused by a residual stress field may be predicted by utilizing either the weight function given by Bückner [*6*] or the stress intensity formula for a point force acting on crack face [*5*]. The latter method was chosen in the present study; a residual stress field is represented as a contiguous group of point forces acting normal on the crack face. The stress intensity caused by a force acting on a point in the crack face of a single-edge-notched specimen is given [*5*] as

$$K_I = \frac{2P}{\sqrt{\pi a}} F\left(\frac{c}{a}, \frac{a}{W}\right) \tag{1}$$

where

$$F\left(\frac{c}{a}, \frac{a}{W}\right) = \frac{3.52\left(1 - \frac{c}{a}\right)}{\left(1 - \frac{a}{W}\right)^{3/2}} - \frac{4.35 - 5.28\frac{c}{a}}{\left(1 - \frac{a}{W}\right)^{1/2}} + \left\{ \frac{1.30 - 0.30\left(\frac{c}{a}\right)^{3/2}}{\sqrt{1 - \left(\frac{c}{a}\right)^2}} + 0.83 - 1.76\frac{c}{a} \right\}\left\{1 - \left(1 - \frac{c}{a}\right)\frac{a}{W}\right\}$$

where P, W, a, and c denote load, specimen width (thickness), crack length, and distance from the specimen face on the crack side to the position of the point force, respectively (Fig. 1). The load P has a dimension of force per unit length (in the breadth direction). The equation may be used to calculate stress intensity changes due to residual stresses of any profile by replacing P with $\sigma_r(c) \times dc$ and integrating over the length of the crack, where $\sigma_r(c)$ signifies the residual stress field expressed as a function of c. Therefore

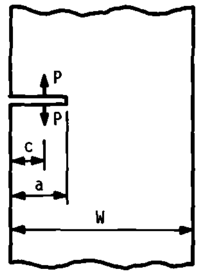

$$K_I = \frac{2P}{\sqrt{\pi a}} F\left(\frac{c}{a}, \frac{a}{W}\right)$$

$$F\left(\frac{c}{a}, \frac{a}{W}\right) = \frac{3.52\left(1-\frac{c}{a}\right)}{\left(1-\frac{a}{W}\right)^{\frac{3}{2}}} - \frac{4.35 - 5.28\frac{c}{a}}{\left(1-\frac{a}{W}\right)^{\frac{1}{2}}}$$

$$+ \left\{\frac{1.30 - 0.30\left(\frac{c}{a}\right)^{\frac{3}{2}}}{\sqrt{1-\left(\frac{c}{a}\right)^2}} + 0.83 - 1.76\frac{c}{a}\right\} \left\{1 - \left(1 - \frac{c}{a}\right)\frac{a}{W}\right\}$$

FIG. 1—*Stress intensity formula for a single-edge-notched specimen with a point force acting on the crack face* [5].

$$K_I = \int_0^a \frac{2\sigma_r\, dc}{\sqrt{\pi a}} F\left(\frac{c}{a}, \frac{a}{W}\right) = \int_0^1 2\sqrt{\frac{a}{\pi}}\,\sigma_r F\left(\frac{c}{a}, \frac{a}{W}\right) d\left(\frac{c}{a}\right) \tag{2}$$

Since Eq 1 contains a term which has $1 - (c/a)^2$ in the denominator, the value of the function is infinite if $c = a$. However, this singularity can be eliminated, and the integral in Eq 2 converges, by expressing c/a as sine or cosine of a new variable. In most cases the integration is best carried out numerically with a computer.

In the following sections, the foregoing computing procedure was applied to analyze the influence of surface residual stress on crack initiation and the influence on fatigue crack propagation of the position of the residual stress peak along the face of the crack.

Crack Initiation and Surface Residual Stress

Application of fracture mechanics to fatigue fracture has been limited only to the propagation of a pre-existing crack, and efforts made in analyzing the crack initiation stage have been relatively meager. Crack initiation is usually reserved for the mechanism by which a crack forms to some finite length, but it could also be defined as that portion of the fatigue process not involved in crack propagation. A crack of a finite length may be present, but if the fatigue stress intensity amplitude is less than the threshold stress intensity amplitude, defined as the value below which no crack propagation occurs, then the system may be considered to be in the crack initiation stage. In this study, crack initiation is defined as that portion of the fatigue process where the stress intensity amplitude is less than the threshold stress intensity amplitude.

Consider a fatigue crack propagation process that obeys Paris's relationship, $da/dN = A(\Delta K_I)^n$. Furthermore, limit the consideration to bend testing of steels for which ΔK_I, the stress intensity amplitude, may be replaced with K_{max}. Then, the influence of compressive residual stress is to decrease K_{max} by the amount predicted from Eq 2. It is known that a threshold value of stress intensity amplitude, ΔK_{th} or K_{th}, exists, below which a crack cannot propagate. Threshold values for steels are about 3 to 8 MPa$\sqrt{\text{m}}$ (3 to 7 ksi$\sqrt{\text{in.}}$) [7]. In the present study, ΔK_{th} will be assumed to have a value of 4.4 MPa$\sqrt{\text{m}}$ (4.0 ksi$\sqrt{\text{in.}}$).

The residual stress profile used to study the influence of surface stress on crack initiation is shown in the upper left corner of Fig. 2; the maximum stress is at the very surface and decreases linearly to zero at a depth of 0.25 mm (0.010 in.). The specimen was assigned to have a 7.0 mm (0.276 in.) thickness, a breadth of 20 mm (0.787 in.), a span-to-thickness ratio of 8, and to be tested in three-point bending in an unnotched condition. Two values were assigned for the surface residual stress, −138 and −276 MPa (−20 and −40 ksi). The stress intensity due to residual stress is plotted as a function of crack length in Fig. 2. Also shown is the maximum stress intensity for various crack lengths caused by an externally applied fatigue load with a constant load-amplitude of 454 kgf (1000 lbf).

The stress intensity values for both the externally applied load and the compressive residual stress are plotted as positive values. Therefore the effective or net stress intensity is calculated by subtracting the residual stress contribution from the stress intensity due to the external loading. Unless the applied stress intensity overcomes the stress intensity due to the compressive residual stress, no crack propagation is expected to occur. In fact, the crack will not propagate until the net stress intensity exceeds the threshold stress intensity.

It is observed in Fig. 2 that only at crack lengths greater than about 0.089 mm (0.0035 in.) does the net stress intensity exceed the threshold stress intensity (ΔK_{th}) of 4.4 MPa$\sqrt{\text{m}}$ (4 ksi$\sqrt{\text{in.}}$) when the surface compressive residual stress is 138 MPa (20 ksi). If the surface residual stress is −276 MPa (−40 ksi), this critical crack length is 0.178 mm (0.007 in.). Without any residual stress, the crack length only has to reach 0.036 mm (0.0014 in.) for the stress intensity to exceed ΔK_{th}. The actual mechanism by which flaws or cracks reach these specific critical lengths pertains to the process of crack initiation and is not discussed in the present paper.

Figure 3 is the same as Fig. 2 except that an externally applied load of 907 kgf (2000 lbf) was also considered and the surface residual stress values ranged from −138 to −689 MPa (−20 to −100 ksi) in increments of 138 MPa (20 ksi). The 907 kgf (2000 lbf) external force corresponds to an outer fiber stress of 779 MPa (113 ksi), which closely approximates typical endurance limits for case-hardened steels [8]. For the combination of a 454 kgf (1000 lbf) external force and surface

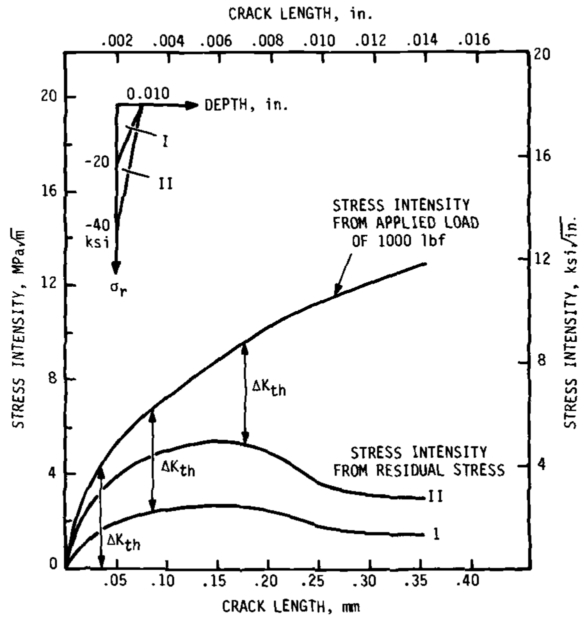

FIG. 2—*Stress intensity profiles due to applied load and two residual stress profiles.*

compressive stresses of 414, 552, and 689 MPa (60, 80, and 100 ksi), the critical crack lengths corresponding to the initiation stage are 0.23, 0.25, and 0.30 mm (0.009, 0.010, and 0.012 in.), respectively. If the externally applied load is increased, the critical crack length for each residual stress condition decreases. For example, critical crack length for the 907 kgf (2000 lbf) external load and −689 MPa (−100 ksi) surface residual stress is 0.15 mm (0.006 in.) compared with 0.30 mm (0.012 in.) for the 454 kgf (1000 lbf) load.

Influence of the Position of Residual Stress Peak on Fatigue Crack Propagation

The discussion made in conjunction with stress profiles shown in Figs. 2 and 3 demonstrates the importance of the surface residual stress on fatigue, but does not consider stress peaks occurring further away from the surface, as often observed in actual carburized cases. Therefore it is of interest to find out which part of the stress field (for example, the part far away from the crack tip or that part very near the crack tip) gives rise to a greater change in stress intensity. To analyze this problem, the contribution to stress intensity by residual stress with a pyramidal profile was computed for various peak positions. The base length of the pyramid profile was fixed at 0.254 mm (0.010 in.). The peak compressive residual stress could be assigned any value, but for this specific analysis was fixed at −345 MPa (−50 ksi). It is seen in Fig. 4 that as the residual stress peak is

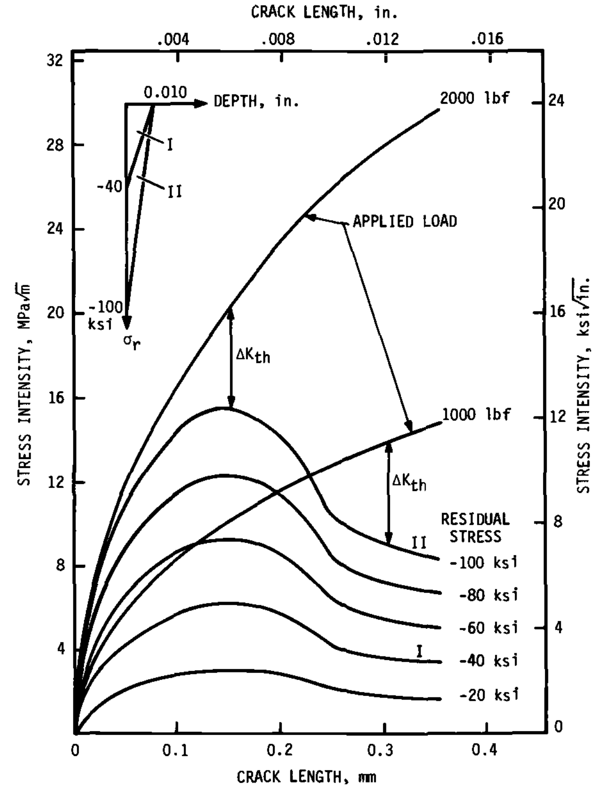

FIG. 3—*Stress intensity profiles due to applied loads and five levels of surface residual stress.*

shifted away from the surface, its contribution to the stress intensity is also shifted. The maximum contribution to stress intensity always occurs when cracks are slightly beyond the peak location of the residual stress profile. Figure 5 is a plot of the maximum stress intensity due to the residual stress peak analyzed in Fig. 4 as the peak is shifted away from the surface. The values remain fairly constant except for a slight increase when the profile and crack are close to the surface. Figure 4 shows that cracks must propagate into the compressive residual stress field before any effect of the residual stress is realized. Also included in Fig. 4 is the stress intensity curve for a constant applied load of 454 kgf (1000 lbf). Because the stress intensity due to the external force increases with crack length, the further the residual stress field is from the surface, the less will be the relative contribution from the residual stress to the net stress intensity.

Fatigue Crack Propagation in Carburized Cases

The stress intensity concept and analytical method explained so far can be used to analyze the fatigue fracture process in a typical residual stress field found in

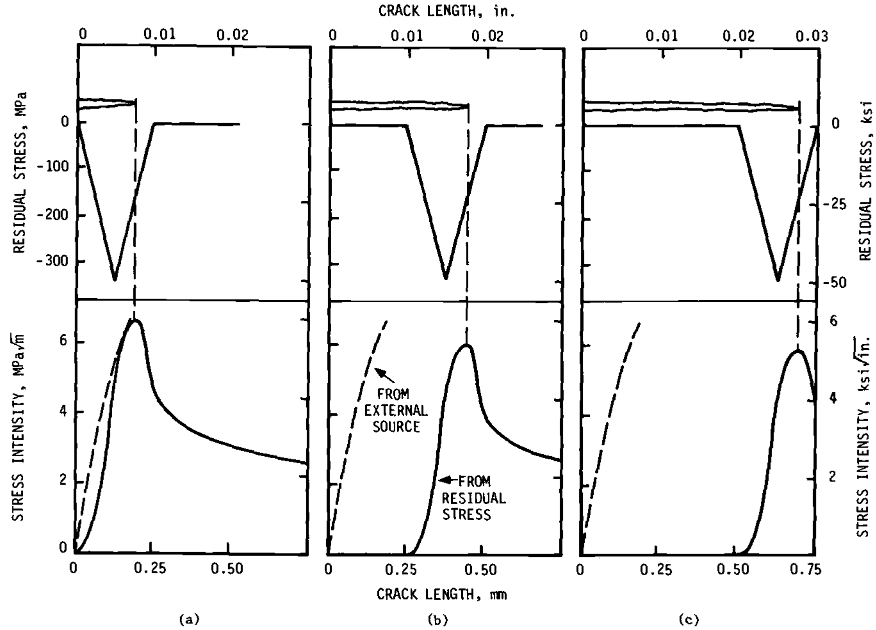

FIG. 4—*Influence of depth of peak residual stress on stress intensity due to residual stress.*

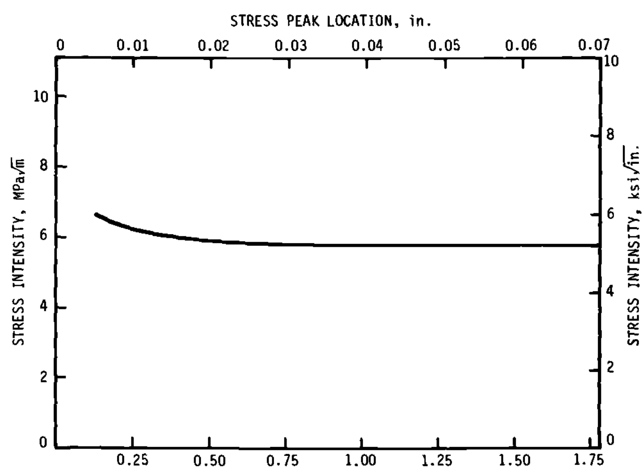

FIG. 5—*Maximum stress intensity changes due to residual stress profiles shown in Fig. 4.*

carburized cases. The assumed typical residual stress field and its contribution to stress intensity as a function of crack length are shown in Fig. 6. The residual stress field has a maximum compressive stress of 345 MPa (50 ksi) at a 1.0 mm

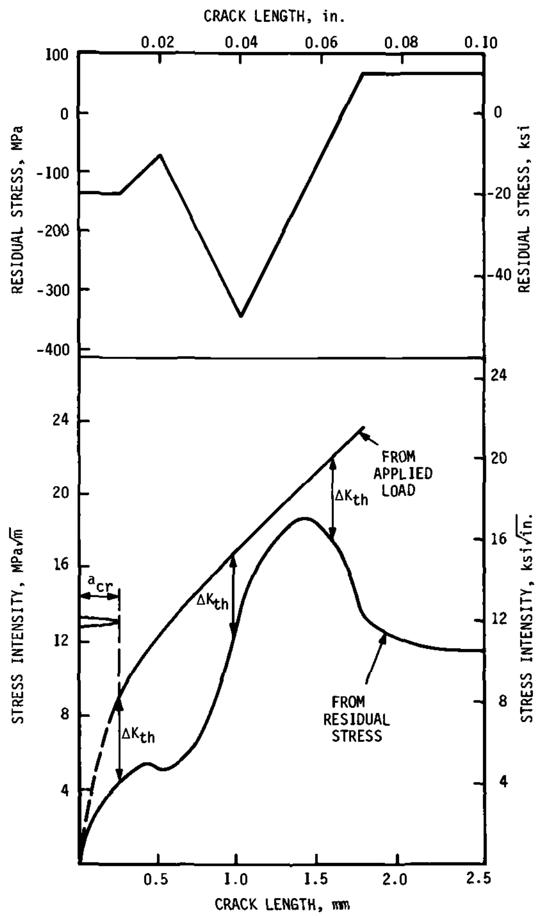

FIG. 6—*Stress intensity change due to a residual stress field typical in carburized steels.*

(0.40 in.) depth. The surface residual stress was assumed to be −138 MPa (−20 ksi), and the same value persists to a 0.25 mm (0.010 in.) depth. Also included in Fig. 6 is a stress intensity curve for an external force of 725 kgf (1600 lbf), which corresponds to a 625 MPa (90 ksi) outer fiber stress. Analogous to the treatment in Figs. 2 and 3, it is the net stress intensity between the applied stress intensity and the residual stress intensity that affects fatigue crack propagation. Only if this net value exceeds the threshold intensity will fatigue propagation occur. Figure 6 shows that crack 0.25 mm (0.010 in.) in length must exist for ΔK to exceed ΔK_{th} under an applied load of 725 kgf (1600 lbf). Once the crack length exceeds this critical value, a_{cr}, the crack will extend to a depth of 1.0 mm (0.039 in.) by the propagation mechanism. At this location, the net stress intensity falls below the threshold value and continues to decrease as the crack length increases. If the applied load never exceeds 725 kgf (1600 lbf), the crack will arrest at this location.

Discussion

The application of fracture mechanics to the fatigue fracture of case-hardened steels with compressive residual stresses in the case has led to a quantitative definition of crack initiation. Crack initiation of case-hardened steels is defined as the process by which a crack of critical length, a_{cr}, is formed. This critical length not only depends on the applied load, but also on the residual stress profile in the case. For applied loads of 454 and 907 kgf (1000 and 2000 lbf) and a residual stress field with a 138 MPa (20 ksi) compressive residual stress at surface, which linearly decreases to zero at a 0.25 mm (0.010 in.) depth (Fig. 3), the critical crack lengths that correspond to the crack initiation stage are 0.08 and 0.005 mm (0.003 and 0.0002 in.), respectively.

For the residual stress profiles shown in Figs. 2 and 3, one can determine the combination of applied load, surface compressive residual stress, and critical crack length necessary for fatigue crack propagation in a carburized case. For any combination which results in a net stress intensity amplitude exceeding ΔK_{th}, assumed to be about 4.4 MPa$\sqrt{m}$ (4 ksi$\sqrt{in.}$), crack propagation will occur.

Oxidized grain boundaries in carburized cases have long been believed to contribute to reduced fatigue lives. The depth of surface oxidation can easily exceed the critical length of crack initiation, especially if the surface compressive residual stress is 138 MPa (20 ksi) or less. A typical depth of surface oxidation is 0.013 mm (0.0005 in.). The fatigue load required to propagate a 0.013-mm (0.0005-in.)-long crack in the compressive residual stress field at the surface of 138 MPa (20 ksi) is 860 kgf (1900 lbf). The outer fiber stress corresponding to this load is 738 MPa (107 ksi), which incidentally is typical of value of fatigue limit for a case-hardened steel. Fatigue limits for carburized steels have been reported to be in the range of 689 to 827 MPa (100 to 120 ksi) [*8*]. A steel with less surface oxidation should have a higher fatigue limit, provided the compressive residual stress at the surface remains constant. Likewise, a steel having a high surface compressive residual stress at the surface can tolerate a greater depth of surface oxidation. Unfortunately, steels having excessive oxidation also tend to form nonmartensitic microstructures at the surface, which in turn decreases compressive residual stresses [*9*].

Shot-peening treatments have been reported to produce surface compressive residual stresses in excess of 690 MPa (100 ksi) [*8*]. The effect of such treatments can easily compensate for the detrimental influences of surface oxidation and other surface flaws. In fact, a fatigue load of 1588 kgf (3500 lbf), corresponding to an outer fiber stress of 1363 MPa (198 ksi), would be required to propagate a crack in a shot-peened specimen with a 550 MPa (80 ksi) surface compressive stress and a surface crack or flaw 0.013 mm (0.0005 in.) in length.

Figure 6 illustrates the stress intensity of cracks extending into a compressive residual stress profile that approximates the shape typical in carburized cases. For the conditions depicted, the net stress intensity amplitude decreases as the crack propagates from a length of 0.76 mm (0.03 in.) to a depth of 1.0 to 1.3 mm (0.04 to 0.05 in.). If the applied fatigue load is low enough, the crack will actually arrest and not propagate again until the applied load is increased.

At the present time, there are no definitions of the initiation and propagation stages in a fatigue fracture process for which there is universal agreement. Socie et al have proposed a definition for crack initiation: a fatigue crack is initiated when the fatigue damage due to propagation mechanisms exceeds that due to crack initiation or strain cycle fatigue mechanisms [*10*]. Low-cycle fatigue concepts and linear elastic fracture mechanics were used to describe crack initiation and propagation stages, respectively. However, for high-carbon, high-hardness, low-toughness materials such as carburized case, the usefulness of the concept of a low-cycle strain-controlled test is doubtful. Such materials do not exhibit an appreciable degree of plasticity in a tension test, and in the fracture toughness test, the plastic zone at the crack tip may be as small as one micron in radius, many orders of magnitude smaller than typical plastic zone sizes found in tough materials. Therefore, defining the initiation and propagation stages of fatigue fracture in terms of the threshold stress intensity amplitude seems to be a reasonable approach to the fatigue fracture of case-hardened steels. In a sense, Socie's and the present authors' definitions of crack initiation may be considered as complementary to each other by providing a means for treating crack initiation in low-strength high-toughness materials and high-strength low-toughness materials, respectively.

The influence of tensile residual stress was not analyzed in the present study. For materials which obey the Paris fatigue equation, crack propagation rate is not affected by tensile residual stress; this is because only the mean stress intensity is raised and not the stress intensity amplitude. It is known, however, that ΔK_{th} can decrease by as much as a factor of 2.5 compared with the residual stress-free condition [*7*]. If such is the case, tensile residual stress is expected to have an effect on the crack initiation life.

It is clearly a difficult task to develop a theory that can describe the fatigue fracture process quantitatively. The authors present this paper as a demonstration of the usefulness of linear elastic fracture mechanics and empirically derived fatigue laws in explaining the influence of residual stress on crack initiation in high-strength low-toughness materials.

Summary

The crack initiation stage of fatigue of carburized steels was defined as the process of formation of a crack whose length is such that the fatigue stress intensity amplitude is equal to the threshold stress intensity amplitude. The process of fatigue crack extension that follows the initiation stage was defined as the propagation stage. The critical initiation crack length depends not only on applied load but also on residual stress. Examples of the effect of various residual stress profiles on the fatigue stress intensity amplitude were given. It was shown that a compressive residual stress at the surface has a greater influence on the critical crack length than a similar residual stress profile existing further inside the case. An analysis of a residual stress profile typical of a carburized case showed

that even after a crack begins to propagate, the stress intensity amplitude may decrease, and at relatively low stress levels this can cause the crack to be arrested.

Carburized cases having surface cracks corresponding in length to the depth of grain boundary oxidation were analyzed. It was found that applied stresses required for crack propagation were similar in magnitude to measured fatigue limits of carburized steels. Steels having greater compressive residual stresses at the surface require greater applied loads for the crack to extend by the propagation mechanism. The influence of surface oxidation on fatigue depends on the depth of the oxidized boundaries as well as the residual stress at the surface. For example, shot-peened specimens having a high compressive residual stress should have a high tolerance for surface oxidation. The high fatigue limit of shot-peened specimens can be explained by the present model, according to which a compressive residual stress field near the surface increases the critical crack size required for propagation.

References

[*1*] Rolfe, S. T. and Barsom, J. M., *Fracture and Fatigue Control in Structures*, Prentice-Hall, Englewood Cliffs, N. J., 1977, p. 209.

[*2*] Sveshnikov, D. A., Kudryavtsev, I. V., Gulyaeva, N. A., and Golubovskaya, L. D., *Metal Science and Heat Treatment*, July 1966, No. 7, p. 527.

[*3*] Throop, J. F., "The Effects of Residual Stress in Fatigue," a summary report from ASTM Task Group No. 3 of E09.90 submitted to ASTM Committee E-9 on Fatigue, 9 Nov. 1980, p. 51.

[*4*] Glinka, Grzegorz, in *Fracture Mechanics, ASTM STP 677*, C. W. Smith, Ed., American Society for Testing and Materials, 1979, pp. 198–214.

[*5*] Tada, H., Paris, P., and Irwin, G., *The Stress Analysis of Cracks Handbook*, Del Research Corp., 1973.

[*6*] Bückner, H. F., *Zeitschrift für Angewandte Mathematik und Mechanik*, Vol. 52, 1971, p. 97.

[*7*] Fuchs, H. O. and Stephens, R. I., *Metal Fatigue in Engineering*, Wiley, New York, 1980.

[*8*] Parrish, Geoffrey, *The Influence of Microstructure on the Properties of Case-Carburized Components*, ASM, 1980.

[*9*] Hildenwall, B. and Ericsson, T., *Journal of Heat Treating*, Vol. 1, No. 3, 1980, p. 3.

[*10*] Socie, D. F., Morrow, JoDean, and Chen, W.-C., *Engineering Fracture Mechanics*, Vol. 11, 1979, p. 851.